Somatotopic organization of the human periaqueductal gray revealed in pain and placebo analgesia

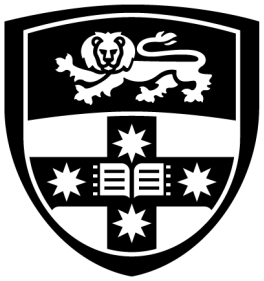

THE UNIVERSITY OF SYDNEY

Fernando Andres Tinoco Mendoza BMedSci (Hons)

Faculty of Medicine and Health

The University of Sydney

A thesis submitted in fulfilment of the requirement for the degree of

Doctor of Philosophy

Laboratory of Neural Imaging

School of Medical Sciences

April 2025

For my family, who have always believed in me.

Table of Contents

Acknowledgements

For years I have questioned my ability to get through this journey, not believed I was capable and doubted whether I was good enough to reach the end. A career in science is no easy path, and I have a profound respect for those who have pursued one. This thesis serves as the greatest achievement of my life, and I hope to have made everyone who has supported me proud.

To all members of the lab, you have given me genuine companionship in times when I needed it the most. The last 5 years would not have been the same without you, and I will always look back fondly to the memories we made together. Rebecca, we've both been side-by-side with one another since the start. I'm glad to have gotten to know and work with you so closely and have no doubt you will become an amazing researcher. Noemi, you were the one to guide me on my first day and have helped me many times when I was feeling down. It has been a pleasure working with you – I'll take good care of your beema. Angela, Alan and Ash, I wish you all the best for the rest of your PhD's! Good luck to you all with your future endeavors.

To the friends that have stuck by me, thank you for putting up with my constant complaints and emotional bursts all these years. All the boyos – Ben, Ethan, Hamish, Jas1ner, Michael, Maffas, Rosh, Yiandogs – thanks for still being by my side after all this time I've dedicated to my studies. Gordon and Luke, I have felt I can always rely on you when I needed to vent and let out my feelings; thank you for listening and convincing me to keep going. Jono, you've been my #1 hype man since starting and you still are; your enthusiasm for my work always pushes me to go further. Faith and Eric, thank you for all the laughs, and for always being there for me all these years.

I would like to give a massive thank you to my supervisor, Luke Henderson. I will never forget the moment we met, when you gave me the opportunity to pitch my business idea after you gave a guest lecture and took the time to listen and give me advice. You have always had nothing but my best interests in mind and I will never forget the work, time and dedication you have spent on me. Thank you for dealing with me for as long as you did, your unwavering support and everything you have done for me over so many years.

Por último, para mi familia: mamá, papá y Nene. Siempre me han dicho que podía lograrlo y me han hecho creer en mí mismo. Nene, eres mi mayor inspiración en la vida y siempre te admiraré como un orgulloso hermanito. Mamá y papá, han estado a mi lado todo los días, y todo lo que han hecho por mí me ha ayudado enormemente. Nunca podré devolverles todo lo que han hecho por mí, pero les prometo que seguiré esforzándome por ser la mejor versión de mí mismo. Gracias por todo. Los amo con todo mi corazón.

Statement of Originality

The work presented in this thesis is, to the best of my knowledge and belief, original except as acknowledged in the text. I hereby declare that I have not submitted this material, either in full or in part, for a degree at this or any other institution.

I certify that the intellectual content of this thesis is the product of my own work and that all the assistance received in preparing this thesis and sources have been acknowledged.

Fernando Andres Tinoco Mendoza

Date: 24 April, 2025

Authorship Attribution Statement

Selected peer-reviewed and/or submitted manuscripts have been used to compose the chapters of this thesis. Below are descriptions of co-authors' contributions to these manuscripts.

Chapter 2 of this thesis is published as:

Fernando A. Tinoco Mendoza, Timothy E. Hughes, Rebecca V Robertson, Lewis S Crawford, Noemi M, Paul M Macey, Vaughan G Macefield, Kevin A Keay, Luke A Henderson, 2023, 'Detailed organisation of the human midbrain periaqueductal grey revealed using ultra-high field magnetic resonance imaging' *Neuroimage*, vol. 266:119828, doi: 10.1016

- Fernando A. Tinoco Mendoza consolidated the data, analyzed the data and wrote the drafts of the manuscript.

Chapter 3 of this thesis is in preparation for publication as:

Fernando A. Tinoco Mendoza, Lewis S. Crawford, Rebecca V. Robertson, Noemi Meylakh, Paul M. Macey, Kirsty Bannister, Tor D. Wager, Vaughan G. Macefield, Kevin A. Keay, Luke A. Henderson, 2024, 'Somatotopic organization of brainstem analgesic circuitry', *Under Review*

- Fernando A. Tinoco Mendoza consolidated the data, analyzed the data and wrote the drafts of the manuscript.

Chapter 4 of this thesis is in preparation for publication as:

Fernando A. Tinoco Mendoza, Lewis S. Crawford, Rebecca V. Robertson, Noemi Meylakh, Paul M. Macey, Kirsty Bannister, Tor Wager, Vaughan G. Macefield, Kevin A. Keay, Luke A. Henderson, 2024, 'Descending cortical and sub-cortical pain modulatory circuits underlying placebo analgesia on different body sites', *Under review*

- Fernando A. Tinoco Mendoza consolidated the data, analyzed the data and wrote the drafts of the manuscript.

Fernando Andres Tinoco Mendoza, 24 April 2025

As supervisor for the candidature upon which this thesis is based, I can confirm that the authorship attribution statements above are correct.

Luke Anthony Henderson, 24 April 2025

Publications and conference presentations

Publications contained in this thesis

Fernando A. Tinoco Mendoza, Timothy E. Hughes, Rebecca V Robertson, Lewis S Crawford, Noemi M, Paul M Macey, Vaughan G Macefield, Kevin A Keay, Luke A Henderson, 2023, 'Detailed organisation of the human midbrain periaqueductal grey revealed using ultra-high field magnetic resonance imaging' *Neuroimage*, vol. 266:119828, doi: 10.1016

CRediT: Conceptualization – FATM, TEH, KAK, LAH; Investigation - FATM, KAK, LAH; Resources – PMM; Data analysis – FATM, TEH, RVR, LSC, PMM; Writing – original draft: FATM

Conference abstracts

2021

Australian Pain Society ASM, 19-20 April (online)

- Poster presentation: "Altered connectivity amongst pain systems underlying trigeminal neuropathic pain"

2023

Australian Pain Society ASM, 2-5 April (Canberra, ACT)

- Free paper presentation: "Altered regional blood flow associated with chronic pain following spinal cord injury"
- Winner of the best free paper award ($1000)

FMH HDR Conference, 19-20 July (Sydney, NSW)

- Free paper presentation: "Altered regional blood flow associated with chronic pain following spinal cord injury"

2024

Australian Pain Society ASM, 21-24 July (Darwin, ACT)

- Free paper presentation: "Somatotopic representation of placebo analgesia in the human brainstem"

IASP World Congress, 5-9 August (Amsterdam, Netherlands)

- Poster presentation: "Somatotopic representation of placebo analgesia in the human brainstem"

Awards and funding

2021-2024	University Postgraduate Award (UPA) ($35,629)
2021-2024	Research Training Program (RTP) Fees Offset
2023	Australian Pain Society (APS) Best free paper award ($1000)
2023-2024	Australian Pain Society (APS) Travel Grant ($500)
2022-2024	Postgraduate Research Support Scheme (PRSS; $500 in 2022; $1060 in 2023; $1000 in 2024)

Other publications during candidature

The following manuscripts, whilst largely unrelated to the topics discussed in this thesis, were published with my academic contribution throughout the course of my candidature:

- Robertson, RV, Meylakh, N, Crawford ,LS, **Tinoco Mendoza, FA**, Macey, PM, Macefield, VG, Keay, KA, Henderson LA, 2024, 'Differential activation of lateral parabrachial nuclei and their limbic projections during head compared with body pain: A 7-Tesla functional magnetic resonance imaging study', *Neuroimage*, vol. 299, no. 120832, https://doi.org/10.1016/j.neuroimage.2024.120832

- Delang, N, Robertson, RV, Tinoco Mendoza, FA, Henderson, LA, Rae, C, McDonald, SJ, Desbrow, B, Irwin, C, Peek, AL, Cairns, EA, Austin, PJ, Green, MA, Jenneke, NW, Cao, J, O'Brien, WT, Ball, S, Buckland, ME, Rae, K, McGregor, IS, McCartney, D, 2024, 'The acute effects of non-concussive head impacts in sport: A randomised control trial', Submitted to *Sports Medicine – Open, Under Review*, https://doi.org/10.21203/rs.3.rs-4765251/v1

List of abbreviations

ACC	Anterior cingulate cortex
BOLD	Blood oxygen level-dependent
CNS	Central nervous system
CSF	Cerebrospinal fluid
DH	Dorsal horn of the spinal cord
dlPFC	Dorsolateral prefrontal cortex
EAA	Excitatory amino acid
fMRI	Functional magnetic resonance imaging
FOV	Field-of-view
MRI	Magnetic resonance imaging
PAG	Periaqueductal gray
PET	Positron emission tomography
PFC	Prefrontal cortex
rACC	Rostral anterior cingulate cortex
RVM	Rostral ventromedial medulla
SpV	Spinal trigeminal nucleus
SRD	Subnucleus reticularis dorsalis
STT	Spinothalamic tract
SUIT	Spatially unbiased infratentorial template
S1	Primary somatosensory cortex
T	Tesla
TENS	Transcutaneous electrical nerve stimulation
TTT	Trigeminothalamic tract
UHF	Ultra-high field

Abstract

Pain is a critical and fundamental homeostatic state that results in the execution of defensive behaviours, one of which is a profound placebo analgesia. Early discoveries on the midbrain periaqueductal gray (PAG) found that its electrical stimulation would evoke analgesia in experimental animals. Subsequent seminal studies led to thorough investigations on the anatomical, behavioural and physiological mechanisms that govern PAG function. Functional and tract-tracing studies revealed a somatotopic organisation of noxious afferent inputs/outputs and defensive behaviours of the PAG from the primary afferent synapse of the medulla and spinal cord. The principal aim of this thesis was to utilize recent advancements in ultra-high field imaging to assess the functional organisation of the human PAG during noxious stimulation and analgesic processing across different body sites, to find whether a somatotopy exists in humans as in animals.

Chapter 2 establishes a somatotopic organisation in the human PAG. We uncovered a rostro-caudal pattern of activation depending on whether pain was induced on the face or body. Building on this work, **Chapter 3** utilized a response conditioning model in the context of placebo analgesia to observe if this same rostro-caudal pattern of activity was preserved in the PAG. **Chapter 4** bridges the cortex, subcortex and brainstem to reveal if a consistent pattern exists in key regions involved in top-down control of pain modulation across the same body sites. This thesis concludes by discussing the behavioural, clinical and experimental implications of our three studies, with a focus on how the delineation of spatially separate face-body circuits within the PAG may be phyletically preserved across species. In addition, we propose how further interrogation of these circuits could aid and assist in the development of new approaches that treat chronic pain, by leveraging the neural mechanisms of a somatotopic organisation within the human PAG.

Chapter 1.

Introduction

“In pain there is as much wisdom as in pleasure:

like the latter, it is one of the best self-preservatives of a species.”

Friedrich Nietzsche, The Gay Science, 1882

1.1 Introduction

Pain is an essential facet of life and survival. When acute in nature, pain exists as an interoceptive state and homeostatic mechanism that motivates certain behavioural responses. By provoking the individual to act, pain functions like a conscious state of emotion. An emotion is accompanied by an individual's subjective experiences, and whether positive or negative, will influence one's decision and conduct (Dąbrowski, 2016). Pain constitutes an emotional experience, often imbued with negativity, shaped by an individual's own beliefs and assessments. Aristotle once proposed that to feel an emotion is to be in a state of pain, pleasure, or both. In his second book of the *Rhetoric*, Aristotle postulated a theory involving four elements that comprise an emotion: (i) cognition, (ii) affection, (iii) behaviour and (iv) physiology (Aristotle, 1984). These elements together provide a crucial framework and hold considerable merit and value for our contemporary theories and knowledge of pain held today.

In his 1662 landmark work *Treatise of Man*, philosopher René Descartes theorised the first physiological idea for pain. He proposed that pain arises when specific pathways are activated by stimulation of receptors within the periphery. Neural signals travel through these pathways via hollow tubes, i.e. nerves, towards a "pain centre" in the brain, where sensory and motor information is processed. This information leads to a perceptual experience (the feeling of pain) and an appropriate behavioural response, such as withdrawing the body from the source of pain (Benini & DeLeo, 1999). Referred to as the 'specificity pain theory', Descartes' stimulus-response model claims that the intensity of pain correlates with the extent of tissue damage, and that removing these pathways should alleviate all pain. However, numerous case studies have disproven this latter component, as demonstrated by the exacerbation of pain symptoms following the severing of nerves and tracts (Nagaro et al., 2001).

Whilst these early reports highlighted the fact that pain acts to motivate an individual to remove themselves from damaging stimuli, clinical observations suggest that the intensity of pain can also be modified by the brain. For example, in the 1950's, when American anaesthesiologist Henry Beecher performed work on wounded war soldiers, a monumental finding related to pain and analgesia was uncovered. In his seminal work "The Powerful Placebo", Beecher summarised the findings of 15 studies and found that 35% of 1082 patients were satisfactorily relieved by a placebo effect alone (Beecher, 1955). That is, simply believing that a particular intervention was going to reduce pain, resulted in a pain reduction even when the treatment was completely inert. Beecher was one of the first to demonstrate a relationship between the pain experience and cognitive/psychological factors associated with the injury (Benedetti, 2022). Since then,

numerous studies have explored the brain pathways capable of producing endogenous pain relief. Extensive work in animals, particularly rodents, have revealed multiple brain sites that, when stimulated, can modulate the intensity of incoming noxious information. One brainstem site, the midbrain periaqueductal gray matter (PAG), has been postulated by many researchers to play a pivotal role in pain modulation. An early experiment performed by Reynolds (1969) noted that electrical stimulation of the PAG produced a profound analgesia in rats such that abdominal surgery could be performed without the need for general anaesthesia. Animal models have since been pivotal in studying the neuroanatomy and functional organisation of the PAG, particularly in the context of pain processing. However, investigating small brain structures, like the PAG, in humans has presented a major challenge for decades due to constraints in the spatial resolution of non-invasive neuroimaging and physiological techniques.

The following literature review aims to collate the animal findings on the role of PAG, notably its lateral column, in pain processing. It will also address the gaps in relation to our understanding of the PAG's functional organisation in how pain and analgesia are processed in different body site.

1.2 Ascending neural pathways

The conscious and subjective experience of pain arises from the activation of specific peripheral receptors called nociceptors. These nociceptors, or specialized nerve endings, can detect a wide range of tissue-threatening stimuli including extreme temperatures, pressures, toxic substances, and inflammatory agents. Nociceptors must be activated by a stimulus deemed to be noxious, and are located throughout peripheral structures, including joints, muscles, skin, and viscera (Hladnik, Bičanić & Petanjek, 2015).

Studies by Mense (1993) revealed several classes of nociceptors according to whether they respond to noxious thermal, chemical, or mechanical stimuli, or a combination of all three, referred to as polymodal nociceptors. Noxious cutaneous stimulation is initially perceived as a sharp, prickling sensation stemming from activation of nociceptors on thinly myelinated Aδ fibers. These nociceptors respond predominantly to heat and mechanosensitive stimuli. In contrast, a slower and throbbing secondary phase of acute pain results from activation of polymodal nociceptors on unmyelinated C-type fibers (Torebjörk & Hallin, 1973). The nociceptive signal travels along these first-order, pseudo unipolar peripheral nerves to the central nervous system (CNS) where they synapse onto second-order neurons. The anatomical junction this site, i.e. the *primary afferent synapse,* is distinct for noxious inputs originating from the body and face.

Noxious information from the body

First-order nociceptor afferents transmitting noxious information from the body enter the CNS and largely terminate in the dorsal horn of the spinal cord (DH). The cell bodies of these afferents are located in the dorsal root ganglia throughout the rostro-caudal extent of the spinal cord. The DH itself is organized into multiple distinct laminae and those that receive and modulate somatosensory inputs, including noxious inputs, are laminae I-VI. More specifically, noxious signals in Aδ and C-fibers terminate in the superficial and deep layers of laminae I-II and V, respectively (D'Mello & Dickenson, 2008) (see Figure 1.1).

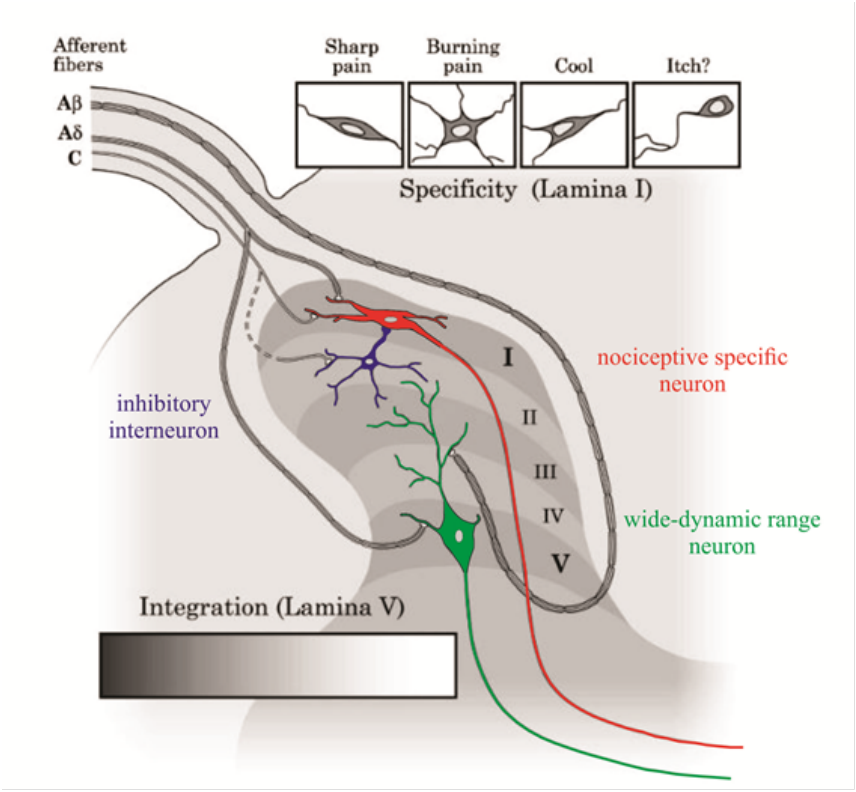

Figure 1.1. Schematic representation of the anatomical basis for afferent inputs into the dorsal horn of the spinal cord. Within the superficial dorsal horn, i.e. laminae I and II, nociceptive specific neurons receive direct input from Aδ and C-fibers, whereas in IV and V of the deeper layers, wide-dynamic range neurons receive (convergent) direct and (interneuron) indirect inputs from all fiber types. Aβ fibers are low-threshold highly myelinated fibers that primarily respond to innocuous stimuli, although may partially respond to noxious stimuli. Note that all laminae receive descending inhibitory or excitatory inputs from supraspinal structures. *Adapted from Craig (2003)*.

It is worth noting that the distribution of nociceptive axons and other somatosensory fibers is segmental throughout the body. That is, the cutaneous area supplied by a single nerve root is distributed in a pattern referred to as a *dermatome*. As shown in Figure 1.2, fine delineations exist between adjacent dermatomes, particularly in fibers that project to the cervical and thoracic spinal cord. Whilst the overall dermatomal pattern exists, influential findings from Foerster (1933) revealed that the precise dermatome locations vary between individuals, a result consistent with previous work performed on primates (Sherrington, 1893; 1898). It remains apparent that current dermatome maps display individual variability and show a high degree of overlap between adjacent dermatomes (Lee, McPhee & Stringer, 2008). Nevertheless, this organization of afferent fibers mapping to unique parts of the body, ultimately enables a finely localized appreciation of a painful sensation to be made at higher areas of the CNS.

Noxious information from the face

In contrast to the body, the skin on the face is innervated largely by the trigeminal nerve. This cranial nerve, i.e. cranial nerve V, conveys noxious and non-noxious somatosensory information from superficial and deep structures of the face and oral cavity. It comprises three peripheral divisions – the ophthalmic (V1), maxillary (V2), and mandibular (V3) – which innervate the face in a segmental manner (see Figure 1.2). This tripartite innervation distribution is segmental like its spinal nerve counterparts in the body, however, despite a convergence of nociceptive processing between trigeminal and cervical afferent systems, they are not dermatomes *per se* (Piovesan et al., 2001).

The cell bodies of the sensory neurons belonging to the trigeminal nerve are located within the trigeminal ganglion. Their axons form the trigeminal sensory root that enters the brainstem at the level of the mid-pons (Waite & Ashwell, 2004). Nociceptor afferents descend caudally from the pons and terminate throughout the rostro-caudal extent of the spinal trigeminal nucleus (SpV) located along the medulla oblongata and upper cervical spinal cord (Sessle, 2000).

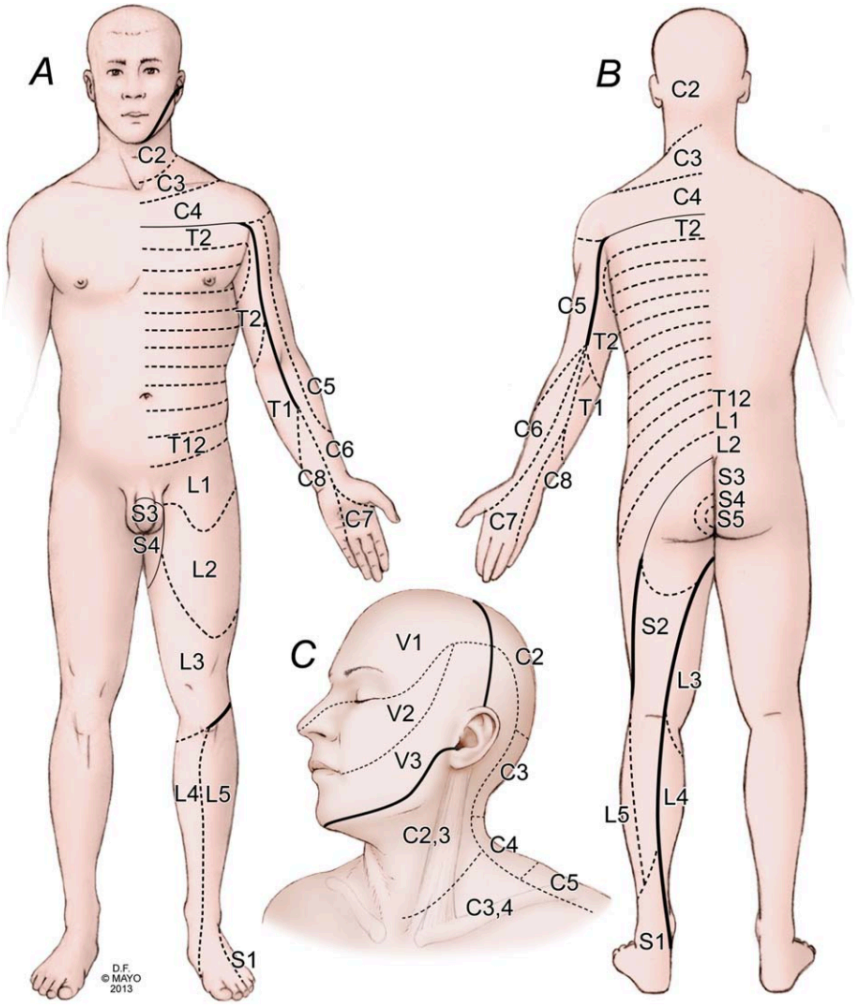

Figure 1.2. Cutaneous dermatome maps of the (a) anterior and (b) posterior surfaces of the body. Spinal nerves from cervical (C), thoracic (T), lumbar (L) and sacral (S) segments of the spinal cord innervate cutaneous and sub-cutaneous parts of the body. Solid axial lines indicate the boundaries between adjacent dermatome segments that do not correspond directly to neighboring spinal levels, whereas dashed lines depict the territories of sensory nerves. In the (c) face, the extent of the ophthalmic (V1), maxillary (V2) and mandibular (V3) divisions of the trigeminal nerve are bounded by the dotted lines. Territories from the cervical spinal segments are displayed due to their distribution input and separated from the trigeminal nerve sensory territories by the axial solid line. *Adapted from Gray's Anatomy*, Standring (2008).

Supraspinal processing

Following termination of nociceptor afferents in either the DH (body) or SpV (face), noxious information is transferred onto second order projection neurons. Within the laminae of the DH, incoming noxious information can be modulated by local interneurons as well as descending facilitatory and inhibitory inputs from the brainstem and cortex (Dubin & Patapoutian, 2010). The SpV can be divided into three major subdivisions - caudalis, interpolaris and oralis – of which the caudalis division of SpV is most analogous with the DH, and also receives descending fibers that modulate incoming noxious information (Sessle, 2000). These second order neurons from the DH and SpV then decussate and cross the midline of the spinal cord or medulla at the corresponding dermatome level, before ascending contralaterally towards thalamic nuclei via multiple ascending neural tracts.

For the body and face respectively, the ascending spinothalamic (STT) and trigeminothalamic tracts (TTT) carry the sensory-discriminative aspects of pain as well as temperature, vibration, and itch sensations (Craig, Zhang & Blomqvist, 2002) (see Figure 1.3A, B). Importantly, the STT and TTT contain a somatotopic arrangement, that is, the point-to-point correspondence for an area of the body to a specific point in the CNS. The STT is organized in a manner that upper and lower body fibers are arranged from most medially to laterally, respectively, within the spinal cord (Vedantam et al., 2019). In the face, a somatotopic map exists as an organized "onion skin" pattern of concentric circles from the perioral to pre-auricular regions. The perioral areas are represented rostrally in the SpV, whereas more posterior facial regions are represented more caudally within SpV, adjacent to sensory input from cervical nerves two and three (DaSilva et al., 2008; Wall & Taub, 1962).

This somatotopic arrangement of ascending noxious information is maintained as fibers from the STT and TTT largely terminate in the ventroposterior lateral and medial nucleus of the thalamus, respectively. The ventroposterior thalamic nuclei then send third-order projection neurons to higher brain regions that comprise the lateral pain system that encodes the sensory-discriminative aspects of pain (Treede et al., 1999).

One key region in the lateral pain system is the primary somatosensory cortex (S1), located in the post-central gyrus of the parietal lobe (Brodmann areas 1, 2, 3a and 3b) (Brodmann, 2006). Penfield and Rasmussen (1950) established that the S1 contains a fine somatotopic arrangement along its mediolateral extent, with distal structures, like the legs, represented medially and proximal structures, such as the hand and face, more laterally (see Figure 1.3C). The secondary somatosensory cortex is also involved and receives projections from S1 and, less extensively, from the thalamus (Liao & Yen, 2008). In addition, the insular cortex is instrumental in the sensory discrimination of noxious stimuli. Like with S1, direct electrical stimulation at sites within the (posterior) insular cortex has shown to elicit tactile paresthesia, though to a lesser extent as exhibited by S1 (Mazzola et al., 2009; Ostrowsky et al., 2002). The insular cortex has also shown to be organized both in a somatotopic arrangement and according to pain modality (Henderson, Gandevia & Macefield, 2007). It is, therefore, through this somatotopic organization of sensory inputs at various levels of the neuroaxis that nociceptive and tactile stimuli can be finely discriminated and localized.

In addition, some ascending noxious information also projects to medial thalamic nuclei, including the mediodorsal and centromedian nuclei (Dostrovsky et al., 2013). These thalamic nuclei, in turn, relay projections to higher order, association cortices that make up the medial pain system and code the emotional and cognitive aspects of pain. These brain regions include the anterior cingulate cortex (ACC), prefrontal cortices and anterior insula (Treede et al., 1999). Indeed, neuroimaging investigations have revealed that noxious stimuli consistently activate these regions (Garcia-Larrea, Frot & Valeriani, 2003) and adjusting the emotional component of pain, i.e. the unpleasantness, without altering the perceived pain intensity, alters ACC activity (Coghill, McHaffie & Yen, 2003). Ultimately, the multifaceted perception of pain is created by the dynamic interplay of these collective regions involved in affective, cognitive, emotional processing, referred to as the 'pain neuromatrix' (Brooks & Tracey, 2005; Tracey, 2005).

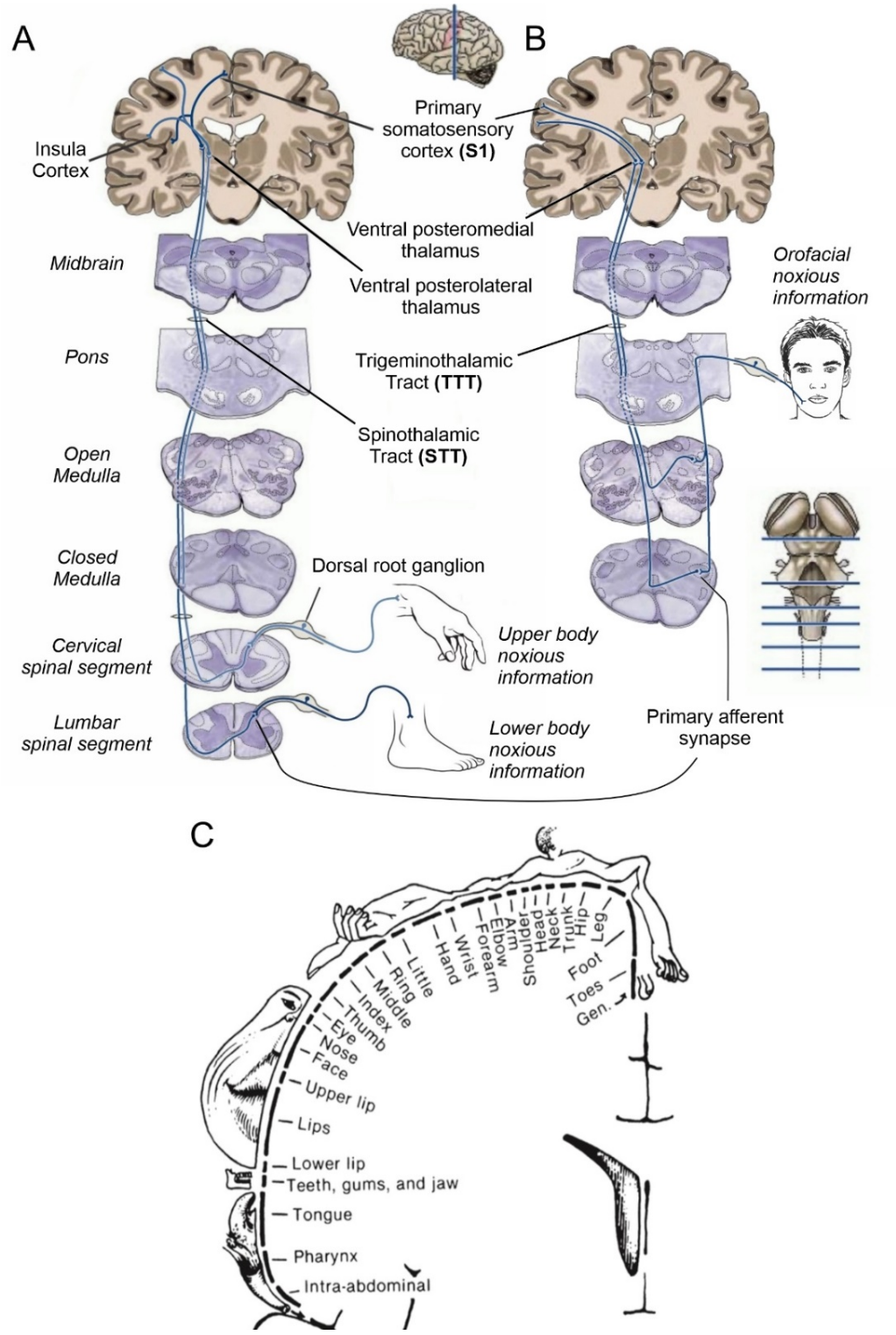

Figure 1.3. Major ascending neural pathways for the discriminatory and sensory aspects of pain perception arising from the (A) Spinothalamic Tract (STT) and (B) Trigeminothalamic Tract (TTT). Primary afferent nociceptors of the body synapse with second order projection neurons in the dorsal horn of the spinal cord, whereas afferents from the face synapse in the spinal trigeminal nucleus at the medulla. Neurons of the STT and TTT decussate and ascend the brainstem to synapse at the contralateral ventroposterior lateral and medial nucleus of the thalamus,

respectively, in which they project to the primary somatosensory cortex (S1) and encode the intensity and location of a noxious stimulus. *Adapted from Purves, Augustine and Fitzpatrick (2001)*. The localization of sensory stimuli across the body and face are distinctly encoded through a somatotopic map of S1 (C). More proximal structures are represented laterally towards the parietal operculum, whilst distal structures are represented medially towards the paracentral lobule. As shown surrounding the cortex, a graphical representation can be made depicting each body part in proportion to the size of the cortical area devoted to that body part – this is known as the somatosensory homunculus. *Modified from Vanderah and Gould (2020), originally taken from Penfield and Rasmussen (1950)*.

1.2.1 The brainstem

Despite long being considered a simple sensation, pain is now considered akin to thirst and hunger, that is, a fundamental need-state that promotes a change in behaviour (Wall, 1979). The sensory-discriminative and emotional dimensions are no doubt important, however it can be argued that the brainstem circuits responsible for behavioural state changes to noxious inputs are more critical for survival. One brainstem region containing all the neural hardware required to produce integrated defensive reactions to noxious stressors is the PAG (Keay & Bandler, 2008). Through distinct neural circuits, the PAG can promote active or passive coping strategies. Respectively, those are confrontational defensive reactions associated with sympathetic activation (tachycardia and hypertension), and conservation-withdrawal strategies characterized by autonomic inhibition (bradycardia and hypotension) (Bandler et al., 2000; Keay & Bandler, 2001).

The importance of the PAG as the site of the midbrain integrating defensive behavioral reactions was underscored from functional experiments performed by Richard Bandler in 1982. Since these seminal findings, which will be discussed in the next section, the relationship between pain and behavior within the PAG has been a topic of continued investigation. While the ascending neural tracts and sensory aspects of pain are established to be somatotopic in nature, a somatotopic organization within the PAG and insight into how it modulates pain-related behavior in humans remains to be shown.

1.3 The midbrain periaqueductal gray (PAG)

Due to their roles in basic survival, primitive behaviours - such as fight or flight defence - and emotions – like anger or fear - are conserved across species. In 1872, Charles Darwin proposed that distant species must share common neuronal circuits and substrates due to the similarity in behaviours and responses that they evoke (Darwin, 1872). Indeed, anatomical structures involved in regulating basic survival appear to have their anatomy conserved across vertebrate species. An advantage of this, is that behaviours are effectively driven and modulated in a selective manner across species, to elicit the most appropriate response against stressors, which is achieved through the PAG.

1.3.1 Structural organization

The PAG is a prominent structure within the mammalian midbrain, consisting of gray matter surrounding the cerebral (mesencephalic) aqueduct (see Figure 1.4). In humans, it measures approximately 14 millimeters long and 4-5 millimeters wide on average and extends from the level of the posterior commissure rostrally to the level of the locus coeruleus caudally (Behbehani, 1995; Linnman et al., 2012). It is bordered laterally by descending tectospinal fibers and the mesencephalic trigeminal nucleus, dorsally by the superior and inferior colliculi and ventrally by the mesencephalic reticular and cuneiform nuclei. The neuronal pool contained within the PAG is considered a separate entity to other nuclei within its own confines, like the dorsal raphe nucleus, the Edinger-Wesphal nucleus, oculomotor nucleus, trochlear nuclei and the dorsal and ventral tegmental nuclei (Linnman et al., 2012). At its rostral extent, the PAG is continuous with the periventricular gray matter of the hypothalamus surrounding the third ventricle. Caudally, the cerebral aqueduct expands into the fourth ventricle where it becomes continuous with the dorsal pons.

Figure 1.4. Transverse section of the rostral human midbrain, indicating the location of the periaqueductal gray (outlined in red). A luxol fast blue histological stain has been used to reveal myelin and a neutral red counterstain for large neurons with prominent Nissl substance. The section is sliced perpendicular to the plane of the cerebral aqueduct. *Adapted from Nolte (2013).*

Initial attempts at sub-dividing the PAG based on cytoarchitecture failed to provide meaningful insights into its structure. Due to being a markedly cell-rich and myelin-poor structure, many experimental methods, such as Nissl staining and Golgi impregnation, were unable to reveal clear boundaries that distinguish a clear cellular organization within the PAG (Carrive & Morgan, 2012). While it was suggested that a relationship existed within the dorsal, lateral and ventral parts of the PAG (Olszewski & Baxter, 1954), there was insufficient evidence, based on neuroanatomy alone, to recognize any strict divisions within the PAG (Mantyh, 1982c). Ultimately, it was through a series of iterative functional experiments that formed the basis of organizing the PAG, reflecting a coupling between somatic and cardiovascular changes of defensive reactions across animal species.

1.3.2 Functional studies: a columnar organization

It is now well accepted that the PAG consists of four longitudinal columns running parallel to the cerebral aqueduct. In the coronal plane along the dorsal-ventral axis, the columns are the dorsomedial PAG, dorsolateral PAG, lateral PAG and ventrolateral PAG (Linnman et al., 2012) (see Figure 1.5). Numerous experimental animal studies have revealed that two of the four PAG columns are involved in pain processing. More specifically, they appear to mediate the active and passive emotional coping strategies to stress, threat and pain (Keay & Bandler, 2001).

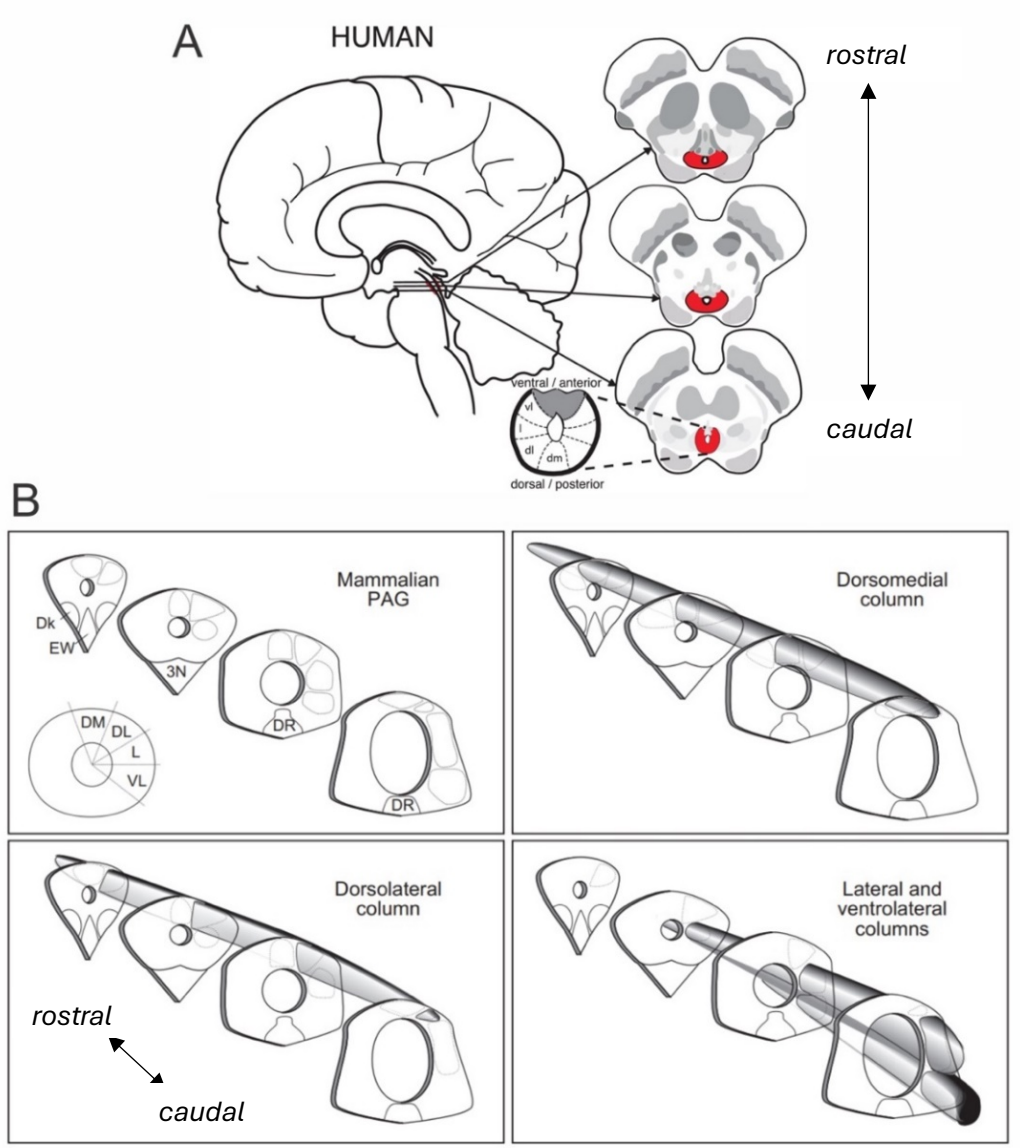

Figure 1.5. The location and columnar organization of the mammalian PAG. (A) The region shaded in red represents the location and changing shape of the human PAG at three separate axial slices (from rostral to caudal) through the midbrain. *Adapted from Faull et al. (2019).* (B) The top left panel illustrates the mammalian PAG at 4 separate rostro-caudal levels, with the most rostral extent in the top left of each panel and most caudal extent in the bottom right of each panel. Note how the shape of the PAG changes depending on its rostro-caudal location, and how the orientation of this PAG is reversed from (A) with the most dorsal aspect represented superiorly in each slice. Moving clockwise through panels, the dorsomedial; lateral and ventrolateral; and dorsolateral longitudinal columns are represented passing through the PAG parallel to the cerebral aqueduct. *Modified from Carrive (1993).*

Abbreviations, Dk = nucleus of Dark-schewitsch; DR = dorsal raphe nucleus; 3N = oculomotor nucleus; dm = dorsomedial; dl = dorsolateral; l = lateral; vl = ventrolateral.

The first suggestions that the PAG may be critical for mediating behavioral state changes resulted from direct electrical stimulation studies in experimental animals. The earliest of these studies was conducted by Brown (1915) who found that uni-polar stimulation applied to the "*gray matter around the* [cerebral] *aqueduct of Sylvius*" of chimpanzees would evoke rapid respiratory movements, characterized by laughter-like vocalizations, alongside a rise in blood pressure. Twenty-two years later, Magoun and colleagues (1937) demonstrated varied vocalization and respirations accompanied by responses in facial musculature in the macaque monkey and cat. Interestingly, the location of stimulation that produced these reactions was obtained along "*the rostrocaudal extent of the central grey matter of the aqueduct"*, i.e. in the PAG. In anaesthetized cats, electrical stimulation of the PAG also elicits rapid respiration and changes in blood pressure (Kabat, Magoun & Ranson, 1935; Sachs, 1911). These vocal behaviors have been explored across animal species and can be replicated by stimulating structures in multiple brain sites. However, PAG stimulation triggers the highest number of vocalization types e.g. cackling, growling, chirping (Jürgens & Ploog, 1970) and its pharmacological blockade can abolish vocal activity induced by limbic structures (Jürgens & Zwirner, 1996).

In addition to changes in vocalization and respiration, a critical role for the PAG in the expression of defensive behaviors was reported in cats, as well as different mammalian species. Bandler (1982) was the first to demonstrate defensive-rage behaviors, identical to those seen in previous experimental studies (Mancia, Baccelli & Zanchetti, 1972), following microinjections of an excitatory amino acid (EAA) (L-glutamic acid) within the PAG. Further studies utilizing the same technique confirmed similar behavioral responses to direct stimulation of neurons in the PAG in rodents (Hilton & Redfern, 1986; Krieger & Graeff, 1985). It was also noted that similar injections into the hypothalamus – a site previously shown to induce rage reactions in cats – did not elicit the same fight-based behaviors that the PAG could evoke (Bandler, 1982). Unlike electrical stimulation, these studies employing chemical stimulation by EAA's provide evidence that dendritic processes within neurons of the PAG are responsible for eliciting the observed defensive behaviors and not fibers of passage that can be activated by direct electrical stimulation techniques.

Strikingly, Carrive and colleagues (1989; 1987) noted a tight coupling between behavioral state changes and cardiovascular changes evoked by stimulation of the PAG. EAA microinjections into the intermediate third of the lateral PAG region in decerebrate cats evoked a distinctive pattern of behavioral and cardiovascular components that always occurred simultaneously. That is, the characteristic *fight* response - strong vocalizations, pupillary dilations, piloerection, arching of the back, striking with claws – together with increases in arterial pressure, heart rate as well as

vasoconstriction of the hindlimb skeletal muscle bed (Carrive, Dampney & Bandler, 1987). In contrast, EAA microinjections in the caudal third of the lateral PAG would evoke a *flight* response and different somatic responses. These were characterized by strenuous hindlimb movement and vasodilation within the hindlimb skeletal muscle bed coupled with increases in arterial blood pressure and heart rate (Carrive, Bandler & Dampney, 1989). The PAG is, therefore, likely to be the locus for the behavioral and cardiovascular responses observed in experimental animals.

A subsequent study found that vasodilation in the extracranial tissues of the face was found to accompany EAA microinjections in the intermediate lateral PAG (fight response region), whilst activation of the caudal lateral PAG (flight response region) was accompanied with vasoconstriction in the extracranial territory of the face (Carrive & Bandler, 1991a). As such, distinct cardiovascular changes were shown to be elegantly coupled to distinct somatomotor changes by the PAG for each type of defensive reaction, ensuring that blood flow is redistributed to anatomical regions of most intense muscle activity (Carrive, 1993). Importantly, these experiments were performed on the acute pre-collicular decerebrate cat, indicating that the neural circuitry responsible for producing a unique, integrated defensive response all reside within, or possibly caudal to, the PAG.

In contrast to the active defensive behaviors (fight/flight) evoked by stimulation of the caudal lateral PAG, Zhang and colleagues (1990) observed that EAA stimulation of the caudal ventrolateral PAG evoked a seemingly opposite behavioral state change. That is, a passive defensive behavior characterized by quiescence and hyporeactive immobility. The vlPAG was later revealed as a site invoking bradycardia and hypotensive cardiovascular changes upon stimulation in the pre-collicular decerebrate cat (Carrive & Bandler, 1991b). Figure 1.6 summaries the findings from the chemical stimulation experiments of the PAG, which demonstrated functional opposition between the lateral and ventrolateral columns of the PAG with respect to somatic and autonomic control. Indeed, these same differential behavioral and autonomic changes during lateral versus ventrolateral PAG stimulation has also been observed in rodents (Depaulis, Bandler & Vergnes, 1989; Depaulis, Keay & Bandler, 1992), providing compelling evidence of a consistent columnar functional organization of the PAG across mammalian species.

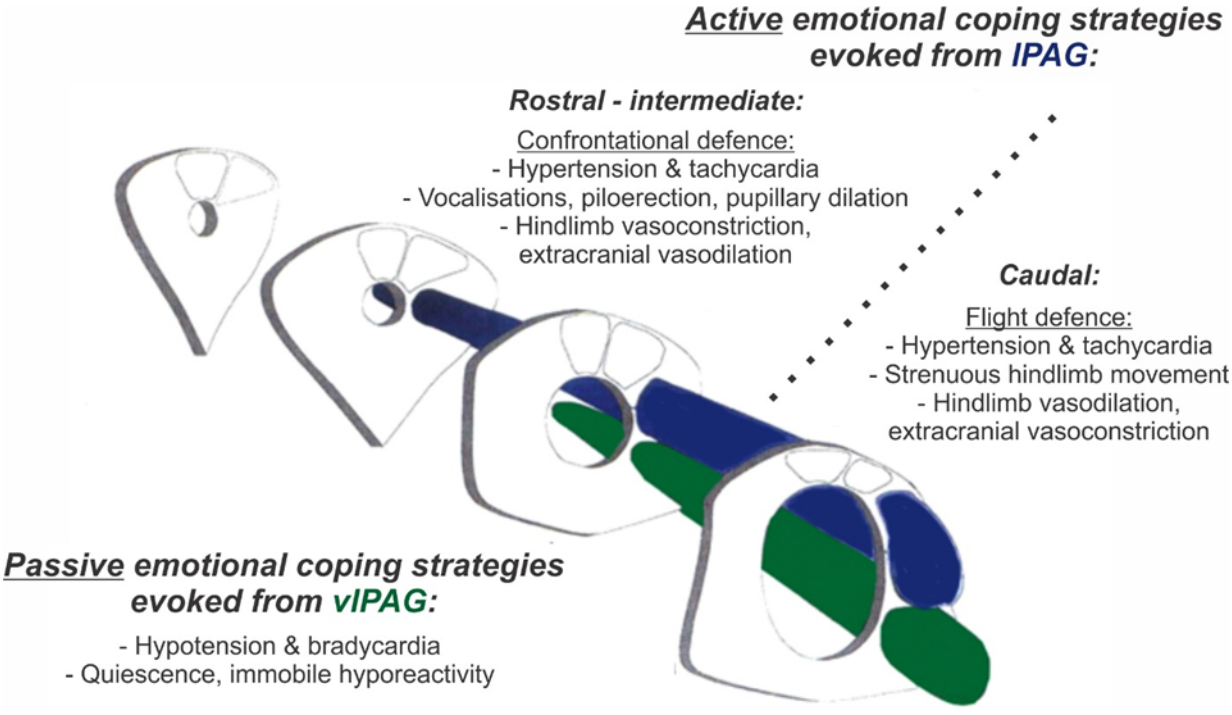

Figure 1.6. Schematic illustration of the neuronal columns within the midbrain periaqueductal gray matter (PAG) and the fundamentally opposite somatic and autonomic responses of the lateral (lPAG) and ventrolateral (vlPAG) columns. Microinjections of excitatory amino acids (EAA) into the rostral and caudal (from left to right) extents of the the lPAG (highlighted in blue) evoke distinct defensive responses dependent on the rostro-caudal level that is activated. That is, activation within the intermediate extents will elicit a confrontational defense response, extracranial vasodilation and hindlimb vasoconstriction. In contrast, activating the caudal lPAG extent produces a flight response amongst extracranial vasoconstriction and hindlimb vasodilation. Hypertension and tachycardia closely accompany lPAG activation regardless of the rostro-caudal level. EAA injections made within the vlPAG (highlighted in green) evokes a passive emotional coping strategy characterized by cessation of all spontaneous activity (quiescence), hypotension and bradycardia. *Adapted from Bandler et al. (2000)*.

1.3.3 Involvement in pain processing

It has long been recognized that distinct coping responses, i.e. active versus passive defensive behaviors, are commonly associated with pain originating in different body tissues. More specifically, there is a notable difference between pain originating from superficial (the skin) and deeper (muscle, viscera and joints) structures. Clinical observations by Lewis (1942) revealed that cutaneous pain most often triggers rapid protective reflexes, tachycardia and invigorating sensations that were linked to active, sympatho-excitatory autonomic changes. Conversely, pain originating in deeper body structures was observed to induce bradycardia and hypotension, along with subdued, socially withdrawing behaviors. These responses later became associated with sympatho-inhibitory changes (Lewis, 1942).

Given these observations and those from experimental animal studies exploring PAG-induced behavioral and cardiovascular changes, subsequent investigations directed attention towards the responses elicited by different origins of noxious stimuli. It was hypothesized that cutaneous pain would preferentially activate the lateral PAG and evoke active defensive behaviors, whereas pain originating in deeper structures would preferentially activate the ventrolateral PAG and evoke passive defensive behaviors. Almost 30 years ago, Keay and Bandler (1993) used immunohistochemical techniques, employing the immediate early gene c-*fos*, a marker of neuronal activation, to explore patterns of PAG activity during cutaneous and deep noxious stimuli. Consistent with this hypothesis, these rodent studies demonstrated a predilection for cutaneous noxious stimulation, specifically radiant heat applied to the skin on the dorsum of the neck, to activate the lateral PAG (see Figure 1.6E). Conversely, muscle pain, evoked by injections of algesic substances, such as formalin or tea-tree oil, into the deep muscles of the neck, preferentially activated the ventrolateral PAG (Keay & Bandler, 1993) (see Figure 1.6D).

Keay and colleagues (1994) also observed that noxious stimulation of various deep somatic structures in rodents preferentially activated the ventrolateral PAG. These structures included the triceps surae muscle, following administration of the algesic substance carrageenan, and the knee joint, after exposure to mechanical algesic agents such as kaolin and carrageenan (see Figure 1.7D). Likewise, noxious stimulation of deep visceral structures, namely intravenous injections of 5-hydroxytrytamine for cardiopulmonary stimulation and intraperitoneal injections of acetic acid (see Figure 1.7C), primarily localized c-*fos* expression to the ventrolateral PAG (Keay et al., 1994). These findings indicate that the PAG serves as a neural substrate mediating a wide range of noxious stimuli and highlight a fundamental separation in the processing of superficial and deep noxious stimuli.

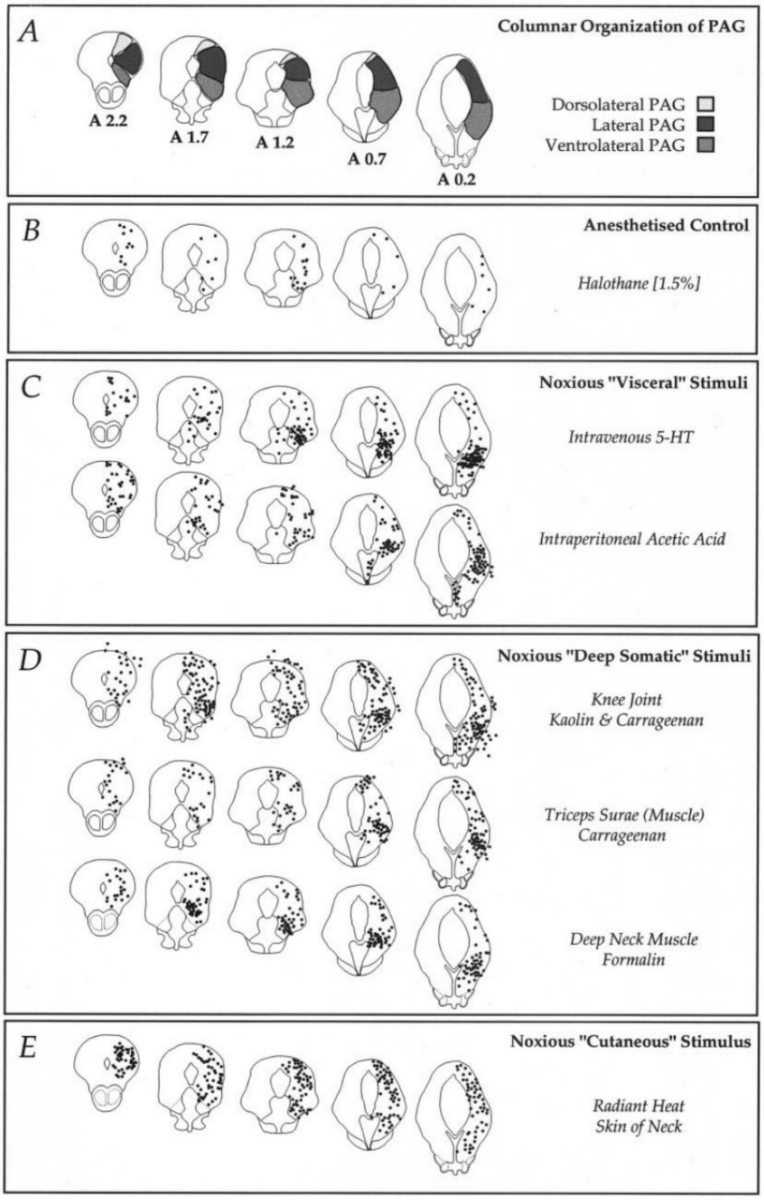

Figure 1.7. Immediate early gene c-fos expression in the periaqueductal gray (PAG) of the rodent on five 50-µm sections (left to right, rostral – caudal) following various types of noxious stimuli. (A) Schematic diagram of the columnar organization of the PAG delineating the boundaries of the dorsolateral, lateral and ventrolateral columns of the PAG. Lower panels (from top to bottom row) illustrate the location of individual *fos*-like immunoreactive cells subsequent to: (B) 1.5% halothane anesthesia (control); (C) intravenous injection of 5-hydroxytryptamine (5-HT), intraperitoneal injection of acetic acid (noxious deep somatic stimulation); (D) intra-articular (knee joint) kaolin and carrageenan injection, intramuscular (triceps surae) carrageenan injection, intramuscular (deep neck muscle) formalin injection (noxious visceral stimulation); (E) radiant heat from an infra-red lamp (five minutes off, five minutes on for two and a half hours) on the skin of the neck (noxious cutaneous stimulation). Note that c-fos expression following

noxious cutaneous stimulation was primarily localised in the lPAG (B), whereas c-fos expression following noxious deep somatic (C) and visceral (D) stimulation was localised in the vlPAG. *Adapted from Bandler et al. (2000).*

1.3.4 Spinal and medullary afferents

Anatomical tract tracing studies have revealed two significant features with respect to a lateral versus ventrolateral PAG organization. First, ascending inputs to the lateral PAG exhibits a crude somatotopic organization, and second, the origins of afferent fibers differ between the lateral and ventrolateral PAG, with each receiving inputs from distinct dorsal horn laminae.

The spinal cord has been identified as a major source of direct afferent input to the PAG. Staining methods that demonstrate degenerating nerve fibres in the CNS have been crucial in showing these spinal connections across different species. Le Gros Clark (1936) was the first to show in monkeys, using Marchi's method, that myelin degeneration following spinal cordotomies would sparsely label the PAG. Extending this work, silver degeneration techniques have revealed similar findings in the PAG of primates (Boivie, 1979; Mehler, 1969; Mehler, Feferman & Nauta, 1960) and rats (Zemlan et al., 1978). Retrograde tract-tracing studies provide the greatest evidence of a somatotopic arrangement within the mammalian PAG due to their ability to trace specific neuronal populations and their termination patterns. In their work on macaque monkeys, Wiberg and colleagues (1987) demonstrated that afferents originating in the: 1) lumbar spinal cord terminated caudally in the lateral PAG, 2) cervical spinal cord terminated in the intermediate part of the lateral PAG, and 3) SpV terminated in the rostral lateral PAG (see Figure 1.8). Similar patterns of input projections have been replicated in primates, rodents and cats (Björkeland & Boivie, 1984; Keay et al., 1997; Wiberg & Blomqvist, 1984; Yezierski, 1988), with most inputs to the lateral PAG originating from the upper cervical segments, and cervical and lumbar enlargements.

In addition to a crude somatotopic map of afferent termination, tract tracing studies have also revealed differences in the lamina inputs to the lateral and ventrolateral columns of the PAG. It has been shown that following injections of an anterograde tracer into cut peripheral nerves in rats, afferent fibres terminate within the superficial laminae (I and II) of the ipsilateral DH. When the tracer is injected into deep tissue (intramuscularly), most anterograde labelling occurs within the deeper laminae (V) of the DH (Mesulam & Brushart, 1979; Mysicka & Zenker, 1981).

Consistent with this afferent input pattern, neurons from within these superficial and deep laminae of the spinal cord are preferentially activated depending on the origin of tissue that is stimulated. Following noxious stimulation of muscle and visceral structures in rodents, *c-fos* expression is reported in the superficial (I and II) and deep (IV and V) laminae of the DH (Clement et al., 2000; Keay et al., 2001). In contrast, cutaneous noxious stimulation almost exclusively expresses c-*fos* in the superficial laminae of the DH (Keay et al., 2001)

Remarkably, retrograde tract tracing reveals that the lateral PAG and ventrolateral PAG follow this same pattern of noxious input from the spinal cord. That is, the lateral PAG receives ascending spinal fibres predominantly from the contralateral superficial laminae of the DH (Keay et al., 1997), as well as the SpV pars caudalis (Mantyh, 1982a). The ventrolateral PAG also receives ascending inputs from both the superficial and deeper laminae of the DH (Keay et al., 1997), in addition to the deep laminae of the SpV pars caudalis (Mantyh, 1982a). These findings have been confirmed with the use of an anterograde tracer into the deep and superficial DH of different animal species (Björkeland & Boivie, 1984; Blomqvist & Craig, 1991; Yezierski, 1988)

Thus, in addition to the somatotopic organisation of spinal and medullary afferents, there is also a topographical organisation to the lateral and ventrolateral PAG that closely resembles that of noxious inputs. In this way, projections towards these columns are tightly regulated and may be able to coordinate a regulated response depending on the type of noxious stimulus and threat.

Figure 1.8. The somatotopic organization of projections to the periaqueductal gray (PAG). Drawings of transverse sections through the midbrain, demonstrating terminal axonal labelling following injections of an anterograde tracer in the lumbar spinal cord (left column), cervical spinal cord (middle column), and nucleus caudalis of the spinal trigeminal nucleus (right column) of macaque monkeys. The sections are ordered with most rostral sections at the top descending to the most caudal sections at the bottom. Red outlines on sections highlight the PAG where significant labelling is present. Injections were made on the left, and labelling was strongly observed in the contralateral lateral and ventrolateral PAG, with spinal trigeminal inputs terminating at more rostral levels, and cervical and lumbar inputs progressively terminating at more caudal levels. *Modified from Wiberg, Westman and Blomqvist (1987).*

1.3.5 Somatotopic organization of the PAG

The somatotopic afferent projection patterns within the lateral PAG, as illustrated in Figure 1.8, is consistent with the observed behavioral and cardiovascular responses during lateral PAG stimulation. That is, noxious cutaneous inputs from the face selectively targets the rostral lateral PAG. Activation of this region elicits a confrontational defensive reaction (see Figure 1.5) characterized by, among others, vasodilation of extracranial tissues of the face, an appropriate response to threats arising from the head or directly in front of the animal. In contrast, noxious cutaneous input from the body preferentially targets the caudal lateral PAG, in which its activation provokes a flight defensive reaction (see Figure 1.5). This escape-based reaction is characterized by vasodilation of hindlimb skeletal muscle beds, meeting the metabolic demands of a fleeing response.

Since defensive behaviors can be elicited in a pre-collicular decerebrate preparation, i.e. with no influence from regions above the midbrain (Carrive, Bandler & Dampney, 1989; Carrive, Dampney & Bandler, 1987), the somatotopic organization of afferent inputs and the organization of appropriate behavioral outputs from the lateral PAG means that this region can drive appropriate behavioral responses in a somewhat reflexive manner. It has been proposed that this somatotopic organization allows for the mediation of specific integrated defensive behaviors in response to noxious cutaneous stimuli at distinct locations along the body (Keay & Bandler, 2001).

It is clear this somatotopic organization exists in experimental animals, however it remains unknown whether a similar pattern exists in humans. A potential somatotopic organization of the human lateral PAG remains unexplored, primarily due to our limited ability to explore the function of small brainstem structures like the PAG. Consequently, this circuitry has not yet been conclusively evaluated in humans, warranting the need the further investigation.

1.4 Cross species homology of the PAG

1.4.1 Higher-order cortical and sub-cortical input

Across animal species, an evolutionary distinction exists between higher mammals, where emotional and higher associative functions are far more developed resulting in growth of association cortices such as the cingulate and prefrontal cortices (PFC). This makes it difficult to directly compare descending inputs pathways that influence the PAG in humans compared with experimental animals. However, cortical and subcortical projection patterns to the PAG appear to be relatively similar as indicated by comparative studies and consistent patterns across primates and rats.

Input to the PAG from the cingulate and PFC has been investigated using retrograde tract tracing techniques in several species including monkeys (Leichnetz et al., 1981; Mantyh, 1982b), rats (Beitz, 1982; Hardy & Leichnetz, 1981; Mantyh, 1982b), cats (Bandler, McCulloch & Dreher, 1985; Mantyh, 1982b) and rabbits(Meller & Dennis, 1986). Early studies revealed a degree of PAG regional specificity, with the PFC terminating primarily in the lateral PAG (Hardy & Leichnetz, 1981; Meller & Dennis, 1986). Indeed, this pattern of termination has also been explored using anterograde tracing in the macaque monkey. Fibres from the medial PFC (areas 25, 32 and 10m), dorsolateral prefrontal cortex (dlPFC) and dorsomedial prefrontal cortex terminate most heavily in the lateral PAG, whereas the orbital prefrontal cortex (13a, 1ai, 12o) projects primarily to the ventrolateral PAG (An et al., 1998). These results were largely replicated in the rat (Floyd et al., 2000), where it was demonstrated that the dorsolateral and ventrolateral PAG receive the densest input from specific PFC regions (see Figure 1.9a).

Other sources of cortical input to the PAG include the ACC, posterior cingulate cortex, primary motor cortex, pre-motor cortex, superior and middle temporal cortices, insular cortices, somatosensory parietal cortex and perirhinal cortices. These regions also terminate focally within discrete PAG columns (An et al., 1998; Bandler, McCulloch & Dreher, 1985; Beitz, 1982; Dujardin & Jürgens, 2005; Floyd et al., 2000; Shipley et al., 1991). It is difficult to determine the conservation of these cortical projection patterns in the human brain, particularly due to its medial and orbital frontal cortex expansion (Floyd et al. 2000). Although, given the role of the PFC in modulating emotions, the topographical organization of cortical inputs to the PFC suggests an organized network for mediating motivational and emotional aspects of behaviour, which could be argued is retained in the human (Bandler, Price & Keay, 2000).

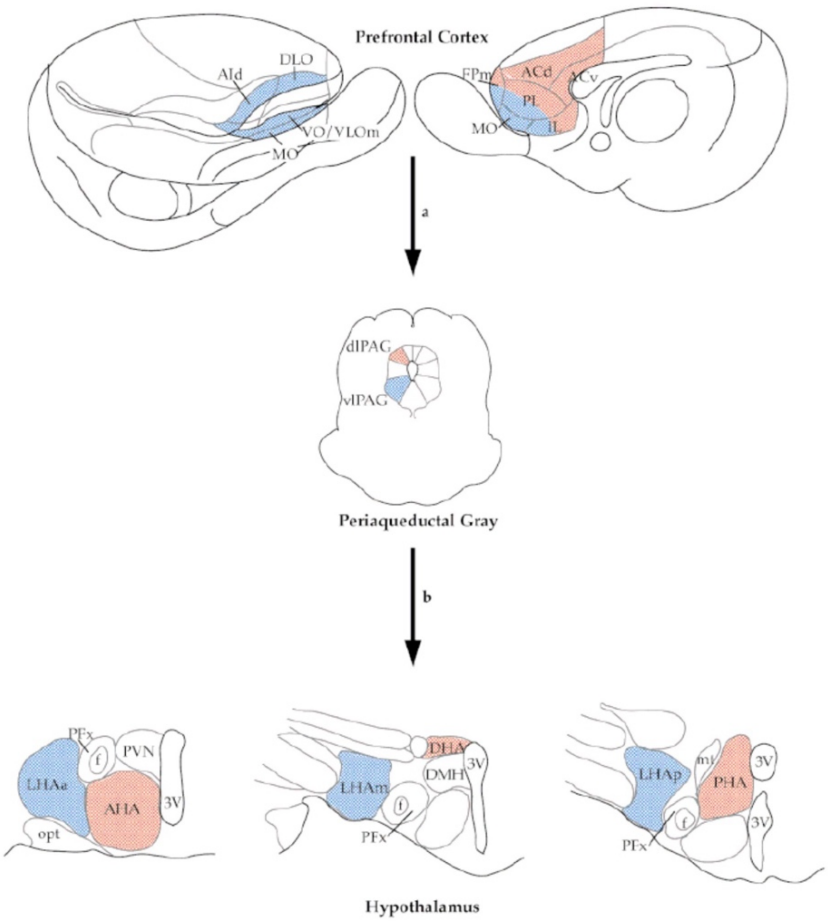

Figure 1.9. Schematic summary of projection patterns of the orbitomedial prefrontal cortex (OMPFC) to specific columns of the periaqueductal gray (PAG) in the rat. Blue shading indicates (a) the OMPFC areas that project to the ventrolateral PAG (vlPAG) and (b) the hypothalamic projections from the vlPAG. Red shadings indicate (a) the OMPFC areas that project to the dorsolateral (PAG) and (b) the hypothalamic projections from the dlPAG. The top row shows lateral and medial views of the rat brain; middle row shows a coronal view of the PAG; bottom row displays the rostral and caudal two thirds of the hypothalamus. *Copied fromFloyd et al. (2001).*

Abbreviations, DLO = dorsolateral orbital cortex; Aid = dorsal agranular insular cortex; MO = medial orbital cortex; VO = ventral orbital cortex; VLOm = medial part of the ventral orbital cortex; FPm = medial frontal polar cortex; AC(d,v) = dorsal agranular cingulate cortex (dorsal, ventral); IL = infralimbic cortex; PL = prelimbic cortex; LHA (a,m,p) = lateral hypothalamic area (anterior, middle, posterior) = PFx = periformal hypothalamic area; f = fornix; opt = optic tract; PVN = paraventricular nucleus of hypothalamus; 3V = third ventricle; DHA = dorsal hypothalamic area; DHM = dorsomedial nucleus of hypothalamus; mt =mammillothalamic tract.

The PAG also receives afferent input from subcortical regions, many of which also provide reciprocal output projections. A number of these structures have been elucidated using anterograde tracers in monkeys, with the thalamus and hypothalamus observed to receive most of the ascending projections (Mantyh, 1982b; Mantyh, 1983a). Indeed, previous autoradiographic and lesion studies have demonstrated a robust connection between the diencephalon and PAG (Eberhart et al., 1985). In particular, the hypothalamus, involved in regulating body and hormonal homeostasis, displays a large degree of input to the PAG (Bandler & McCulloch, 1984). Furthermore, specific PAG columns and hypothalamic nuclei are projected upon by the same PFC areas (Floyd et al., 2001), which are themselves interconnected. For detailed PFC-PAG-hypothalamic projection patterns, see Figure 1.9.

In addition, the amygdala also possesses a paucity of projections to and from the PAG (Mantyh, 1982b). The amygdala - a subcortical structure with important roles in the expression of behavioural and physiological manifestations of fear (LeDoux et al., 1988) – has been shown to project to dorsomedial, lateral PAG and ventrolateral columns of the PAG in monkeys (Price & Amaral, 1981). While the amygdala processes affective and emotional information, it also regulates defence and anti-nociception via the central nucleus. This central nucleus, among the other nuclei, is a major target to the PAG (Beitz, 1982; Mantyh, 1982b; Price & Amaral, 1981) and projects to different PAG columns along its rostro-caudal extent (Shipley et al., 1991).

Importantly, sources of projections to the PAG from forebrain structures offer a means to modulate PAG functions in relation to affective or cognitive status. While the lateral and ventrolateral PAG columns can mediate behavioral state changes, their function is likely influenced by the different afferent and efferent pathways involving motor, sensory and limbic structures.

1.4.2 Descending brainstem targets

The PAG has also shown to exhibit dense projections to much of the brainstem predominantly on the ipsilateral side. In turn, many of these brainstem connections are often reciprocal and their projection patterns somewhat differ depending on the PAG column from which they stem from. Tract tracing studies have revealed robust bilateral PAG connections between the mesencephalic reticular formation, cuneiform nucleus and pre-tectal area, including the superior and inferior colliculi (Mantyh, 1983b). Midbrain afferents to the PAG also originate in the substantia niagra

(more so in the pars reticulata) and dorsal raphe nucleus (Dujardin & Jürgens, 2005; Mantyh, 1983b).

PAG projections to the pons primarily target the locus coeruleus and lateral parabrachial nucleus in the dorsal pons. Efferent PAG projections target caudal pontine structures including the ventral pons, rostral ventromedial medulla (RVM), which comprises the median raphe nuclei (magnus and pallidus) and paramedian gigantocellular and paragigantocellular nuclei (Mantyh, 1983b). Notably, the projections to the raphe magnus nucleus and gigantocellular reticular nucleus are reciprocal as revealed through retrograde tract tracing (Chung et al., 1983; Dujardin & Jürgens, 2005). The PAG also has outputs to the caudal medulla, at the retroambiguus nucleus and the surrounding reticular formation, as well as inputs by the vestibular, gracile and solitary tract nucleus (Dujardin & Jürgens, 2005; Mantyh, 1983b) (see Figure 1.10).

Afferent projections from the brainstem to the PAG do not appear to selectively target specific PAG columns, however adrenergic and noradrenergic groups of the lower brainstem tend to target the lateral PAG and vlPAG columns (Carrive & Morgan, 2012). As many of these regions are premotor centres for sensory, motor or autonomic nuclei of the brainstem or spinal cord, this suggests the importance of the PAG in coordinating expression of basic behavioural responses (Holstege, 1998).

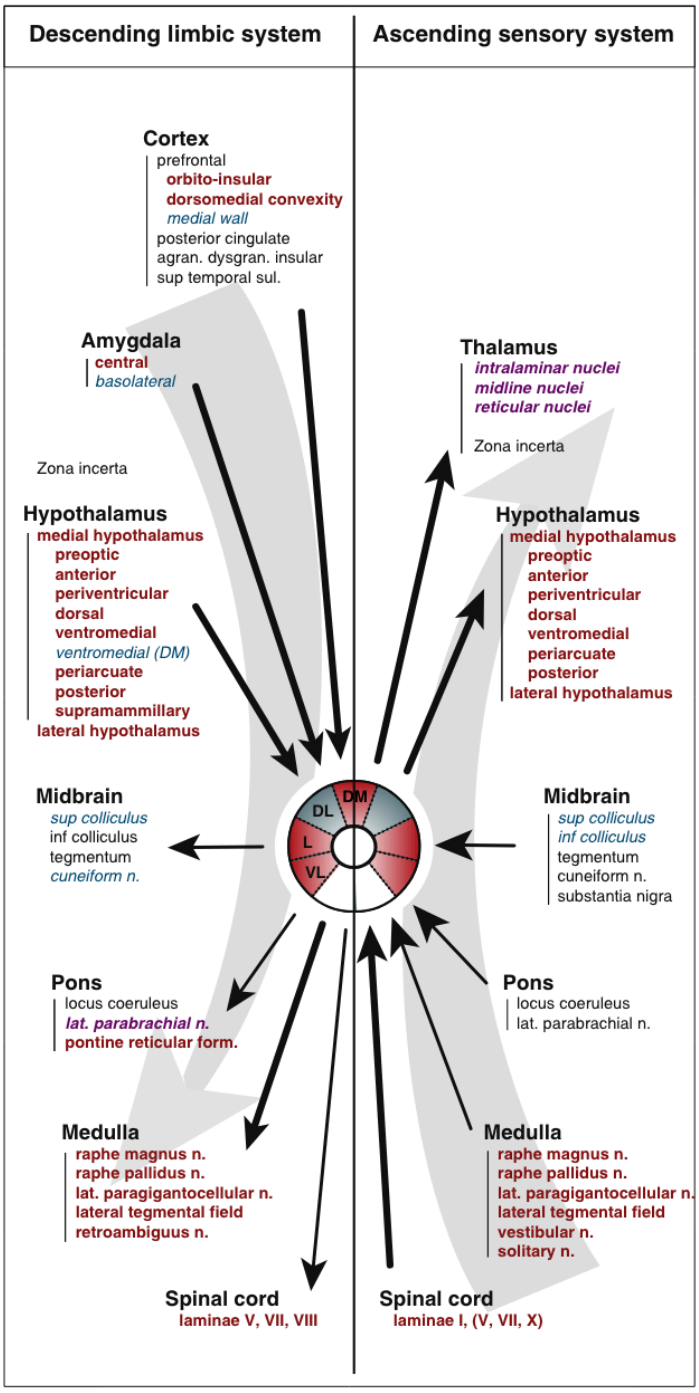

Figure 1.10. A schematic overview of afferent and efferent connections of the periaqueductal gray (PAG). Represented on the left are descending projections from limbic structures and on the right are the connections that form the ascending sensory system. Structures indicated in red and bold are connected to either the dorsomedial, lateral, or ventrolateral columns, or a combination of them. Structures indicated in blue and italic are connected to the dorsolateral column exclusively. Structures indicated in purple, bold and italic are connected to all four columns. The ascending and descending systems closely interact with the PAG and influence its different functions. *Adapted from Carrive and Morgan (2012)*.

1.5 Pain-modulatory circuits

It has been known for some time that stimulation of the PAG can evoke a profound analgesia. At first this may appear counterintuitive, given the critical role of the PAG in responding to noxious inputs. However, it is thought that once the PAG evokes a behavioural response following noxious inputs, it is no longer advantageous for the individual to remain in pain during a defensive behavioural response. Consequently, it was thought that the PAG contains the neural circuitry able to produce analgesia, likely by descending inputs that inhibit incoming noxious inputs.

1.5.1 Cortico-brainstem circuitry

Initial landmark studies in rodents revealed that direct electrical stimulation of the PAG could induce a profound analgesia (Mayer & Liebeskind, 1974; Mayer et al., 1971; Reynolds, 1969). Subsequently, it was established that the μ-opioid receptor antagonist naloxone could inhibit this PAG-mediated analgesia (Akil, Mayer & Liebeskind, 1976), revealing that the analgesic response involved an opioid-related mechanism. Future studies then began to determine if the PAG also mediated analgesic responses in humans.

A method for producing analgesia in humans is through a placebo paradigm. Placebo analgesia is characterized by a reduction in pain experienced by an individual due to the belief in the analgesic efficacy of an intervention, even when that intervention lacks pharmacologically active components. Seminal research by Levine, Gordon and Fields (1978) was the first to demonstrate opioids likely mediate placebo analgesia in humans, revealing that combining naloxone with placebo resulted in less relief of post-surgical dental pain when compared to the effects of placebo alone. Thereby, this evidence suggests that the engagement of endogenous opioids is essential for a placebo response to be mounted and raised the prospect of PAG involvement.

In the early 2000's, human neuroimaging studies began to elucidate the circuits involved in placebo analgesia. A pivotal region identified as being responsive to both opioid administration and placebo analgesia was the rostral portion of the ACC (rACC). Notably, the rACC has been shown to covary with the PAG during placebo analgesia responses, a result not observed during acute pain (Petrovic et al., 2002). Supporting the importance of coupling between the rACC and PAG in placebo analgesia, Eippert and colleagues (2009a) revealed that naloxone administration disrupts the functional connectivity between these regions. This observation aligns with animal tract tracing studies that have shown direct connections between the nociceptive areas of the rACC and the PAG (An et al., 1998).

In addition to the rACC, other discrete cortical sites are consistently activated in placebo pain studies, with the dlPFC emerging as a particularly critical region. Krummenacher and colleagues (2010) demonstrated that transient disruption of the right dlPFC through repetitive transcranial magnetic stimulation abolishes anticipated analgesic effects and subsequent placebo responses. Conversely, Tu and colleagues (2021) demonstrated that modulating the excitability of the right dlPFC through transcranial direct current stimulation can enhance placebo responses and facilitate specific changes in connectivity between the dlPFC and other frontotemporal regions. The dlPFC also possesses reciprocal connections with both the rACC and PAG. In this context, positron emission tomography (PET) studies have shown that placebo analgesia is associated with activation and the release of endogenous opioids within the rACC, dlPFC and PAG (Bingel & Tracey, 2008; Petrovic et al., 2002). These structures are consistently active across different placebo analgesia paradigms (Bingel et al., 2006; Kong et al., 2006; Wager et al., 2004), thereby establishing a cortico-brainstem circuit capable of modulating pain through mechanisms of placebo conditioning and expectations.

In addition to cortical and brainstem sites, subcortical areas are also critical for placebo analgesia. Placebo-induced responses have been associated with increased opioid neurotransmissions in the amygdala (Scott et al., 2008) as well as increased activity within the hypothalamus which can be abolished by naloxone (Eippert et al., 2009a). Altered activity within the amygdala has also been consistently reported in both placebo- and expectancy-induced reductions of pain (Atlas & Wager, 2014).

Evidently, placebo analgesia is mediated by a distributed neural network encompassing cortical and sub-cortical structures. While this network is extensive, key regions such as the nucleus accumbens, insula and ventromedial prefrontal cortex have also been implicated in placebo responses (Schafer, Geuter & Wager, 2018). Within this broader circuitry, four regions – the rACC, dlPFC, amygdala and hypothalamus – emerge as critical nodes due to their convergence of cognitive, affective and modulatory functions. Recent findings have highlighted that these regions exhibit altered functional connectivity with the lateral PAG during a placebo response, suggesting a role in mediating PAG sensitivity and engaging endogenous pain inhibition (Crawford et al., 2023). The involvement of a sub-cortical network comprising the amygdala, PAG and rACC has also been proposed as essential for the cognitive appraisal of pain (Bingel et al., 2006). Importantly, for these regions to exert pain modulatory effects, they must interface with various modulatory nuclei within the brainstem for descending pain control.

1.5.2 Descending pain control system

Experimental animal studies have shown that the neural circuits capable of directly inhibiting incoming noxious inputs lie within the brainstem. The most well-described brainstem analgesic circuit involves a projection from the PAG to the RVM, which in turn directly modulates nociceptive activity at the DH or SpV (Fields & Heinricher, 1985; Heinricher, Barbaro & Fields, 1989). The RVM itself can produce analgesia upon opioid microinjection and block PAG-evoked analgesia following injection of opioid receptor antagonists (Heinricher et al., 2009; Kiefel, Rossi & Bodnar, 1993). It encompasses the midline nucleus raphe magnus and adjacent nucleus reticularis gigantocellularis, both of which send efferent to the DH and SpV (Fields, Malick & Burstein, 1995). Throughout these RVM nuclei, there are scattered populations of neurons containing distinct nociceptive-modulating properties (Fields, Malick & Burstein, 1995). These cell populations include "ON" cells – that fire directly preceding behavioral pain responses, and "OFF" cells – which are pain inhibitory and cease firing during pain responses (Fields et al., 1983; Heinricher, Barbaro & Fields, 1989). The mechanism by which the PAG dynamically alters pain perception is believed to involve switching between these ON and OFF cells, thereby changing the balance of nociceptive transmission within the DH and SpV (Heinricher et al., 1994). Functional imaging of the spinal cord has also revealed that placebo analgesia is indeed associated with changes in DH activity (Eippert et al., 2009b).

It is imperative to note that the PAG-RVM system can be modulated by higher cortical regions. Indeed, the PAG is situated in an optimal position to receive and integrate top-down information (Cedarbaum & Aghajanian, 1978; Linnman et al., 2012). Numerous human imaging investigations have demonstrated top-down modulation of this PAG-RVM system, particularly during attentional and placebo paradigms (Eippert et al., 2009a; Tracey et al., 2002). Notably, the rACC and dlPFC appear to engage the PAG and RVM most heavily to mediate placebo analgesia (Eippert et al., 2009a).

These studies suggest that the PAG is driving anti-nociception at the DH under placebo conditions, and that this circuitry involves opioid mechanisms. Indeed, it has been a long-held view that a specific column of the PAG, the ventrolateral PAG, is the primary mediator of placebo analgesia. This view emerged from the combination of two findings; firstly, that direct stimulation of neurons in the ventrolateral PAG of experimental animals produces an opioid-mediated analgesia. Secondly, in humans, placebo analgesia is inhibited by administration of opiate antagonists (Sauro & Greenberg, 2005). However, a recent functional imaging study has

suggested that it is the lateral PAG column which is responsible for opioid-independent analgesia, as is the case in placebo (Crawford et al., 2021).

Other brainstem nuclei are also sites of inhibitory control over pain perception. The locus coeruleus, an adrenergic cell group, sends projection neurons rostrally to pain processing regions of the thalamus and cortex (Chandler, 2016; Llorca-Torralba et al., 2016), as well as caudally to the RVM and DH (Cross, 1994). Similarly, the parabrachial complex and subnucleus reticularis dorsalis (SRD) have also demonstrated roles in modulating how pain is processed (Bouhassira et al., 1992; Roeder et al., 2016). The PAG interacts with the locus coeruleus and parabrachial complex, each of which either directly or indirectly communicates to the DH/SpV via the RVM or SRD (Chebbi et al., 2014; Roeder et al., 2016). Collectively, these brainstem regions operate as a descending modulation network that finely regulates the excitability of the primary synapse and information transfer along the ascending pathways (Chebbi et al., 2014) (see Figure 1.11).

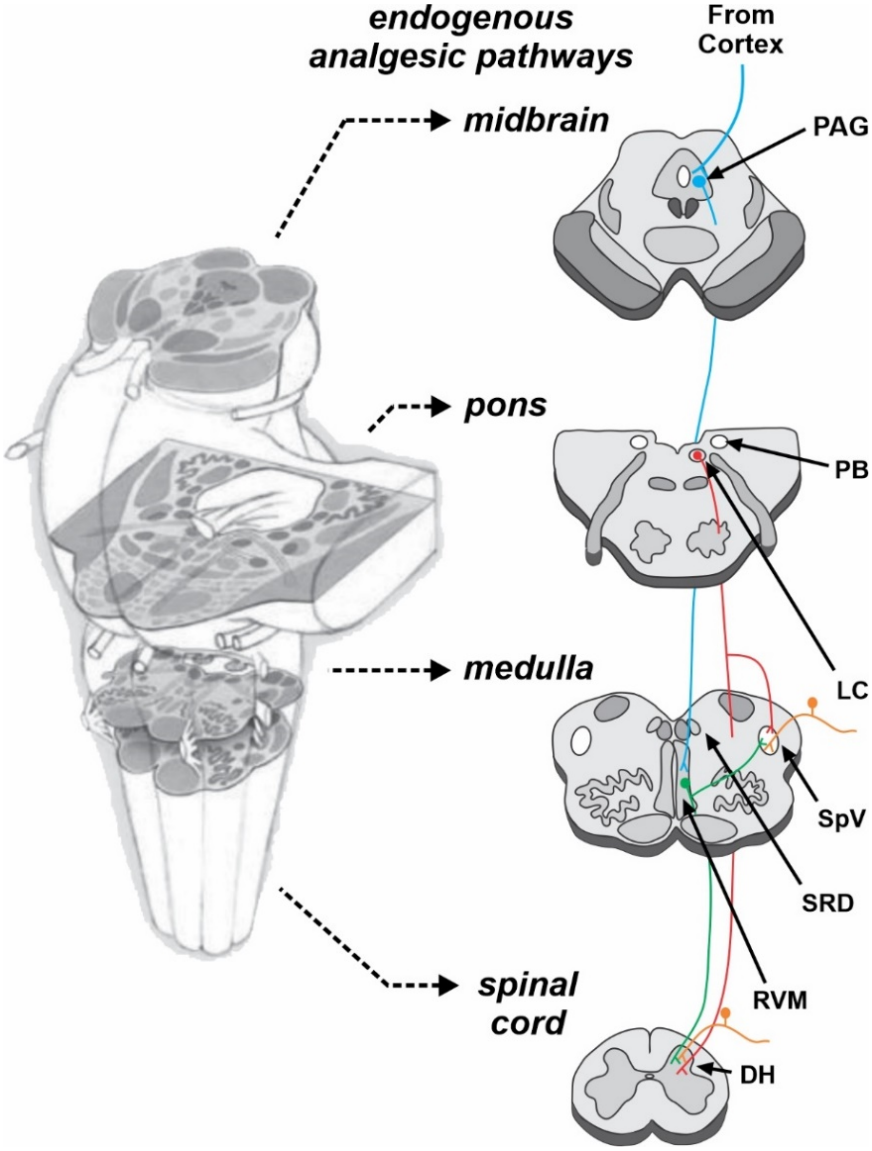

Figure 1.11. Descending brainstem circuits involved in the modulation of pain. Descending inputs from higher cortical and sub-cortical structures act on the periaqueductal gray (PAG) which, in turn, has top-down control over the rostral ventromedial medulla (RVM). The PAG-RVM axis and other pain-modulating brainstem regions, like the subnucleus reticularis dorsalis (SRD), parabrachial complex (PB) and locus coeruleus (LC), exert dynamic control over the transmission of ascending nociceptive signals located at the spinal dorsal horn (DH) and spinal trigeminal nucleus (SpV).

1.5.3 Is PAG-induced analgesia body site specific?

We know that noxious PAG inputs and associated behavioral outputs are organized in a rostro-caudal somatotopic fashion in cats, rats and primates (Yezierski, 1988). This raises the possibility that not only are the inputs to the PAG somatotpically organized in humans, but that the neural substrate for analgesic responses is also topographically segregated. Indeed, analgesia produced by electrically stimulating the PAG has been shown to retain this same somatotopic pattern in rodents. That is, caudal PAG stimulation produces a strong analgesia in the tail and hindlimb, whereas stimulation of the middle and rostral PAG induces analgesia in the forepaw and ear, respectively (Soper & Melzack, 1982). Proving whether analgesia is somatotopically organized in humans has important implications, particularly when we know certain treatments can exert analgesic effects on selective body areas.

In contemporary medical practice, transcutaneous electrical nerve stimulation (TENS) is a therapeutic modality that can produce pain relief in targeted areas of the body. TENS is theorized to promote hypoalgesia by targeting sensory nerves and activating the large peripheral Aδ fibers. In doing so, inhibitory interneurons are activated which decrease nociceptive transmission by overriding the smaller diameter C-fibers, thereby preventing nociceptive signals from ascending to supraspinal centers (Song et al., 2024). Importantly, TENS is thought to act at the level of the spinal cord and is known to produce pain relief only in the area of the body at which specific nerves are activated.

It is clear then that the CNS has the ability to modulate noxious information at specific body sites. This raises an important question: can the PAG also regulate pain in a specific body region? If so, does the rostral lateral PAG, when stimulated, produce an analgesia restricted to the face, and caudal lateral PAG stimulation evoke analgesia restricted to the body? Alternatively, it may be that lateral PAG stimulation produces a generalized analgesic response over a broader body area. Essentially, descending modulation originating from the lateral PAG may be capable of targeting specific body areas in a manner consistent with differential behavioral and cardiovascular responses observed during rostral and caudal lateral PAG stimulation.

1.6 Neural imaging of pain perception

1.6.1 Challenges of brainstem imaging

Whilst non-invasive functional neural imaging techniques have revolutionized our understanding of the human brain over the past 30 years, imaging of the brainstem has traditionally proved challenging for several reasons. Firstly, brainstem nuclei are on average only several millimeters in diameter (Afshar et al., 1978) and are hence considerably smaller than higher cortical and subcortical structures that can be relatively easily explored with standard 1.5 and 3 Tesla (T) magnetic resonance imaging (MRI) machines. In the case of 3T MRI, achieving an adequate signal-to-noise ratio for each fMRI voxel of the brain requires an in- plane isotropic spatial resolution of between 2-4mm (Sclocco et al., 2018), meaning that functional imaging of many brainstem nuclei involves working at the limit of spatial resolution (Beissner, 2015). This has the capacity to impart partial volume effects, where the limited spatial resolution of the scanner may cause a displacement of activity between neighboring voxels, and the relatively large voxel size may cause multiple tissue types, such as gray matter and cerebrospinal fluid (CSF), to be represented within that voxel (Linnman et al., 2012) (see Figure 1.12).

Furthermore, imaging the brainstem is susceptible to various sources of physiological noise: magnetic field changes due to the subject's chest movements during the respiratory cycle(Raj, Anderson & Gore, 2001); pulsations of the arteries in the vicinity of the brainstem (Dagli, Ingeholm & Haxby, 1999); and motion of CSF within the cerebral aqueduct and surrounding cisterns (Greitz et al., 1992). These can have a range of effects on the functional MRI (fMRI) scan, such as producing movement artefact and signal changes which are unrelated to blood oxygen level-dependent (BOLD) activity (Beissner, 2015). Moreover, the brainstem's proximity to air-filled cavities and bone of the posterior cranial fossa can similarly induce image distortions which may hamper image co-registration and transformation to a standard space template (Napadow, Sclocco & Henderson, 2019). Finally, standard strength MRI predominantly reveals the brainstem as both an anatomically heterogeneous structure, with grey and white matter often indistinguishable (Sclocco et al., 2018), and as a functionally heterogeneous structure, with nuclei mediating disparate and unrelated functions often located in very close proximity (Beissner, 2015). As such, stimuli chosen for functional mapping of certain brainstem nuclei must be thoughtfully chosen with respect to the specific functions that those nuclei subserve (Beissner, 2015).

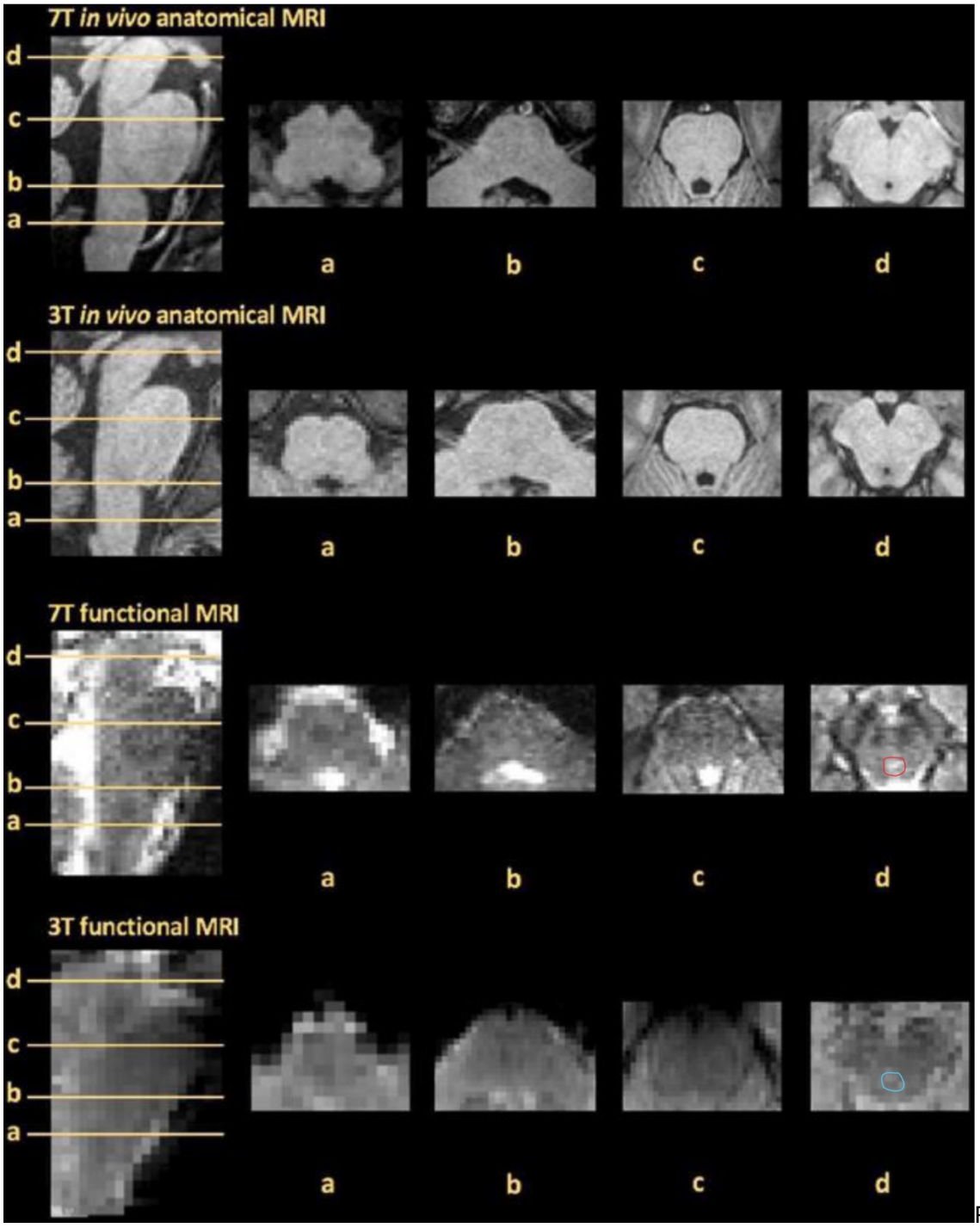

PAG

Figure 1.12. Examples of T1 anatomical and fMRI brainstem data obtained by MRI scanners of differing magnetic field strengths. In comparing T1 scans obtained at 7 Tesla (T) (top row) and 3 T (second row), smaller isotropic voxel sizes and increased signal to noise at 7 T result in improved visualization of brainstem regions such as the caudal medulla (axial slice a). Moreover, an fMRI image at 7 T (third row) demonstrates the abilities of 7 T scanning to resolve structures such as the PAG and cerebral aqueduct (axial slice d, encircled in red) compared to an fMRI image at 3 T (bottom row), which does not resolve these regions as clearly (axial slice d, encircled in blue). *Modified from Napadow, Sclocco and Henderson (2019).*

1.6.2 Ultra-high field MRI

Improving our understanding of the structure and function of the human brainstem is important, given that alterations to brainstem nuclei underlie many pathophysiological conditions (Henderson & Macefield, 2013). Indeed, the adoption of ultra-high field (UHF) MRI scanning (7 T and above) in recent years has seen several of the limitations of standard strength brainstem neuroimaging overcome, paving the way for significant advances in the field. Through the increased strength of the UHF magnet and the subsequently increased signal-to-noise ratio, sub millimeter spatially resolved voxel sizes can be collected, revealing detail otherwise undetectable at standard MRI strengths (see Figure 1.10) (Cho et al., 2014). Combining the capabilities of UHF MRI with specific processing pipelines tailored to resolving brainstem BOLD signal, such as the Spatially Unbiased Infratentorial Template (SUIT) toolbox (Diedrichsen, 2006), allows us to greatly accentuate fMRI signal within small brainstem nuclei like the PAG.

UHF imaging of the human PAG promises to build upon the well-defined animal research and provide greater insights into the structure and function of this brainstem center of integration. Using 7T fMRI to collect 0.75 mm isotropic voxels, Satpute and colleagues (2013) were able to demonstrate discrete columnar activity in the PAG of subjects exposed to emotionally aversive images. The observation that PAG activity was concentrated along a spiral pattern, from the dorsomedial and lateral columns most rostrally to the ventrolateral most caudally, was particularly consistent with the expression of c-*fos* in the PAG of rodents following the administration of a range of anxiogenic drugs (Singewald & Sharp, 2000). These findings illustrate that the pattern of functional PAG activation in states of anxiety may be conserved across mammalian species.

The efficacy of 7T fMRI in exploring the structure of the human PAG was again demonstrated by Faull and colleagues (2015), who observed that deactivations within the lateral PAG and the caudal section of the dorsomedial PAG were associated with short expiratory breath holds. In a follow up study, activations of the lateral PAG were associated with difficulty in inspiration, whilst activity of the ventrolateral PAG was associated with cues signaling impending breathing difficulty (Faull et al., 2016). Together, these findings have demonstrated the potential for UHF fMRI to elucidate functional roles of subdivisions of the PAG involved in conscious and subconscious respiratory control networks.

1.7 Aims and Hypotheses

Given what is currently understood about the PAG in regulating behaviors and pain modulation across animal species, there is still much to uncover about this small yet intricate brainstem structure in humans. As such, this thesis presents a series of studies which sought to explore three core aims:

1) To explore how noxious cutaneous stimuli on various sites on the body (face, arm and leg) are processed within the human PAG. More specifically, we first aim to determine a pattern of activation within columns of the PAG, and whether this activation is somatotopically organized based on the location of the applied stimulus. We also aim to compare columnar activity between cutaneous and sub-cutaneous noxious stimuli. (Chapter 2).

2) To investigate the role of the PAG and associated brainstem circuits during placebo analgesia on the same body sites previously studied, and whether a similar somatotopic pattern of activation is observed in brainstem analgesic circuitry (Chapter 3).

3) To explore descending cortical and sub-cortical pain modulatory circuits previously implicated in placebo analgesia and uncover whether there is a somatotopic pattern of top-down inhibition on different sites of the body (Chapter 4).

Our hypotheses tied to each aim align closely with the results from the animal literature and preliminary findings in humans and, therefore, are discussed within the summary and text of each experimental chapter. The final chapter of this thesis (Chapter 5) will discuss the findings of these three experimental studies, outlining their scientific and clinical relevance and how they extend on the current animal and human literature of pain and analgesic processing.

Chapter 2.

Detailed organization of the human periaqueductal gray revealed in humans using ultra-high field magnetic resonance imaging

"It is not our abilities that show what we truly are,
it is our choices"

Albus Dumbledore, Harry Potter and the Chamber of Secrets

2.1 Overview

This Chapter contains the following publication: **Fernando A. Tinoco Mendoza,** Timothy E. Hughes, Rebecca V Robertson, Lewis S Crawford, Noemi M, Paul M Macey, Vaughan G Macefield, Kevin A Keay, Luke A Henderson, 2023, 'Detailed organisation of the human midbrain periaqueductal grey revealed using ultra-high field magnetic resonance imaging' *Neuroimage*, vol. 266:119828, doi: 10.1016

Animal models have demonstrated a columnar structure that sub-divides the PAG into four columns on each side, and these subdivisions have different functions in response to noxious stimuli. While the PAG has been extensively studied in animals, human imaging work on the PAG is predominantly based off imaging protocols with resolutions of 2-5mm, enough to cover the entire PAG with only a few voxels (Linnman et al., 2012). As such, attempting to localize pain-related activity to specific columns of the human PAG is an immensely difficult feat. Investigating this columnar activity in relation to noxious stimulation on different body sites, as well as differing types of noxious stimuli, has, to our knowledge, not previously been investigated.

In this chapter, we used UHF fMRI alongside a brainstem-specific analysis to image the PAG at a high resolution (0.5mm^3 voxels) in healthy control participants. We aimed to identify activation within specific PAG columns associated with acute cutaneous noxious stimuli at different body sites. These sites included three proximal regions on the face (ear, cheek and lip) and two distal areas on the body (thenar and toe). Additionally, we sought to assess whether a difference in columnar activity could be revealed when a sub-cutaneous (deep) noxious stimulus was applied.

It was hypothesized that a moderately noxious cutaneous stimulus will preferentially activate the lateral PAG. This lateral PAG activation will follow a somatotopic organization, with noxious stimulation to the face activating the rostral PAG, whilst noxious stimulation to the body activating more caudal PAG regions. Furthermore, superficial noxious stimulation (heat pain) will preferentially activate the lateral PAG as opposed to the ventrolateral PAG during a deep noxious stimulus.

Our results showed activity can be localized to specific PAG columns, and that noxious stimuli to the face and body elicits a separate rostral and caudal activation pattern, respectively. Importantly, the rostro-caudal difference was almost identical between three sites on the face and two distal sites on the body. Acute cutaneous pain also preferentially activates the lateral column as opposed to the ventrolateral column during deep pain. This Chapter reveals the opportunities of 7T fMRI to non-invasively investigate the PAG such that a somatotopic organization can be demonstrated during noxious stimulation across different body sites.

NeuroImage 266 (2023) 119828

Contents lists available at ScienceDirect

NeuroImage

journal homepage: www.elsevier.com/locate/neuroimage

Detailed organisation of the human midbrain periaqueductal grey revealed using ultra-high field magnetic resonance imaging

Fernando A Tinoco Mendoza[a], Timothy E S Hughes[a], Rebecca V Robertson[a], Lewis S Crawford[a], Noemi Meylakh[a], Paul M Macey[b], Vaughan G Macefield[c], Kevin A Keay[a], Luke A Henderson[a,*]

[a] School of Medical Sciences (Neuroscience), Brain and Mind Centre, University of Sydney, NSW 2050, Australia
[b] UCLA School of Nursing and Brain Research Institute, University of California, Los Angeles, CA 90095, USA
[c] Baker Heart & Diabetes Institute, Melbourne, VIC 3004, Australia

ARTICLE INFO

Keywords:
Functional MRI
Pain
Brainstem
Periaqueductal grey
Somatotopy

ABSTRACT

The midbrain periaqueductal grey (PAG) is a critical region for the mediation of pain-related behavioural responses. Neuronal tract tracing techniques in experimental animal studies have demonstrated that the lateral column of the PAG (lPAG) displays a crude somatotopy, which is thought to be critical for the selection of contextually appropriate behavioural responses, without the need for higher brain input. In addition to the different behavioural responses to cutaneous and muscle pain – active withdrawal versus passive coping – there is evidence that cutaneous pain is processed in the region of the lPAG and muscle pain in the adjacent ventrolateral PAG (vlPAG). Given the fundamental nature of these behavioural responses to cutaneous and muscle pain, these PAG circuits are assumed to have been preserved, though yet to be definitively documented in humans. Using ultra-high field (7-Tesla) functional magnetic resonance imaging we determined the locations of signal intensity changes in the PAG during noxious cutaneous heat stimuli and muscle pain in healthy control participants. Images were processed and blood oxygen level dependant (BOLD) signal changes within the PAG determined. It was observed that noxious cutaneous stimulation of the lip, cheek, and ear evoked maximal increases in BOLD activation in the rostral contralateral PAG, whereas noxious cutaneous stimulation of the thumb and toe evoked increases in the caudal contralateral PAG. Analysis of individual participants demonstrated that these activations were located in the lPAG. Furthermore, we found that deep muscular pain evoked the greatest increases in signal intensity in the vlPAG. These data suggest that the crude somatotopic organization of the PAG may be phylletically preserved between experimental animals and humans, with a body-face delineation capable of producing an appropriate behavioural response based on the location and tissue origin of a noxious stimulus.

1. Introduction

It has long been recognised that acute pain warns an individual of danger to motivate them to either escape the source of the noxious stimulus, or to confront it with the possibility of exerting control over it, i.e., the classically described flight or fight defensive behaviours (Fields, 1999). Experimental animal investigations have shown that these defensive behaviours are integrated by the periaqueductal grey matter (PAG). More specifically, it is neurons in the region lying immediately lateral to the midbrain aqueduct, i.e., the lateral PAG (lPAG), that control these escape/flight, or confront/fight behavioural responses (Bandler and Depaulis, 1991; Zhang et al., 1990). Since the lPAG can drive these basic survival responses without the requirement of descending cortical drive (Koutsikou et al., 2017), having somatotopically organized somatosensory inputs able to produce a spatially appropriate behavioural response would be of great adaptive value. Indeed, it could be considered essential since one would require accurate information about stimulus location to drive rapid and potentially life-saving behavioural outputs. Direct brain stimulation studies in both cats and rats have shown that the rostral lPAG evokes confrontation/fight behaviours, whereas stimulation of the more caudal lPAG evokes escape/flight behaviours (Bandler and Keay, 1996b). Consistent with the rostro-caudal organisation of these behaviourally patterned responses, anatomical studies in rats, cats, and primates have revealed that neurons in the spinal trigeminal nucleus (SpV) project to the contralateral, rostral lPAG and those in the dorsal horn of the spinal cord project to the contralateral, intermediate, and caudal lPAG (Keay et al., 1997; Wiberg et al., 1987).

In addition to having a somatotopic organization, there is also evidence for a differential representation of body tissues within the PAG.

* Corresponding author at: School of Medical Sciences (Neuroscience), Brain and Mind Centre, University of Sydney, Australia
E-mail address: luke.henderson@sydney.edu.au (L.A. Henderson).

https://doi.org/10.1016/j.neuroimage.2022.119828.
Received 28 March 2022; Received in revised form 15 December 2022; Accepted 19 December 2022
Available online 20 December 2022.

Clinical observations made almost 80 years ago by Lewis (1942) noted that cutaneous pain triggered quick-protective reflexes, tachycardia and invigorating sensations, whereas pain derived from muscle or deeper structures elicited quiescence and social disengagement coupled with bradycardia and hypotension. Indeed, experimental animal investigations have revealed that these distinctive behavioural responses evoked by pain arising from different tissues are mediated by different parts of the PAG (Keay and Bandler, 1993). As already described, stimulation of the lPAG evokes fight and flight behaviours, which are associated with increases in vigilance, tachycardia, and hypertension; these active coping behaviours are identical to those triggered by cutaneous pain. Furthermore, using c-fos expression, a marker of neural activation, it has been shown in rats that cutaneous noxious stimuli preferentially activate neurons in the lPAG (Keay and Bandler, 1993). In contrast, direct stimulation of the region of the PAG ventrolateral to the aqueduct (vlPAG) evokes quiescence, accompanied by bradycardia and hypotension (Keay and Bandler, 2001; Keay and Bandler, 2002). In studies using c-fos expression, a range of noxious stimuli applied to muscle, joints, and viscera preferentially activated neurons of the vlPAG (Keay et al., 1994; Keay and Bandler, 2001). Once more, these vlPAG-evoked passive coping behaviours closely resemble the behavioural changes described by Lewis in his clinical observations of patients with muscular or deep pain.

While experimental animal studies suggest a clear somatotopic and deep versus superficial organization in the PAG, it remains unknown if this organizational principle is conserved in humans. In this study we use ultra-high field MRI (7-Tesla) to explore regional activation of the PAG in awake healthy humans. In line with the anatomical and functional data from experimental animal studies, we hypothesised that: i) noxious stimuli would preferentially activate the contralateral PAG; ii) noxious cutaneous stimuli would preferentially activate the lPAG; iii) noxious stimulation of skin on the face will activate the rostral lPAG, iv) noxious stimulation of skin on the hand and foot would activate the caudal lPAG, and iv) noxious stimulation of muscle would preferentially activate the vlPAG.

2. Materials and methods

Participants: A total of 25 healthy participants (17 males; mean±SEM age: 27.3 ± 1.3 years; range: 20–45 years) were recruited for this study, which was approved by the University of Sydney Human Research Ethics Committee. All procedures were conducted with written and informed consent of the participants in accordance with the Declaration of Helsinki, with exception of registration in a database. All participants were able to withdraw from the study at any time.

MRI scans: Prior to entering the MRI scanner, in 24 of the 25 participants, a 3 × 3 cm magnetic resonance imaging (MRI) compatible Peltier-element thermode device was secured to the skin of the volar surface of their right forearm (Medoc LTD Advanced Medical Systems, Rimat Yishai, Israel). One of the 25 participants did not partake in the noxious cutaneous stimuli experiments, having only the saline injection component. To determine a temperature that evoked moderate pain ratings in each individual, the thermode temperature was raised with a Thermal Sensory Analyser (TSA-II, Medoc) from a baseline temperature of 32 ˚C to various temperatures at 0.5 ˚C intervals between 44- 49 ˚C. Temperatures were randomly applied in 15-second intervals for a duration of 10 s. The temperature which generated a pain intensity rating of approximately 6 out of 10 was then used for the remainder of the experiment.

2.1. Acute cutaneous pain

Each participant was then positioned supine onto the MRI scanner bed and placed into a 7-Tesla MRI scanner (MAGNETOM, Siemens Healthcare, Erlangen, Germany) with a combined single-channel transmit and the head immobilized in a 32-channel receive head coil (Nova Medical, Wilmington, MA, USA) to which padding was added to minimise head movement. A T1-weighted anatomical image covering the whole brain was initially acquired (repetition time = 5000 ms, echo time = 3.1 ms, raw voxel size = 0.73×0.73×0.73 mm, 224 sagittal slices, scan time = 7mins). Following this, in 16 of the 24 participants, three continuous series of 134 gradient echo, echo-planar image sets with Blood Oxygen Level dependant (BOLD) contrast were collected. Each image volume covered the entire brain, extending caudally to include the upper cervical spinal cord (124 axial slices, repetition time = 2500ms^{-1}, echo time = 26.0 ms^{-1}, flip angle = 34˚, multiband factor = 4, multislice mode = interleaved, acceleration factor = 3, phase encoding direction = anterior-to-posterior, phase partial fourier = 6/8, image matrix = 224×224, raw voxel size = 1.0 × 1.0 × 1.2 mm thick; no inter-slice gap). During each of the three fMRI scans, noxious stimuli were applied to skin overlaying one of three different parts of the right side of the body: i) skin over corner of mouth (upper and lower lips), ii) thenar eminence (thumb), and iii) plantar surface of the hallux (toe). In the remaining 8 of 24 participants, two fMRI scans which noxious stimuli was applied to skin overlaying two areas of the right side of the face were also collected: iv) cheek, and v) temporomandibular joint immediately anterior to the ear. During each of these five fMRI scans, following a 60-second baseline period, a series of eight noxious thermal stimuli reaching the target (moderate) temperature were applied. The thermode temperature was raised over 2.5-seconds and held at the target temperature for 10-seconds before being lowered over 2.5-seconds to the baseline temperature (32 ˚C), which was held for 15-seconds. This was repeated seven times for a total of eight noxious stimulation periods. At the end of each fMRI scan, subjects were asked to rate the mean maximum pain intensity of all 8 stimuli on a scale from 0 (no pain) to 10 (most extreme pain imaginable).

2.2. Muscular saline pain

In 17 of the 25 participants, a fine stainless steel butterfly cannula (23 G), connected via a 10 cm tube to a 1 ml syringe filled with sterile hypertonic (5%) saline, was placed ~1 cm into the belly of the anterior flexor carpi radialis muscle of the right forearm. An fMRI scan with the same parameters as those described above was then performed during which, following a 90 second baseline period, a bolus injection of 1 ml of hypertonic saline was made into the right flexor carpi radialis muscle. The participant was not informed as to when any of either the cutaneous or muscle noxious stimuli would be delivered. During the scan, participants were asked to press a buzzer when the pain began, immediately following the peak pain intensity and when the pain subsided completely. At the end of the fMRI scan, participants were asked to rate the maximum pain intensity on a scale from 0 (no pain) to 10 (most extreme pain imaginable). A table indicating stimulus paradigms performed on each of the 25 participants is provided in the supplementary materials (Table S1).

MRI scan analysis: Using SPM12 (Friston et al., 1994) and custom software, fMRI images were slice-time corrected and realigned. The first five volumes were removed to allow for signal stabilisation, leaving 129 vol for analysis. Movement parameters were examined to ensure no participant displayed >1 mm volume-to-volume movement in the X, Y and Z planes, or 0.05 radians in the pitch, roll and yaw directions. In addition, for each of the 6 movement parameters, the mean±SEM values were calculated and plotted and significant differences between all baseline periods and all stimulation periods determined (p<0.05, two-sample, two-tailed t-tests). Physiological (cardiovascular [60–120 beats per minute +1 harmonic] and respiratory [8–25 breaths per minute +1 harmonic]) noise was then modelled and removed using the Dynamic Retrospective Filtering (DRIFTER) toolbox (Särkkä et al., 2012). The resulting fMRI images were linear detrended to remove global signal intensity changes, and signal at all voxels had any signal matching movement parameters modelled and removed. To improve the spatial normalization of the PAG, the spatially unbiased infra-tentorial template (SUIT)

toolbox was used (Diedrichsen, 2006). For both the fMRI and T1 image sets, the brainstem and cerebellum were isolated and then normalised to the brainstem- and cerebellum-only SUIT template in Montreal Neurological Institute (MNI) space. During this process, both the T1 structural and functional image sets were resliced into 0.5 mm isotropic voxels and these images were spatially smoothed using a 1 mm full-width-at-half maximum (FWHM) Gaussian filter. A small smoothing kernel was used to allow for the accurate investigation of signal intensity changes within small brainstem nuclei (Sclocco et al., 2018).

Somatotopic organization*:* For each participant, the mean of the maximum pain intensity ratings (eight trials) for each of the five regions where noxious cutaneous stimuli were applied, was determined. Then, for each of these five regions, the mean pain intensity ratings (±SEM) across all participants were calculated. For each of the five regions, significant changes in signal intensity were determined using a repeated box-car model convolved with a canonical hemodynamic response function. To explore PAG activations, a volume of interest (VOI) of the entire rostro-caudal extent of the PAG (MNI *z* co-ordinates −3 to −13 mm) was created on the mean brainstem fMRI image set created from all 25 participants. To construct these VOI's, the mean image was first manually inspected and cross referenced with both the Bandler and Keay (1996a) localisation of PAG subregions as well as Paxinos and Huang's 'Atlas of the Human Brainstem' (Paxinos and Huang, 2013). Voxels which constituted any PAG subregion were included, and further defined in subsequent analyses as either the dorsomedial (dmPAG), dorsolateral (dlPAG), lateral (lPAG), or ventrolateral (vlPAG) PAG column. Two additional VOI's were also created of both the ipsi-lateral and contra-lateral PAG by dividing this initial VOI along the brainstem midline. Such an approach has previously been employed to resolve structural and functional organizations of discrete brainstem nuclei (Crawford et al., 2021a; Ezra et al., 2015)

Two separate analyses were then performed. Firstly, a random-effects second-level group analysis ($p<0.01$, uncorrected, minimum cluster size of 5 contiguous voxels) whereby the resulting contrast maps were used to record the maximally activated cluster from the VOI of the entire PAG for each of the five cutaneous regions (i.e. the lip, cheek, ear, thumb, and toe). For each significant cluster, the coordinates were overlaid onto the mean fMRI brainstem image set, and beta-values (effect size) extracted and mean (±SEM) values calculated for each of the 5 stimulation sites. Secondly, to explore in detail activation patterns in individual participants, the maximally activated voxel during the noxious stimulation of each of the five regions was determined separately using each participant's 1st-level contrast maps ($p<0.01$, uncorrected, minimum cluster size of 5 contiguous voxels) and the contralateral and ipsilateral mask of the entire PAG. The co-ordinates from each individual participant were recorded, and the mean (±SEM) X, Y and Z co-ordinates calculated. These mean contralateral coordinates were then overlaid onto the mean fMRI brainstem image set. Beta-values were extracted from a 1 mm diameter sphere centred at the highest activated contralateral co-ordinate for each of the 5 individual participant analyses and mean (±SEM) values calculated. Percentage signal intensity changes during noxious stimuli relative to the baseline period were calculated and averaged across all participants to create mean% (±SEM) change in signal intensity plots for each of the five cutaneous regions.

Significant differences in X, Y and Z co-ordinates between the five cutaneous stimuli were analysed using a one-way analysis of variance (ANOVA) test ($p<0.05$). The Levene test was first used to ensure the assumption of homogeneity of variances was met across all three sets of co-ordinates. In addition, the Shapiro-Wilk test was used to assess normality of the X, Y and Z coordinates. While the X-coordinates did not meet the assumption of normality, we were more interested in comparison of the Y and Z coordinates. The ipsilateral Z-coordinates did not meet the assumptions of equal variances or normality, and so the Kruskal-Wallis test was used to determine significance for the ipsilateral Z-coordinates between the cutaneous stimuli. Post-hoc analyses were performed using the Tukey's honest significance (HSD) test to assess whether the mean differences between the contralateral X, Y and Z coordinates of each group of stimuli were significant.

In addition, for each participant, the X, Y and Z co-ordinates for the lip, cheek and ear noxious cutaneous stimuli were averaged to create a mean "face" coordinate, and those for the thumb and toe averaged to create a mean "body" co-ordinate. With regards to the mean "face" coordinate, the lip coordinate was used in the 7 participants for which no cheek or ear stimulation was conducted. In each participant, the face and body co-ordinates were plotted in three-dimensional space. To determine the PAG location of the maximum co-ordinates for each stimulus, in each participant, the maximum co-ordinates were overlaid onto the mean fMRI brainstem image set and their locations in either the vlPAG, lPAG, dlPAG or dmPAG column determined. The total number of maximum voxels for each column from each stimulus was calculated, expressed as a percentage of the total number of participants and then plotted.

Cutaneous versus muscle pain organization*:* Following each scan, participants were asked to provide a mean pain score out of 10 for each noxious stimulus that they received. To determine muscle pain activation of the PAG, significant signal intensity changes evoked by the hypertonic saline injection into the forearm muscle were determined using a box-car model convolved with a canonical hemodynamic response function. Like the cutaneous pain conditions, two second-level analyses were performed. Firstly, a random-effects group analysis to record the maximum significantly activated voxel in the whole PAG using each subject's contrast maps. The whole PAG masque was used for the group-level analysis to establish on which side the maximally activated voxel was relative to the stimulus. Beta-values were extracted at the peak activation and the mean (±SEM) value calculated to determine the directions of signal change. Secondly, an individual analysis using the ipsilateral and contralateral PAG masque was used to determine the maximally activated voxel during noxious muscle pain separately for each participant. Individual participant X, Y, and Z co-ordinates were recorded for both the ipsi- and contra-lateral sides of the PAG and the mean coordinates calculated. Signal intensity changes as well as beta-values were extracted from a 1 mm diameter sphere centred at the highest activated mean co-ordinates from all participants. Percentage changes relative to the baseline period were then calculated and averaged across all participants to create mean (±SEM)% change signal intensity plots.

To assess which PAG column the maximum co-ordinate was located in, for each participant, the maximum co-ordinates were overlaid onto the mean fMRI brainstem image set and their locations in either the vlPAG, lPAG, dlPAG or dmPAG columns determined. The total number of maximum voxels for each column for muscle and cutaneous pains were calculated, expressed as a percentage of the total number of participants, and plotted.

3. Results

The mean (±SEM) heat pain intensity ratings (VAS 0–10) reported by the participants were as follows: lip 5.7 ± 0.3; cheek 5.4 ± 0.5; ear 5.2 ± 0.4; thumb 5.8 ± 0.3; and toe 3.5 ± 0.3. While pain intensity ratings of the toe were lower than those of the four other stimuli locations, each participant reported the stimulus as being moderately painful. On average, the forearm muscle pain intensity ratings peaked at 7.7 ± 0.3 which was 10–15 s after the injection, and the ratings declined to low levels approximately 150 s after the injection began. Additionally, plots of the 6 movement parameters revealed no significant difference in any parameters during the noxious stimuli compared with baseline periods for any of the 6 noxious stimuli (Figure S1).

Somatotopic organization- Group Analysis: The patterns of afferents to the PAG revealed by tract tracing studies in primates is shown in Fig. 1A. Note that the projection pattern is predominantly contralateral to the injection site. Furthermore, the SV receives afferents from the orofacial region projects most rostrally, whereas the regions of the spinal cord that receive afferents from both the upper and lower limbs,

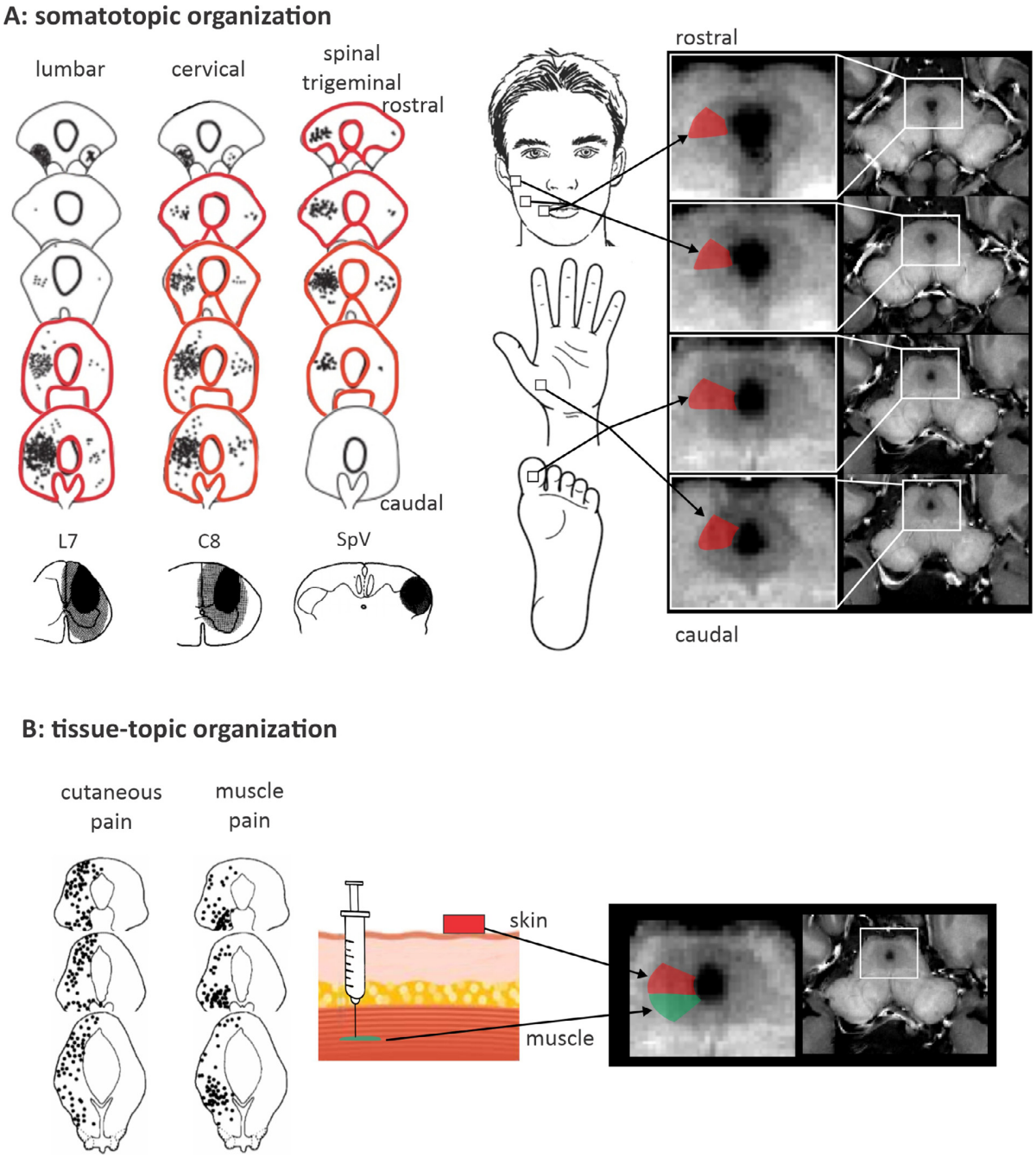

Fig. 1. **A:** Left panel shows a series of line drawings of the midbrain periaqueductal grey matter (PAG) of the macaque monkey with the location of direct projections from the lumber 7 (L7) dorsal horn, cervical 8 (C8) dorsal horn and the spinal trigeminal nucleus (SpV) in the caudal medulla. Note the crude somatotopic projection to regions of the contralateral PAG immediately lateral to the midbrain aqueduct (lPAG). To the right are the locations of the five cutaneous noxious stimuli we applied and the hypothesised activation patterns overlaid onto a T1-weighted anatomical MRI. The red shading indicates the location of the lPAG. **B:** Left panel shows line drawings of the rodent PAG with the location of neural activation (c-fos expression) evoked by cutaneous pain and muscle pain. Note that cutaneous pain activates the lPAG primarily, whereas muscle pain activates the ventrolateral PAG (vlPAG). To the right is the hypothesised locations of regional signal intensity changes during cutaneous and muscle pain in the contralateral PAG. The green shading indicates the location of the vlPAG. Figures adapted with permission from Wiberg and colleagues, 1987 and Keay and Bandler, 1993.

project most strongly to the caudal lPAG. Consistent with these neuroanatomically defined projection patterns, our assessment of group analysis peak activations for each of the five cutaneous pain stimuli revealed, that the regions of strongest activation were found in the contralateral PAG (Fig. 2A and Table 1). Furthermore, a crude rostro-caudal somatotopic organization was quite clear, with face activations located rostral to those of the body (Fig. 2A). There were, however, some inconsistencies with respect to the boundaries of the peak activation for the facial and body stimuli and whether the peak activation was found in the region of the lPAG (Figure S2). While the group peak co-ordinate during cheek and thumb noxious stimuli were found in the lPAG, those during ear and lip stimulations were found in the dorsolateral PAG and during toe stimulation in the vlPAG (Fig. 2A).

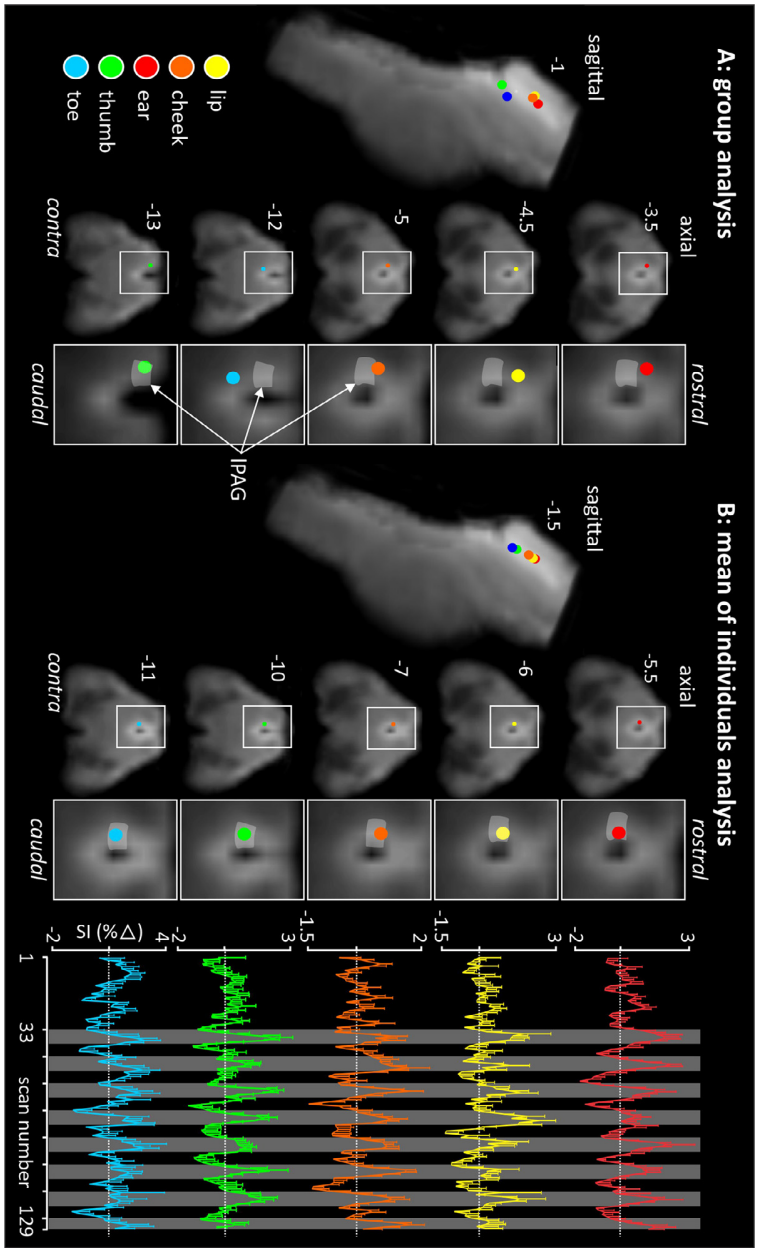

Fig. 2. A: Locations of maximum activations in the midbrain periaqueductal grey matter (PAG) during noxious stimulation of each of the 5 cutaneous sites in 24 participants using group-level analysis. Maximum activated voxel locations are indicated by the coloured circles overlaid onto a mean functional MRI image set in the sagittal and axial planes. The slice location in Montreal Neurological Institute space is indicated at the top left of each slice. Note the crude rostrocaudal somatotopic organization with noxious inputs from the body (thumb and big toe) activating the caudal PAG and the head (lip, cheek and ear) the rostral PAG. The grey shading in the enlarged panels shows the location of the lateral PAG (lPAG). Note the relative inconsistency with respect to locations of maximum points and the lPAG column. **B:** The same series of overlays as in A, however the locations were derived from individual participant analysis. Note that the maximal activation points show a rostrocaudal somatotopic organization and are also all located in the region of the lPAG. To the right are the percentage signal intensity changes for the individual peaks averaged across all participants. The vertical grey bars indicate the periods of noxious stimulation.

Somatotopic organization- Individual Analysis: As identified in the group analysis, individual participant analysis also revealed that the mean peak co-ordinates during cutaneous stimuli were organized in a crude rostro-caudal somatotopic organization, with face activations located rostral to those of the body for both the contralateral (Fig. 3A and Table 1) and ipsilateral side (Table S2) of the PAG. Indeed, the mean contralateral Y and Z co-ordinates between groups of cutaneous stimulation were significant (ANOVA, $p<0.001$), but not the X-coordinate (ANOVA, $p>0.05$). There was no significant difference between the groups of cutaneous stimuli in the ipsilateral Y-coordinates (ANOVA $p>0.05$) and Z-coordinates ($\chi^2(4)) = 3.97, p = 0.41$, Kruskal-Wallis test).

Post-hoc Tukey's HSD test revealed that for the contralateral Z-coordinates of both the thumb and toe, activations were significantly more caudal than those of the lip, cheek and ear ($p<0.05$). In addition, the mean difference between the Y coordinates of the: lip and toe ($p<0.01$) and ear and toe ($p<0.01$) were also significant. Plots of coordinates of mean face pain (lip, cheek, ear) and body pain activations (thumb, toe) in each participant, confirmed this somatotopic organization (Fig. 3B). An inspection of individual participants revealed that 22 of 24 displayed body pain activation caudal to face pain activation (Fig. 3C). Extraction of signal intensity changes from the peak activations revealed robust signal intensity increases during each noxious stimulus period (Fig. 2B). Importantly, the analysis of the PAG column of each individual participant activations revealed that for all five stimuli, the greatest percentage of activations were clearly located in the lPAG column (vlPAG / lPAG / dlPAG / dmPAG%: lip: 13 / 54 /29 /4; cheek: 12 / 47 / 41 / 0; ear: 12 / 70 / 18 / 0; thumb: 38 /46 / 16 / 0; toe: 13 / 71 / 12 / 4) (Fig. 3C).

Tissue-topic organization: Assessment of group analysis peak activation during muscle pain again revealed the highest activated cluster was located in the contralateral PAG (Table 1). Analysis of individual participant peak activations revealed no significant differences in mean peak coordinates during muscle pain compared with that during cutaneous heat pain on the cheek (X: $p = 0.88$; Y: $p = 0.34$; Z: $p = 0.88$) (Table 1, Fig. 4A and B). Extraction of signal intensity changes from the peak acti-

Table 1
Mean (±SEM) peak X, Y and Z Montreal Neurological Institute (MNI) co-ordinates and beta-values in the contralateral midbrain periaqueductal grey matter during noxious stimuli applied to various parts of the body and in different tissues.

	MNI co-ordinates				
	X (mm)	Y (mm)	Z (mm)	Beta value (mean ± SEM)	T-Value
Cutaneous pain					
Group analysis					
lip	−0.5	−32.0	−4.5	0.81 ± 0.33	2.69
cheek	−1.5	−30.5	−5.0	0.76 ± 0.32	2.28
ear	−1.5	−30.5	−3.5	1.30 ± 0.4	3.71
thumb	−1.5	−36.0	−13.0	0.44 ± 0.13	3.68
toe	−0.5	−32.0	−12.0	0.49 ±- 0.13	3.37
Individual participant analysis					
lip	−0.80 ± 0.13	−31.04 ± 0.68	−6.09 ± 0.62	0.35 ± 0.28	3.13
cheek	−0.85 ± 0.19	−31.76 ± 0.61	−6.79 ± 0.79	0.37± 0.21	4.07
ear	−0.97 ± 0.16	−30.88 ± 0.45	−5.41 ± 0.43	1.44 ± 0.28	4.56
thumb	−0.60 ± 0.15	−32.85 ± 0.69	−9.67 ± 0.77	0.26 ± 0.19	3.94
toe	−0.77 ± 0.14	−33.61 ± 0.53	−10.66 ± 0.70	0.21 ± 0.12	3.40
Muscle pain					
Group analysis					
forearm	−1.0	−31.5	−8.0	0.79 ± 0.24	3.19
Individual participant analysis					
forearm	−1.00 ± 0.12	−30.76 ± 0.73	−6.79 ± 0.77	0.66 ± 0.14	3.00

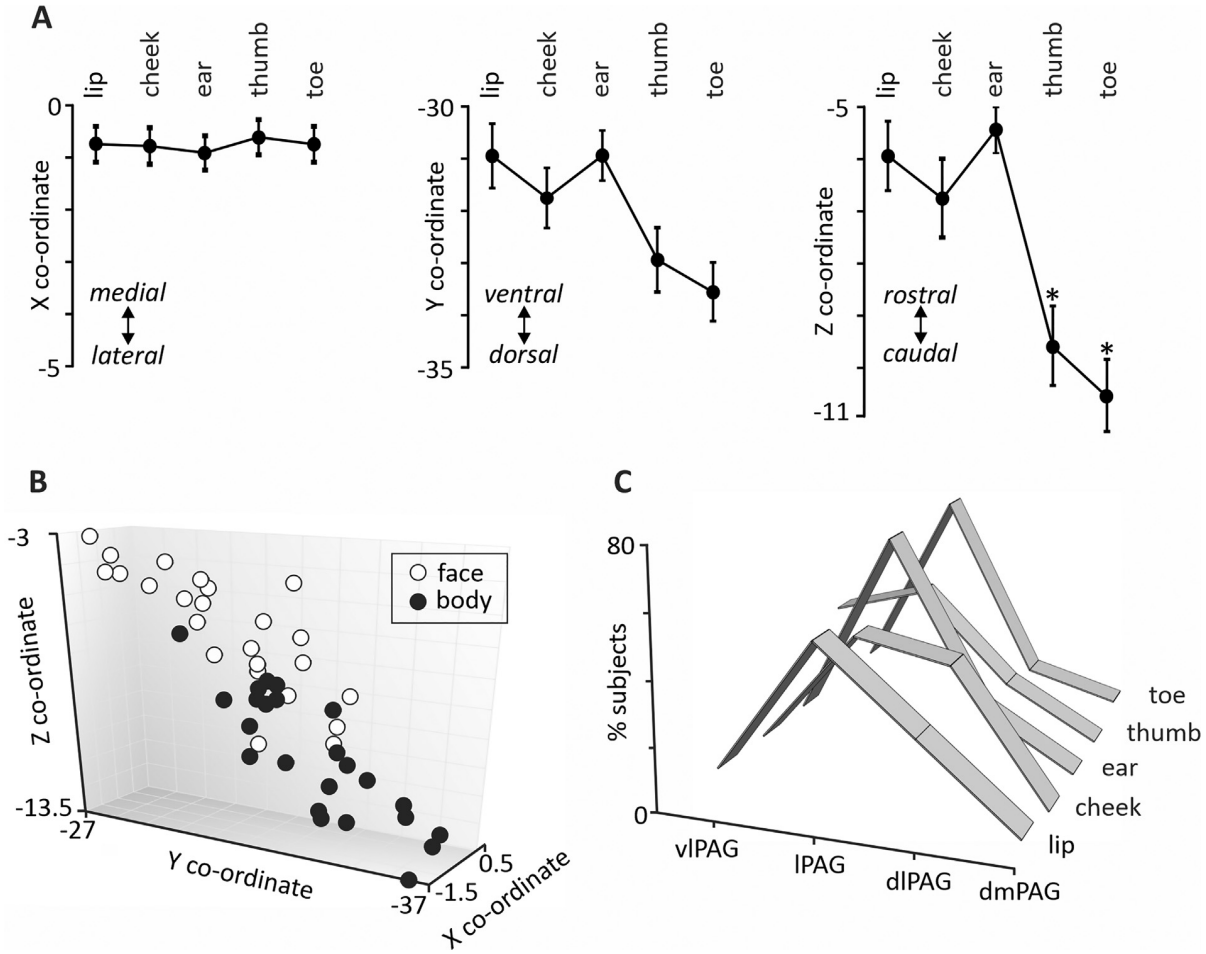

Fig. 3. A: Plots of mean (±SEM) X, Y and Z co-ordinates in Montreal Neurological Institute (MNI) space during noxious stimulation to each of the 5 cutaneous sites. Note that in the Z direction, the thumb and toe activations are located significantly caudal to those of the face activations (* $p<0.05$). **B:** 3D plot of individual participant X, Y and Z co-ordinates show cutaneous face pain activated the PAG more rostral than that of body cutaneous pain **C:** Plots of the percentage of individuals in which the maximum activations were located in each of the PAG columns: ventrolateral (vlPAG), lateral (lPAG), dorsolateral (dlPAG) and dorsomedial (dmPAG). Note that during all cutaneous stimuli the greatest proportion of activations occurred in the lPAG.

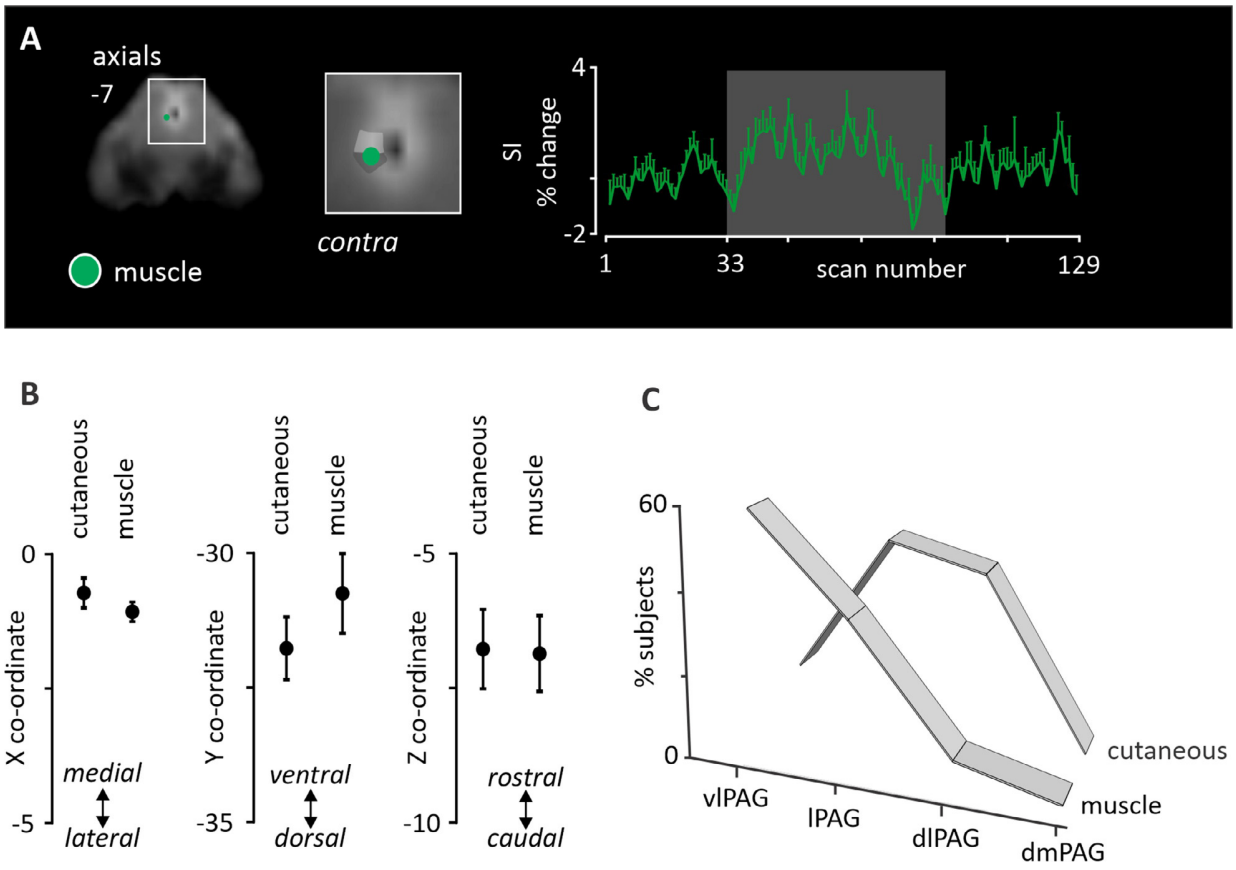

Fig. 4. **A:** Location of maximum activations in the midbrain periaqueductal grey matter (PAG) during muscle pain applied to 17 participants. The maximum activated voxel location is indicated by the green circle overlaid onto a mean axial functional MRI image. The slice location in Montreal Neurological Institute (MNI) space is indicated at the top left of the slice. Note that muscle pain activates the region of the ventrolateral PAG (dark grey shading). To the right is the percentage signal intensity changes for the individual peaks averaged across all participants. The vertical grey bars indicate the period of muscle pain. **B:** Plots of mean (±SEM) X, Y and Z co-ordinates in MNI space during muscle pain and cutaneous pain on the cheek. Note there are no significant differences. **C:** Plots of the percentage of individuals in which the maximum activations were located in each of the PAG columns: ventrolateral (vlPAG), lateral (lPAG), dorsolateral (dlPAG) and dorsomedial (dmPAG). Note that muscular pain evoked the greatest proportion of activations in the vlPAG.

vations revealed robust signal intensity increases during the muscle pain stimulus (Fig. 4B). Whilst there was no significant difference in the overall dorso-ventral locations, plots of cutaneous and muscle co-ordinates in nine individuals who had both the cutaneous cheek and deep muscle pain stimuli revealed that in six of the nine participants, muscle pain activated the PAG in a more ventral location than did cutaneous pain (Fig. 4C). Finally, analysis of the PAG column of each individual participant activations revealed that for muscle pain, the greatest percentage of activations were located in the lPAG column (vlPAG 59%, lPAG 35%, dlPAG 6%, dmPAG 0%) (Fig. 4C).

4. Discussion

These experiments provide evidence of a crude somatotopic map for acute cutaneous pain in the human PAG. Noxious cutaneous stimuli applied to the face, evoked signal intensity changes in the rostral PAG contralateral to the side stimulated, and noxious cutaneous stimuli applied to the body surface, activated the caudal PAG, again contralateral to the side of stimulation. When considered at the level of each individual participant, the cutaneous pain, evoked activation at sites located predominantly in the lPAG region, immediately adjacent to the midbrain aqueduct. As for the cutaneous stimuli, noxious stimulation of muscle was also observed to specifically activate the contralateral PAG. However, we did not find overall significant differences in the dorso-ventral location of activation sites following noxious muscle stimulation when compared with noxious cutaneous stimuli. However, cutaneous pain most often activated the lPAG, whereas muscle pain most often activated the region of the vlPAG. These findings suggest a strong phylogenetic consistency in the longitudinal functional organisation of the mammalian PAG, with regards to the organisation of nociceptive input.

Neuroanatomical tract tracing studies using both retrograde and anterograde tracers have shown, in several species, that there is a somatotopic organisation of spinal and spinal trigeminal inputs to the PAG (Wiberg and Blomqvist, 1984), and specifically, to its lateral column (Keay et al., 1997; Keay and Bandler, 1992). In non-human primates (macaque), it has been shown that neurons in the lumbar spinal cord send significant projections to the PAG which terminate predominantly in the caudal lateral region (lPAG), whereas neurons in the spinal trigeminal nuclei send projections to the PAG that preferentially target the rostral lPAG (Wiberg et al., 1987) (Fig. 1A). This pattern of head to rostral PAG and body to caudal PAG is also seen clearly in the spinal projections investigated in both cats and rodents (Bandler et al., 2000). While there is a clear preferential targeting of these PAG regions, the boundaries of termination are not exclusive and there may well be a blurring of the body maps, in rather the same way that nociceptive inputs to the spinal cord and SpV do not follow the precision of somatotopy as seen in the pathways carrying inputs from the specialised mechanoreceptors (Mantyh, 1983). Our results are largely consistent with these projection patterns, with similar rostrally located peaks of activation following stimulation at the three facial sites and a similar

caudally located peak of activations for stimulation of distal sites on the body. Moreover, when considered individually, it was evident that cutaneous noxious stimuli evoked the greatest signal intensity increases clearly within the boundaries of the lPAG. The importance of taking an individual focus when evaluating the functional organisation of the PAG with such a high-resolution approach is highlighted by our observations that the details of columnar organization are lost in group level analyses. Our data argues for the importance of parallel analyses of individual differences in activation strengths during voxel-by-voxel group analyses to increase the overall ability of detecting fine organizational details in small brain nuclei, as exemplified here by the PAG.

The somatotopic organisation of nociceptive inputs to the PAG, and particularly to the lateral column, has been argued as being central to its function in generating the behavioural responses to acute, painful events (Lumb, 2002). Experimental animal studies have shown that the lPAG, and its descending projections are all that are required for an animal to mount an integrated behavioural response to a painful stimulus (Carrive et al., 1989). Acute noxious stimuli applied in the region of the head provoke confrontation and attack (fight) behaviours, driven predominantly by activation of spinal trigeminal afferents to the rostral lPAG; whereas acute noxious stimuli applied to the body usually trigger escape responses (flight) (Keay and Bandler, 1993). In addition to these strong motor reactions, activation of these lPAG sites also produces changes in regional blood-flow, cardiac output, and respiration to support the successful execution of these behaviours (Carrive et al., 1987; Carrive and Bandler, 1991a). Consistent with these experimental animal findings, direct stimulation of the dorsal PAG in awake human evokes increases in blood pressure whereas direct stimulation of the vlPAG evokes a decrease in blood pressure (Green et al., 2005). These repertoires of active coping behaviours are also accompanied by heightened vigilance, as well as a non-opioid mediated analgesia (Carrive et al., 1987; Fleischmann and Urca, 1989; Keay and Bandler, 2001). It has been argued that this analgesic response facilitates the successful execution of confrontation (fight) or escape (flight), by preventing the potential interruption of the "conscious appreciation" of the pain state (Keay and Bandler, 2002). It is also suggested from earlier studies that the analgesia evoked from the lPAG accompanying these active coping responses are somatotopic in nature (Fardin et al., 1984; Nichols and Thorn, 1990). That is, the analgesia is specific to the area of the body from which the noxious inputs originate. Consistent with this idea, we showed recently that placebo analgesia evoked by applying multiple noxious stimuli to the arm resulted in altered analgesia-related signal changes in the lPAG at the same rostro-caudal location that was activated in response to noxious stimulation of the thumb in this study (Crawford et al., 2021a). These observations raise the possibility that in some experimental paradigms, placebo analgesia may also have a somatotopic representation in the PAG.

In addition to its clear somatotopic organisation, the lPAG is also selectively activated by noxious stimulation of cutaneous (superficial) structures. It has been further suggested that this region of the PAG is activated primarily by stimuli for which an active coping reaction would be the most successful in either controlling and/or escaping from, a noxious, stressful, or threatening stimulus (Keay and Bandler 2002). By contrast, experimental animal experiments have shown that the vlPAG is preferentially activated during deep noxious stimuli (Keay et al., 1994; Keay and Bandler, 2001; Lumb, 2002; Parry et al., 2002). This preferential activation is consistent with our findings that muscle pain most often activates the vlPAG, although in a significant number of individuals we also observed that muscle pain preferentially activated the lPAG. It is interesting to note that the activation of neurons in the lPAG have been observed in animal experiments using c-fos expression as an indicator of neuronal activation following deep noxious stimuli that required superficial points of access, although our cannula was inserted into the skin at least 15 mins prior to the muscle pain stimulation (Clement et al., 1996; Keay et al., 2002). The selectivity of the vlPAG to deep pain may be best evaluated during naturally occurring deep pain if it were possible to capture such an episode. Alternatively, the lack of specificity with respect to identifying PAG activation in less spatially distinct regions during muscle pain may simply result from spatial acuity limitations present even at ultra-high field strengths.

Observations from experimental animal studies have shown that deep pain (i.e., that originating in muscle, tendons, ligaments, bones, joints and viscera) selectively activates the vlPAG (Keay et al., 1994; Keay et al., 2000; Keay and Bandler, 2002). Furthermore, the vlPAG receives convergent inputs from neurons in spinal laminae and regions of the nucleus of the solitary tract which relay noxious inputs from deep structures (Clement et al., 2000; Keay et al., 1997). When considered together with the observations that direct stimulation of the vlPAG evokes quiescence, hyporeactivity, hypotension, bradycardia and an opioid-mediated analgesia, these findings have led to the suggestion that the vlPAG is critical for integrating the responses to stimuli that are essentially inescapable, or uncontrollable (Carrive and Bandler, 1991b; Depaulis et al., 1994; Keay and Bandler, 2002). Consistent with these findings in experimental animals, direct stimulation of the PAG has been used for the treatment of pain for over fifty years (Duncan et al., 1991), with conflicting reports on whether the analgesia can be blocked with an opiate antagonist (Barbaro, 1988; Sims-Williams et al., 2017; Young and Chambi, 1987). It is tempting to suggest, based on observations in experimental animals, that these differences reflect different dorso-ventral placements of the stimulating electrodes in the PAG of each patient. In the context of the design of human MR studies, any noxious stimulus applied acquires a quality of inescapability, due to the requirement for the participant to remain in the MRI scanner. In this context, the propensity to escape from a noxious stimulus may be supressed in the scanning environment and a more adaptive response would be to disengage attention from the stimulus and the pain experience (Kucyi et al., 2013; Oliva et al., 2021). Such a response may indeed alter the extensive descending cortical projections onto the PAG that shifts activity between lateral to ventrolateral PAG columns and therefore, result in individual variability in the location of muscle pain activation.

We now address limitations arising from this study. Firstly, as identified above, it is thought that the primary role of the PAG is to drive behavioural responses to acute noxious stimuli. Since the MRI scanner environment requires the participant to remains as still as possible, it is inherent that during noxious stimuli, the brain is likely acting to inhibit the normal "reflexive" behavioural PAG outputs. This may have a profound effect on the degree of activation within areas like the PAG, although it is unlikely to result in a change in its somato- and cutaneous versus muscle pain organization. Secondly, consistent and robust spatial normalization of small structures such as the PAG can be difficult and could have resulted in some individual variations in the precise location of different PAG columns. We attempted to reduce such variability by using a brainstem-specific template for the normalization process and by using a small smoothing kernel. All results were also laid onto a mean fMRI brainstem image set to reduce any differences in the co-registration between fMRI and anatomical image sets. Moreover, we did not collect and use a field map to correct for potential distortions in this investigation. Whilst we did not see any distortion in the PAG and did not expect that any signal due to noise would saturate the signal resulting from functional activation of the PAG in response to acute pain, collection of a field map may have improved the overall significance of the peak activations. We overlaid all results onto a mean fMRI brainstem image set to reduce any differences in the co-registration between fMRI and anatomical image sets. Furthermore, we tested a number of fMRI protocols to balance signal:noise, distortion and voxel size and found that $1 \times 1 \times 1.2$ mm gave us the best combination. Of course in future studies with improvements in hardware, smaller voxels with greater signal:noise could provide an even greater ability to explore somatotopy in small structure like the PAG. We also asked participants to rate the intensity of pain at the end of each scan and not during each noxious stimulation period. Given this, the potential effects of differences in individual stimulation period pain intensity ratings on signal intensity

changes could not be determined. Moreover, we did not find significant differences between the locations of cutaneous and muscle pain stimuli, even though muscle pain was found to more commonly activate the vl-PAG column. Increasing the number of participants may result in a clear significant difference. Finally, our chosen statistical threshold was not corrected for multiple comparisons, since we had an a priori hypothesis of response based on the literature on experimental animal models and tract tracing studies.

Using ultra high-field fMRI we have shown, for the first time, evidence of a crude somatotopic map for acute cutaneous pain in the human PAG. In support of animal models asserting a somatotopic organisation of noxious inputs, we have provided evidence that these projection patterns as well as their functional activation is retained phyletically across species.

5. Credit author statement

Fernando A Tinoco Mendoza: Formal analysis, Data curation, Writing - Original Draft; **Timothy E S Hughes:** Data curation and preliminary analysis; **Lewis S Crawford:** Investigation, Data curation, Writing - Review and Editing; **Rebecca Robertson:** Investigation, Data curation, Writing - Review and Editing; **Noemi Meylakh:** Investigation, Writing-Reviewing and Editing; **Paul M Macey:** Software, Writing- Reviewing and Editing; **Vaughan G Macefield:** Investigation, Writing- Reviewing and Editing; **Kevin A Keay**: Conceptualization, Writing- Reviewing and Editing, **Luke A Henderson:** Conceptualization, Methodology, Supervision, Writing - Review & Editing, Funding acquisition.

Declaration of competing interest

The authors declare that there are no conflicts of interest.

Data Availability

The authors do not have permission to share data.

Acknowledgements

We wish to thank the many volunteers in this study. The authors acknowledge the facilities and scientific and technical assistance of the Australian National Imaging Facility, a National Collaborative Research Infrastructure Strategy (NCRIS) capability, at Melbourne Brain Centre Imaging Unit, University of Melbourne. This work was funded by the National Health and Medical Research Council of Australia Grant 1130280.

Supplementary materials

Supplementary material associated with this article can be found, in the online version, at doi:10.1016/j.neuroimage.2022.119828.

References

Bandler, R., Depaulis, A., 1991. Midbrain periaqueductal gray control of defensive behavior in the cat and the rat. In: Depaulis, A., Bandler, R. (Eds.), The Midbrain Periaqueductal Gray Matter: Functional, Anatomical, and Neurochemical Organization. Springer, Boston, MAUS.

Bandler, R., Keay, K.A., 1996a. Chapter 17 Columnar organization in the midbrain periaqueductal gray and the integration of emotional expression. In: Holstege, G., Bandler, R., Saper, C.B. (Eds.), Progress in Brain Research. Elsevier.

Bandler, R., Keay, K.A., 1996b. Columnar organization in the midbrain periaqueductal gray and the integration of emotional expression. Prog. Brain Res. 107, 285–300.

Bandler, R., Price, J.L., Keay, K.A., 2000. Brain mediation of active and passive emotional coping. Prog. Brain Res. 122, 333–349.

Barbaro, N.M., 1988. Chapter 8 Studies of PAG/PVG stimulation for pain relief in humans. In: FIELDS, H.L., BESSON, J.M. (Eds.), Progress in Brain Research. Elsevier.

Carrive, P., Bandler, R., 1991a. Control of extracranial and hindlimb blood flow by the midbrain periaqueductal grey of the cat. Exp. Brain Res. 84, 599–606.

Carrive, P., Bandler, R., 1991b. Viscerotopic organization of neurons subserving hypotensive reactions within the midbrain periaqueductal grey: a correlative functional and anatomical study. Brain Res. 541, 206–215.

Carrive, P., Bandler, R., Dampney, R.A.L., 1989. Somatic and autonomic integration in the midbrain of the unanesthetized decerebrate cat: a distinctive pattern evoked by excitation of neurones in the subtentorial portion of the midbrain periaqueductal grey. Brain Res. 483, 251–258.

Carrive, P., Dampney, R.A., Bandler, R., 1987. Excitation of neurones in a restricted portion of the midbrain periaqueductal grey elicits both behavioural and cardiovascular components of the defence reaction in the unanaesthetised decerebrate cat. Neurosci. Lett. 81, 273–278.

Clement, C.I., Keay, K.A., Owler, B.K., Bandler, R., 1996. Common patterns of increased and decreased fos expression in midbrain and pons evoked by noxious deep somatic and noxious visceral manipulations in the rat. J. Comp. Neurol. 366, 495–515.

Clement, C.I., Keay, K.A., Podzebenko, K., Gordon, B.D., Bandler, R., 2000. Spinal sources of noxious visceral and noxious deep somatic afferent drive onto the ventrolateral periaqueductal gray of the rat. J. Comp. Neurol. 425, 323–344.

Crawford, L.S., Mills, E.P., Hanson, T., Macey, P.M., Glarin, R., Macefield, V.G., Keay, K.A., Henderson, L.A., 2021a. Brainstem Mechanisms of Pain Modulation: a within-Subjects 7T fMRI Study of Placebo Analgesic and Nocebo Hyperalgesic Responses. J. Neurosci. 41, 9794–9806.

Depaulis, A., Keay, K., Bandler, R., 1994. Quiescence and hyporeactivity evoked by activation of cell bodies in the ventrolateral midbrain periaqueductal gray of the rat. Experimental brain research. Experimentelle Hirnforschung. Expérimentation cérébrale 99, 75–83.

Diedrichsen, J., 2006. A spatially unbiased atlas template of the human cerebellum. Neuroimage 33, 127–138.

Duncan, G.H., Bushnell, C.M., Marchand, S., 1991. Deep brain stimulation: a review of basic research and clinical studies. Pain 45, 49–59.

Ezra, M., Faull, O.K., Jbabdi, S., Pattinson, K.T., 2015. Connectivity-based segmentation of the periaqueductal gray matter in human with brainstem optimized diffusion MRI. Hum. Brain Mapp. 36, 3459–3471.

Fardin, V., Oliveras, J.L., Besson, J.M., 1984. A reinvestigation of the analgesic effects induced by stimulation of the periaqueductal gray matter in the rat. II. Differential characteristics of the analgesia induced by ventral and dorsal PAG stimulation. Brain Res. 306, 125–139.

FIELDS, H.L., 1999. Pain: an unpleasant topic. Pain 82.

Fleischmann, A., Urca, G., 1989. Clip-induced analgesia: noxious neck pinch suppresses spinal and mesencephalic neural responses to noxious peripheral stimulation. Physiol. Behav. 46, 151–157.

Friston, K.J., Holmes, A.P., Worsley, K.J., Poline, J.P., Frith, C.D., Frackowiak, R.S.J., 1994. Statistical parametric maps in functional imaging: a general linear approach. Hum. Brain Mapp. 2, 189–210.

Green, A.L., Wang, S., Owen, S.L., Xie, K., Liu, X., Paterson, D.J., Stein, J.F., Bain, P.G., Aziz, T.Z., 2005. Deep brain stimulation can regulate arterial blood pressure in awake humans. Neuroreport 16, 1741–1745.

Keay, K., Li, Q., Bandler, R., 2000. Muscle pain activates a direct projection from ventrolateral periaqueductal gray to rostral ventrolateral medulla in rats. Neurosci. Lett. 290, 157–160.

Keay, K.A., Bandler, R., 1992. Anatomical evidence for segregated input from the upper cervical spinal cord to functionally distinct regions of the periaqueductal gray region of the cat. Neurosci. Lett. 139, 143–148.

Keay, K.A., Bandler, R., 1993. Deep and superficial noxious stimulation increases Fos-like immunoreactivity in different regions of the midbrain periaqueductal grey of the rat. Neurosci. Lett. 154, 23–26.

Keay, K.A., Bandler, R., 2001. Parallel circuits mediating distinct emotional coping reactions to different types of stress. Neurosci. Biobehav. Rev. 25, 669–678.

Keay, K.A., Bandler, R., 2002. Distinct central representations of inescapable and escapable pain: observations and speculation. Exp. Physiol. 87, 275–279.

Keay, K.A., Clement, C.I., Matar, W.M., Heslop, D.J., Henderson, L.A., Bandler, R., 2002. Noxious activation of spinal or vagal afferents evokes distinct patterns of fos-like immunoreactivity in the ventrolateral periaqueductal gray of unanaesthetised rats. Brain Res. 948, 122–130.

Keay, K.A., Clement, C.I., Owler, B., Depaulis, A., Bandler, R., 1994. Convergence of deep somatic and visceral nociceptive information onto a discrete ventrolateral midbrain periaqueductal gray region. Neuroscience 61, 727–732.

Keay, K.A., Feil, K., Gordon, B.D., Herbert, H., Bandler, R., 1997. Spinal afferents to functionally distinct periaqueductal gray columns in the rat: an anterograde and retrograde tracing study. J. Comp. Neurol. 385, 207–229.

KOUTSIKOU, S., Apps, R., Lumb, B.M., 2017. Top down control of spinal sensorimotor circuits essential for survival. J. Physiol. (Lond.) 595, 4151–4158.

Kucyi, A., Salomons, T.V., Davis, K.D., 2013. Mind wandering away from pain dynamically engages antinociceptive and default mode brain networks. Proc. Natl. Acad. Sci. U.S.A. 110, 18692–18697.

Lewis, T., 1942. Pain. Macmillan.

Lumb, B.M., 2002. Inescapable and escapable pain is represented in distinct hypothalamic-midbrain circuits: specific roles for Adelta- and C-nociceptors. Exp. Physiol. 87, 281–286.

Mantyh, P.W., 1983. Connections of midbrain periaqueductal gray in the monkey. II. Descending efferent projections. J. Neurophysiol. 49, 582–594.

Nichols, D.S., Thorn, B.E., 1990. Stimulation-produced analgesia and its cross-tolerance between dorsal and ventral PAG loci. Pain 41, 347–352.

Oliva, V., Gregory, R., Davies, W.-.E., Harrison, L., Moran, R., Pickering, A.E., Brooks, J.C.W., 2021. Parallel cortical-brainstem pathways to attentional analgesia. Neuroimage 226 117548-117548.

PARRY, D.M., SEMENENKO, F.M., CONLEY, R.K., LUMB, B.M., 2002. Noxious somatic inputs to hypothalamic-midbrain projection neurones: a comparison of the columnar organisation of somatic and visceral inputs to the periaqueductal grey in the rat. Exp. Physiol. 87, 117–122.

Paxinos, G., Huang, X.-F., 2013. Atlas of the Human Brainstem. Elsevier.
Särkkä, S., Solin, A., Nummenmaa, A., Vehtari, A., Auranen, T., Vanni, S., Lin, F.H, 2012. Dynamic retrospective filtering of physiological noise in BOLD fMRI: DRIFTER. Neuroimage 60, 1517–1527.
Sclocco, R., Beissner, F., Bianciardi, M., Polimeni, J.R., Napadow, V., 2018. Challenges and opportunities for brainstem neuroimaging with ultrahigh field MRI. Neuroimage 168, 412–426.
Sims-Williams, H., Matthews, J.C., Talbot, P.S., Love-Jones, S., Brooks, J.C.W., Patel, N.K., Pickering, A.E., 2017. Deep brain stimulation of the periaqueductal gray releases endogenous opioids in humans. Neuroimage 146, 833–842.
Wiberg, M., Blomqvist, A., 1984. The spinomesencephalic tract in the cat: its cells of origin and termination pattern as demonstrated by the intraaxonal transport method. Brain Res. 291, 1–18.
Wiberg, M., Westman, J., Blomqvist, A., 1987. Somatosensory projection to the mesencephalon: an anatomical study in the monkey. J. Comp. Neurol. 264, 92–117.
Young, R.F., Chambi, V.I., 1987. Pain relief by electrical stimulation of the periaqueductal and periventricular gray matter: evidence for a non-opioid mechanism. J. Neurosurg. 66, 364–371.
Zhang, S.P., Bandler, R., Carrive, P., 1990. Flight and immobility evoked by excitatory amino acid microinjection within distinct parts of the subtentorial midbrain periaqueductal gray of the cat. Brain Res. 520, 73–82.

Chapter 3.

Somatotopic organisation of brainstem analgesic circuitry

"What is more important for us, at an elemental level, than the control, the owning and operation, of our own physical selves?"

Oliver Sacks, The Man Who Mistook His Wife for a Hat, 1998

3.1 Overview

The execution of active defensive behaviors depends on our body's ability to induce analgesia, as continued pain perception may hinder these protective responses. Following our findings of lateral PAG involvement during noxious cutaneous stimuli, here we address **Aim 2** by investigating whether the lateral PAG is also involved in placebo analgesia across the face, arm and leg. A previous 7T fMRI study has recently shown the caudal lateral PAG to be most involved during placebo analgesia on the arm (Crawford et al., 2021). Thus, we hypothesized that a rostro-caudal somatotopy in the lateral PAG would be conserved between analgesia on the face and body.

This study involved three sessions: conditioning, reinforcement, and testing – conducted over two successive days. Participants were deceptively conditioned to believe a placebo "lidocaine" and nocebo "capsaicin" cream were modulating their pain relative to a control vaseline cream. Whilst collecting fMRI scans, both creams received identical thermal noxious stimuli, so that any difference in reported pain across the fMRI scans reflected a placebo response. Importantly, our experimental design had participants report an expectation of pain immediately prior to each series of noxious stimuli, as well as rate their pain continuously during conditioning and throughout scanning – overcoming prior limitations of series-position or experimenter biases associated with participants being asked to reflect on their previously experienced pain. A total of 70 subjects completed the study, with placebo responses successfully elicited in 41%, 48% and 61% of subjects in the face, arm and leg paradigms, respectively.

Using 7T fMRI, our results showed that, 1) placebo responders exhibit a rostro-caudal pattern of lateral PAG activity following analgesia on the face and body, and 2) RVM activity linearly increases with placebo ability which also follows a similar somatotopic organization. Remarkably, the coordinates of activity within the rostral and caudal PAG in our analgesia paradigm were almost identical to those found in the previous chapter during acute noxious stimulation.

Our results provide the first human evidence of a somatototopic organization within the PAG and RVM, two key regions of the brainstem's analgesic circuitry. In this way, it appears that the brain can selectively target and inhibit noxious information coming from either the body or head. We propose a model whereby separate face-body circuits originating from the lateral PAG enable both spatially appropriate behavioral responses and a somatotopic analgesia.

Title: Somatotopic Organization of Brainstem Analgesic Circuitry

Running Title: Analgesia somatotopy

Authors: Fernando A Tinoco Mendoza[1,2], Lewis S Crawford[1,2], Rebecca V Robertson[1,2], Noemi Meylakh[1,2], Paul M Macey[3], Kirsty Bannister[4], Tor D. Wager[5], Vaughan G Macefield[6], Kevin A Keay[1,2] and Luke A Henderson[1,2]

Affiliations: [1]School of Medical Sciences (Neuroscience), and [2]Brain and Mind Centre, University of Sydney, Australia, 2006; [3] UCLA School of Nursing and Brain Research Institute, University of California, Los Angeles, California, 90095, USA; [4]Department of Pharmacology and Therapeutics, Institute of Psychiatry, Psychology and Neuroscience, King's College London, London, United Kingdom; [5]Department of Psychological and Brain Sciences, Dartmouth College, Hanover, NH, USA.; [6] Baker Heart & Diabetes Institute, Melbourne, VIC, Australia.

Corresponding author: Luke A. Henderson, School of Medical Sciences (Neuroscience), Brain and Mind Centre, University of Sydney, Australia. luke.henderson@sydney.edu.au (email); +612 9351 7063 (Tel) +612 9351 6556 (Fax).

Acknowledgements: We wish to thank the many volunteers in this study, and to Benjamin Goldsmith for his technical assistance on distortion correction. The authors acknowledge the facilities and scientific and technical assistance of the National Imaging Facility, a National Collaborative Research Infrastructure Strategy (NCRIS) capability, at Monash University. This work was funded by the National Health and Medical Research Council of Australia Grant 1130280.

Abstract:

The lateral periaqueductal gray (lPAG) evokes somatotopically appropriate defensive behaviours, including an analgesia that allows the animal to escape or fight unimpeded. Whether the lPAG and its descending targets are also able to drive somatotopically specific analgesic responses is not known. In seventy participants, we assessed lPAG ultra-high field functional magnetic resonance imaging signals during analgesia at different body locations. We found that analgesic responses are somatotopically organized in the lPAG and its descending outputs to the rostral ventromedial medulla. These data show for the first time, that the PAG can regulate analgesic responses in a highly spatially localised manner and thus has the ability to mediate body site-selective control over pain.

Main Text:

A paramount need for all living organisms is to preserve bodily integrity and prevent harm. Organisms faced with pain and other signs of danger to bodily integrity must make rapid choices in a context-sensitive manner, including the classically described 'fight or flight' decision (*1*). Experimental animal investigations have shown that these active defensive behaviours are integrated by neurons in the periaqueductal gray (PAG), an integrative midbrain structure that plays key roles in producing coordinated responses to threat. The PAG has a columnar structure, with dorsolateral, ventrolateral (vlPAG), and lateral PAG (lPAG) playing distinct roles in different behaviors. Whereas the vlPAG is central for so-called 'passive coping' responses to threat, the lPAG mediates active 'fight' or 'flight' responses (*2, 3*). lPAG neurons receive direct inputs from cells in the dorsal horn and spinal trigeminal nucleus (SpV), providing direct access by nociceptive systems conveying pain-related information. These projections are organized in a crude somatotopic fashion, that is SpV neurons project to the rostral lPAG, whereas dorsal horn neurons project to the caudal lPAG (*4, 5*). This somatotopy is linked directly to behavioural states changes, with rostral lPAG stimulation evoking confrontation/fight behaviours and caudal lPAG stimulation evoking escape/flight behaviours (*3*). This organizational lPAG scheme is conserved across species as it appears to also be a feature of human PAG organisation, with a recent ultra-high field functional magnetic resonance imaging (fMRI) study reporting rostro-caudal lPAG activation patterns during noxious stimulation to the face compared with the body (*6*). Although the lPAG and is an integrative decision centre that is driven and/or modulated by inputs from higher brain regions (*7*), it can also produce defensive behaviours without such descending inputs (*8*). The somatotopically organised projections to, and from, the lPAG drive spatially appropriate behavioural responses in an essentially reflexive manner, which confers a potentially life-saving behavioural importance to these circuits.

A key component for the successful execution of active defensive behaviours is a profound analgesia, which allows the behavioural response to be expressed unimpeded following an initial painful event (*9*). We know that spatially restricted analgesia is possible since expectancy of pain relief in one body region can evoke pain reduction in that region but simultaneously have no pain-relieving effects at other body sites (*10*). Whether the lPAG can also drives spatially appropriate, and restricted analgesic responses remains unknown. One way to explore the organization of lPAG analgesic responses is using a placebo analgesia paradigm. It is well known that when one expects pain relief, an inert treatment can produce a profound reduction in perceived pain

intensity, i.e. placebo analgesia. Placebo analgesia is mediated by forebrain regions that recruit brainstem circuits to inhibit noxious inputs at the level of the dorsal horn or SpV(*7, 11, 12*). While it has been a long-held view that the brainstem circuit recruited during placebo analgesia depends specifically on neurons in ventrolateral column of the PAG, a recent fMRI study found that the lPAG column is primarily responsible (*11*).

Given that placebo analgesia results from activity changes in the lPAG, which has a clear somatotopic organisation it is possible that the circuitry underpinning placebo analgesia shares this somatotopy. Specifically, that placebo analgesia induced on the face and the body are driven by the rostral and caudal lPAG, respectively. This organizational principle may also be conserved in the major descending output targets of the lPAG that drive analgesic responses, for example, the rostral ventromedial medulla (RVM). Thus, specific parts of the RVM may preferentially contact and modulate incoming noxious inputs from the head, whereas other RVM regions contact the dorsal horn and modulate noxious inputs from the body. Such an organization would fundamentally change our understanding of how the brain controls pain and would reveal a level of regional analgesic control previously unappreciated. We hypothesise that analgesia in the face and body will be paralleled by distinct somatotopic patterns of activity in the lPAG - RVM circuitry.

By deceptively applying different intensity thermal stimuli onto sites in the face, forearm and/or leg, we conditioned healthy participants (face n=22, arm n=46, leg=41) to believe that a placebo cream (a sham “lidocaine”) was acting to reduce their pain relative to an adjacent control cream (“vaseline”). In a subsequent session, whilst collecting ultra-high-field (7-Tesla) fMRI, we applied identical intensity stimuli to both cream-sites (“vaseline"/control; “lidocaine”/placebo) and recorded the subjective pain intensity continuously using a visual analogue scale (VAS) extending from 0 (no pain) to 10 (worst pain imaginable) (Fig 1A). We first found an overall effect of all the placebo paradigms on pain ratings (paired t-test, $p<0.05$) and then classified participants as either responders or non-responders for each stimulus site and conducted group-level analyses using SPM12 to explore changes in signal intensity changes and stimulus-independent connectivity changes associated with analgesic responses. Despite all participants expecting reduced pain on the placebo-treated site (Fig 1B; Table 1), only 41%, 48% and 61% of participants demonstrated significant pain reductions when identical stimuli were applied to both sites on either the face, arm or leg, respectively (Fig 2C; Table 1). These proportions were not affected by sex distribution or thermode temperatures (Table 2).

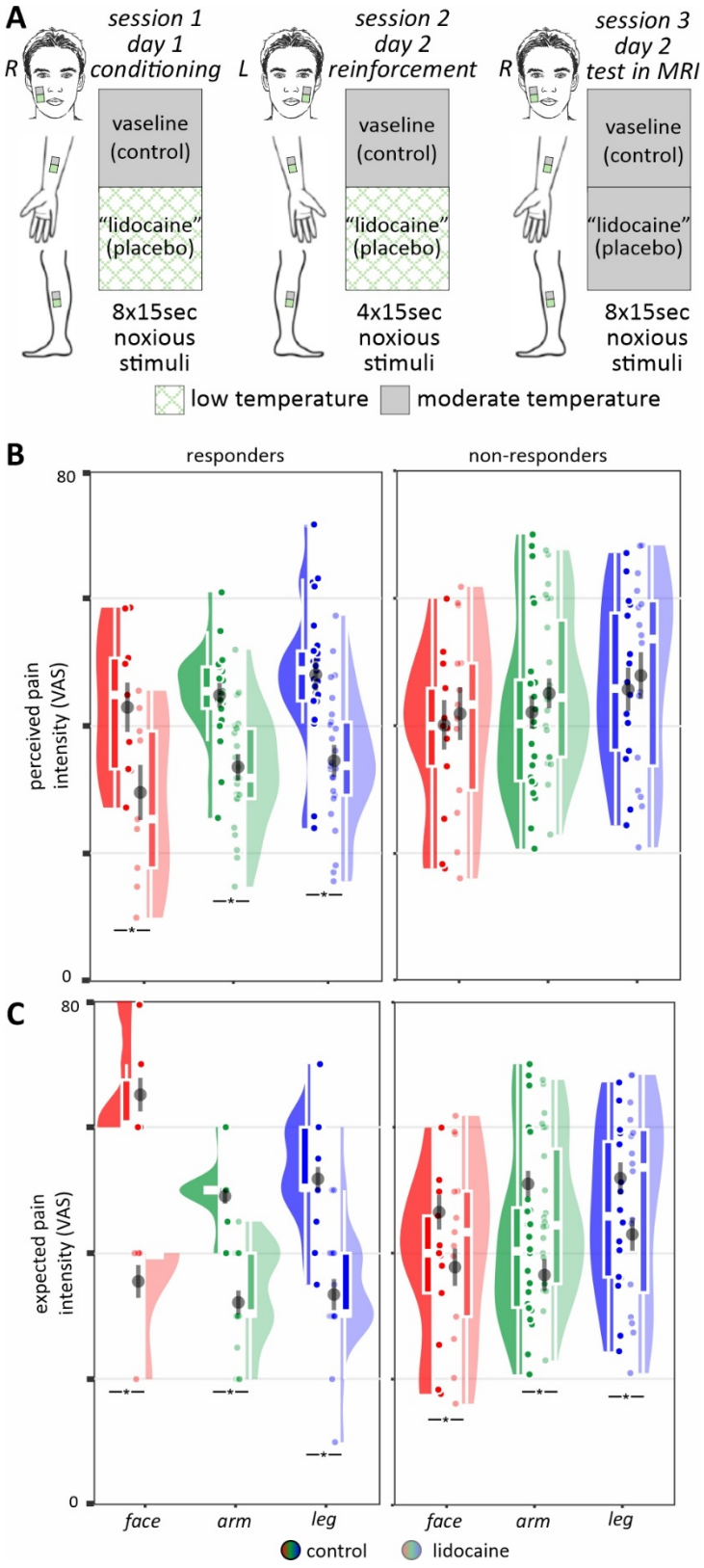

Fig 1: Experimental protocol and placebo-related pain changes. A) Placebo response paradigm. Conditioning was performed by applying low intensity noxious stimuli to the "lidocaine" site and moderate intensity to the vaseline site; crucially, during this phase participants deceptively believed stimuli of moderate intensity were being applied to both sites.

On the following day, a reinforcement phase was conducted using the low and moderate temperatures on the opposite side of the body. Following a washout period, two independent functional magnetic resonance imaging (fMRI) series were collected where identical moderate intensity noxious stimuli to the control vaseline (scan 1), and placebo "lidocaine" cream (scan 2) sites were applied sequentially. During these two series, participants rated their expected and perceived pain on an MR-compatible visual analogue scale (*0 = no pain, 100 = worst pain imaginable*). R: right, L: left. **B) Perceived pain intensities during control and placebo stimulations.** Raincloud plot displaying the distribution of perceived pain scores during control and placebo cream stimulation. The coloured circles, horizontal white line on the box plot and black circle with error bars indicate individual pain scores, median perceived pain intensity and mean (±SEM) perceived pain intensity, respectively, across the face, arm and leg in placebo responder and non-responder groups. **C) Expected pain intensities during control and placebo stimulations.** Raincloud plot displaying the distribution of expected pain scores during control and placebo cream stimulation. The coloured circles, horizontal white line on the box plot and black circle with error bars indicate individual pain scores, median expected pain intensity and mean (±SEM) expected pain intensity, respectively, across the face, arm and leg in placebo responder and non-responder groups. * $p<0.05$.

Consistent with our hypothesis, analysis of fMRI activation patterns in placebo responders compared with non-responders revealed a crude somatotopic organization within the PAG (Figure 2A, Table 1). That is, placebo analgesia on the face evoked signal intensity change differences in the rostral PAG, whereas placebo analgesia on the arm and leg evoked signal differences more caudally in the PAG (Z co-ordinates; face: -5, arm: -9.5; leg: -9.0). Consistent with this organization, linear regression analysis of signal intensity change differences (control versus "lidocaine" scans) with analgesic ability (percentage change in mean pain intensity ratings during the control compared with the placebo scan) also revealed the same somatotopic pattern. Signal intensity changes were negatively correlated with placebo ability and localised to the rostral PAG for the face (Z co-ordinate) and, again, more caudally for the body sites (Z co-ordinates; arm: -9.5; leg: -9.5) (Figure 2B, Table 1). For all three stimulus sites, placebo analgesia responders displayed signal intensity changes decreases whereas non-responders displayed signal intensity change increases.

Individual analysis of greatest (nadir) differences between control and placebo scans in responders again confirmed a rostro-caudal PAG organization (mean ±SEM Z-coordinate: face -

5.94±1.08; arm: -9.05±0.65; leg: -8.38±0.58; Figure 2B, Table 1). A one-way ANOVA revealed that there was a statistically significant difference in the mean ipsilateral Z co-ordinate between at least two body sites (F(2, 9) = [3.4], p=0.04]. Tukey's HSD test found that the mean Z co-ordinate was significantly different between the face and arm (p=0.03) but not the face and leg (p=0.1), revealing a somatotopic organisation between face and arm placebo. Both responder/non-responder and correlation group analyses resulted in clusters located across different PAG columns. However, analysis of the X, Y, Z co-ordinates of nadir signal intensity change differences in responders, revealed the mean locations for the face, arm and leg were localised within the lPAG column when overlaid onto a mean brainstem fMRI image set created from all participants (Figure 2C, Table 1).

Also, consistent with our hypothesis we found that placebo analgesia preferentially activates distinct regions of the RVM depending on whether analgesia was elicited on the face or body. Although a responder versus non-responder analysis of the face, arm and leg did not reveal significant RVM signal intensity change differences, our correlation analyses revealed significant positive correlations for each placebo site in distinct RVM regions. That is, signal intensity changes were positively correlated with placebo ability within different RVM locations during face, arm and leg placebo scans (Figure 3, Table 3). Face placebo was associated with signal intensity correlations more caudally than that evoked by arm and leg analgesia responses Z co-ordinates; face: -52.0, arm: -46.5; leg: -48.5). Furthermore, these correlations were unique for each placebo site. That is, while signal change differences for each cluster derived from the placebo face analysis were correlated with placebo ability, values extracted from this cluster for the arm or leg placebo scans were not significantly correlated.

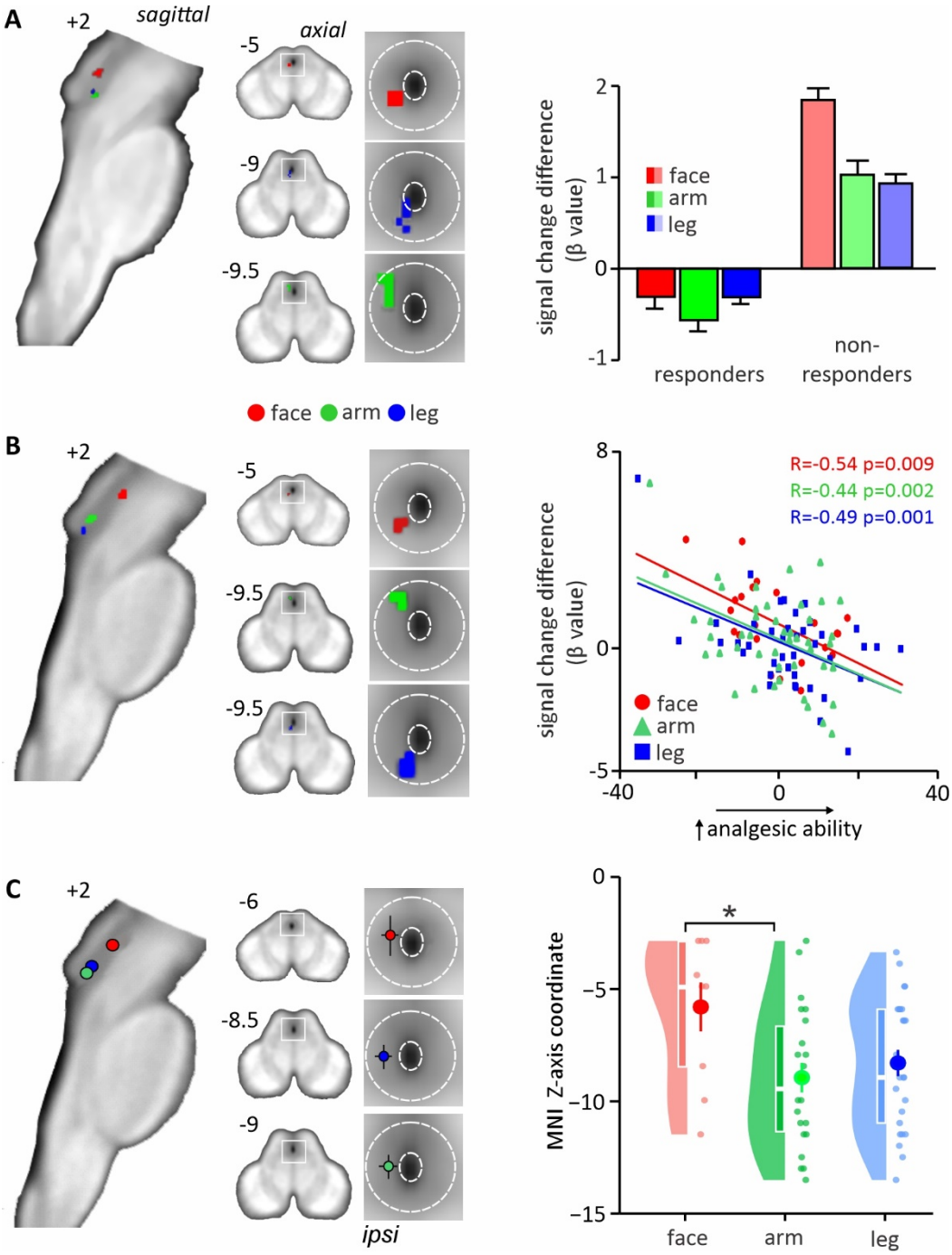

Fig 2: Somatotopic organization of the PAG during placebo analgesia. A) Responder versus non-responder. Analysis of noxious stimuli evoked signal intensity change differences (placebo lidocaine-control scan) revealed a somatotopic PAG organization with placebo analgesia on the face evoking signal intensity change differences (placebo-control) in the rostral PAG, and placebo analgesia on the arm and leg evoking signal change differences more caudally in the PAG. To the right are plots of signal intensity change differences (β value change) for responders and non-responder for each site. **B) Signal change correlation with analgesic ability.** Analysis of noxious stimulus evoked signal intensity change differences correlated with analgesia strength also revealed a rostro-caudal, face-body, PAG organization. To the right are plots of signal intensity

change differences versus analgesia strength for each site. **C) Individual responder participant signal intensity change differences.** Analysis of individual signal intensity change differences in responders also revealed a rostro-caudal organization for face versus arm placebo. Furthermore, these peaks were located immediately lateral to the aqueduct in the lateral PAG column. To the right are raincloud plots of individual peaks for the face, arm and leg placebo with the mean and median shown by the circle and box plot, respectively. *p<0.05.

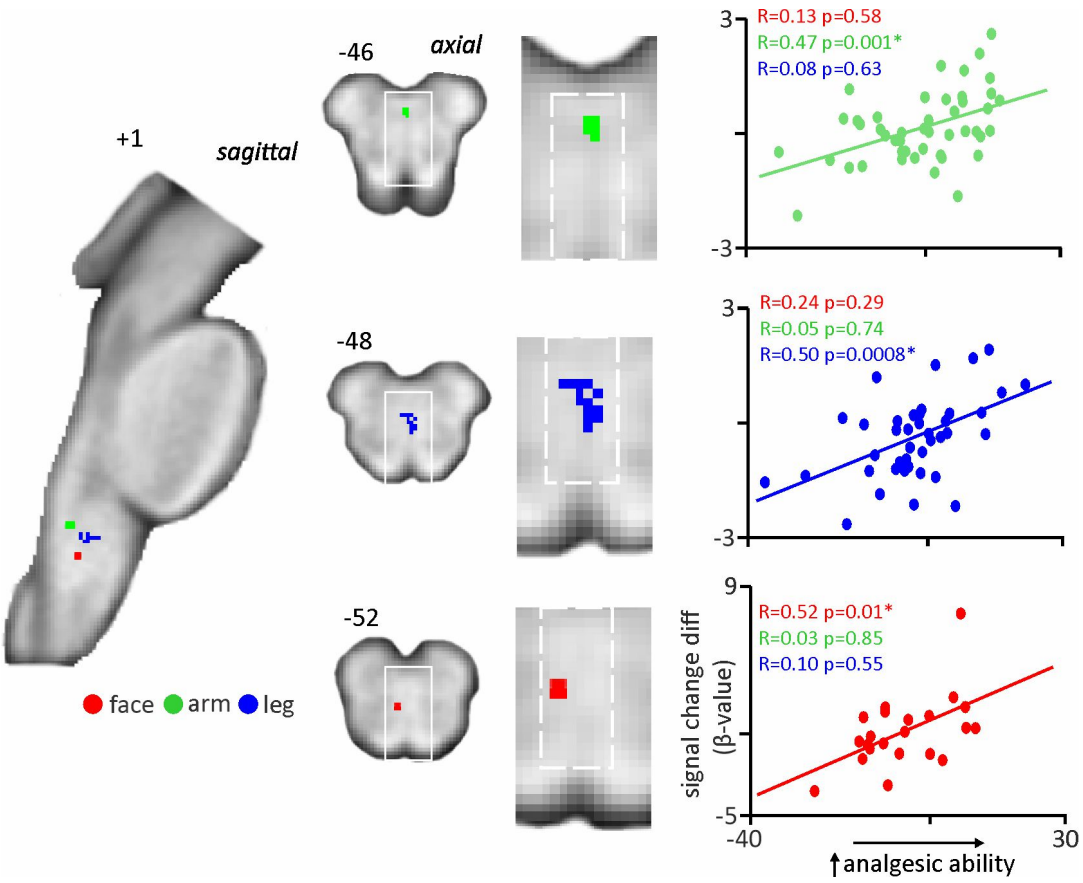

Fig 3: Organization of the RVM during placebo analgesia. Signal intensity change difference correlated with placebo ability. Analysis of noxious stimuli evoked signal intensity change differences (placebo lidocaine-control scan) revealed a discrete RVM organization when placebo analgesia is elicited on the face, arm and leg. Placebo analgesia on the face was associated with a signal correlation within a more caudal aspect of the RVM when compared with placebo analgesia evoked on the arm and leg. To the right are plots of signal intensity change differences (β value change) correlated against placebo analgesia ability for each site. Note that for each site, the cluster identified was uniquely correlated with analgesia strength. That is, the cluster identified during the face placebo voxel-by-voxel analysis was significantly correlated only for the

face placebo scan and not for the arm or leg placebo scans; the same applies for arm and leg placebo clusters.

Our data reveals for the first time that brainstem circuits, involving the PAG and RVM, activated by placebo analgesia have a clear somatotopic organisation. These findings show that the brainstem has the ability to selectively modulate incoming noxious inputs entering from a specific part of the body/head. This specificity is consistent with the idea that during active defensive behaviours, the body regions in which noxious inputs occur, drive not only spatially appropriate behavioural responses, but that these responses are coupled with a somatotopically appropriate analgesia. It has been proposed that at the level of the spinal cord, stimulation of large diameter non-noxious sensory afferents can interfere with incoming small-diameter afferent noxious inputs to produce a regionally specific analgesia, i.e. the pain-gate theory (*13*). Our data are the first to show that circuits within the brain are also organized such that incoming noxious inputs can be modulated in a regionally specific manner. This fundamentally changes our understanding of how the brain regulates noxious information and raises the prospect that altered function in these anatomically specific brainstem analgesic circuits may underlie the presence of regionally restricted persistent pain.

Despite all subjects expecting the "lidocaine" cream to modulate pain intensity, in only a proportion of individuals was a significant reduction in pain intensity reported. This variability is consistent with reports that pain modulation relies on concordance between expectations and experience of prior painful events (*14, 15*). Despite this variability, we found that similar numbers of individuals displayed an analgesic response during placebo applied to the face (41%), arm (49%) and leg (61%), proportions similar to those reported by others (*16*), indicating that body site does not impact placebo analgesia rates. We also confirm that, contrary to accepted hypotheses that placebo analgesia is opiate-dependent (*17-19*) and, by extension, mediated by the ventrolateral PAG (*20, 21*), it is the lPAG which, when stimulated, drives placebo analgesia without the influence of endogenous opiates (*22*). Although group level analyses resulted in variability with respect to the columnar distribution of PAG signal changes for placebo on the face, arm and leg, -similar to our previous study exploring PAG organization during noxious stimuli (*6*)- individual level analyses revealed a consistent peak signal change in the ipsilateral lPAG column. Higher brain regions involved in expectation, such as the anterior cingulate cortex and amygdala, have been shown to be recruited during placebo analgesia (*23-25*). These areas

project strongly to the lPAG, therefore, opioid activity at these sites could provide a key input in driving the lPAG mediated pain modulation.

The patterns of placebo-induced lPAG signal changes are consistent with the organization of afferent inputs from the dorsal horn and SpV (*4, 5*) as well as patterns of lPAG activation following noxious stimuli (*26*). That is, the caudal lPAG: 1) receives projections from the spinal dorsal horn, 2) is activated by noxious stimulation of the forelimb and hindlimb, and 3) evokes signal changes following placebo analgesia responses in the leg and arm. This pattern exists also for the face and the rostral lPAG. In addition to describing somatotopic organization in the lPAG, we also found that the RVM displays regionally specific signal intensity changes during face, arm and leg analgesia. It is well-established from experimental animal investigations that the lPAG modulates incoming noxious information via projections to the RVM, which then project directly to the SpV and dorsal horn (*21, 27-30*). The RVM contains both "off" and "on" neurons that strongly inhibit and facilitate neurotransmission at the primary nociceptive synapse, respectively (*31-35*). We found opposing relationships with greater placebo ability associated with reduced PAG signal changes and increased signal changes. These findings suggest that during placebo analgesia, reduced lPAG synaptic activity evokes an overall increase in RVM "off" compared to "on" cell firing, which, in turn, results in increased inhibition of incoming nociceptive drive at the dorsal horn or SpV.

Our results reveal that RVM signal changes during face, arm and leg placebo are discrete and spatially separated, consistent with the idea that the RVM contains groups of neurons that preferentially target specific parts of the dorsal horn or the SpV. While evidence for a somatotopic organization within the RVM is novel, earlier pre-clinical studies have shown a degree of anatomical specificity within the RVM. For example, anterograde tracing has revealed that midline neurons in the RVM (raphe magnus) project preferentially to deep laminae (V-VI), whereas more laterally placed RVM neurons (lateral paragigantocellular neurons) project to the superficial laminae (I-II) of the dorsal horn (*36*). Moreover, it has been reported that RVM projections to spinal dorsal horn are predominantly GABAergic and are more likely to contact neuronal somata, whereas projections to SpV have only modest numbers of GABAergic cells which preferentially target dendrites (*37*). We know of no preclinical study that has specifically addressed the question of somatotopic organization of the RVM, our human data shows that, like the lPAG, the RVM is activated in a regionally specific manners during placebo-mediated analgesic responses.

It is important to note some limitations. Firstly, it was not possible to fully counterbalance the ordering of stimuli since the experimental design required a pairing of modulated with non-modulated responses. Secondly, conditioning-based pain modulation paradigms are prone to response bias (*38*), to counteract this bias, each participant rated their pain continuously during the scan instead of afterwards. Finally, the statistical threshold we employed was $p<0.005$ uncorrected for multiple comparisons with a cluster extent threshold of 5 contiguous voxels. Our results were limited solely to the PAG and RVM, two regions previously shown to be critical for placebo analgesia. Thus, signal changes in these regions are consistent with our hypothesis on these two specific regions and align with decades of preclinical studies describing a role for these areas in pain modulation.

Using ultra high-field fMRI we have shown, for the first time, a somatotopic organization within the PAG and RVM following analgesia in the face and body. Ultimately, these findings provide evidence that the brain is capable of modulating incoming noxious information in a regionally specific manner which may allow for the rapid coordination of the most appropriate defensive behaviors.

Methods:

Ethics: All experimental procedures were approved by the University of Sydney Human Research Ethics Committee and were consistent with the Declaration of Helsinki. Written informed consent was obtained from participants at the commencement of the study. Participants were provided with an emergency buzzer while inside the scanner so that they could stop the experiment at any time. At the conclusion of testing, participants were informed verbally, and through a written statement, of the necessary deception and true methodology of the experiment and were invited to seek clarification of what they had just experienced.

Participants: Seventy participants were recruited for the study (33 male, 37 female; mean ±SEM age, 24.6±0.5 years; range 20 - 38 years). In order to evaluate the necessary number of participants required for this study, an *a priori* power analysis was performed using results from a previous imaging study investigating cortico-brainstem connectivity during placebo analgesia (*24*). This revealed a total sample size of 40 across all groups in the study design to be necessary to detect similar effect sizes with 95% power ($d = 0.31$, $\alpha = 0.05$, power = 0.95). Before beginning

the study, participants completed a data sheet recording current medication(s), and any alcohol or caffeine ingested in the 24 hours prior to testing.

Experimental Design: The study included three sessions occurring on two successive days: a conditioning session on day 1, and a reinforcement and MRI scanning session on day 2 (Figure 1A). Throughout the study, noxious stimuli were administered to one of three places: the right cheek, volar surface of the forearm or on the shin of the lower leg. Brief noxious stimuli were delivered using a 3x3cm MR-compatible Peltier element thermode, which delivered a heat stimulus at a pre-programmed temperature via a Thermal Sensory Analyzer (TSA-II) (Medoc LTD Advanced Medical Systems, Rimat Yishai, Israel). Each stimulus lasted 15 seconds, including a ramp-up period (four degrees per second), a plateau period at a noxious temperature and a ramp-down period (four degrees per second). Each stimulus was separated by a 15 second inter-stimulus-interval (ISI) at a non-painful baseline temperature of 32°C. Throughout conditioning, participants rated their pain on-line using a horizontal 10 cm visual analogue scale (VAS) ranging between 0 and 100, where 0 was described as "no pain" and 100 as "the worst pain imaginable". During scanning, participants used an MR-compatible button box to continuously report their pain perception. The VAS scale was shown on a reflected digital screen at the end of the magnet bore, and participants controlled the position of a slider to report their pain continuously by holding the left (moved slider towards zero) or right (moved slider towards ten) buttons with their left middle and index finger.

Conditioning: Session 1 was conducted outside the MRI and consisted of two rounds of a conditioning protocol. Participants were first informed both verbally and via a written statement that the study was designed to investigate the modulatory effects of a topical anaesthetic containing lidocaine, which had been shown to provide pain relief in some individuals. A second control cream was stated to be purely Vaseline and was stated as being necessary to evaluate typical pain responses. In reality, both creams contained Vaseline, and differed only in colour and their described properties. Individual low and moderate pain responses were calculated by applying a series of randomised stimuli to the right face, arm or leg ranging from 44-48.5 degrees, asking participants to rate their perceived pain during each stimulus. Participants were informed that we were only recording a temperature which elicited a moderate subjective pain response (40–50 VAS rating), and that this temperature would be used throughout the remainder of the experiment. However, using the ratings provided during this process, we recorded two different temperatures: one which was rated between 20-30 on the VAS (low temperature); and one which

was rated between 40-50 (moderate temperature). These three temperatures were then deceptively applied to the "lidocaine" and Vaseline cream sites throughout the conditioning and reinforcement experimental phases.

Creams were then applied to two adjacent 3x3 cm squares on the participants' right face, arm or leg. To enhance the believability that the "lidocaine" cream contained an active analgesic, a false label was attached to the cream bottle and green food colouring was added. The positions of the "lidocaine" and vaseline creams were counterbalanced between participants to reduce potential confounders of local sensitivity. Ten minutes following cream application, we conducted two rounds of conditioning. Participants believed they would receive eight identical moderate thermal stimuli and were instructed to report their perceived pain intensity using the VAS. Participants were also asked prior to each set of stimuli for an average expectation of the pain they would experience, which acted both to measure belief that lidocaine was working to modulate their subjective pain, and to reinforce the pain-relieving quality of the cream. During the two conditioning rounds we deceptively applied a moderate temperature to the vaseline cream site, and a low temperature to the green 'lidocaine' cream site.

Reinforcement and Test: At approximately the same time on the following day, sessions 2 and 3 were conducted with participants inside the MRI scanner and consisted of a reinforcement protocol (session 2) and a test protocol (session 3). The creams were applied to the same part of the face, arm or leg, in the same order and locations as session 1, but on both the left and right sides, and participants were reminded of the "lidocaine's" pain-relieving qualities. Reinforcement was conducted by applying four noxious stimuli at the same low and moderate temperatures that were used throughout session 1 applied to the left face, arm or leg. This reinforcement protocol was conducted to ensure that participants continued to report different expectations and pain ratings between the two cream sites despite the change in day and environment (inside the MRI).

Following reinforcement, we waited 15 minutes for residual pain and sensitivity to dissipate before beginning the test protocol. During this 15-minute period, structural brain scans were collected. Dissimilar to conditioning and reinforcement, during the test phase we applied *identical moderate temperature stimuli* to both the control Vaseline and placebo "Lidocaine" cream sites on the right side of face, arm or leg (Figure 1A). We asked each participant for an average expectation of pain intensity directly prior to stimulation and instructed them to report

the pain intensity experienced over the duration of the scan using the button box and the projected digital VAS. Each participant received two consecutive series of eight stimuli, with a separate functional series collected during each series of stimuli. The control cream site was always stimulated during the first series, and the 'lidocaine' site was stimulated during the second series, so that we generated a "pre" and "post" condition, or, functional brain images encoding typical and placebo pain responses, respectively.

MRI data acquisition and preprocessing: Brain images were acquired using a whole-body Siemens MAGNETOM 7 Tesla (7T) MRI system (Siemens Healthcare, Erlangen, Germany) with a combined single-channel transmit and 32-channel receive head coil (Nova Medical, Wilmington MA, USA). Participants were positioned supine with their head in the coil and sponges supporting the head laterally to minimise movement. A T1-weighted anatomical image set covering the whole brain was collected (repetition time=5000 ms, echo time=3.1ms, raw voxel size=0.73x0.73x0.73mm, 224 sagittal slices, scan time=7mins). The three fMRI acquisitions each consisted of a series of 134 gradient echo echo-planar measurements using blood oxygen level dependant (BOLD) contrast covering the entire brain. Images were acquired in an interleaved collection pattern with a multi-band factor of four and an acceleration factor of three (repetition time=2500ms, echo time=26ms; raw voxel size=1.0x1.0x1.2mm, 124 axial slices, scan time=6:25mins). In 31 of the 70 participants, only a single placebo scan was collected: 25 for the arm, 4 for the face and 2 for the leg. In the remaining 39 out of 70 participants, two placebo scans were collected; 21 for both the arm and leg placebo, and 18 for both the face and leg placebo.

Image preprocessing and statistical analyses were performed using SPM12 and custom software. The first five volumes of each scan were removed from the model due to excessive signal saturation from the scanner. The remaining 129 functional images were slice-time, motion corrected, and the resulting 6 directional movement parameters inspected to ensure that all fMRI scans had no greater than 1mm of linear movement or 0.5 degrees of rotation movement in any direction. Images were linearly detrended to remove global signal changes, physiological noise relating to cardiac and respiratory frequency filtered and removed using the DRIFTER toolbox (*39*), and the 6-parameter movement related signal changes were modelled and removed using a linear modelling of realignment parameters (LMRP) procedure. Each individual's fMRI image sets were then co-registered to their own T1-weighted anatomical and underwent distortion correction using the SynBOLD DisCO toolbox (*40*).

Following anatomical co-registration, the T1-weighted image was then spatially normalized to the DARTEL template in Montreal Neurological Institute (MNI) space and the parameters applied to the fMRI image sets. To focus on the brainstem specifically, the brainstem and cerebellum were isolated using the spatially unbiased infra-tentorial template (SUIT) toolbox (*41*), for both the fMRI and T1 image sets, and then normalised to the brainstem- and cerebellum-only SUIT template in Montreal Neurological Institute (MNI) space. During this process, both the T1 structural and functional image sets were resliced into 0.5mm isotropic voxels and these images were spatially smoothed using a 1mm FWHM Gaussian filter. A small smoothing kernel was used to allow for the accurate investigation of signal intensity changes within small brainstem nuclei (*42*).

Dichotomizing placebo responder and non-responder groups: The overall effect of the placebo on pain perception was first tested against all participants using a paired t-test. Participants were then grouped as either a responder or non-responder to placebo analgesia based on a bootstrapped permutation procedure (*43*). Briefly, mean VAS ratings to each of the 8 noxious stimuli delivered during the control stimulated series were entered to a permutation model, where 10,000 artificial sample were generated with replacement. This artificial sample was significance tested to 10,000 artificial samples generated from the VAS ratings to each 8 noxious stimuli delivered during the 'lidocaine' stimulated series. If the mean difference between the two series was significant, with the 'lidocaine' significantly lower than the control, a participant was considered a responder. If not, they were considered a non-responder. Significant differences between groups with respect to expected changes in pain intensities immediately prior to testing were determined using paired t-tests (two-tailed, $p<0.05$). Since participants were grouped into either responder or non-responder categories based on their perceived pain intensities during the fMRI scans (session 3), we did not assess significant differences between groups for the perceived pain intensity changes. A single factor ANOVA ($p<0.05$) was also used to determine if there were differences in the temperature applied or pain intensity ratings reported between responder and non-responder groups during the control stimulated series to ensure any reported placebo effects did not relate to baseline thermal sensitivity. In addition, we calculated each participant's analgesic ability by calculating the percentage change in mean pain intensity ratings during the control compared with the placebo scan. A greater analgesic ability value represents a greater pain reduction during the placebo compared with control scan.

fMRI statistical analysis: To determine significant changes in signal intensity during each noxious thermal period, a repeating boxcar model convolved with a canonical hemodynamic

response function was applied to each of the fMRI series. The contrast images generated for each functional image series were then used in group analyses. Following the creation of a PAG and RVM mask drawn on a mean brainstem fMRI image set calculated from one image from each of the 70 participants, we conducted two separate analyses to determine PAG and RVM signal changes during placebo:

responders versus non-responders: significant differences between PAG and RVM signal intensity changes of responder and non-responder groups were determined by subtracting the control scan contrast map from the placebo scan contrast map in each individual. The signal intensity change difference maps (placebo lidocaine – control scan) were then compared between responder and non-responder groups using random effects, two-sample voxel-by-voxel analyses. The greatest significantly different PAG or RVM cluster in the responder<non-responder contrast was determined using a minimum threshold of $p<0.005$ (cluster extent threshold of five contiguous voxels) and overlaid onto a mean brainstem T1-weighted anatomical image set located in the same exact location as the mean brainstem fMRI image set. The signal change differences (β values) were extracted from each significant cluster and the mean ±SEM values plotted.

linear correlation with analgesia: significant relationships between PAG and RVM signal change differences and analgesic responses were determined by placing the signal intensity change difference maps (placebo-control scan) compared with analgesic ability values into a random effects, one-sample, voxel-by-voxel analyses. The greatest negative or positive correlation PAG and RVM cluster was determined using a minimum threshold of $p<0.005$ (cluster extent threshold of five contiguous voxels) and overlaid onto a mean brainstem T1-weighted anatomical image set. The signal change differences (β values) were extracted from each significant cluster and plotted against analgesic abilities and rho and p values (Pearsons's correlation coefficient) calculated.

In addition, since we have previously shown that the columnar organization of the PAG is more accurately determined by assessing the location of signal intensity changes at an individual participant level, we performed a third analysis:

individual placebo analgesia PAG peaks in responders: we determined the location of the lowest nadir of the placebo – control contrast maps in the PAG in each responder for the face, arm and leg. To determine the location of this peak with respect to PAG columns, masks encompassing

the dorsomedial (dmPAG), dorsolateral (dlPAG), lateral (lPAG) and ventrolateral PAG (vlPAG) columns as defined by Bandler and Keay (*3*) were created at 1mm intervals throughout its rostro-caudal extent (Z co-ordinate -3 to -13). We then recorded and plotted the mean±SEM MNI co-ordinates onto a mean brainstem T1-weighted anatomical image set. As the focus of this study was on investigating rostro-caudal differences within the PAG, a one-way ANOVA was performed to compare the effect of body site (face, arm and leg) on the mean ipsilateral Z co-ordinate. The Levene test was first used to ensure the assumption of homogeneity of variances was met as well as the Shapiro-Wilk test for normality across the Z-coordinates for the face, arm and leg. Post-hoc analyses were then performed using Tukey's honest significance difference (HSD) test to determine whether there was a significant difference in the mean Z-coordinates between the face, arm and leg.

References:

1. H. L. Fields, Pain: An unpleasant topic. *Pain* **82** (1999).
2. S. P. Zhang, R. Bandler, P. Carrive, Flight and immobility evoked by excitatory amino acid microinjection within distinct parts of the subtentorial midbrain periaqueductal gray of the cat. *Brain Res* **520**, 73-82 (1990).
3. R. Bandler, K. A. Keay, Columnar organization in the midbrain periaqueductal gray and the integration of emotional expression. *Prog Brain Res* **107**, 285-300 (1996).
4. K. A. Keay, K. Feil, B. D. Gordon, H. Herbert, R. Bandler, Spinal afferents to functionally distinct periaqueductal gray columns in the rat: an anterograde and retrograde tracing study. *J Comp Neurol* **385**, 207-229 (1997).
5. M. Wiberg, J. Westman, A. Blomqvist, Somatosensory projection to the mesencephalon: an anatomical study in the monkey. *J Comp Neurol* **264**, 92-117 (1987).
6. F. A. Tinoco Mendoza *et al.*, Detailed organisation of the human midbrain periaqueductal grey revealed using ultra-high field magnetic resonance imaging. *Neuroimage* **266**, 119828 (2023).
7. L. S. Crawford *et al.*, Stimulus-independent and stimulus-dependent neural networks underpin placebo analgesia responsiveness in humans. *Commun Biol* **6**, 569 (2023).
8. S. Koutsikou, R. Apps, B. M. Lumb, Top down control of spinal sensorimotor circuits essential for survival. *J Physiol* **595**, 4151-4158 (2017).
9. N. M. Barbaro, Studies of PAG/PVG stimulation for pain relief in humans. *Prog Brain Res* **77**, 165-173 (1988).
10. F. Benedetti, C. Arduino, M. Amanzio, Somatotopic activation of opioid systems by target-directed expectations of analgesia. *J Neurosci* **19**, 3639-3648 (1999).
11. L. S. Crawford *et al.*, Brainstem Mechanisms of Pain Modulation: A within-Subjects 7T fMRI Study of Placebo Analgesic and Nocebo Hyperalgesic Responses. *J Neurosci* **41**, 9794-9806 (2021).
12. L. S. Crawford *et al.*, Function and biochemistry of the dorsolateral prefrontal cortex during placebo analgesia: how the certainty of prior experiences shapes endogenous pain relief. *Cereb Cortex* **33**, 9822-9834 (2023).
13. R. Melzack, P. D. Wall, Pain mechanisms: a new theory. *Science* **150**, 971-979 (1965).
14. A. Grahl, S. Onat, C. Büchel, The periaqueductal gray and Bayesian integration in placebo analgesia. *Elife* **7**, (2018).

15. P. Tétreault *et al.*, Brain Connectivity Predicts Placebo Response across Chronic Pain Clinical Trials. *PLOS Biology* **14**, e1002570 (2016).
16. R. Meister *et al.*, Placebo response rates and potential modifiers in double-blind randomized controlled trials of second and newer generation antidepressants for major depressive disorder in children and adolescents: a systematic review and meta-regression analysis. *European Child & Adolescent Psychiatry* **29**, 253-273 (2020).
17. J.-K. Zubieta *et al.*, Placebo Effects Mediated by Endogenous Opioid Activity on μ-Opioid Receptors. *The Journal of Neuroscience* **25**, 7754 (2005).
18. D. J. Scott *et al.*, Placebo and nocebo effects are defined by opposite opioid and dopaminergic responses. *Arch Gen Psychiatry* **65**, 220-231 (2008).
19. R.-R. Zhang, W.-C. Zhang, J.-Y. Wang, J.-Y. Guo, The opioid placebo analgesia is mediated exclusively through μ-opioid receptor in rat. *International Journal of Neuropsychopharmacology* **16**, 849-856 (2013).
20. G. P. McNally, M. Pigg, G. Weidemann, Opioid Receptors in the Midbrain Periaqueductal Gray Regulate Extinction of Pavlovian Fear Conditioning. *The Journal of Neuroscience* **24**, 6912 (2004).
21. D. R. Loyd, A. Z. Murphy, The Role of the Periaqueductal Gray in the Modulation of Pain in Males and Females: Are the Anatomy and Physiology Really that Different? *Neural Plasticity* **2009**, 462879 (2009).
22. R. Bandler, K. A. Keay, N. Floyd, J. Price, Central circuits mediating patterned autonomic activity during active vs. passive emotional coping. *Brain Research Bulletin* **53**, 95-104 (2000).
23. I. Tracey, P. W. Mantyh, The cerebral signature for pain perception and its modulation. *Neuron* **55**, 377-391 (2007).
24. F. Eippert *et al.*, Activation of the Opioidergic Descending Pain Control System Underlies Placebo Analgesia. *Neuron* **63**, 533-543 (2009).
25. S. Freeman *et al.*, Distinct neural representations of placebo and nocebo effects. *NeuroImage* **112**, 197-207 (2015).
26. K. A. Keay, R. Bandler, Parallel circuits mediating distinct emotional coping reactions to different types of stress. *Neurosci Biobehav Rev* **25**, 669-678 (2001).
27. P. W. Mantyh, Connections of midbrain periaqueductal gray in the monkey. II. Descending efferent projections. *J Neurophysiol* **49**, 582-594 (1983).
28. P. Petrovic, K. M. Petersson, P. Hansson, M. Ingvar, Brainstem involvement in the initial response to pain. *Neuroimage* **22**, 995-1005 (2004).

29. M. Mokhtar, P. Singh, Neuroanatomy, Periaqueductal Gray. *StatPearls [Internet]*, (2020).
30. A. G. Hohmann *et al.*, An endocannabinoid mechanism for stress-induced analgesia. *Nature* **435**, 1108-1112 (2005).
31. H. Fields, State-dependent opioid control of pain. *Nature Reviews Neuroscience* **5**, 565-575 (2004).
32. H. Vanegas, H. G. Schaible, Descending control of persistent pain: inhibitory or facilitatory? *Brain Res Brain Res Rev* **46**, 295-309 (2004).
33. E. E. Benarroch, Descending monoaminergic pain modulation: bidirectional control and clinical relevance. *Neurology* **71**, 217-221 (2008).
34. M. M. Heinricher, I. Tavares, J. L. Leith, B. M. Lumb, Descending control of nociception: Specificity, recruitment and plasticity. *Brain Res Rev* **60**, 214-225 (2009).
35. M. H. Ossipov, G. O. Dussor, F. Porreca, Central modulation of pain. *The Journal of clinical investigation* **120**, 3779-3787 (2010).
36. A. Gautier, D. Geny, S. Bourgoin, J. F. Bernard, M. Hamon, Differential innervation of superficial versus deep laminae of the dorsal horn by bulbo-spinal serotonergic pathways in the rat. *IBRO Rep* **2**, 72-80 (2017).
37. S. A. Aicher, S. M. Hermes, K. L. Whittier, D. M. Hegarty, Descending projections from the rostral ventromedial medulla (RVM) to trigeminal and spinal dorsal horns are morphologically and neurochemically distinct. *J Chem Neuroanat* **43**, 103-111 (2012).
38. A. Hróbjartsson, T. J. Kaptchuk, F. G. Miller, Placebo effect studies are susceptible to response bias and to other types of biases. *Journal of clinical epidemiology* **64**, 1223-1229 (2011).
39. S. Särkkä *et al.*, Dynamic retrospective filtering of physiological noise in BOLD fMRI: DRIFTER. *NeuroImage* **60**, 1517-1527 (2012).
40. T. Yu *et al.*, SynBOLD-DisCo: Synthetic BOLD images for distortion correction of fMRI without additional calibration scans. *Proc SPIE Int Soc Opt Eng* **12464**, (2023).
41. J. Diedrichsen, A spatially unbiased atlas template of the human cerebellum. *Neuroimage* **33**, 127-138 (2006).
42. R. Sclocco, F. Beissner, M. Bianciardi, J. R. Polimeni, V. Napadow, Challenges and opportunities for brainstem neuroimaging with ultrahigh field MRI. *Neuroimage* **168**, 412-426 (2018).
43. K. J. Berry, J. E. Johnston, P. W. Mielke, Jr., Permutation methods. *WIREs Computational Statistics* **3**, 527-524 (2011).

Table 1: Mean (±SEM) pain ratings from responders and non-responders across face, arm) and leg sites prior to (expected) and during (perceived) stimulation of the control and lidocaine (placebo) cream sites. The grey shaded boxes indicate where pain (expected or perceived) was significantly lower during the placebo compared with the control scans. Note that for the non-responders there was a significant increase in perceived pain during the placebo compared with the control scan.

	Responders			**Non-Responders**		
	face	arm	leg	face	arm	leg
Expected pain ratings						
Control	65.0±2.5	49.3±0.8	52.9±1.6	47.3±2.7	51.2±1.9	52.8±2.3
Placebo	36.7±2.5	33.5±1.6	34.8±2.0	38.5±3.3	37.1±2.6	43.4±2.6
t-test	p<0.05	p<0.05	p<0.05	p<0.05	p<0.05	p<0.05
Perceived pain ratings						
Control	43.7±3.6	45.2±1.5	48.4±2.0	40.6±3.5	42.2±2.8	46.3±3.1
Placebo	28.5±4.1	33.0±1.9	34.9±2.1	42.7±3.8	45.9±2.4	48.4±3.8
t-test	p<0.05	p<0.05	p<0.05	p>0.05	p=0.04	p>0.05

Table 2: Mean (±SEM*)* age, sex distribution and thermode temperature (used to induce moderate pain in both control and placebo scans) for responder (R) and non-responder (NR) groups for face (n=22), arm (n=46), and leg placebo (n=41). Note that the total sample size was n=70, with 31 subjects completing one placebo scan and the remaining 39 subjects completing two out of three placebo scans. * p<0.05 R vs NR.

face		arm		leg	
R	NR	R	NR	R	NR
Age (mean±SEM)					
23.6±1.6*	25.5±1.5	24.6±0.7*	24.5±0.9	24.7±0.7*	26.2±1.3
Sex distribution (male:female)					
2:7	6:7	14:8	10:14	12:13	8:8
Thermode temperature (mean±SEM)					
46.3±0.3	46.3±0.2	46.9±0.2	46.8±0.2	46.4±0.1	46.2±0.2

Table 3: Mean peak X, Y and Z Montreal Neurological Institute (MNI) co-ordinates and t-values in the ipsilateral midbrain periaqueductal gray matter (PAG) and rostral ventromedial medulla (RVM) during placebo analgesic responses applied to the face, arm and leg.

	MNI co-ordinate			**t-value**
	X	**Y**	**Z**	
PAG negative correlation with placebo ability				
face	2.5	-28.5	-5.0	2.87
arm	2.0	-34.5	-9.5	3.10
leg	1.5	-30.5	-9.5	3.40
PAG responder vs non-responder				
face	2.5	-29.5	-5.0	3.59
arm	2.5	-34.5	-9.5	2.85
leg	2.0	-30.5	-9.0	2.64
PAG individual nadir signal change analysis (mean±SEM)				
face	1.61±0.23	-31.39±0.94	-5.94±1.08	-
arm	1.78±0.14	-32.39±0.54	-9.05±0.65	-
leg	1.78±0.14	-32.48±0.45	-8.38±0.58	-
RVM positive correlation with placebo ability				
face	0	-37.5	-52.0	2.75
arm	1.5	-40.0	-46.5	3.34
leg	1.0	-36.5	-48.5	3.67

Chapter 4.

Descending cortical and sub-cortical pain modulatory circuits underlying placebo analgesia on different body sites

"It is the power of the mind to be unconquerable"

Seneca, The Stoic Philosophy: Essays and Letters

4.1 Overview

Whilst the previous chapters provided direct evidence of a somatotopic organization within the PAG and RVM during pain and analgesia on the face and body, a major limitation was the restriction of our investigations to the brainstem. Although necessary for achieving the highest resolution and spatial acuity offered by UHF imaging, as discussed in section 1.6.2, these brainstem nuclei are heavily influenced by top-down projections from the cortex.

This study involved a similar method of response conditioning conducted in Chapter 3. To improve the interpretations of our findings within Chapter 3, this investigation sought to identify how cortical and sub-cortical regions previously implicated in descending pain modulation process placebo analgesia across different body sites. We focused our attention to four key sites - the rACC, dlPFC, amygdala and hypothalamus – critically involved in placebo analgesia and which have showed altered functional connectivity with the lateral PAG during a placebo analgesia response (Crawford et al., 2023). Assessing their functional activation and connectivity in response to placebo analgesia on the face, arm and leg, we sought to identify a complete cortical network capable of driving endogenous pain modulation in a spatially separate manner, thus addressing **Aim 3.** We hypothesized spatially separate activation patterns and lateral PAG connectivity strength changes in the ACC and dlPFC for placebo responses on the face and body, but since somatotopy appears to be absent in the amygdala and hypothalamus, we predicted no such spatially separate patterns in these regions.

Regarding functional connectivity, we used the previous mean peak coordinate of the rostral and caudal PAG during pain and analgesia to create two 'face' and 'body' PAG seeds and determine a difference between PAG seed connectivity. Functional analyses revealed an increase in signal intensity in the rACC and dlPFC in placebo responders, however only the rACC showed an overlap in activation and a crude somatotopic pattern between face and body analgesia. Additionally, lateral PAG coupling increased with the rACC and dlPFC in placebo responders, whereas a decrease was observed with the amygdala and hypothalamus. The amygdala and hypothalamus showed a regionally similar change in PAG connectivity that was common between face and body analgesia.

Together, these findings provide a basis of a primitive pain modulatory network that is able to recognize where in the body an analgesic response should be mounted. We suggest that during placebo analgesia, the active integration of cognitive evaluation is largely driven by the dlPFC, and forebrain regions likely mediate the key aspects of a successful placebo analgesia response.

Title: Descending cortical and sub-cortical pain modulatory circuits underlying placebo analgesia on different body sites

Running title: Cortical placebo circuits

Authors: Fernando A Tinoco Mendoza[1], Lewis S Crawford[1], Rebecca V Robertson[1], Noemi Meylakh[1], Paul M Macey[2], Kirsty Bannister[3], Tor Wager[4], Vaughan G Macefield[5], Kevin A Keay[1] and Luke A Henderson[1]

Affiliations: [1] School of Medical Sciences (Neuroscience), Brain and Mind Centre, University of Sydney, Australia, 2006; [2] UCLA School of Nursing and Brain Research Institute, University of California, Los Angeles, California, 90095, USA; [3]Department of Pharmacology and Therapeutics, Institute of Psychiatry, Psychology and Neuroscience, King's College London, London, United Kingdom; [4]Department of Psychological and Brain Sciences, Dartmouth College, Hanover, NH, USA; [5] Department of Neuroscience, Monash University, Australia.

Corresponding author: Luke A. Henderson, School of Medical Sciences (Neuroscience), Brain and Mind Centre, University of Sydney, Australia. luke.henderson@sydney.edu.au (email); +612 9351 7063 (Tel) +612 9351 6556 (Fax).

Acknowledgements: We wish to thank the many volunteers in this study. The authors acknowledge the facilities and scientific and technical assistance of the National Imaging Facility, a National Collaborative Research Infrastructure Strategy (NCRIS) capability, at Monash University. This work was funded by the National Health and Medical Research Council of Australia Grant 1130280. The authors declare no competing financial interests.

Abstract:

The successful execution of active defensive behaviors is contingent upon our body's capacity to induce analgesia. The midbrain periaqueductal gray (PAG) has a well-established role in pain modulation, and one way to explore this is through a placebo analgesia paradigm. Noxious stimulation to the face and body has recently shown to elicit a rostro-caudal somatotopic organization within the lateral PAG that is also preserved during placebo analgesia on similar body sites. It remains unknown whether the underlying top-down circuits responsible for descending pain modulation from the cortex and sub-cortex are also somatotopically organized like in the brainstem. We used ultra-high field functional magnetic resonance imaging (7-tesla) to determine whether placebo analgesia on the face, arm and leg evoke differential activation and PAG-connectivity patterns within the rostral anterior cingulate cortex (rACC), dorsolateral prefrontal cortex (dlPFC), amygdala and hypothalamus in healthy subjects (n=70). In comparison to the arm, placebo analgesia on the face elicits significant signal intensity changes in spatially separate areas of the rACC and dlPFC. However, a significant difference between analgesia induced on the face and arm is observed only when the cluster values from the rACC are extracted. Decreases in PAG-connectivity with the amygdala were found in the basolateral complex in both face and arm placebo responders. Leg analgesia only showed one significant change across both analyses being a decrease in PAG-hypothalamus connectivity, of which the cluster was significant in both face and leg analgesia subjects. These results extend on anatomical studies showing profuse projections between limbic structures and the rostro-caudal extent of the PAG. Our findings suggest a conserved analgesic circuit involving primitive limbic structures and an evolved cognitive circuit utilizing the dlPFC to generate an expectation of pain relief at a specific body site.

Key words: periaqueductal gray; somatotopy; placebo analgesia; pain modulation; functional MRI.

Introduction:

The ability of an individual to perceive and modulate incoming sensory information is critical for survival. In stressful and threatening situations, the brain can profoundly inhibit incoming noxious sensory information, allowing individuals to perceive less pain despite a significant injury driving noxious input (Best and Neuhauser, 2010). Experimental animal studies have defined a number of brainstem regions that, upon activation, modulate incoming noxious information (Aimone et al., 1987, Basbaum and Fields, 1984, Behbehani and Fields, 1979) and are themselves modulated by higher brain regions such as the hypothalamus, amygdala and the cerebral cortex (Eippert et al., 2009). However, determining whether these brainstem circuits are conserved in humans has remained challenging due to the small intricate nature of the structures involved.

One way to explore the brains pain modulatory circuits is through the use of a placebo analgesia paradigm. Placebo analgesia occurs when one expects a treatment to relieve pain, and a subsequent pain reduction occurs even though the treatment is inert. Importantly, placebo analgesia requires cognitive appraisal, therefore requiring input from higher order brain regions. Numerous brain imaging studies in humans have revealed that the hypothalamus, amygdala, anterior cingulate cortex (ACC) and the dorsolateral prefrontal cortex (dlPFC) are involved in mediating a placebo analgesic response (Bingel et al., 2006, Crawford et al., 2023a, Eippert et al., 2009). These regions appear to drive a key brainstem pain modulatory region, the midbrain periaqueductal gray matter (PAG), which in turn modulates incoming noxious information in the dorsal horn and spinal trigeminal nucleus via connections with the rostral ventromedial medulla (RVM) (Cheng et al., 1986, Crawford et al., 2021, Heinricher et al., 1994, Ossipov et al., 2010).

The ventrolateral PAG has long been associated with mediating placebo analgesia, primarily due to its opiate-mediated analgesic effects and the ability of opiate antagonists to attenuate placebo responses (Benedetti, 1996, Eippert et al., 2009, Grevert et al., 1983, Levine et al., 1978). However, a recent ultra-high field functional magnetic resonance imaging (fMRI) study has revealed that the lateral PAG (lPAG) column mediates non-opiate placebo analgesia (Crawford et al., 2021).

The lateral PAG exhibits a somatotopic organization, with pain experienced in the face and body eliciting signal increases in the rostral and caudal lateral PAG, respectively (Tinoco Mendoza et al., 2023). Previous animal research has demonstrated that the PAG can also produce a somatotopically organized analgesia, as electrical stimulation and morphine injection into the rostral and caudal PAG results in analgesia localized to the face and hindlimb regions of rodents, respectively (Soper and Melzack, 1982, Yaksh et al., 1976). Notably, we have recently shown that

placebo analgesic responses in humans also displays a similar pattern of somatotopy that was confined within the lateral PAG (Tinoco Mendoza et al., 2024). This functional organization raises two possibilities regarding top-down neural control. First, distinct descending neuronal populations may selectively activate the rostral and caudal PAG to induce regionally specific placebo analgesia. Second, a single descending neuronal population may drive the entire rostro-caudal extent of the lateral PAG, with somatotopically organized ascending noxious inputs then mediating this regionally restricted placebo analgesia.

Interestingly, a previous fMRI study has reported that noxious and innocuous median and tibial nerve electrical stimulation evoked fMRI signal intensity changes in spatially separate parts of the ACC. That is, ACC activation is more anterior from median nerve stimulation than with tibial nerve stimulation (Arienzo et al., 2006). Furthermore, we have recently demonstrated that noxious face stimuli evoked signal intensity decreases in the dlPFC whereas noxious body stimuli evoked signal increases (Robertson et al., 2024). Whilst these studies do not reveal a somatotopic organization, they suggest that the ACC and dlPFC display differential signal changes and a potential somatotopy during face versus body analgesia.

The aim of this study was to use ultra-high field fMRI to identify forebrain circuits mediating placebo analgesia across different body sites. Within the placebo network, four regions – the rACC, dlPFC, amygdala and hypothalamus – are critical nodes and have recently been shown to exhibit altered functional connectivity with the lateral PAG during a placebo analgesia response on the arm (Crawford et al., 2023). We hypothesized that placebo responses on the face and body would be characterized by activation patterns and lateral PAG connectivity strength changes in the ACC and dlPFC that are spatially separate. Since we know of no evidence of somatotopy in the amygdala and hypothalamus, we hypothesize that face and body placebo will not display spatially separate activation and lateral PAG connectivity patterns in these regions.

Methods:

Ethics:

All experimental procedures were approved by the University of Sydney Human Research Ethics Committee and were consistent with the Declaration of Helsinki. Written informed consent was obtained from participants at the commencement of the study. Participants were also provided with an emergency buzzer while inside the scanner so that they could stop the experiment at any time. At the conclusion of testing, participants were informed both verbally and through a written

statement of the necessary deception and true methodology of the experiment and were invited to seek clarification of what they had just experienced.

Participants:

Seventy healthy control participants were recruited for the study (33 male, 37 female; mean±SEM age, 24.6±0.5 years; range 20–38 years). In order to evaluate the necessary number of participants required for this study, an apriori power analysis was performed using results from a previous imaging study investigating brainstem connectivity during placebo analgesia (Crawford et al., 2021). This revealed a total sample size of 40 would be necessary to detect similar effect sizes with 95% power ($d = 0.31$, $\alpha = 0.05$, power = 0.95). Before beginning the study, participants completed a data sheet recording current medication(s), and any alcohol or caffeine ingested in the 24 hours prior to testing.

Experimental Design:

The study included three sessions occurring on two successive days: a conditioning session on day 1, and a reinforcement and MRI scanning session on day 2 (Figure1A). Throughout the study, noxious stimuli were administered to one of three places: the left and right cheek, volar surface of the forearm or on the shin of the lower leg. Brief noxious stimuli were delivered using a 3x3cm MR-compatible Peltier element thermode, which provided a heat stimulus at a pre-programmed temperature via a Thermal Sensory Analyzer (TSA-II) (Medoc LTD Advanced Medical Systems, Rimat Yishai, Israel). Each stimulus lasted 15 seconds, including a ramp-up period (four degrees per second), a plateau period at a noxious temperature and a ramp-down period (four degrees per second). Each stimulus was separated by a 15 second inter-stimulus-interval (ISI) at a non-painful baseline temperature of 32°C. Throughout conditioning, participants rated their pain on-line using a horizontal 10 cm visual analogue scale (VAS) ranging between 0 and 100, where 0 was described as “no pain” and 100 as “the worst pain imaginable”. During scanning, participants used an MR-compatible button box to continuously report their pain perception. The VAS scale was shown on a reflected digital screen at the end of the magnet bore, and participants controlled the position of a slider to report their pain continuously by holding the left (moved slider towards zero) or right (moved slider towards ten) buttons with their left middle and index finger.

Conditioning:

Session 1 was conducted outside the MRI and consisted of two rounds of a conditioning protocol. Participants were first informed both verbally and via a written statement that the study was designed to investigate the modulatory effects of a topical anesthetic containing lidocaine, which

had been shown to provide pain relief in some individuals. A second control cream was stated to be purely Vaseline and was stated as being necessary to evaluate typical pain responses. In reality, both creams contained vaseline and only differed in color and their described properties. We calculated individual low and moderate pain responses by applying a series of randomised stimuli to the right face, arm or leg ranging from 44-48.5 degrees, asking participants to rate their perceived pain during each stimulus. Participants were informed that we were only recording a temperature which elicited a moderate subjective pain response (40-50 VAS rating), and that this temperature would be used throughout the remainder of the experiment. However, using the ratings provided during this process, we recorded two different temperatures: one which was rated between 20-30 on the VAS (low temperature); and one which was rated between 40-50 (moderate temperature). These two temperatures were then deceptively applied to the "lidocaine" and Vaseline cream sites throughout the conditioning and reinforcement experimental phases.

Creams were then applied to two adjacent 3x3 cm squares on the participants' right face, arm or leg. To enhance the believability that the "lidocaine" cream contained an active analgesic, a false label was attached to the cream bottle and green food coloring was added. The positions of the "lidocaine" and vaseline creams were counterbalanced between participants to reduce potential confounders of local sensitivity. Ten minutes following cream application, we conducted two rounds of conditioning. Participants believed they would receive eight identical moderate thermal stimuli and were instructed to report their perceived pain intensity using the VAS. Participants were also asked prior to each set of stimuli for an average expectation of the pain they would experience, which acted both to measure belief that lidocaine was working to modulate their subjective pain, and to reinforce the pain-relieving quality of the cream. During the two conditioning rounds we deceptively applied a moderate temperature to the control vaseline-site, and a low temperature to the placebo lidocaine-site.

Reinforcement and Test:

At approximately the same time on the following day, sessions 2 and 3 were conducted with participants inside the MRI scanner and consisted of a reinforcement protocol (session 2) and a test protocol (session 3). The creams were applied to the same part of the face, arm or leg, in the same order and locations as session 1, but on both the left and right sides, and participants were reminded of the "lidocaine's" pain-relieving qualities. Reinforcement was conducted by applying four noxious stimuli at the same low and moderate temperatures that were used throughout session 1 applied to the left face, arm or leg. This reinforcement protocol was conducted to

ensure that participants continued to report different expectations and pain ratings between the two cream sites despite the change in day and environment (inside the MRI). Furthermore, the reinforcement was performed on the opposite sites of testing (the left face, arm and leg) to prevent sensitization.

Following reinforcement, we waited 15 minutes for residual pain and sensitivity to dissipate from all three body sites before beginning the test protocol. During this 15-minute period, structural brain scans were collected. Unlike conditioning and reinforcement, during the test phase we applied *identical moderate temperature stimuli* to both the control vaseline- and placebo lidocaine-sites (Figure 1A). We asked each participant for an average expectation of pain intensity directly prior to each stimulation series and instructed them to report the pain intensity continuously throughout the duration of the scan using the button box and the projected digital VAS. VAS responses were recorded every 0.5 seconds, and values during each pain period were averaged providing a pain intensity for each noxious stimulus period. Each participant received two consecutive series of eight stimuli, with a separate functional series collected during each series of stimuli. Each fMRI series began with a 90-second baseline period prior to the eight stimuli presentations. The control vaseline-site was always stimulated during the first series, and the placebo lidocaine-site stimulated during the second series, so that we generated a "pre" and "post" condition, or, functional brain images encoding typical and placebo pain responses, respectively.

MRI data acquisition and preprocessing:

Brain images were acquired using a whole-body Siemens MAGNETOM 7 Tesla (7T) MRI system (Siemens Healthcare, Erlangen, Germany) with a combined single-channel transmit and 32-channel receive head coil (Nova Medical, Wilmington MA, USA). Participants were positioned supine with their head in the coil and sponges supporting the head laterally to minimize movement. A T1-weighted anatomical image set covering the whole brain was collected (repetition time=5000ms, echo time=3.1ms, raw voxel size=0.73x0.73x0.73mm, 224 sagittal slices, scan time=7mins). The two fMRI acquisitions each consisted of a series of 134 gradient echo echo-planar measurements using blood oxygen level dependent (BOLD) contrast covering the entire brain. Images were acquired in an interleaved collection pattern with a multi-band factor of four and an acceleration factor of three (repetition time=2500ms, echo time=26ms; raw voxel size=1.0x1.0x1.2mm, 124 axial slices, scan time=5:35mins).

Image preprocessing and statistical analyses were performed using SPM12 and custom software. The first five volumes of each scan were removed from the model due to excessive signal

saturation from the scanner. The remaining 129 functional images were slice-time, motion corrected, and the resulting 6 directional movement parameters inspected to ensure that all fMRI scans had no greater than 1mm of linear movement or 0.5 degrees of rotation movement in any direction. Images were linearly detrended to remove global signal changes, physiological noise relating to cardiac and respiratory frequency filtered and removed using the DRIFTER toolbox (Särkkä et al., 2012), and the 6-parameter movement related signal changes were modelled and removed using a linear modelling of realignment parameters (LMRP) procedure. Each individual's fMRI image sets were then co-registered to their own T1-weighted anatomical and underwent distortion correction using the SynBOLD DisCO toolbox (Yu et al., 2023).

Following anatomical co-registration, the T1-weighted image was then spatially normalized to the DARTEL template in Montreal Neurological Institute (MNI) space and the parameters applied to the fMRI image sets. The normalized fMRI images were then resliced into 1mm isotropic voxels, and spatially smoothed using a 2mm and 6mm full width at half maximum Gaussian filter. These smoothing kernels were used to investigate subcortical structures and cortical structures, respectively. In addition, the brainstem and cerebellum were isolated using the spatially unbiased infra-tentorial template (SUIT) toolbox (Diedrichsen, 2006), for both the fMRI and T1 image sets, and then normalized to the brainstem- and cerebellum-only SUIT template in Montreal Neurological Institute (MNI) space. During this process, both the T1 structural and functional image sets were resliced into 0.5mm isotropic voxels and these images were spatially smoothed using a 1mm FWHM Gaussian filter. A small smoothing kernel was used to allow for the accurate seed selection and signal intensity extraction from the rostral and caudal lateral PAG.

Dichotomizing placebo responder and non-responder groups:

Participants were grouped as either a responder or non-responder to placebo analgesia based on a permutation procedure. Briefly, mean VAS ratings to each of the 8 noxious stimuli delivered during the control stimulated series were entered to a permutation model, where 10,000 artificial sample were generated with replacement. This artificial sample was significance tested to 10,000 artificial samples generated from the VAS ratings to each 8 noxious stimuli delivered during the 'lidocaine' stimulated series. If the mean difference between the two series was significant, with the 'lidocaine' significantly lower than the control, a participant was considered a responder. If not, they were considered a non-responder.

Significant differences between groups with respect to expected changes in pain intensities immediately prior to testing were determined using paired t-tests (two-tailed, $p<0.05$). Since

participants were grouped into either responder or non-responder categories based on their perceived pain intensities during the fMRI scans (session 3), we did not assess significant differences between groups for the perceived pain intensity changes. A single factor ANOVA ($p<0.05$) was also used to determine if there were differences in the temperature applied or pain intensity ratings reported between responder and non-responder groups during the control stimulated series to ensure any reported placebo effects did not relate to baseline thermal sensitivity. In addition, we calculated each participants analgesic ability by calculating the percentage change in mean pain intensity ratings during the control compared with the placebo scan. A greater analgesic ability value represents a greater pain reduction during the lidocaine compared with vaseline scan.

fMRI statistical analysis:

To determine significant changes in signal intensity during each noxious thermal period, a repeating boxcar model convolved with a canonical hemodynamic response function was applied to each of the fMRI series. Within this model, scanning volumes overlying stimulus plateau periods were assigned a value of 1, and inter-stimulus-intervals and the initial 90-second baseline period were assigned a value of 0. The contrast images generated for each functional image series were then used in two separate group analyses.

Firstly, a random-effects paired, voxel-by-voxel analysis was conducted in placebo responders comparing the vaseline and lidocaine scans for the face, arm and leg separately. Since we aimed to explore signal changes in the rACC and dlPFC, we created bilateral masks of these regions using parcels derived from the extended Human Connectome Project atlas (HCPex) (Huang et al., 2022). Similarly, subcortical masks encompassing the entire bilateral amygdala and hypothalamus were also created using the HCPex atlas and based on Neudorfer and colleagues' (2020) atlas with slight adjustments (Figure 1C). Restricted to these four brain regions, we determined analgesia-related signal intensity changes between the vaseline and lidocaine cream scans in the placebo responder groups for the face (n=9), arm (n=22) and leg (n=25) by placing the contrast images into three separate second-level, random-effects analyses ($p<0.005$ uncorrected with a cluster extent threshold of 20 and 4 contiguous voxels for cortical and sub-cortical structures, respectively). Significant clusters were overlayed onto an anatomical MNI T1 template for visualization purposes. For each significant cluster, signal intensity change differences (lidocaine-vaseline) were extracted from each individual and for each of the three stimulation sites– face, arm and leg. For the stimulation sites not related to the generation of the significant cluster, significant signal intensity changes were determined using a one-sample

paired t-tests ($p<0.05$, vaseline versus lidocaine scans). That is, for a cluster derived from the face analgesia analysis, we extracted β-value changes for the face as well as the arm and leg analgesia scans. To avoid double dipping, we did not assess the significance of the face β values, but instead restricted this to the arm and leg β-value changes.

In the second analysis, a seed-based functional connectivity analysis was performed to explore how signal intensity changes covary between the lateral PAG and our cortical and subcortical regions of interest. Previously, we have identified that the ipsilateral (to side of stimulation) lateral PAG displays significant signal intensity changes during placebo analgesia, and that this signal change is located in the rostral lateral PAG during face and in the caudal lateral PAG during body analgesia (Tinoco Mendoza et al. 2024). Using the peak location of these two clusters, we generated two 1mm radius spherical volume of interest (VOI) in the rostral and caudal lateral PAG and used these as "seeds" to explore connectivity during face and body analgesia responses (X, Y, Z MNI co-ordinates: face: 2, -31, -6; arm/leg: 2, -32, -9). We extracted the signal intensity changes from the SUIT-isolated brainstem images over the entire vaseline and lidocaine scans and determined coupling between these two lPAG seed signal changes and signal changes in each voxel of the brain restricted to our regions of interest (Figure 1D).

The resulting contrast images for the vaseline and lidocaine scans in each individual were then placed into a random-effects, paired, voxel-by-voxel analysis for the face, arm and leg in the responder group ($p<0.005$ uncorrected with a cluster extent threshold of 20 and 4 contiguous voxels for cortical and sub-cortical structures, respectively). For each significant cluster, lateral PAG connectivity change differences (lidocaine-vaseline) were extracted from each individual and for each of the three stimulation sites – face, arm and leg. For the stimulation sites not related to the generation of the significant cluster, significant signal intensity changes were determined using one-sample, paired t-tests ($p<0.05$, vaseline versus lidocaine scans). Significant clusters were overlayed onto an anatomical MNI T1 template for visualization purposes. For cluster localization and identification, we used the atlas by Huang and colleagues (2022) in addition to Mai and Majtanik (2017) for nuclei of the amygdala and hypothalamus.

Results:

Psychophysics: Despite all participants expecting pain relief, only 9 of the 22 (41%) face placebo participants, 22 of the 46 (48%) arm placebo participants and 25 of the 41 (61%) leg participants displayed a significant reduction in perceived pain intensity during the lidocaine compared with

vaseline cream scans (Figure 1B). There were no significant differences between the responder and non-responder groups with respect to thermode temperature (mean±SEM ^{0}Celcius responder versus non-responder: face 46.6±0.3 vs 46.3±0.2; arm 46.9±0.2 vs 46.8±0.2; leg 46.4±0.1 vs 46.2±0.2, all $p>0.05$).

Analgesia-evoked signal intensity increases:

Comparison of signal intensity changes during vaseline versus lidocaine scans in the responder group resulted in significant signal intensity changes in the rostral ACC (rACC) and dlPFC during face and arm analgesia but not during leg analgesia (Figure 2A). In addition, we found no significant signal intensity changes in either the amygdala or the hypothalamus. Whilst both face and arm analgesia were associated with signal intensity increases in the left rACC, the location of signal changes during arm analgesia were anterior/rostral to those during face analgesia. Similarly, whilst both face and arm analgesia evoked signal intensity increases in the right dlPFC at the same dorso-ventral level, the location of signal changes during arm analgesia were anterior to those during face analgesia (Figure 2B). Extraction of rACC signal intensity changes from the face cluster across all three sites revealed signal intensity increases in face analgesia (as expected) as well as arm analgesia, but not leg analgesia (mean±SEM β value changes: *face:* vaseline 0.16±0.10, lidocaine 0.52±0.12; *arm:* vaseline -0.28±0.15, lidocaine 0.13±0.17; *leg:* vaseline 0.04±0.09, lidocaine 0.28±0.17; face, arm $p<0.05$; leg $p>0.05$). In contrast, the arm cluster was associated with signal increases during arm analgesia (as expected), but no significant changes during face or leg analgesia (mean±SEM β value changes: *face:* vaseline 0.37±0.22, lidocaine 0.07±0.13; *arm:* vaseline -0.29±0.15, lidocaine 0.13±0.17; *leg:* vaseline -0.24±0.10, lidocaine -0.31±0.15; arm $p<0.05$; face, leg $p>0.05$). For the right dlPFC, extraction of signal changes revealed the face cluster was associated with signal intensity increases during face analgesia (as expected) and no significant change during arm or leg analgesia (mean±SEM β value changes: *face:* vaseline -0.06±0.19, lidocaine 0.66±0.18; *arm:* vaseline 1.58±0.27, lidocaine 1.61±0.30; *leg:* vaseline 0.81±0.18, lidocaine 0.66±0.34; face $p<0.05$; arm, leg $p>0.05$). Similarly, for the arm cluster, arm placebo evoked signal intensity increases (as expected) and again no significant change during face or leg analgesia (mean±SEM β value changes: *face:* vaseline 0.19±0.25, lidocaine 0.10±0.25; *arm:* vaseline -0.03±0.25, lidocaine 0.46±0.23; *leg:* vaseline -0.01±0.16, lidocaine -0.27±0.33; arm $p<0.05$; face, leg $p>0.05$).

Analgesia-evoked lateral PAG connectivity increases with cortical regions:

Functional connectivity analysis revealed significantly greater lateral PAG connectivity across the entire vaseline scan compared with lidocaine scans for the face and arm but not leg analgesia in

the rACC and dlPFC (Figure 3). In contrast to rACC signal intensity changes, both the face and arm connectivity changes were on the right side of the rACC and in different locations, with the face more rostral to the arm. Extraction of rACC connectivity strength changes from the face cluster across all three sites revealed that face analgesia evoked connectivity increases (as expected), but no change during the arm and leg analgesia (mean±SEM β value changes $x10^2$: *face:* vaseline -0.80±0.47, lidocaine 3.08±0.82; *arm:* vaseline 1.89±0.91, lidocaine 1.62±0.99; *leg:* vaseline 2.06±1.41, lidocaine 2.36±1.41; face $p<0.05$, arm, leg $p>0.05$). In contrast, the arm cluster was associated with connectivity strength increases during both arm (as expected) and face analgesia, but not leg analgesia (mean±SEM β value changes: *face:* vaseline -0.52±1.25, lidocaine 3.01±1.29; *arm:* vaseline -0.52±0.82, lidocaine 2.49±0.73; *leg:* vaseline 1.78±1.01, lidocaine -0.17±0.95; face, arm $p<0.05$; leg $p>0.05$). Similarly, functional connectivity analysis revealed greater lPAG connectivity for the face and arm but not leg analgesia in the dlPFC on the left side of the brain, i.e. again on the opposite side to the signal intensity change differences, and with the face more rostral to the arm. Extraction of dlPFC connectivity strength changes from the face cluster across all three sites revealed that face analgesia evoked connectivity increases (as expected), but no change during the arm and leg analgesia (mean±SEM β value changes $x10^2$: *face:* vaseline -0.07±2.26, lidocaine 5.97±1.52; *arm:* vaseline 0.63±1.14, lidocaine 1.35±0.98; *leg:* vaseline 0.65±1.30, lidocaine 0.25±1.47; face $p<0.05$; arm, leg $p>0.05$), with a similar pattern for the arm cluster (mean±SEM β value changes: *face:* vaseline -0.99±1.30, lidocaine -0.63±1.56; *arm:* vaseline -0.30±0.93, lidocaine 3.07±1.00; *leg:* vaseline 2.72±1.27, lidocaine 1.00±1.62; arm $p<0.05$; face, leg $p>0.05$).

Analgesia-evoked lateral PAG connectivity decreases with the amygdala and hypothalamus:

Functional connectivity analysis revealed significantly reduced lateral PAG connectivity with the amygdala again for the face and arm but not leg analgesia (Figure 4A). Both face and arm connectivity changes were in the right amygdala and in the same nucleus, the basolateral complex. Extraction of connectivity strength changes from the face cluster across all three sites revealed that both face and arm analgesia evoked connectivity decreases, whereas during the leg analgesia there was a small increase (mean±SEM β value changes $x10^2$: *face:* vaseline 2.41±3.07, lidocaine -5.49±3.36; *arm:* vaseline 2.52±2.61, lidocaine -3.18±1.84; *leg:* vaseline 0.22±1.49, lidocaine 3.54±1.45; face, arm, leg $p<0.05$). In contrast, the arm cluster was associated with connectivity strength decreases during arm, but not face and leg analgesia (mean±SEM β value changes: *face:* vaseline 2.57±1.24, lidocaine -3.13±3.34; *arm:* vaseline 6.45±1.99, lidocaine -3.68±1.48; *leg:* vaseline 1.79±1.53, lidocaine 0.08±0.95; arm $p<0.05$; face, leg $p>0.05$).

Functional connectivity analysis also revealed significantly reduced lateral PAG connectivity with the hypothalamus for the face and leg but not the arm analgesia (Figure 4B). This is the only region where either signal or connectivity change differences reached significance for the leg and not for arm analgesia. Extraction of connectivity strength changes from the arm cluster across all three sites revealed that only arm analgesia evoked lPAG-hypothalamus connectivity decreases (mean±SEM β value changes $x10^2$: *face:* vaseline -14.45±3.33, lidocaine -7.72±6.51; *arm:* vaseline 5.05±1.48, lidocaine -1.05±1.82; *leg:* vaseline 0.10±1.65, lidocaine -0.53±1.83; arm $p<0.05$; face, leg $p>0.05$). However, whilst the voxel-by-voxel analysis did not reveal significant connectivity changes during face analgesia, extraction of connectivity strength values from the leg cluster revealed that both the leg and face analgesia evoked decreases in lateral PAG-hypothalamus connectivity (mean±SEM β value changes: *face:* vaseline -1.75±2.26, lidocaine -6.55±4.16; *arm:* vaseline 1.87±1.78, lidocaine -1.21±2.05; *leg:* vaseline 3.54±1.26, lidocaine -2.52±1.35; face, leg $p<0.05$; arm $p>0.05$).

Discussion:

Our results reveal the first exploration of descending circuits involved in generating a placebo response across different body sites. The convergent activity and connectivity changes observed within the rACC, amygdala and hypothalamus across different body sites may potentially form a core descending pain modulatory circuit. That is, regardless of whether placebo is mounted in the face or body, the PAG communicates with these three regions in a fashion where there is cortical cross-communication between face and body circuits. On the contrary, the dlPFC appears to be more selective in its regional changes in activity, depending on where in the body analgesia occurs. The presence of overlapping and divergent signal and connectivity changes suggests that these forebrain regions likely drive different aspects of the placebo analgesia response.

Our data reveals that although analgesia on the arm evokes increases in signal intensity at a location in the rACC that is more anterior/rostral than during face analgesia there is also some overlap between sites. Similarly, whilst lateral PAG-rACC connectivity changes during face placebo are located rostrally than lateral PAG-rACC connectivity during arm placebo, again there is some overlap between sites. We have previously shown that rACC signal intensity changes drive lateral PAG signal changes during placebo analgesia, strongly suggesting that this circuit is critical in driving the brainstem circuitry responsible for placebo analgesia (Crawford et al., 2023a). The largely spatially separate signal and connectivity changes in the rACC may underpin

a somatotopic drive onto the lateral PAG to mediate a body specific analgesia. While a somatotopic organization within the lateral PAG is well-established in animals (Wiberg et al., 1987, Yezierski, 1988) this has only recently been demonstrated in humans (Tinoco Mendoza et al., 2023). This organizational principle extends across multiple brain regions, even outside those thought to consciously code stimulus location such as S1. For example, thermal noxious stimulation of the face relative to the hand and leg activates a anterior-posterior somatotopic arrangement in the dorso-posterior insula in humans (Brooks et al., 2005), a result replicated during muscular pain on the hand and leg (Macefield et al., 2007). While similar somatotopic patterns have also been observed in S2 (Bingel et al., 2004), these studies across multiple body sites are rare and often do not focus on pain modulatory regions. One such experiment focusing on the ACC found that electrical noxious stimulation of the median nerve results in a more anterior activation than tibial nerve stimulation (Arienzo et al., 2006). While we did not observe this same pattern of activation between arm and leg analgesia, the ACC seems to exhibit a degree of somatotopy during pain processing that might drive different rostro-caudal regions of the lateral PAG.

Anatomical tract-tracing studies have shown that the ACC targets the lateral as well as the ventrolateral and dorsomedial columns of the PAG (An et al., 1998, Leichnetz et al., 1981, Müller-Preuss and Jürgens, 1976). Critically, anterograde tracing in rodents has revealed that multiple injections into the medial cortical field, encompassing the ACC and pre-limbic areas, densely labels the PAG bilaterally but more heavily on the ipsilateral side (Shipley et al., 1991). Whilst this tract tracing study did not explore the lateral PAG specifically, it did reveal that projections from individual regions of the medial and lateral cortical fields terminate with a high degree of specificity along the rostro-caudal axis of PAG. They suggest that these highly specific patterns could preferentially influence specific rostro-caudal parts of the PAG. Indeed, our results are consistent with these tract-tracing findings revealing that there is separation between rACC activity and lateral PAG connectivity changes during analgesia evoked on the face compared with the body.

Spatially restricted analgesia has been shown to occur only at sites of ongoing pain where pain reduction is expected (Benedetti et al., 1999, Montgomery and Kirsch, 1996). The opioid antagonist naloxone can abolish this specificity, indicating that endogenous opioids are organized topographically and play a role in analgesia that is spatially specific (Benedetti et al., 1999). As such, the opioid response is likely to heavily influence higher brain centers, like the ACC, when a placebo response is mounted; on the contrary, the lateral PAG appears to be primarily involved in non-opiate placebo analgesia. This highly organized network of endogenous

opioids could link cognitive, sensory and emotional factors to create a spatially specific placebo analgesic response via the somatotopic organization of the PAG. It is possible that during placebo analgesia, rACC-lateral PAG connections are able to drive specific rostro-caudal parts of the lateral PAG, which in turn targets incoming noxious inputs from either the head or the body to produce a spatially restricted analgesia.

We also found spatially separate dlPFC signal and lateral PAG connectivity changes during analgesia evoked in the head compared with the body. Placebo analgesia is driven by cognitive and evaluative mechanisms, and it has been reported that increased dlPFC activity has been associated with placebo analgesia and correlated with activity in the PAG (Crawford et al., 2023b, Wager et al., 2004), and the analgesic effects of perceived pain control is correlated with dlPFC activity (Wiech et al., 2006). It has also been reported that analgesia-related dlPFC activation and altered dlPFC-lateral PAG connectivity correlated with dlPFC glutamate levels (Crawford et al., 2023b). The dlPFC is involved in expectations, decision making and error-prediction (Hibi et al., 2020, Rosenbloom et al., 2012, Schenk and Colloca, 2019, Wager et al., 2004) and demonstrates reduced activation, alongside altered coupling patterns with pain processing areas such as the posterior insula, S1 and the PAG, in individuals who express greater variation in perceived pain intensity during a series of identical noxious stimuli (Crawford et al., 2022). Furthermore, repetitive transcranial magnetic stimulation can relieve capsaicin-induced pain (Brighina et al., 2011) and transient direct current dlPFC stimulation boosts placebo analgesia responses (Tu et al., 2021). It should also be noted that we know of no other studies that has demonstrated a somatotopic organization of nociceptive or anti-nociceptive processing in the dlPFC. In this way, we posit that the dlPFC can preferentially modulate specific parts of the lateral PAG as does the rACC.

In addition to changes in cortical structures we found significant differences in PAG connectivity with the amygdala and hypothalamus between face and arm analgesia. Humans exhibit greater complexity in how thought and emotion influence pain perception than other mammals. Indeed, the ACC, a cortical region, and the amygdala, a subcortical region, are highly developed in humans due to their key roles in emotion and mood (Bandler et al., 2000), although their projections to the PAG appear evolutionarily stable across animal species (An et al., 1998, Floyd et al., 2000). The amygdala has direct projections to the ACC and bidirectional connections with the PAG; that is, inputs to the basolateral complex and outputs from the central nucleus (Olucha-Bordonau et al., 2015, Vogt, 2015). Our results demonstrate decreased lateral PAG-amygdala connectivity in face and arm analgesia in the region of the basolateral complex. This nucleus plays a prominent role in modulating pain by relating information to the hypothalamus

(Neugebauer et al., 2009) and integrating sensory inputs across the prefrontal cortex, ACC and PAG (Romanski et al., 1993). Similarly, the observed decrease in hypothalamus-lateral PAG connectivity during leg analgesia, that was also significant during in face analgesia subjects, appears to correspond with the ventromedial hypothalamus, a nucleus crucial for defensive behaviors and which targets the lateral PAG (Wang et al., 2015, Yates, 2015).

Importantly, we did not find any significant signal intensity changes associated with placebo analgesia induced on the leg. In our experimental paradigms, we attempted to match perceived pain intensities during face and body pain by assessing pain intensity placed on the arm prior to entering the MRI scanner. Using the same temperature on all three body sites resulted in a slightly lower perceived pain intensity during leg stimulation compared with the arm and face. Indeed, there are fewer and sparser tactile cutaneous afferent fibers in the lower leg relative to the arm and especially the face (Corniani and Saal, 2020, Löken et al., 2022). The trigeminal nerve tributaries also have the highest density of thermal-sensitive receptors and proportion of A-fiber nociceptors compared to the limbs at the spinal level (Cohen, 2006, Sharav and Benoliel, 2008). Furthermore, pain on the head and orofacial region elicits a higher fear response than pain on the hand and leg region and has been associated with enhanced signal activation and connectivity changes in the amygdala (Meier et al., 2014, Schmidt et al., 2016, Robertson et al., 2024). Therefore, while our participants experienced a placebo response, the nociceptive drive and fear response from noxious stimulation to the leg may have resulted in lower activity that was not detectable at our significance threshold, in the areas we focused on that are implicated in affective and emotional processing.

There are several limitations of this investigation worth noting. Firstly, whilst our focus was to identify a functional network responsible for placebo responders, it would be of interest to better understand the difference in this same network in individuals that fail to generate significant analgesic responses to placebo. In this way, we could assess whether the network involving the rACC, amygdala and hypothalamus in modulating pain-related activity within the lateral PAG is a hard-wired nociceptive circuit or a corollary of an analgesic response. Secondly, there was a variable number of placebo responders across our placebo paradigms on each body site, particularly for the face, and no participant had placebo analgesia paradigms applied to all three body sites. As such, we were unable to localize individual differences in our regions-of-interest in a placebo responder across all three body sites, which would be of interest in future investigations to compare. Thirdly, functional analyses utilized a threshold at $p<0.005$, uncorrected for multiple comparisons. To reduce the chances of Type II errors, we implemented a minimum cluster threshold of 20 and 4 contiguous voxels in the whole brain and restricted our

analysis to the voxels that comprised our cortical and sub-cortical structures, respectively. Also, although we measured pain intensity, we did not measure the emotional component of the noxious stimulus, such as fear of pain, threat anticipation or pain catastrophizing. Exploring a possible relationship between the affective quality of each stimulus and significant regional brain activity could have allowed us to investigate possible variables related to fear and anxiety that may have an influence as to where in the body analgesia occurs. Fourthly, it was not possible to fully counterbalance the ordering of stimuli since the experimental design required a pairing of modulated with non-modulated responses. Lastly, we restricted our analyses to only four regions involved in placebo analgesia to conduct a seed-to-seed analysis and improve statistical power. While they are key structures involved in endogenous pain modulation, the neural circuits underlying placebo analgesia are extensive and it is likely that other structures are also heavily involved in mediating analgesia through the lateral PAG.

Ultimately, we provide evidence for separate descending modulatory networks involving the rACC, dlPFC, amygdala and hypothalamus that mediate analgesia evoked in either the face or body. The dlPFC has most likely evolved within the top-down modulatory pain pathways in humans and is necessary to localize the body area where analgesia should occur during a placebo response. Our findings highlight the need to account for body location when exploring pain-related signal changes in cortical and sub-cortical regions and warrant future investigations to explore this further using other analgesic paradigms.

Tables:

Table 1. Locations, cluster sizes (number of voxels) and t-values for cortical and sub-cortical seed regions that displayed significantly different signal intensity changes between vaseline and lidocaine cream sites for the face and arm stimulation sites in responders. Co-ordinates are shown in Montreal Neurological Institute (MNI) space. *rACC* = rostral anterior cingulate cortex; *dlPFC* = dorsolateral prefrontal cortex.

		MNI coordinates				
		X	**Y**	**Z**	**cluster size**	**t-value**
rACC	face	-11	26	30	15	5.08
lidocaine > vaseline	arm	-11	39	8	38	3.11
dlPFC	face	41	7	33	34	7.24
lidocaine > vaseline	arm	23	28	34	140	4.11

Table 2. Locations, cluster sizes (number of voxels) and t-values for regions that displayed altered connectivity across the entire vaseline compared with lidocaine scans for the face, arm and leg in responders. Co-ordinates are shown in Montreal Neurological Institute (MNI) space. dlPFC: dorsolateral prefrontal cortex, rACC: rostral anterior cingulate cortex.

		MNI coordinates				
		X	**Y**	**Z**	**cluster size**	**t-value**
rACC	face	2	37	30	96	4.86
lidocaine > vaseline	arm	8	36	22	51	3.25
dlPFC	face	-37	22	38	77	4.37
lidocaine > vaseline	arm	-43	4	37	26	4.48
amygdala	face	-20	-1	-22	4	4.88
vaseline > lidocaine	arm	-22	-1	-20	17	4.36
	leg	23	-5	-27	4	2.72
hypothalamus	arm	3	2	-9	5	3.36
vaseline > lidocaine	leg	-3	-2	-16	12	4.13

Figure Legends:

Figure 1. Experimental protocol and pain intensity changes. A) Analgesia paradigm. Conditioning was performed by applying low intensity noxious stimuli to the lidocaine site and moderate intensity to the vaseline site; crucially, during this phase participants deceptively believed stimuli of moderate intensity were being applied to both sites. On the following day, a reinforcement phase was conducted using the low and moderate temperatures on the opposite side of the body. Following a washout period, two independent functional magnetic resonance imaging (fMRI) series were collected where identical moderate intensity noxious stimuli to the vaseline (scan 1), and lidocaine cream (scan 2) sites were applied sequentially. During these two series, participants rated their expected and perceived pain on an MR-compatible visual analogue scale (0 = no pain, 100 = worst pain imaginable). R: right, L: left. **B) Perceived pain intensity changes.** Raincloud plot displaying the distribution of perceived pain scores during control and placebo cream stimulation. The coloured circles, horizontal white line on the box plot and black circle with error bars indicate individual pain scores, median perceived pain intensity and mean (±SEM) perceived pain intensity, respectively, across the face, arm and leg in placebo responders. *p<0.05. **C) Cortical and sub-cortical seeds of interest.** The bilateral rostral anterior cingulate cortex (rACC), dorsolateral prefrontal cortex (dlPFC), amygdala and hypothalamus were selected based on their demonstrated roles in placebo analgesia. The rACC and dlPFC are only showing one side for visualisation purposes. **D) Functional connectivity analysis.** Control vaseline- and placebo lidocaine-site functional scans were analyzed, allowing us to determine which seeds of interest altered their ongoing coupling with the lateral midbrain periaqueductal gray (PAG) during placebo analgesia. For placebo effects on the face and body (arm and leg), rostral and caudal seeds of the lateral PAG were derived from the peak coordinates of a previously shown somatotopic organization in the PAG (Tinoco Mendoza et al. 2024).

Figure 2. Analgesia evoked signal intensity changes between vaseline and lidocaine cream stimulation in the rostral anterior cingulate cortex and dorsolateral prefrontal cortex. A) Significant signal intensity increases (*hot* colour scale) in the rostral anterior cingulate cortex (rACC) during placebo analgesia on the face and arm overlaid onto a T1-weighted anatomical template. Slice locations in Montreal Neurological Institute Space are indicated at the top left of each slice. Below each slice are plots of mean±SEM signal intensity changes (β values) from extracting the significant cluster from each individual and for each of the three stimulation sites on the face, arm and leg. **B)** Significant signal intensity increases (*hot* colour scale) in the

dorsolateral prefrontal cortex (dlPFC) during placebo analgesia on the face and arm overlaid onto a T1-weighted anatomical template. Below each slice are plots of mean±SEM signal intensity changes (β values) from extracting the significant cluster from each individual and for each of the three stimulation sites on the face, arm and leg. *p<0.005 and #p<0.05

Figure 3. Analgesia evoked functional connectivity changes between the lateral midbrain periaqueductal gray matter and the rostral anterior cingulate cortex and dorsolateral prefrontal cortex. A) Significant increases in functional coupling (*hot* colour scale) in the rostral anterior cingulate cortex (rACC) during placebo analgesia on the face and arm overlaid onto a T1-weighted anatomical template. Slice locations in Montreal Neurological Institute Space are indicated at the top left of each slice. Below each slice are plots of mean±SEM connectivity changes (β values) from extracting the significant cluster from each individual and for each of the three stimulation sites on the face, arm and leg. **B)** Significant increases in functional coupling (*hot* colour scale) in the dorsolateral prefrontal cortex (dlPFC) during placebo analgesia on the face and arm overlaid onto a T1-weighted anatomical template. Slice locations in Montreal Neurological Institute Space are indicated at the top left of each slice. Below each slice are plots of mean±SEM connectivity changes (β values) from extracting the significant cluster from each individual and for each of the three stimulation sites on the face, arm and leg. The seeds used in this analysis are the rostral and caudal lateral PAG corresponding to the face-and body (arm and leg) placebo paradigms, respectively. *p<0.005 and #p<0.05

F**igure 4. Analgesia evoked functional connectivity changes between the lateral midbrain periaqueductal gray matter and the amygdala and hypothalamus. A)** Significant decreases in functional coupling (*hot* colour scale) in the amygdala during placebo analgesia on the face and arm overlaid onto a T1-weighted anatomical template. Slice locations in Montreal Neurological Institute Space are indicated at the top left of each slice. Below each slice are plots of mean±SEM connectivity changes (β values) from extracting the significant cluster from each individual and for each of the three stimulation sites on the face, arm and leg. **B)** Significant decreases in functional coupling (*hot* colour scale) in the hypothalamus during placebo analgesia on the arm and leg overlaid onto a T1-weighted anatomical template. Slice locations in Montreal Neurological Institute Space are indicated at the top left of each slice. Below each slice are plots of mean±SEM connectivity changes (β values) from extracting the significant cluster from each individual and for each of the three stimulation sites on the face, arm and leg. The seeds used in this analysis are the rostral and caudal lateral PAG corresponding to the face-and body (arm and leg) placebo paradigms, respectively. *p<0.005 and #p<0.05

Figure 1:

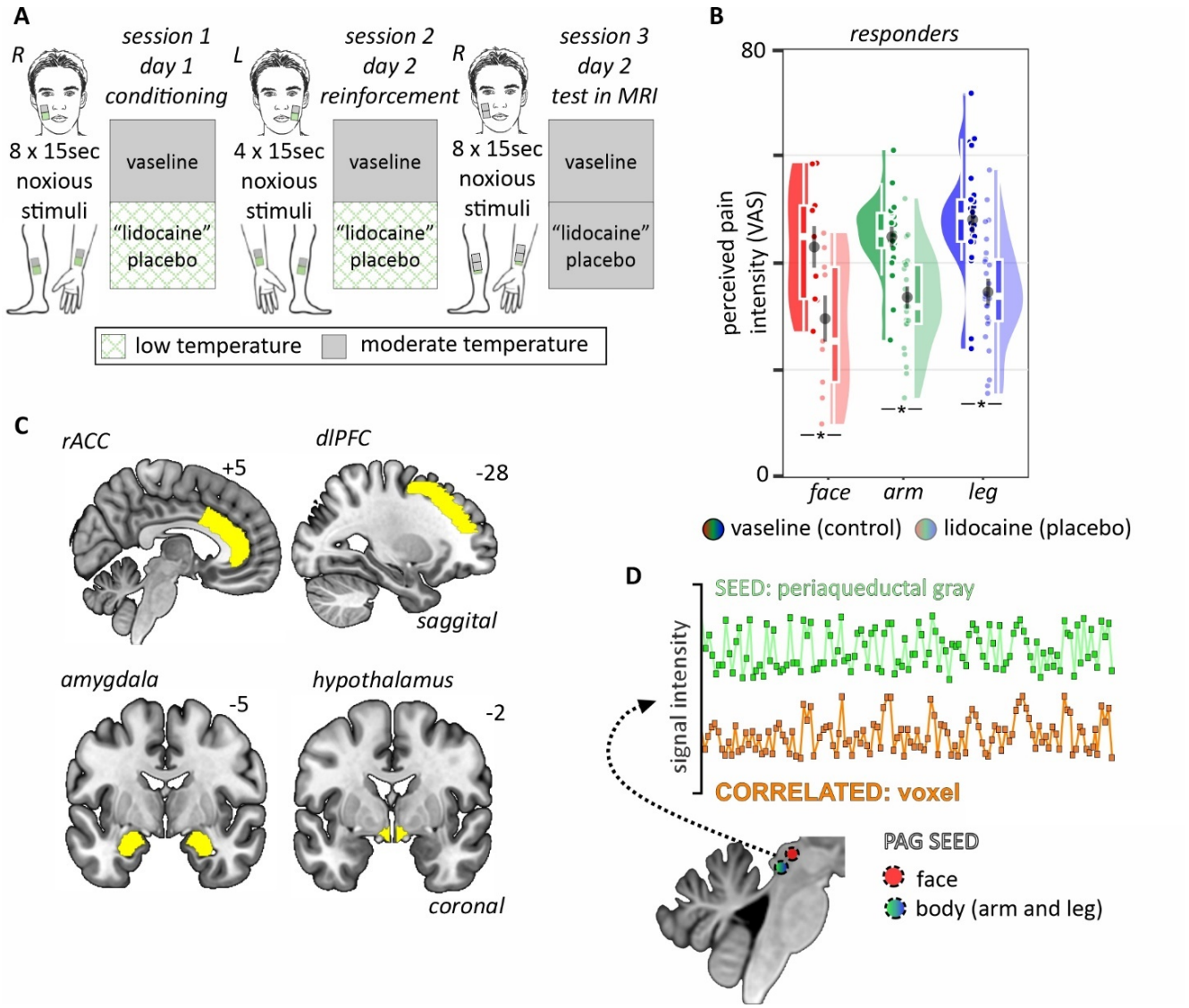
A
R
session 1
day 1
conditioning
8 x 15sec
noxious
stimuli
vaseline
"lidocaine"
placebo
L
session 2
day 2
reinforcement
4 x 15sec
noxious
stimuli
vaseline
"lidocaine"
placebo
R
session 3
day 2
test in MRI
8 x 15sec
noxious
stimuli
vaseline
"lidocaine"
placebo
low temperature
moderate temperature
B
responders
80
0
perceived pain
intensity (VAS)
face
arm
leg
vaseline (control)
lidocaine (placebo)
C
rACC
+5
dlPFC
-28
saggital
amygdala
-5
hypothalamus
-2
coronal
D
SEED: periaqueductal gray
signal intensity
CORRELATED: voxel
PAG SEED
face
body (arm and leg)

Figure 2:

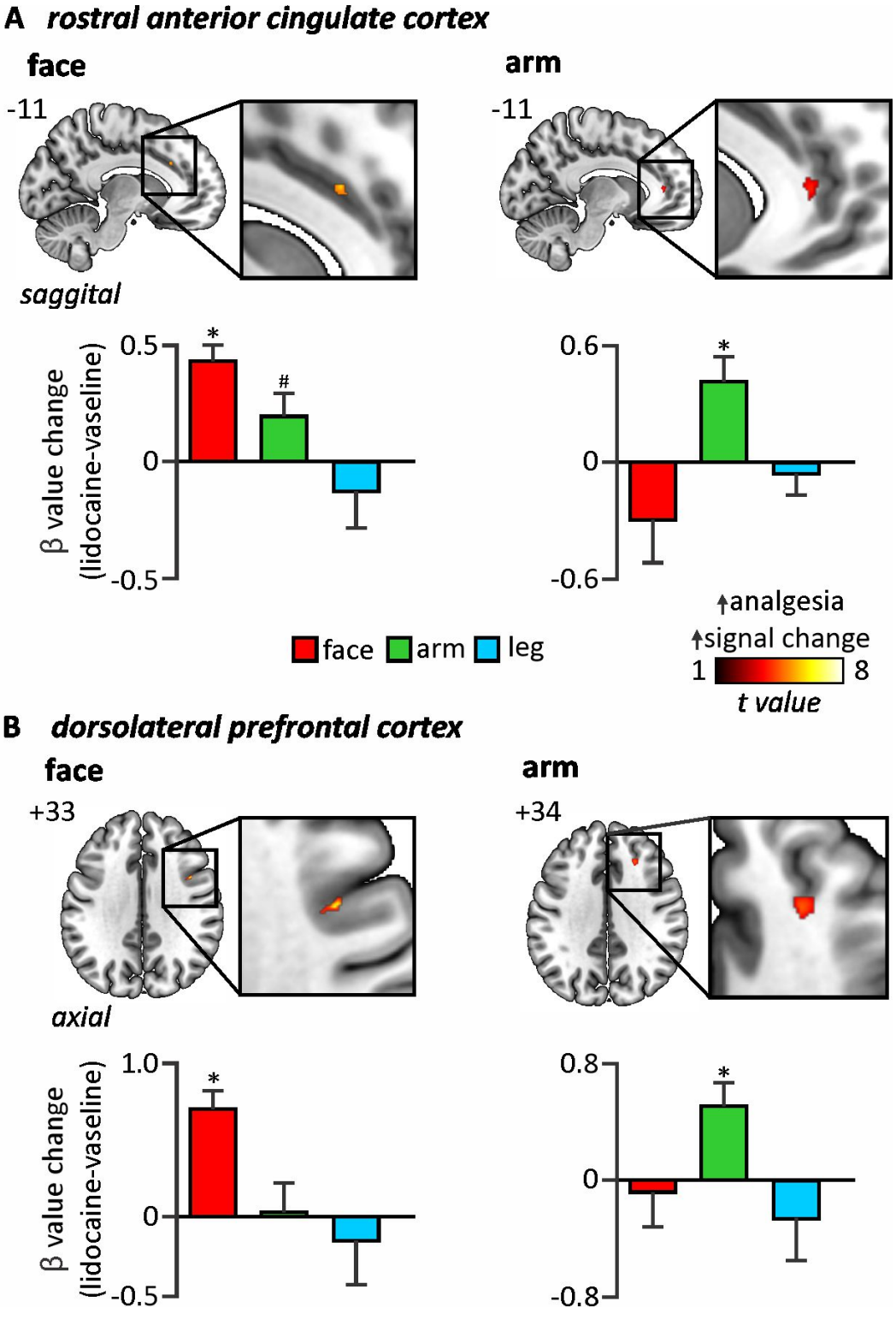
A rostral anterior cingulate cortex
face
arm
-11
-11
saggital
β value change (lidocaine-vaseline)
0.5
0
-0.5
*
#
0.6
0
-0.6
*
face
arm
leg
analgesia
signal change
1
8
t value
B dorsolateral prefrontal cortex
face
arm
+33
+34
axial
β value change (lidocaine-vaseline)
1.0
0
-0.5
*
0.8
0
-0.8
*

Figure 3:

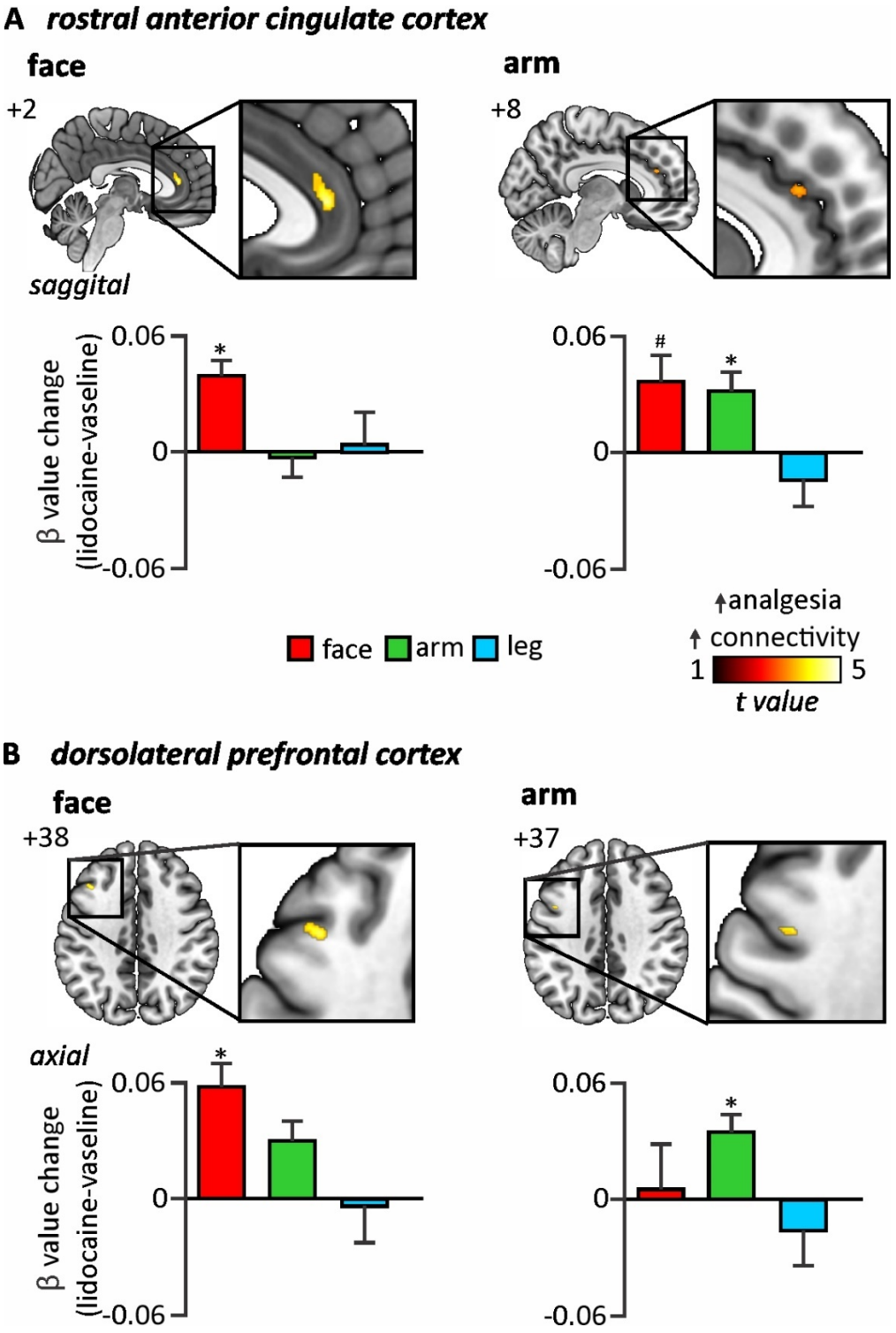
A rostral anterior cingulate cortex
face
arm
+2
+8
saggital
β value change (lidocaine-vaseline)
0.06
0
-0.06
*
#
face
arm
leg
analgesia
connectivity
1
5
t value
B dorsolateral prefrontal cortex
face
arm
+38
+37
axial

Figure 4:

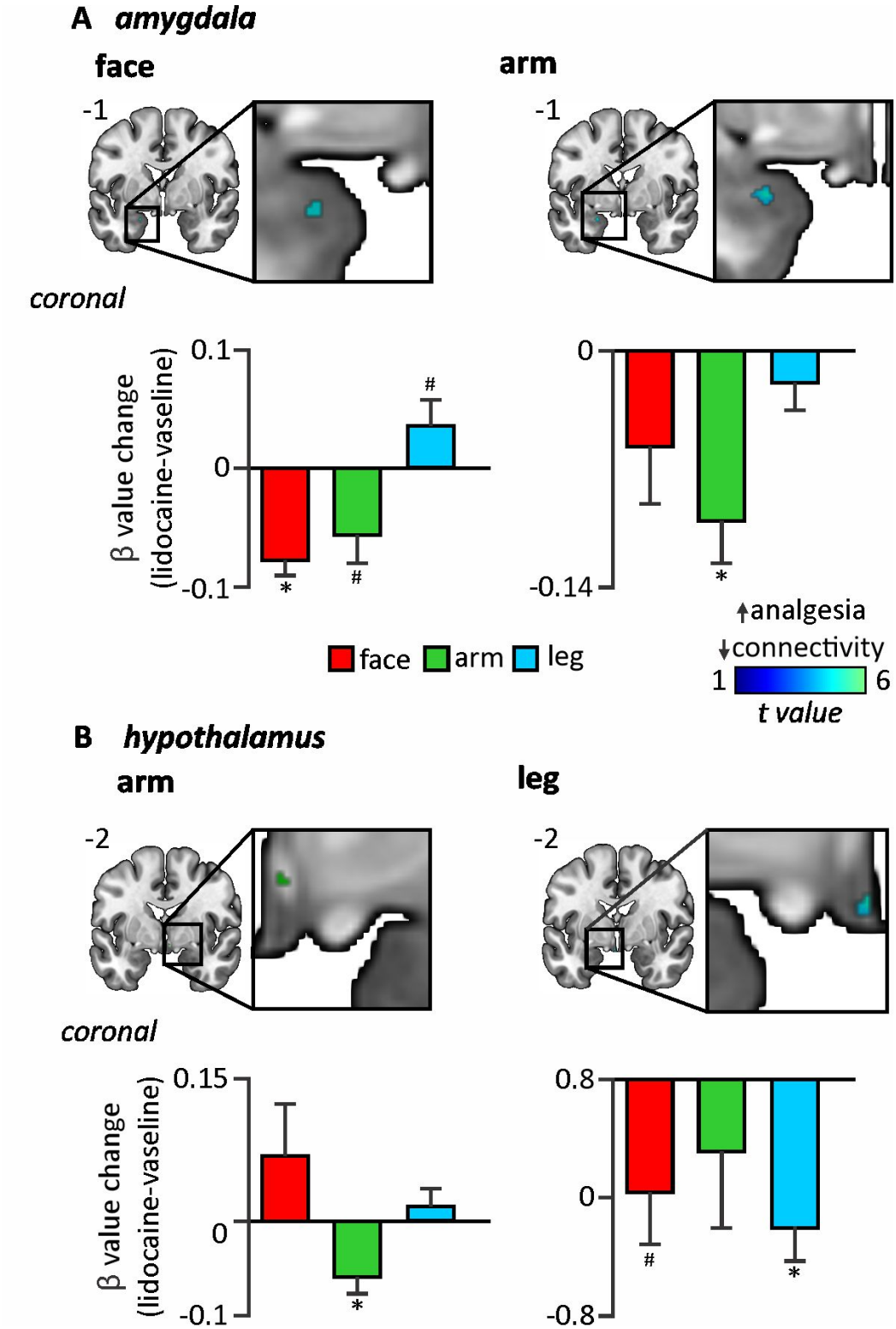
A amygdala
face
arm
-1
-1
coronal
β value change (lidocaine-vaseline)
0.1
0
-0.1
*
#
#
0
-0.14
*
face
arm
leg
analgesia
connectivity
1
6
t value
B hypothalamus
arm
leg
-2
-2
coronal
β value change (lidocaine-vaseline)
0.15
0
-0.1
*
0.8
0
-0.8
#
*

References

AIMONE, L. D., JONES, S. L. & GEBHART, G. F. 1987. Stimulation-produced descending inhibition from the periaqueductal gray and nucleus raphe magnus in the rat: mediation by spinal monoamines but not opioids. *Pain,* 31**,** 123-136.

AN, X., BANDLER, R., ONGÜR, D. & PRICE, J. L. 1998. Prefrontal cortical projections to longitudinal columns in the midbrain periaqueductal gray in macaque monkeys. *J Comp Neurol,* 401**,** 455-79.

ARIENZO, D., BABILONI, C., FERRETTI, A., CAULO, M., DEL GRATTA, C., TARTARO, A., ROSSINI, P. M. & ROMANI, G. L. 2006. Somatotopy of anterior cingulate cortex (ACC) and supplementary motor area (SMA) for electric stimulation of the median and tibial nerves: an fMRI study. *Neuroimage,* 33**,** 700-5.

BANDLER, R., PRICE, J. L. & KEAY, K. A. 2000. Brain mediation of active and passive emotional coping. *Prog Brain Res,* 122**,** 333-49.

BASBAUM, A. I. & FIELDS, H. L. 1984. Endogenous pain control systems: brainstem spinal pathways and endorphin circuitry. *Annu Rev Neurosci,* 7**,** 309-38.

BEHBEHANI, M. M. & FIELDS, H. L. 1979. Evidence that an excitatory connection between the periaqueductal gray and nucleus raphe magnus mediates stimulation produced analgesia. *Brain Res,* 170**,** 85-93.

BENEDETTI, F. 1996. The opposite effects of the opiate antagonist naloxone and the cholecystokinin antagonist proglumide on placebo analgesia. *Pain,* 64**,** 535-543.

BENEDETTI, F., ARDUINO, C. & AMANZIO, M. 1999. Somatotopic activation of opioid systems by target-directed expectations of analgesia. *J Neurosci,* 19**,** 3639-48.

BEST, M. & NEUHAUSER, D. 2010. Henry K Beecher: Pain, belief and truth at the bedside. The powerful placebo, ethical research and anaesthesia safety. *BMJ Quality & Safety,* 19**,** 466-8.

BINGEL, U., LORENZ, J., GLAUCHE, V., KNAB, R., GLÄSCHER, J., WEILLER, C. & BÜCHEL, C. 2004. Somatotopic organization of human somatosensory cortices for pain: a single trial fMRI study. *Neuroimage,* 23**,** 224-32.

BINGEL, U., LORENZ, J., SCHOELL, E., WEILLER, C. & BÜCHEL, C. 2006. Mechanisms of placebo analgesia: rACC recruitment of a subcortical antinociceptive network. *Pain,* 120**,** 8-15.

BRIGHINA, F., DE TOMMASO, M., GIGLIA, F., SCALIA, S., COSENTINO, G., PUMA, A., PANETTA, M., GIGLIA, G. & FIERRO, B. 2011. Modulation of pain perception by transcranial magnetic stimulation of left prefrontal cortex. *J Headache Pain,* 12**,** 185-91.

BROOKS, J. C., ZAMBREANU, L., GODINEZ, A., CRAIG, A. D. & TRACEY, I. 2005. Somatotopic organisation of the human insula to painful heat studied with high resolution functional imaging. *Neuroimage,* 27**,** 201-9.

CHENG, Z. F., FIELDS, H. L. & HEINRICHER, M. M. 1986. Morphine microinjected into the periaqueductal gray has differential effects on 3 classes of medullary neurons. *Brain Research,* 375**,** 57-65.

COHEN, M. M. 2006. *Perspectives on the Face,* New York, Oxford University Press.

CORNIANI, G. & SAAL, H. P. 2020. Tactile innervation densities across the whole body. *J Neurophysiol,* 124**,** 1229-1240.

CRAWFORD, L., MILLS, E., MEYLAKH, N., MACEY, P. M., MACEFIELD, V. G. & HENDERSON, L. A. 2022. Brain activity changes associated with pain perception variability. *Cerebral Cortex*.

CRAWFORD, L. S., MEYLAKH, N., MACEY, P. M., MACEFIELD, V. G., KEAY, K. A. & HENDERSON, L. A. 2023a. Stimulus-independent and stimulus-dependent neural networks underpin placebo analgesia responsiveness in humans. *Commun Biol,* 6**,** 569.

CRAWFORD, L. S., MILLS, E. P., HANSON, T., MACEY, P. M., GLARIN, R., MACEFIELD, V. G., KEAY, K. A. & HENDERSON, L. A. 2021. Brainstem Mechanisms of Pain Modulation: A within-Subjects 7T fMRI Study of Placebo Analgesic and Nocebo Hyperalgesic Responses. *The Journal of Neuroscience,* 41**,** 9794-9806.

CRAWFORD, L. S., MILLS, E. P., PEEK, A., MACEFIELD, V. G., KEAY, K. A. & HENDERSON, L. A. 2023b. Function and biochemistry of the dorsolateral prefrontal cortex during placebo analgesia: how the certainty of prior experiences shapes endogenous pain relief. *Cerebral Cortex,* 33**,** 9822-9834.

DIEDRICHSEN, J. 2006. A spatially unbiased atlas template of the human cerebellum. *Neuroimage,* 33**,** 127-38.

EIPPERT, F., BINGEL, U., SCHOELL, E. D., YACUBIAN, J., KLINGER, R., LORENZ, J. & BÜCHEL, C. 2009. Activation of the opioidergic descending pain control system underlies placebo analgesia. *Neuron,* 63**,** 533-43.

FLOYD, N. S., PRICE, J. L., FERRY, A. T., KEAY, K. A. & BANDLER, R. 2000. Orbitomedial prefrontal cortical projections to distinct longitudinal columns of the periaqueductal gray in the rat. *J Comp Neurol,* 422**,** 556-78.

GREVERT, P., ALBERT, L. H. & GOLDSTEIN, A. 1983. Partial antagonism of placebo analgesia by naloxone. *Pain,* 16**,** 129-143.

HEINRICHER, M. M., MORGAN, M. M., TORTORICI, V. & FIELDS, H. L. 1994. Disinhibition of off-cells and antinociception produced by an opioid action within the rostral ventromedial medulla. *Neuroscience,* 63**,** 279-88.

HIBI, D., TAKAMOTO, K., IWAMA, Y., EBINA, S., NISHIMARU, H., MATSUMOTO, J., TAKAMURA, Y., YAMAZAKI, M. & NISHIJO, H. 2020. Impaired hemodynamic activity in the right dorsolateral prefrontal cortex is associated with impairment of placebo analgesia and clinical symptoms in postherpetic neuralgia. *IBRO Rep,* 8**,** 56-64.

HUANG, C. C., ROLLS, E. T., FENG, J. & LIN, C. P. 2022. An extended Human Connectome Project multimodal parcellation atlas of the human cortex and subcortical areas. *Brain Struct Funct,* 227**,** 763-778.

LEICHNETZ, G. R., SPENCER, R. F., HARDY, S. G. & ASTRUC, J. 1981. The prefrontal corticotectal projection in the monkey; an anterograde and retrograde horseradish peroxidase study. *Neuroscience,* 6**,** 1023-41.

LEVINE, J. D., GORDON, N. C. & FIELDS, H. L. 1978. The mechanism of placebo analgesia. *Lancet,* 2**,** 654-7.

LÖKEN, L. S., BACKLUND WASLING, H., OLAUSSON, H., MCGLONE, F. & WESSBERG, J. 2022. A topographical and physiological exploration of C-tactile afferents and their response to menthol and histamine. *J Neurophysiol,* 127**,** 463-473.

MACEFIELD, V. G., GANDEVIA, S. C. & HENDERSON, L. A. 2007. Discrete changes in cortical activation during experimentally induced referred muscle pain: a single-trial fMRI study. *Cereb Cortex,* 17**,** 2050-9.

MAI, J. K. & MAJTANIK, T. 2017. *Human Brain in Standard MNI Space: A Comprehensive Pocket Atlas*, Elsevier.

MEIER, M. L., DE MATOS, N. M. P., BRÜGGER, M., ETTLIN, D. A., LUKIC, N., CHEETHAM, M., JÄNCKE, L. & LUTZ, K. 2014. Equal pain—Unequal fear response: enhanced susceptibility of tooth pain to fear conditioning. *Frontiers in Human Neuroscience,* 8.

MONTGOMERY, G. & KIRSCH, I. 1996. Mechanisms of Placebo Pain Reduction: An Empirical Investigation. *Psychological Science,* 7**,** 174-176.

MÜLLER-PREUSS, P. & JÜRGENS, U. 1976. Projections from the 'Cingular' vocalization area in the squirrel monkey. *Brain Research,* 103**,** 29-43.

NEUDORFER, C., GERMANN, J., ELIAS, G. J. B., GRAMER, R., BOUTET, A. & LOZANO, A. M. 2020. A high-resolution in vivo magnetic resonance imaging atlas of the human hypothalamic region. *Scientific Data,* 7**,** 305.

NEUGEBAUER, V., GALHARDO, V., MAIONE, S. & MACKEY, S. C. 2009. Forebrain pain mechanisms. *Brain Res Rev,* 60**,** 226-42.

OLUCHA-BORDONAU, F. E., FORTES-MARCO, L., OTERO-GARCÍA, M., LANUZA, E. & MARTÍNEZ-GARCÍA, F. 2015. Chapter 18 - Amygdala: Structure and Function. *In:* PAXINOS, G. (ed.) *The Rat Nervous System (Fourth Edition)*. San Diego: Academic Press.

OSSIPOV, M. H., DUSSOR, G. O. & PORRECA, F. 2010. Central modulation of pain. *J Clin Invest,* 120**,** 3779-87.

ROBERTSON, R. V., MEYLAKH, N., CRAWFORD, L. S., TINOCO MENDOZA, F. A., MACEY, P. M., MACEFIELD, V. G., KEAY, K. A. & HENDERSON, L. A. 2024. Differential activation of lateral parabrachial nuclei and their limbic projections during head compared with body pain: A 7-Tesla functional magnetic resonance imaging study. *Neuroimage,* 299**,** 120832.

ROMANSKI, L. M., CLUGNET, M. C., BORDI, F. & LEDOUX, J. E. 1993. Somatosensory and auditory convergence in the lateral nucleus of the amygdala. *Behav Neurosci,* 107**,** 444-50.

ROSENBLOOM, M. H., SCHMAHMANN, J. D. & PRICE, B. H. 2012. The functional neuroanatomy of decision-making. *J Neuropsychiatry Clin Neurosci,* 24**,** 266-77.

SÄRKKÄ, S., SOLIN, A., NUMMENMAA, A., VEHTARI, A., AURANEN, T., VANNI, S. & LIN, F. H. 2012. Dynamic retrospective filtering of physiological noise in BOLD fMRI: DRIFTER. *Neuroimage,* 60**,** 1517-27.

SCHENK, L. A. & COLLOCA, L. 2019. The neural processes of acquiring placebo effects through observation. *Neuroimage***,** 116510.

SCHMIDT, K., FORKMANN, K., SINKE, C., GRATZ, M., BITZ, A. & BINGEL, U. 2016. The differential effect of trigeminal vs. peripheral pain stimulation on visual processing and memory encoding is influenced by pain-related fear. *Neuroimage,* 134**,** 386-395.

SHARAV, Y. & BENOLIEL, R. 2008. *Orofacial Pain and Headache,* Edingburgh, Mosby Elsevier.

SHIPLEY, M. T., ENNIS, M., RIZVI, T. A. & BEHBEHANI, M. M. 1991. Topographical Specificity of Forebrain Inputs to the Midbrain Periaqueductal Gray: Evidence for Discrete Longitudinally Organized Input Columns. *In:* DEPAULIS, A. & BANDLER, R. (eds.) *The Midbrain Periaqueductal Gray Matter: Functional, Anatomical, and Neurochemical Organization*. Boston, MA: Springer US.

SOPER, W. Y. & MELZACK, R. 1982. Stimulation-produced analgesia: Evidence for somatotopic organization in the midbrain. *Brain Research,* 251**,** 301-311.

TINOCO MENDOZA, F. A., CRAWFORD, L. S., ROBERTSON, R. V., MEYLAKH, N., MACEY, P. M., BANNISTER, K., WAGER, T. D., MACEFIELD, V. G., KEAY, K. A. & HENDERSON, L. A. 2024. Somatotopic organisation of brainstem analgesic circuitry. *Under Review*.

TINOCO MENDOZA, F. A., HUGHES, T. E. S., ROBERTSON, R. V., CRAWFORD, L. S., MEYLAKH, N., MACEY, P. M., MACEFIELD, V. G., KEAY, K. A. & HENDERSON, L. A. 2023. Detailed organisation of the human midbrain periaqueductal grey revealed using ultra-high field magnetic resonance imaging. *Neuroimage,* 266**,** 119828.

TU, Y., WILSON, G., CAMPRODON, J., DOUGHERTY, D. D., VANGEL, M., BENEDETTI, F., KAPTCHUK, T. J., GOLLUB, R. L. & KONG, J. 2021. Manipulating placebo analgesia and nocebo hyperalgesia by changing brain excitability. *Proc Natl Acad Sci U S A,* 118.

VOGT, B. 2015. Cingulate Cortex and Pain Architecture.

WAGER, T. D., RILLING, J. K., SMITH, E. E., SOKOLIK, A., CASEY, K. L., DAVIDSON, R. J., KOSSLYN, S. M., ROSE, R. M. & COHEN, J. D. 2004. Placebo-induced changes in FMRI in the anticipation and experience of pain. *Science,* 303**,** 1162-1167.

WANG, L., CHEN, I. Z. & LIN, D. 2015. Collateral pathways from the ventromedial hypothalamus mediate defensive behaviors. *Neuron,* 85**,** 1344-58.

WIBERG, M., WESTMAN, J. & BLOMQVIST, A. 1987. Somatosensory projection to the mesencephalon: an anatomical study in the monkey. *J Comp Neurol,* 264**,** 92-117.

WIECH, K., KALISCH, R., WEISKOPF, N., PLEGER, B., STEPHAN, K. E. & DOLAN, R. J. 2006. Anterolateral prefrontal cortex mediates the analgesic effect of expected and perceived control over pain. *J Neurosci,* 26**,** 11501-9.

YAKSH, T. L., YEUNG, J. C. & RUDY, T. A. 1976. Systematic examination in the rat of brain sites sensitive to the direct application of morphine: Observation of differential effects within the periaqueductal gray. *Brain Research,* 114**,** 83-103.

YATES, D. 2015. Going on the defensive. *Nature Reviews Neuroscience,* 16**,** 247-247.

YEZIERSKI, R. P. 1988. Spinomesencephalic tract: projections from the lumbosacral spinal cord of the rat, cat, and monkey. *J Comp Neurol,* 267**,** 131-46.

YU, T., CAI, L. Y., MORGAN, V. L., GOODALE, S. E., ENGLOT, D. J., CHANG, C. E., LANDMAN, B. A. & SCHILLING, K. G. 2023. SynBOLD-DisCo: Synthetic BOLD images for distortion correction of fMRI without additional calibration scans. *Proc SPIE Int Soc Opt Eng,* 12464.

Chapter 5.

General discussion and future directions

"Nothing in this world that's worth having comes easy"

Dr. Bob Kelso, Scrubs

5.1 Abstract

The overarching aim of this thesis was to investigate the functional organization of the PAG in pain and analgesic processing and establish whether the human PAG is somatotopically organized. The PAG is believed to be a crucial component of ancient neural circuits that evolved to detect and avoid threats. Rooted in the PAG, this primitive defensive system coordinates diverse biological responses to environmental dangers and motivates recuperative behaviors to facilitate healing when pain is perceived (Wall, 1979).

In Chapter 2, we presented an investigation that revealed activity within the human PAG during acute noxious stimuli applied to different sites on the face and body. For the first time we revealed that the (contralateral) lateral PAG is somatotopically organized such that noxious stimulation of the face and body activates separate rostro-caudal levels in the lateral PAG. These results are consistent with the ascending afferent projection patterns in experimental animal studies and strongly suggests that this somatotopic organization is phyletically preserved in humans.

Correspondingly, in Chapter 3, we showed that the (ipsilateral) lateral PAG is involved in placebo analgesia, in a manner that is also somatotopically organized. That is, placebo analgesia on the face elicits activation in the lateral PAG at an identical rostral level to that during facial noxious stimulation. Likewise, placebo analgesia on the body, be it the arm or leg, elicits activation at a similar caudal level during noxious stimulation on similar body sites. Thus, the PAG has the ability to generate analgesia which is spatially restricted to either the head or body.

Lastly, in Chapter 4, we determined cortical and sub-cortical circuits that mediate placebo analgesia across the head and body. We focused on two cortical regions, the rACC and dlPFC, and two sub-cortical regions, the amygdala and hypothalamus, due to their established role in pain control. We found activation patterns that were spatially separate in the rACC, dlPFC and amygdala when analgesia was induced on the face and body. This finding was also seen during analysis of functional connectivity with spatially separate sites connecting with the lateral PAG during face versus body analgesia.

In this final chapter, we extend on the main findings of this thesis and how they reveal a critical role of the PAG in driving spatially specific responses. We then discuss the importance of anatomically separate PAG circuits, particularly in the context of analgesic processing. We will address the methodological considerations of the use of 7T fMRI in imaging the brainstem, before concluding with an outline of the importance of this research in our understanding of the PAG in humans for future research.

5.2 The role of a somatotopic organization

Somatotopy is a common organizational principle of the CNS and is critical for the accurate localization of a stimulus as well as to drive appropriate behavioral responses. In Chapters 2 and 3, we have identified that incoming noxious information is processed and modulated in a regionally selective manner within the lateral PAG in humans. Therefore, it is apparent that animals and humans contain a robust somatotopic organization within the PAG that has significant implications in driving the most appropriate behaviors for defense and survival.

Humans are known to share ancient phylogenetic forebrain and brainstem structures with other animal species. Among the most evolutionarily ancient species, the sea lamprey (*Petromyzon marinus*), an extant jawless vertebrate, provides insight into the deep ancestry of neural systems, having remained relatively conserved for over 500 million years (Smith et al., 2018; Xu, Zhu & Li, 2016). Strikingly, a homologous structure corresponding to the mammalian PAG has been identified in the sea lamprey, as well as in zebrafish, including its afferent and efferent connections to forebrain structures (Olson et al., 2017; Stephenson-Jones et al., 2011).

The physiological response to stress, an evolutionarily conservative anti-predator mechanism, is also present in the sea lamprey as it possesses components necessary to mount the fight or flight response. Accordingly, this behavioral response is widespread across taxa and mobilizes an organism for rapid action in the face of a threat (Charmandari, Tsigos & Chrousos, 2005). Central to the fight or flight response is the activation of the sympatho-adrenal system, whereby perceived threats stimulate the release of adrenaline and noradrenaline from the adrenal gland (Cannon, 1915). Notably, recent discoveries have shown that the sea lamprey harbors sympathetic neurons, overturning the prevailing dogma that the sympathetic nervous system evolved in jawed vertebrates (Edens et al., 2024). These findings imply that the rudimentary neural circuits governing active survival behaviors, such as fight or flight, were present in the earliest vertebrates and have been retained throughout vertebrate evolution.

Given the presence of both a homologous PAG and a sympathetic nervous system in the sea lamprey, it is thus plausible that the functional components of the PAG in humans, including its somatotopic organization, have been conserved across vertebrate lineages. Therefore, we propose that the somatotopic organization of nociceptive circuits observed in Chapters 2 and 3 represents a sophisticated elaboration of a deeply rooted defensive system that dates to the earliest species across animal taxa.

It is also clear that the behavioral outputs elicited by the PAG underscore its essential role in survival. When confronted with stressors or threats, animals employ adaptive strategies driven by fear and aversion to enhance survival (Mobbs et al., 2015). In mammals, the PAG mediate active emotional coping strategies, such as fight or flight, in response to escapable stressors like cutaneous pain, as examined in our experiments (Keay & Bandler, 2001). These responses are reflexive and context-specific, differing based on whether the threat is perceived on the face or the body (see Section 1.3.2). Such a spatially-dependent reflex requires minimal latency and is initiated within the confines of the lateral PAG, as evidenced in decerebrate models (Carrive, Bandler & Dampney, 1989; Carrive, Dampney & Bandler, 1987). Our findings further support the notion that, in humans, the PAG exhibits a functional topography, with distinct rostral defensive and caudal avoidance zones (Bandler & Depaulis, 1991). Collectively, the conservation of these structural and functional features from the sea lamprey to human provides compelling evidence that a somatotopically organized PAG is a fundamental and ancestral feature across all mammals.

In Chapter 2, we identified a somatotopy within the human PAG where noxious stimuli applied to the face and body activates separate rostral and caudal levels. Notably, this somatotopy is crude in nature i.e. different sites on the face and body activate similar rostro-caudal levels of the PAG. A crude somatotopy matches the nature of neuronal cells within the PAG having large receptive fields (Liebeskind & Mayer, 1971) and is critical in the context of defense as it would enable the most rapid behavioral response to occur. That is, regardless of where exactly in the face or body a threat or stimulus occurs, the PAG can recognize whether a fighting or fleeing response would be most appropriate. In this way, a crude somatotopic organization of the human lateral PAG would drive defensive behaviors that are most appropriately adapted to the location of a threat, as has been observed across the evolution of animal species.

There is an important distinction that must be made between behavioral and sensory somatotopy. A common property of sensory projections, such as the ascending pain pathways, is that they retain a spatial arrangement throughout the entire nervous system (see Section 1.2). This spatial arrangement is extremely specific in both animals and humans. For example, rodents contain a connection between each individual whisker and specific cylinders/barrels within S1. In humans, 7T fMRI studies have shown detailed somatotopic maps at the level of individual phalanges in S1 (Sanchez-Panchuelo et al., 2012) and motor representations of each digit within M1 (Schellekens, Petridou & Ramsey, 2018). Thus, our bodies can precisely discriminate the location of sensory stimuli across proximal body areas.

Whilst such a detailed spatial map is essential for the precise localization of stimuli, this level of fidelity may not be as beneficial for triggering appropriate defensive behaviors. An underlying dilemma with increasing topographical detail is the associated increase in complexity and functional capacity of the neural pathways. With increasing specificity, the number of neurons increases, which can increase redundancy and functional diversification. As a consequence, total energy consumption rises which reduces the energy efficiency of information processing per neuron (Niven & Laughlin, 2008). Given that active defensive behaviors are relatively global, patterned responses, a relatively crude somatotopically organized afferent drive from general body regions would be sufficient to initiate such responses with minimal energetic cost.

To our knowledge, no other study has also identified this kind of crude somatotopy of the human PAG during noxious stimulation. Interestingly, after our publication, a study demonstrated a highly specific somatotopic representation of facial nociceptive inputs in the human PAG using 3T fMRI (Mehnert et al., 2024). By electrically stimulating the three peripheral branches of the trigeminal nerve (V1, V2 and V3), they showed a rostro-caudal activation pattern within the PAG. However, the voxel sizes from a 3T MRI exceed 1mm, impacting the overall detail and resolution of the PAG, which are also susceptible to partial volume effects (Linnman et al., 2012). From an evolutionary standpoint, it is unlikely that modern humans encounter the kind of frequent predatory threats that would perhaps require a more detailed somatotopy than the one we have observed. Future work is warranted on discerning a crude versus specific somatotopic pattern within the human PAG, which would be best done using the high-resolution capabilities of 7T MRI given the small intricate size of this midbrain structure.

While our studies support a crude somatotopy within the lateral PAG, it is important to note that this likely arises from adaptive specializations tuned to varying functional demands. In certain contexts, a crude somatotopy – lacking detailed face-body distinctions – may be beneficial for rapidly initiating global defensive responses without the need for precise stimulus localization. Conversely, we also observed a rostro-caudal somatotopic organization within the PAG which appears to be a conserved feature across animal species. Having a somatotopy that has been preserved would potentially facilitate faster and more contextually appropriate responses when specific body parts are being targeted. This specificity in representing the face versus the body would enable the PAG to prioritize motor strategies suited to the location of a threat. Therefore, a crude and refined rostro-caudal PAG somatotopy are likely not mutually exclusive and could coexist, supporting flexible behavioral outputs depending on the environmental context.

5.3 Face-body circuits underpinning placebo analgesia

Once a defensive behavioral response has been generated by incoming noxious inputs, the perception of pain is no longer advantageous and could limit the ability of an animal to continue to remove themselves from the initial noxious stimulus. Given this, it is well established that the same lateral PAG region that mediates active defensive behaviors also mediates a non-opioid mediated profound analgesia (Bandler & Shipley, 1994). Since we found a crude somatotopic activation pattern within the lateral PAG during acute noxious stimuli, we hypothesized that the lateral PAG may also be able to mount a somatotopically organized analgesia.

Extending on our findings from Chapter 2, we sought to examine whether the same rostro-caudal organization in the lateral PAG occurs when analgesic responses are exhibited across different head and body sites. In Chapter 3 we showed, for the first time, that placebo analgesia on the face and body (arm and leg) was associated with altered signal intensity changes in the ipsilateral rostral and caudal lateral PAG, respectively. Remarkably, the location of these changes in the PAG occurred at similar rostro-caudal levels as identified in Chapter 2. We thus propose that the downstream anti-nociceptive properties of the human PAG, as well as its noxious inputs, are separated into separate circuits for the head and body.

Previous animal studies support our proposed framework by demonstrating that the PAG can induce anti-nociceptive effects in a somatotopic manner. Firstly, electrical stimulation of the PAG at various rostro-caudal levels produces analgesia in specific regions; a notable finding is that rostral PAG stimulation affects fewer regions compared to caudal stimulation. There is also a clear distinction in electrode sites where analgesia is observed in the ears but not in the hindlimbs or tail of rodents (Soper & Melzack, 1982). Secondly, morphine injection into the rostral PAG leads to analgesia restricted to the ipsilateral face, whereas caudal PAG stimulation evokes a whole-body analgesia (Yaksh, Yeung & Rudy, 1976). These findings indicate the existence of "*two anatomically separate systems related to analgesia of the ears and forelimbs*" (Soper & Melzack, 1982), reinforcing our assertion that separate face-body circuits operate within the human PAG.

In Chapters 2 and 3, we observed altered signal intensity change along the lateral PAG on the contralateral and ipsilateral sides, respectively. Anatomical tract tracing studies have revealed that spinal and medullary afferents project predominantly to the contralateral PAG, with much fewer projections to the ipsilateral PAG (see Section 1.3.4) (Wiberg, Westman & Blomqvist, 1987). In the context of analgesia, electrical stimulation of the caudal PAG in rats has been shown to

inhibit nociception bilaterally in the tail and hind paw, though the effect is stronger and more preferentially expressed on the ipsilateral side (Levine et al., 1991). In Chapter 2, we examined both sides of the PAG and found a somatotopic pattern of activation across the contralateral and ipsilateral side. However, only the contralateral side demonstrated statistically significant changes, emphasizing a critical role of PAG laterality in pain processing. Our findings thus support pre-clinical evidence that the side of the PAG activation differs depending on whether pain is being processed or inhibiting – highlighting laterality as a key factor in the neural dynamics of pain modulation and nociception.

Placebo analgesic responses have, in the past, shown to be spatially specific to the body site where expectancy is directed (Benedetti, Arduino & Amanzio, 1999). These findings argue against the widespread premise that the underlying mechanisms of a placebo analgesia response are non-specific and affect the entire body. Interestingly, this spatially restricted analgesia can be blocked by the opioid antagonist naloxone (Benedetti, Arduino & Amanzio, 1999; Montgomery & Kirsch, 1996), suggesting that endogenous opioids play a key role in mediating a precise and targeted analgesia. Given we have shown that the lateral PAG is critical in regulating non-opiate placebo analgesia, it is possible that the opioid effect from a successful placebo response originates from higher brain centers, likely in the rACC. The neural circuits involved in a spatially specific analgesia could be regulated by a topographical relationship between expectancies and endogenous opioid systems, which are driven via the somatotopic organization of the lateral PAG.

In Chapter 3, we reported that placebo analgesia on the arm, face and leg evoked signal intensity changes in the lateral/dorsolateral PAG. These signal intensity changes were again organized in a somatotopic fashion with analgesia on the face recruiting the rostral lateral PAG and analgesia on the arm and leg recruiting the caudal lateral PAG. As discussed in Section 1.5.2, the PAG mediates analgesia via its projections to the RVM, with the PAG-RVM system undoubtedly the most well-documented descending pain modulatory pathway of the brainstem and has become a cornerstone in pain research since its first discovery (Fields & Heinricher, 1985; Heinricher, Barbaro & Fields, 1989). Although the RVM was not of primary interest for this thesis, in Chapter 3 we also found a remarkably consistent somatotopic pattern of signal intensity changes in the RVM during placebo analgesia on the face, arm and leg. Since the RVM is the neural link between the PAG and the SpV/dorsal horn for pain modulation, one would expect that the somatotopic organization of the PAG to also be preserved in the RVM.

No previous study has ever presented evidence of a somatotopic organization within the RVM in humans. Although, one experimental animal retrograde tract-tracing study has shown a crude

somatotopy of RVM (nucleus raphe magnus) projections to the four divisions of the spinal cord (Watkins et al., 1980). There is also evidence demonstrating that different RVM cell types project to either the superficial or deep nociceptive laminae of the spinal cord (Gautier et al., 2017), which has previously been proposed to result in the separation of medullo-spinal projections (Basbaum, Clanton & Fields, 1978). However, like the PAG, no definable border exists between the cellular groups of the RVM due to an identical cytoarchitecture in the adjoining reticular formation (Taber, Brodal & Walberg, 1960). As such, it is an immensely difficult feat to prove a functional segregation within the RVM. Altogether, our data provides improved knowledge on the anatomical organization of medullo-spinal projections from the PAG-RVM system regulating descending pain modulation in humans.

5.3.1 Cortical circuits subserving PAG-induced analgesia

Whilst the PAG can generate defensive behaviors without cortical input, its sensitivity is modulated by descending inputs from higher brain regions such as the hypothalamus and cerebral cortex (Beitz, 1982). In response to tissue-damaging stimuli, these defensive behaviors engage motivational states that are thought to involve neural networks in both primordial limbic forebrain regions and more recently evolved higher-order areas.

In Chapter 4, we showed that the dlPFC and parts of the ACC exhibit distinct areas of activation and connectivity with the lateral PAG during analgesia on the face compared with the body. The PAG serves as a central hub for descending modulatory signals regulated by limbic structures such as the ACC, amygdala and hypothalamus (Cao et al., 2024). It is possible that these forebrain regions constitute a conserved defense system, capable of accessing the PAG's intrinsic anti-nociceptive circuits. Our findings suggest that the ACC, dlPFC and amygdala are all involved in initiating spatially restricted analgesia, by potentially activating independent circuits from the same cortical and subcortical location that project to either the rostral or caudal lateral PAG.

One strategy for actively controlling threat-avoidance behaviors involves predictive learning. In learning the most optimal manner to escape, cognitive appraisal – the ability to reframe and evaluate a threat- is required. Placebo analgesia is a paradigm that relies on cognitive evaluation, a trait particularly well-developed in higher species like humans. Our results in Chapter 4 demonstrated that placebo-induced activity and PAG connectivity within the dlPFC are regionally specific, varying depending on the body area targeted for analgesia. This spatial specificity

suggests that the cognitive appraisal of a placebo response, likely mediated by the dlPFC, may be part of an evolved circuit that can selectively modulate nociceptive information in different body regions. In this way, the dlPFC does not directly drive the biological demand for analgesia but rather leverages the face-body circuits within the PAG to exert selective analgesic effects on specific body areas.

By integrating the results from our experimental chapters, we propose a model of pain modulation in which ascending and descending nociceptive information is spatially segregated for facial and bodily regions. The spatial separation of face-body circuits is maintained within the descending inhibitory pathway via the PAG-RVM system, ultimately targeting the primary afferent synapse (Figure 5.1). Although these investigations were conducted using a placebo paradigm, existing literature suggests that other analgesic paradigms may recruit similar if not identical brainstem circuitry. Future research should explore the directionality of this analgesic network using techniques like dynamic causal modelling to determine whether the activation and connectivity patterns exert influence in a unidirectional manner.

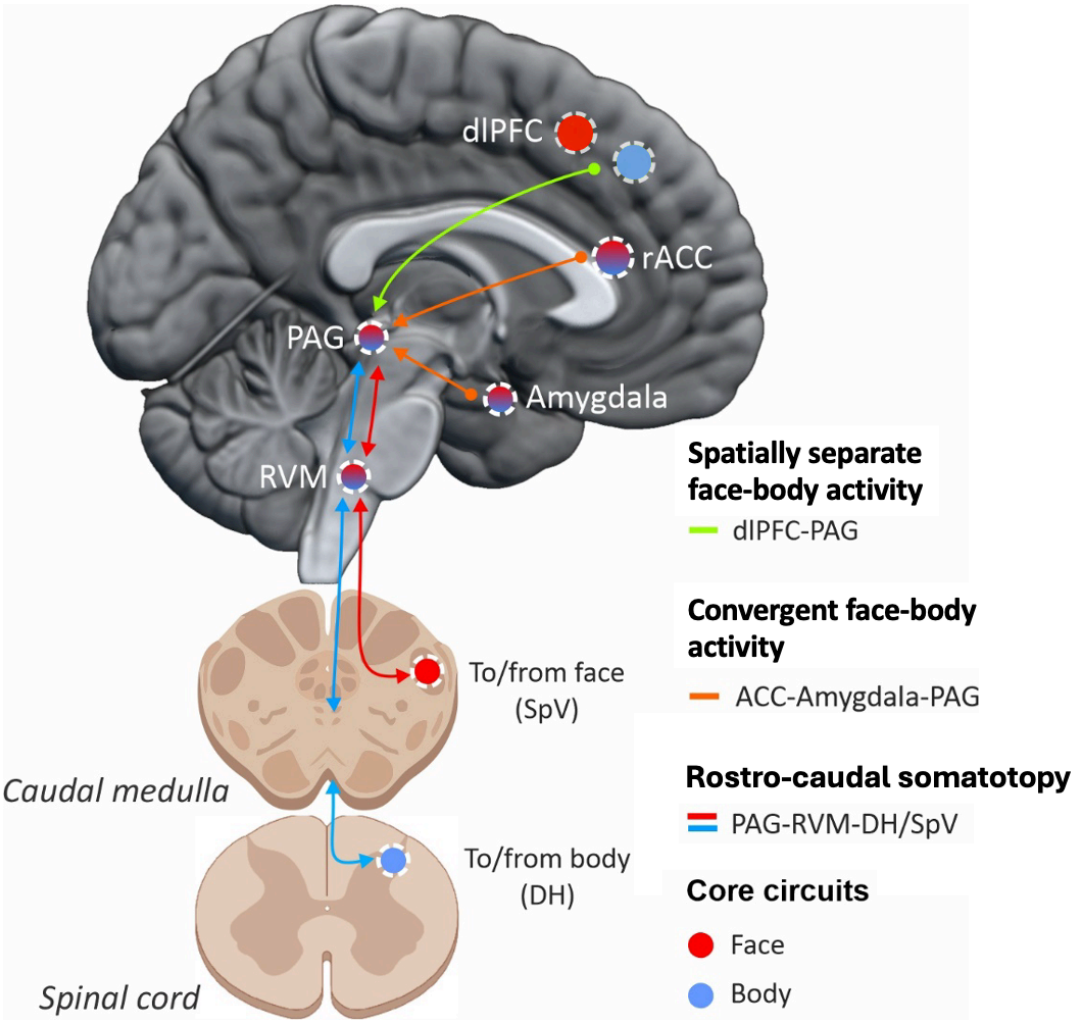

Figure 5.1. A proposed theoretical model for spatially separate neural circuits underlying descending pain modulation for different body sites. Upon encountering a noxious stimulus, nociceptive information ascends via distinct circuits from the SpV (red), for face stimuli, or DH of the spinal cord (blue), for body stimuli. This information converges onto the PAG (red-blue) at separate rostro-caudal levels, where it is modulated through the RVM (red-blue) via these same face-body circuits. In humans, top-down cognitive modulation of the PAG during placebo analgesia utilizes an evolved circuit involving the dlPFC (green) which is regionally activated depending on the body location where analgesia is to be mounted. To induce a fundamental analgesic response, primitive circuits involving the ACC and amygdala (red-blue) are activated in overlapping regions in a convergent manner (orange), irrespective of the specific body region targeted for analgesia. These limbic regions subsequently project to the PAG-RVM system, activating the descending analgesic pathway in a somatotopically segregated manner.

Abbreviations, DH = dorsal horn; dlPFC = dorsolateral prefrontal cortex; PAG = periaqueductal gray; rACC = rostral anterior cingulate cortex; RVM = rostral ventromedial medulla; SpV = spinal trigeminal nucleus.

5.4. Limitations and future directions

This thesis presents several novel discoveries about the human brainstem and cortical systems that underlie functionally organized responses to pain and analgesia. Our findings are not, however, without limitations which must be considered when guiding future research endeavors.

Firstly, we constrained our study to healthy individuals to examine a somatotopy within the PAG. A primary drawback of this approach is that we can only theorize about the role of this somatotopic organization in chronic pain populations. Considering that placebo interventions have been demonstrated to alleviate pain and disability in chronic pain patients (Kaptchuk, Hemond & Miller, 2020; Vase, Skyt & Hall, 2016), further research on placebo analgesia offers the greatest potential. Thereby, the delineation of face-body circuits we have presented within the PAG has widespread therapeutic implications for future studies on chronic pain and analgesia.

Over the past two decades, numerous studies have indicated that chronic pain is associated with a diminished ability to mount an analgesic response (Julien et al., 2005; King et al., 2009; Wilder-Smith et al., 2004). Crucially, these studies have only tested body sites in which there is chronic pain, neglecting other areas without ongoing pain. It is possible that previous analgesic research has overlooked differences in analgesic capacity across various body sites, emphasizing the need for future analgesic experiments to examine multiple body sites simultaneously. As our data suggests that analgesic responses are somatotopically organized within the lateral PAG, we propose that the brain is structured to selectively modulate noxious inputs from specific body regions. This regional specificity for analgesic responses raises the possibility that chronic pain patients may experience impaired placebo analgesia in the area of ongoing pain, but not in pain-free regions. Considering this finding, we have put forth a model where somatotopically appropriate circuits for chronic pain relief can be targeted (Figure 5.2). The basis of this model is most applicable to conditions where individuals experience spatially restricted chronic pain in the face or body.

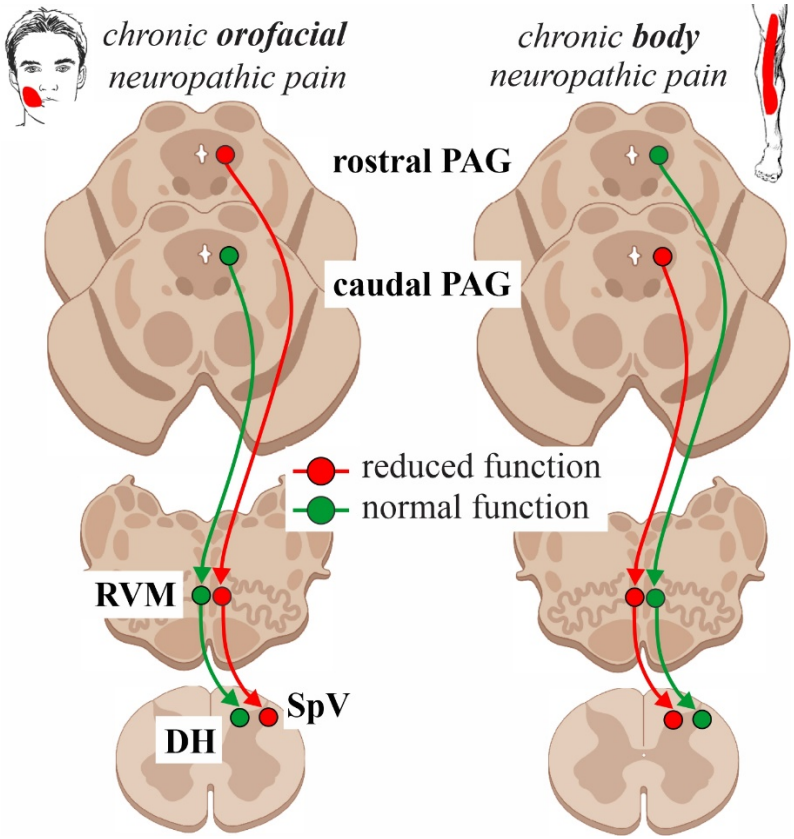

Figure 5.2. A proposed theoretical model of altered function in analgesic circuits affecting chronic orofacial versus body pain. Analgesic ability may be affected in the area of chronic pain depending on whether it is in the face or body. In the pain-free regions, there is regular analgesic function, allowing for reductions in pain despite experiencing chronic pain in a separate body area.

Abbreviations; DH, dorsal horn; PAG, periaqueductal gray; RVM, rostral ventromedial medulla; SpV, spinal trigeminal nucleus

In this thesis, we have used placebo analgesia as a means to explore analgesic circuitry. However, placebo analgesia is just one type of fundamental analgesia. Conditioned pain modulation, stress-induced analgesia and offset analgesia are distinct phenomena that rely on the neurobiological mechanisms of endogenous pain modulation. Evidence suggests that all three of these pain modulatory phenomena engage the PAG-RVM system (Derbyshire & Osborn, 2009; Harrison et al., 2022; Szikszay et al., 2020; Youssef, Macefield & Henderson, 2016). A within-subjects imaging study that assesses each of these fundamental types of analgesia alongside placebo would allow for a direct comparison of similarities and differences in the underlying neural circuits. Furthermore, it would be insightful to determine whether the PAG-RVM somatotopy we have observed is consistent across these fundamental types of analgesia when assessed between sites on the face and body.

Secondly, the field-of-view (FOV) we acquired in our fMRI series was quite large, considering our focus on a small structure like the PAG. By encompassing the entire cerebrum and brainstem, we have limited the highest possible resolution attainable with 7T-MRI. While reducing the FOV would enhance the overall resolution of our fMRI scans, a large coverage was necessary for the purposes of this thesis, as we aimed to explore the entire descending pain modulatory pathway. With the use of UHF imaging, sub-millimeter detail can be resolved making it feasible to distinguish activity within specific columns of the PAG (Cho et al., 2014; Satpute et al., 2013). Despite this, determining the optimal resolution for a PAG-specific fMRI analysis remains challenging. While increasing spatial resolution would minimize partial volume effects, it would compromise signal-to-noise ratio and sensitivity to detect functional activation (Blazejewska et al., 2019). Therefore, we believe the fMRI acquisition we employed is optimal for this thesis, with future research warranted on the limitations of the BOLD effect on high-resolution MRI data.

Thirdly, the number of participants varied across our experiments. In Chapter 2, fewer participants received noxious cutaneous stimulation to the cheek and ear (n=17) compared to those who had lip, thenar and toe stimulation (n=24). Likewise, there were fewer participants who received the noxious deep stimulus (n=17) compared to noxious cutaneous stimulation (n=24). This may have reduced the statistical power that contributed to our finding that there was no significant difference in activation between the lateral and ventrolateral PAG columns. In Chapters 3 and 4, approximately half as many subjects underwent the placebo analgesia paradigm on the face (n=23) compared to the arm (n=46) and leg (n=41). Additionally, no subject completed all three placebo paradigms, preventing us from directly differentiating the rostro-caudal location of PAG signal intensity changes between the face, arm and leg in individual subjects. Future analgesic experiments should consider utilizing a within-subjects design to identify individuals who are consistent placebo responders across different face and body sites. In these consistent responders, it would be interesting to investigate whether the rostro-caudal pattern of activity in the PAG we observed is conserved in the PAG and RVM across the face and body.

Finally, our results and interpretations of functional activation and connectivity are based on fMRI data. The fundamental constraint of fMRI is that it is not a direct measure of neural activity; instead, it measures the corresponding hemodynamic effects using BOLD responses. Other imaging modalities, like arterial spin labeling or PET, can localize signal to specific neuronal tissue by quantifying cerebral blood flow. Although, these methods lack the resolution needed to accurately investigate small structures like the PAG, which fMRI can achieve. The hemodynamic response of fMRI is additionally limited by its poor temporal resolution (in the order of seconds)

relative to neural dynamics (in the order of milliseconds). Recent advancements in custom ultra-fast fMRI sequences have pushed repetition times closer to the range required to decode marked neuronal processes (Cabral, Fernandes & Shemesh, 2023; McDowell & Carmichael, 2019; Nagy et al., 2023). One promising technique, known as “direct imaging of neuronal activity”, has demonstrated the ability to trace somatosensory information along thalamocortical pathways in anesthetized mice following whisker stimulation (Toi et al., 2022). As these novel techniques become available for human MRI technologies, their application to experimental pain modulation will further our understanding of how the cortex and brainstem influence the pain experience.

5.5 Conclusion

The findings of this thesis have revealed that the human PAG contains a crude somatotopic organization with respect to noxious inputs and analgesia. We have demonstrated a rostro-caudal somatotopic organization within the lateral PAG that is active in response to noxious stimuli on the face and body. Intriguingly, this somatotopic organization persists during placebo analgesia, and shows that the rACC and amygdala exhibit spatially separate activation and connectivity with the lateral PAG depending on where analgesia on the body occurs. The observed data suggests that the PAG and its connected limbic structures form a defence system with deep evolutionary roots. This system appears to orchestrate a spatially specific analgesia in response to threats targeting either the head or the body, a capability likely facilitated by the functional organization of the PAG along its rostro-caudal axis.

Ultimately, our knowledge of the human PAG is largely based on research conducted on experimental animals. Our findings challenge the conventional understanding of sensory inhibitory circuits, as they suggest a crude somatotopic organization within the PAG that is phyletically conserved between animal species and humans. A deeper understanding of the PAG’s role in various pain and analgesic contexts could pave the way for innovative treatments for chronic pain conditions associated with aberrant analgesic responses at specific body sites.

References

Afshar, F, Watkins, ES, Watkins, S & Yap, JC 1978, *Stereotaxic Atlas of the Human Brainstem and Cerebellar Nuclei: A Variability Study*, Raven Press.

Akil, H, Mayer, DJ & Liebeskind, JC 1976, 'Antagonism of Stimulation-Produced Analgesia by Naloxone, a Narcotic Antagonist', *Science,* vol. 191, no. 4230, pp. 961-962.

An, X, Bandler, R, Öngür, D & Price, JL 1998, 'Prefrontal cortical projections to longitudinal columns in the midbrain periaqueductal gray in Macaque monkeys', *Journal of Comparative Neurology,* vol. 401, no. 4, pp. 455-479.

Aristotle 1984, *The Rhetoric and Poetics of Aristotle*, McGraw-Hill Education.

Atlas, LY & Wager, TD 2014, 'A Meta-analysis of Brain Mechanisms of Placebo Analgesia: Consistent Findings and Unanswered Questions', in Benedetti, F, Enck, P, Frisaldi, E & Schedlowski, M (eds.), *Placebo*, Springer Berlin Heidelberg, Berlin, Heidelberg.

Bandler, R 1982, 'Induction of 'rage' following microinjections of glutamate into midbrain but not hypothalamus of cats', *Neuroscience letters,* vol. 30, no. 2, pp. 183-188.

Bandler, R & Depaulis, A 1991, 'Midbrain Periaqueductal Gray Control of Defensive Behavior in the Cat and the Rat', in Depaulis, A & Bandler, R (eds.), *The Midbrain Periaqueductal Gray Matter: Functional, Anatomical, and Neurochemical Organization*, Springer US, Boston, MA.

Bandler, R, Keay, KA, Floyd, N & Price, J 2000, 'Central circuits mediating patterned autonomic activity during active vs. passive emotional coping', *Brain research bulletin,* vol. 53, no. 1, pp. 95-104.

Bandler, R & Mcculloch, T 1984, 'Afferents to a midbrain periaqueductal grey region involved in the ‘defense reaction’ in the cat as revealed by horseradish peroxidase. II. The diencephalon', *Behavioural Brain Research,* vol. 13, no. 3, pp. 279-285.

Bandler, R, Mcculloch, T & Dreher, B 1985, 'Afferents to a midbrain periaqueductal grey region involved in the ‘defence reaction’ in the cat as revealed by horseradish peroxidase. I. The telencephalon', *Brain Research,* vol. 330, no. 1, pp. 109-119.

Bandler, R, Price, JL & Keay, KA 2000, 'Brain mediation of active and passive emotional coping', *Progress in Brain Research,* vol. 122, pp. 333-349.

Bandler, R & Shipley, MT 1994, 'Columnar organization in the midbrain periaqueductal gray: modules for emotional expression?', *Trends Neurosci,* vol. 17, no. 9, pp. 379-89.

Basbaum, AI, Clanton, CH & Fields, HL 1978, 'Three bulbospinal pathways from the rostral medulla of the cat: an autoradiographic study of pain modulating systems', *J Comp Neurol,* vol. 178, no. 2, pp. 209-24.

Beecher, HK 1955, 'THE POWERFUL PLACEBO', *Journal of the American Medical Association,* vol. 159, no. 17, pp. 1602-1606.

Behbehani, MM 1995, 'Functional characteristics of the midbrain periaqueductal gray', *Progress in Neurobiology,* vol. 46, no. 6, pp. 575-605.

Beissner, F 2015, 'Functional MRI of the Brainstem: Common Problems and their Solutions', *Clin Neuroradiol,* vol. 25 Suppl 2, pp. 251-7.

Beitz, AJ 1982, 'The organization of afferent projections to the midbrain periaqueductal gray of the rat', *Neuroscience,* vol. 7, no. 1, pp. 133-59.

Benedetti, F 2022, 'Historical evolution of the scientific investigation of the placebo analgesic effect', *Frontiers in Pain Research,* vol. 3.

Benedetti, F, Arduino, C & Amanzio, M 1999, 'Somatotopic activation of opioid systems by target-directed expectations of analgesia', *J Neurosci,* vol. 19, no. 9, pp. 3639-48.

Benini, A & Deleo, JA 1999, 'René Descartes' physiology of pain', *Spine (Phila Pa 1976),* vol. 24, no. 20, pp. 2115-9.

Bingel, U, Lorenz, J, Schoell, E, Weiller, C & Büchel, C 2006, 'Mechanisms of placebo analgesia: rACC recruitment of a subcortical antinociceptive network', *Pain,* vol. 120, no. 1-2, pp. 8-15.

Bingel, U & Tracey, I 2008, 'Imaging CNS modulation of pain in humans', *Physiology (Bethesda),* vol. 23, pp. 371-80.

Björkeland, M & Boivie, J 1984, 'The termination of spinomesencephalic fibers in cat. An experimental anatomical study', *Anat Embryol (Berl),* vol. 170, no. 3, pp. 265-77.

Blazejewska, AI, Fischl, B, Wald, LL & Polimeni, JR 2019, 'Intracortical smoothing of small-voxel fMRI data can provide increased detection power without spatial resolution losses compared to conventional large-voxel fMRI data', *Neuroimage,* vol. 189, pp. 601-614.

Blomqvist, A & Craig, AD 1991, 'Organization of Spinal and Trigeminal Input to the PAG', in Depaulis, A & Bandler, R (eds.), *The Midbrain Periaqueductal Gray Matter: Functional, Anatomical, and Neurochemical Organization*, Springer US, Boston, MA.

Boivie, J 1979, 'An anatomical reinvestigation of the termination of the spinothalamic tract in the monkey', *J Comp Neurol,* vol. 186, no. 3, pp. 343-69.

Bouhassira, D, Villanueva, L, Bing, Z & Le Bars, D 1992, 'Involvement of the subnucleus reticularis dorsalis in diffuse noxious inhibitory controls in the rat', *Brain Res,* vol. 595, no. 2, pp. 353-7.

Brodmann, K 2006, *Brodmann's Localisation in the Cerebral Cortex: The Principles of Comparative Localisation in the Cerebral Cortex Based on Cytoarchitectonics*, Springer US, Boston, MA.

Brooks, J & Tracey, I 2005, 'From nociception to pain perception: imaging the spinal and supraspinal pathways', *Journal of anatomy,* vol. 207, no. 1, pp. 19-33.

Brown, TG 1915, 'Note on the physiology of the basal ganglia and mid-brain of the anthropoid ape, especially in reference to the act of laughter', *The Journal of physiology,* vol. 49, no. 4, pp. 195-207.

Cabral, J, Fernandes, FF & Shemesh, N 2023, 'Intrinsic macroscale oscillatory modes driving long range functional connectivity in female rat brains detected by ultrafast fMRI', *Nat Commun,* vol. 14, no. 1, pp. 375.

Cannon, WB 1915, *Bodily changes in pain, hunger, fear and rage : an account of recent researches into the function of emotional excitement*, D. Appleton and Company, New York ;.

Cao, B, Xu, Q, Shi, Y, Zhao, R, Li, H, Zheng, J, Liu, F, Wan, Y & Wei, B 2024, 'Pathology of pain and its implications for therapeutic interventions', *Signal Transduction and Target Therapy,* vol. 9, no. 1, pp. 155.

Carrive, P 1993, 'The periaqueductal gray and defensive behavior: Functional representation and neuronal organization', *Behavioural brain research,* vol. 58, no. 1, pp. 27-47.

Carrive, P & Bandler, R 1991a, 'Control of extracranial and hindlimb blood flow by the midbrain periaqueductal grey of the cat', *Experimental brain research,* vol. 84, no. 3, pp. 599-606.

Carrive, P & Bandler, R 1991b, 'Viscerotopic organization of neurons subserving hypotensive reactions within the midbrain periaqueductal grey: a correlative functional and anatomical study', *Brain research,* vol. 541, no. 2, pp. 206-215.

Carrive, P, Bandler, R & Dampney, RaL 1989, 'Somatic and autonomic integration in the midbrain of the unanesthetized decerebrate cat: a distinctive pattern evoked by excitation of neurones in the subtentorial portion of the midbrain periaqueductal grey', *Brain research,* vol. 483, no. 2, pp. 251-258.

Carrive, P, Dampney, RaL & Bandler, R 1987, 'Excitation of neurones in a restricted portion of the midbrain periaqueductal grey elicits both behavioural and cardiovascular components of the defence reaction in the unanaesthetised decerebrate cat', *Neuroscience letters,* vol. 81, no. 3, pp. 273-278.

Carrive, P & Morgan, MM 2012, 'The periaqueductal Gray', in Mai, JK & Paxinos, G (eds.), *The Human Nervous System,* Third edn, Academic Press, London.

Cedarbaum, JM & Aghajanian, GK 1978, 'Activation of locus coeruleus neurons by peripheral stimuli: modulation by a collateral inhibitory mechanism', *Life Sci,* vol. 23, no. 13, pp. 1383-92.

Chandler, DJ 2016, 'Evidence for a specialized role of the locus coeruleus noradrenergic system in cortical circuitries and behavioral operations', *Brain Res,* vol. 1641, no. Pt B, pp. 197-206.

Charmandari, E, Tsigos, C & Chrousos, G 2005, 'Endocrinology of the stress response', *Annu Rev Physiol,* vol. 67, pp. 259-84.

Chebbi, R, Boyer, N, Monconduit, L, Artola, A, Luccarini, P & Dallel, R 2014, 'The nucleus raphe magnus OFF-cells are involved in diffuse noxious inhibitory controls', *Experimental Neurology,* vol. 256, pp. 39-45.

Cho, ZH, Kang, CK, Son, YD, Choi, SH, Lee, YB, Paek, SH, Park, CW, Chi, JG, Calamante, F, Law, M & Kim, YB 2014, 'Pictorial review of in vivo human brain: from anatomy to molecular imaging', *World Neurosurgery,* vol. 82, no. 1-2, pp. 72-95.

Chung, JM, Kevetter, GA, Yezierski, RP, Haber, LH, Martin, RF & Willis, WD 1983, 'Midbrain nuclei projecting to the medial medulla oblongata in the monkey', *J Comp Neurol,* vol. 214, no. 1, pp. 93-102.

Clement, CI, Keay, KA, Podzebenko, K, Gordon, BD & Bandler, R 2000, 'Spinal sources of noxious visceral and noxious deep somatic afferent drive onto the ventrolateral periaqueductal gray of the rat', *J Comp Neurol,* vol. 425, no. 3, pp. 323-44.

Coghill, RC, Mchaffie, JG & Yen, Y-F 2003, 'Neural correlates of interindividual differences in the subjective experience of pain', *Proceedings of the National Academy of Sciences,* vol. 100, no. 14, pp. 8538-8542.

Craig, AD 2003, 'PAIN MECHANISMS: Labeled Lines Versus Convergence in Central Processing', *Annual Review of Neuroscience,* vol. 26, no. 1, pp. 1-30.

Craig, AD, Zhang, ET & Blomqvist, A 2002, 'Association of spinothalamic lamina I neurons and their ascending axons with calbindin-immunoreactivity in monkey and human', *Pain (Amsterdam),* vol. 97, no. 1, pp. 105-115.

Crawford, LS, Meylakh, N, Macey, PM, Macefield, VG, Keay, KA & Henderson, LA 2023, 'Stimulus-independent and stimulus-dependent neural networks underpin placebo analgesia responsiveness in humans', *Commun Biol,* vol. 6, no. 1, pp. 569.

Crawford, LS, Mills, EP, Hanson, T, Macey, PM, Glarin, R, Macefield, VG, Keay, KA & Henderson, LA 2021, 'Brainstem Mechanisms of Pain Modulation: A within-Subjects 7T fMRI Study of Placebo Analgesic and Nocebo Hyperalgesic Responses', *The Journal of Neuroscience,* vol. 41, no. 47, pp. 9794.

Cross, SA 1994, 'Pathophysiology of pain', *Mayo Clin Proc,* vol. 69, no. 4, pp. 375-83.

D'mello, R & Dickenson, AH 2008, 'Spinal cord mechanisms of pain', *BJA: British Journal of Anaesthesia,* vol. 101, no. 1, pp. 8-16.

Dąbrowski, A 2016, 'Emotions in Philosophy. A Short Introduction', *Studia Humana,* vol. 5.

Dagli, MS, Ingeholm, JE & Haxby, JV 1999, 'Localization of cardiac-induced signal change in fMRI', *Neuroimage,* vol. 9, no. 4, pp. 407-15.

Darwin, C 1872, *The expression of the emotions in man and animals*, John Murray, London.

Dasilva, AF, Becerra, L, Pendse, G, Chizh, B, Tully, S & Borsook, D 2008, 'Colocalized structural and functional changes in the cortex of patients with trigeminal neuropathic pain', *PloS one,* vol. 3, no. 10, pp. e3396.

Depaulis, A, Bandler, R & Vergnes, M 1989, 'Characterization of pretentorial periaqueductal gray matter neurons mediating intraspecific defensive behaviors in the rat by microinjections of kainic acid', *Brain Res,* vol. 486, no. 1, pp. 121-32.

Depaulis, A, Keay, KA & Bandler, R 1992, 'Longitudinal neuronal organization of defensive reactions in the midbrain periaqueductal gray region of the rat', *Exp Brain Res,* vol. 90, no. 2, pp. 307-18.

Derbyshire, SW & Osborn, J 2009, 'Offset analgesia is mediated by activation in the region of the periaqueductal grey and rostral ventromedial medulla', *Neuroimage,* vol. 47, no. 3, pp. 1002-6.

Diedrichsen, J 2006, 'A spatially unbiased atlas template of the human cerebellum', *Neuroimage,* vol. 33, no. 1, pp. 127-38.

Dostrovsky, JO, Craig, AD, Tracey, IMaPF, Mcmahon, SBFFSB, Turk, DCP & Koltzenburg, MMDF 2013, 'Ascending Projection Systems', *Wall and Melzack's Textbook of Pain,* Sixth Edition edn, Elsevier - Health Sciences Division, Philadelphia.

Dubin, AE & Patapoutian, A 2010, 'Nociceptors: the sensors of the pain pathway', *The Journal of clinical investigation,* vol. 120, no. 11, pp. 3760-3772.

Dujardin, E & Jürgens, U 2005, 'Afferents of vocalization-controlling periaqueductal regions in the squirrel monkey', *Brain Res,* vol. 1034, no. 1-2, pp. 114-31.

Eberhart, JA, Morrell, JI, Krieger, MS & Pfaff, DW 1985, 'An autoradiographic study of projections ascending from the midbrain central gray, and from the region lateral to it, in the rat', *J Comp Neurol,* vol. 241, no. 3, pp. 285-310.

Edens, BM, Stundl, J, Urrutia, HA & Bronner, ME 2024, 'Neural crest origin of sympathetic neurons at the dawn of vertebrates', *Nature,* vol. 629, no. 8010, pp. 121-126.

Eippert, F, Bingel, U, Schoell, ED, Yacubian, J, Klinger, R, Lorenz, J & Büchel, C 2009a, 'Activation of the Opioidergic Descending Pain Control System Underlies Placebo Analgesia', *Neuron,* vol. 63, no. 4, pp. 533-543.

Eippert, F, Finsterbusch, J, Bingel, U & Büchel, C 2009b, 'Direct Evidence for Spinal Cord Involvement in Placebo Analgesia', *Science,* vol. 326, no. 5951, pp. 404-404.

Faull, OK, Jenkinson, M, Clare, S & Pattinson, KT 2015, 'Functional subdivision of the human periaqueductal grey in respiratory control using 7 tesla fMRI', *Neuroimage,* vol. 113, pp. 356-64.

Faull, OK, Jenkinson, M, Ezra, M & Pattinson, KTS 2016, 'Conditioned respiratory threat in the subdivisions of the human periaqueductal gray', *eLife,* vol. 5, pp. e12047.

Faull, OK, Subramanian, HH, Ezra, M & Pattinson, KTS 2019, 'The midbrain periaqueductal gray as an integrative and interoceptive neural structure for breathing', *Neuroscience and biobehavioral reviews,* vol. 98, pp. 135-144.

Fields, HL, Bry, J, Hentall, I & Zorman, G 1983, 'The activity of neurons in the rostral medulla of the rat during withdrawal from noxious heat', *J Neurosci,* vol. 3, no. 12, pp. 2545-52.

Fields, HL & Heinricher, MM 1985, 'Anatomy and physiology of a nociceptive modulatory system', *Philos Trans R Soc Lond B Biol Sci,* vol. 308, no. 1136, pp. 361-74.

Fields, HL, Malick, A & Burstein, R 1995, 'Dorsal horn projection targets of ON and OFF cells in the rostral ventromedial medulla', *J Neurophysiol,* vol. 74, no. 4, pp. 1742-59.

Floyd, NS, Price, JL, Ferry, AT, Keay, KA & Bandler, R 2000, 'Orbitomedial prefrontal cortical projections to distinct longitudinal columns of the periaqueductal gray in the rat', *J Comp Neurol,* vol. 422, no. 4, pp. 556-78.

Floyd, NS, Price, JL, Ferry, AT, Keay, KA & Bandler, R 2001, 'Orbitomedial prefrontal cortical projections to hypothalamus in the rat', *J Comp Neurol,* vol. 432, no. 3, pp. 307-28.

Foerster, O 1933, 'THE DERMATOMES IN MAN', *Brain (London, England : 1878),* vol. 56, no. 1, pp. 1-39.

Garcia-Larrea, L, Frot, M & Valeriani, M 2003, 'Brain generators of laser-evoked potentials: from dipoles to functional significance', *Neurophysiologie clinique,* vol. 33, no. 6, pp. 279-292.

Gautier, A, Geny, D, Bourgoin, S, Bernard, JF & Hamon, M 2017, 'Differential innervation of superficial versus deep laminae of the dorsal horn by bulbo-spinal serotonergic pathways in the rat', *IBRO Reports,* vol. 2, pp. 72-80.

Greitz, D, Wirestam, R, Franck, A, Nordell, B, Thomsen, C & Ståhlberg, F 1992, 'Pulsatile brain movement and associated hydrodynamics studied by magnetic resonance phase imaging. The Monro-Kellie doctrine revisited', *Neuroradiology,* vol. 34, no. 5, pp. 370-80.

Hardy, SG & Leichnetz, GR 1981, 'Frontal cortical projections to the periaqueductal gray in the rat: a retrograde and orthograde horseradish peroxidase study', *Neurosci Lett,* vol. 23, no. 1, pp. 13-7.

Harrison, R, Gandhi, W, Van Reekum, C & Salomons, T 2022, 'Conditioned pain modulation is associated with heightened connectivity between the periaqueductal grey and cortical regions', *PAIN Reports,* vol. 7, pp. e999.

Heinricher, MM, Barbaro, NM & Fields, HL 1989, 'Putative nociceptive modulating neurons in the rostral ventromedial medulla of the rat: firing of on- and off-cells is related to nociceptive responsiveness', *Somatosens Mot Res,* vol. 6, no. 4, pp. 427-39.

Heinricher, MM, Morgan, MM, Tortorici, V & Fields, HL 1994, 'Disinhibition of off-cells and antinociception produced by an opioid action within the rostral ventromedial medulla', *Neuroscience,* vol. 63, no. 1, pp. 279-88.

Heinricher, MM, Tavares, I, Leith, JL & Lumb, BM 2009, 'Descending control of nociception: Specificity, recruitment and plasticity', *Brain Res Rev,* vol. 60, no. 1, pp. 214-25.

Henderson, AL, Gandevia, CS & Macefield, GV 2007, 'Somatotopic organization of the processing of muscle and cutaneous pain in the left and right insula cortex: A single-trial fMRI study', *Pain,* vol. 128, no. 12, pp. 20-30.

Henderson, LA & Macefield, VG 2013, 'Functional Imaging of the Human Brainstem during Somatosensory Input and Autonomic Output', *Frontiers in Human Neuroscience,* vol. 7, pp. 569.

Hilton, SM & Redfern, WS 1986, 'A search for brain stem cell groups integrating the defence reaction in the rat', *The Journal of physiology,* vol. 378, no. 1, pp. 213-228.

Hladnik, A, Bičanić, I & Petanjek, Z 2015, 'Functional neuroanatomy of nociception and pain', *Periodicum Biologorum,* vol. 117, no. 2, pp. 195-204.

Holstege, G 1998, 'The emotional motor system in relation to the supraspinal control of micturition and mating behavior', *Behav Brain Res,* vol. 92, no. 2, pp. 103-9.

Julien, N, Goffaux, P, Arsenault, P & Marchand, S 2005, 'Widespread pain in fibromyalgia is related to a deficit of endogenous pain inhibition', *PAIN,* vol. 114, no. 1.

Jürgens, U & Ploog, D 1970, 'Cerebral representation of vocalization in the squirrel monkey', *Experimental brain research,* vol. 10, no. 5, pp. 532-554.

Jürgens, U & Zwirner, P 1996, 'The role of the periaqueductal grey in limbic and neocortical vocal fold control', *Neuroreport,* vol. 7, no. 18, pp. 2921-2924.

Kabat, H, Magoun, HW & Ranson, SW 1935, 'ELECTRICAL STIMULATION OF POINTS IN THE FOREBRAIN AND MIDBRAIN: THE RESULTANT ALTERATIONS IN BLOOD PRESSURE', *Archives of Neurology & Psychiatry,* vol. 34, no. 5, pp. 931-955.

Kaptchuk, TJ, Hemond, CC & Miller, FG 2020, 'Placebos in chronic pain: evidence, theory, ethics, and use in clinical practice', *BMJ,* vol. 370, pp. m1668.

Keay, K & Bandler, R 2008, 'Emotional and Behavioral Significance of the Pain Signal and the Role of the Midbrain Periaqueductal Gray (PAG)', in Masland, RH, Albright, TD, Albright, TD, Masland, RH, Dallos, P, Oertel, D, Firestein, S, Beauchamp, GK, Catherine Bushnell, M, Basbaum, AI, Kaas, JH & Gardner, EP (eds.), *The Senses: A Comprehensive Reference*, Academic Press, New York.

Keay, KA & Bandler, R 1993, 'Deep and superficial noxious stimulation increases Fos-like immunoreactivity in different regions of the midbrain periaqueductal grey of the rat', *Neuroscience letters,* vol. 154, no. 1, pp. 23-26.

Keay, KA & Bandler, R 2001, 'Parallel circuits mediating distinct emotional coping reactions to different types of stress', *Neuroscience and biobehavioral reviews,* vol. 25, no. 7-8, pp. 669-678.

Keay, KA, Clement, CI, Depaulis, A & Bandler, R 2001, 'Different representations of inescapable noxious stimuli in the periaqueductal gray and upper cervical spinal cord of freely moving rats', *Neuroscience Letters,* vol. 313, no. 1, pp. 17-20.

Keay, KA, Clement, CI, Owler, B, Depaulis, A & Bandler, R 1994, 'Convergence of deep somatic and visceral nociceptive information onto a discrete ventrolateral midbrain periaqueductal gray region', *Neuroscience,* vol. 61, no. 4, pp. 727-732.

Keay, KA, Feil, K, Gordon, BD, Herbert, H & Bandler, R 1997, 'Spinal afferents to functionally distinct periaqueductal gray columns in the rat: An anterograde and retrograde tracing study', *Journal of comparative neurology (1911),* vol. 385, no. 2, pp. 207-229.

Kiefel, JM, Rossi, GC & Bodnar, RJ 1993, 'Medullary mu and delta opioid receptors modulate mesencephalic morphine analgesia in rats', *Brain Res,* vol. 624, no. 1-2, pp. 151-61.

King, CD, Wong, F, Currie, T, Mauderli, AP, Fillingim, RB & Riley, JL, 3rd 2009, 'Deficiency in endogenous modulation of prolonged heat pain in patients with Irritable Bowel Syndrome and Temporomandibular Disorder', *PAIN,* vol. 143, no. 3.

Kong, J, Gollub, RL, Rosman, IS, Webb, JM, Vangel, MG, Kirsch, I & Kaptchuk, TJ 2006, 'Brain Activity Associated with Expectancy-Enhanced Placebo Analgesia as Measured by Functional Magnetic Resonance Imaging', *The Journal of Neuroscience,* vol. 26, no. 2, pp. 381.

Krieger, JE & Graeff, FG 1985, 'Defensive behavior and hypertension induced by glutamate in the midbrain central gray of the rat', *Braz J Med Biol Res,* vol. 18, no. 1, pp. 61-7.

Krummenacher, P, Candia, V, Folkers, G, Schedlowski, M & Schönbächler, G 2010, 'Prefrontal cortex modulates placebo analgesia', *Pain,* vol. 148, no. 3, pp. 368-374.

Le Gros Clark, WE 1936, 'The Termination of Ascending Tracts in the Thalamus of the Macaque Monkey', *Journal of Anatomy,* vol. 71, no. Pt 1, pp. 7-40.

Ledoux, JE, Iwata, J, Cicchetti, P & Reis, DJ 1988, 'Different projections of the central amygdaloid nucleus mediate autonomic and behavioral correlates of conditioned fear', *J Neurosci,* vol. 8, no. 7, pp. 2517-29.

Lee, MWL, Mcphee, RW & Stringer, MD 2008, 'An evidence-based approach to human dermatomes', *Clinical anatomy (New York, N.Y.),* vol. 21, no. 5, pp. 363-373.

Leichnetz, GR, Spencer, RF, Hardy, SG & Astruc, J 1981, 'The prefrontal corticotectal projection in the monkey; an anterograde and retrograde horseradish peroxidase study', *Neuroscience,* vol. 6, no. 6, pp. 1023-41.

Levine, JD, Gordon, NC & Fields, HL 1978, 'The mechanism of placebo analgesia', *Lancet,* vol. 2, no. 8091, pp. 654-7.

Levine, R, Morgan, MM, Cannon, JT & Liebeskind, JC 1991, 'Stimulation of the periaqueductal gray matter of the rat produces a preferential ipsilateral antinociception', *Brain Research,* vol. 567, no. 1, pp. 140-144.

Lewis, T 1942, *Pain*, MacMillan, New York.

Liao, C-C & Yen, C-T 2008, 'Functional Connectivity of the Secondary Somatosensory Cortex of the Rat', *The Anatomical Record,* vol. 291, no. 8, pp. 960-973.

Liebeskind, JC & Mayer, DJ 1971, 'Somatosensory evoked responses in the mesencephalic central gray matter of the rat', *Brain Research,* vol. 27, no. 1, pp. 133-151.

Linnman, C, Moulton, EA, Barmettler, G, Becerra, L & Borsook, D 2012, 'Neuroimaging of the periaqueductal gray: State of the field', *NeuroImage (Orlando, Fla.),* vol. 60, no. 1, pp. 505-522.

Llorca-Torralba, M, Borges, G, Neto, F, Mico, JA & Berrocoso, E 2016, 'Noradrenergic Locus Coeruleus pathways in pain modulation', *Neuroscience,* vol. 338, pp. 93-113.

Magoun, HW, Atlas, D, Ingersoll, EH & Ranson, SW 1937, 'Associated Facial, Vocal and Respiratory Components of Emotional Expression: An Experimental Study', *Journal of neurology, neurosurgery and psychiatry,* vol. s1-17, no. 67, pp. 241-255.

Mancia, G, Baccelli, G & Zanchetti, A 1972, 'Hemodynamic responses to different emotional stimuli in the cat: patterns and mechanisms', *Am J Physiol,* vol. 223, no. 4, pp. 925-33.

Mantyh, PW 1982a, 'The ascending input to the midbrain periaqueductal gray of the primate', *J Comp Neurol,* vol. 211, no. 1, pp. 50-64.

Mantyh, PW 1982b, 'Forebrain projections to the periaqueductral gray in the monkey, with observations in the cat and rat', *Journal of Comparative Neurology,* vol. 206, no. 2, pp. 146-158.

Mantyh, PW 1982c, 'The midbrain periaqueductal gray in the rat, cat, and monkey: A Nissl, Weil, and Golgi analysis', *Journal of comparative neurology (1911),* vol. 204, no. 4, pp. 349-363.

Mantyh, PW 1983a, 'Connections of midbrain periaqueductal gray in the monkey. I. Ascending efferent projections', *J Neurophysiol,* vol. 49, no. 3, pp. 567-81.

Mantyh, PW 1983b, 'Connections of midbrain periaqueductal gray in the monkey. II. Descending efferent projections', *J Neurophysiol,* vol. 49, no. 3, pp. 582-94.

Mayer, DJ & Liebeskind, JC 1974, 'Pain reduction by focal electrical stimulation of the brain: An anatomical and behavioral analysis', *Brain Research,* vol. 68, no. 1, pp. 73-93.

Mayer, DJ, Wolfle, TL, Akil, H, Carder, B & Liebeskind, JC 1971, 'Analgesia from Electrical Stimulation in the Brainstem of the Rat', *Science,* vol. 174, no. 4016, pp. 1351.

Mazzola, L, Isnard, J, Peyron, R, Guénot, M & Mauguière, F 2009, 'Somatotopic organization of pain responses to direct electrical stimulation of the human insular cortex', *Pain,* vol. 146, no. 12, pp. 99-104.

Mcdowell, AR & Carmichael, DW 2019, 'Optimal repetition time reduction for single subject event-related functional magnetic resonance imaging', *Magnetic Resonance in Medicine,* vol. 81, no. 3, pp. 1890-1897.

Mehler, WR 1969, 'SOME NEUROLOGICAL SPECIES DIFFERENCES - A POSTERIORI', *Annals of the New York Academy of Sciences,* vol. 167, no. 1, pp. 424-468.

Mehler, WR, Feferman, ME & Nauta, WJH 1960, 'ASCENDING AXON DEGENERATION FOLLOWING ANTEROLATERAL CORDOTOMY. AN EXPERIMENTAL STUDY IN THE MONKEY', *Brain (London, England : 1878),* vol. 83, no. 4, pp. 718-750.

Mehnert, J, Tinnermann, A, Basedau, H & May, A 2024, 'Functional representation of trigeminal nociceptive input in the human periaqueductal gray', *Science Advances,* vol. 10, no. 12, pp. eadj8213.

Meller, ST & Dennis, BJ 1986, 'Afferent projections to the periaqueductal gray in the rabbit', *Neuroscience,* vol. 19, no. 3, pp. 927-64.

Mense, S 1993, 'Nociception from skeletal muscle in relation to clinical muscle pain', Elsevier B.V.

Mesulam, MM & Brushart, TM 1979, 'Transganglionic and anterograde transport of horseradish peroxidase across dorsal root ganglia: A tetramethylbenzidine method for tracing central sensory connections of muscles and peripheral nerves', *Neuroscience,* vol. 4, no. 8, pp. 1107-1117.

Mobbs, D, Hagan, CC, Dalgleish, T, Silston, B & Prévost, C 2015, 'The ecology of human fear: survival optimization and the nervous system', *Frontiers in Neuroscience,* vol. 9.

Montgomery, G & Kirsch, I 1996, 'Mechanisms of Placebo Pain Reduction: An Empirical Investigation', *Psychological Science,* vol. 7, no. 3, pp. 174-176.

Mysicka, A & Zenker, W 1981, 'Central projections of muscle afferents from the sternomastoid nerve in the rat', *Brain Res,* vol. 211, no. 2, pp. 257-65.

Nagaro, T, Adachi, N, Tabo, E, Kimura, S, Arai, T & Dote, K 2001, 'New pain following cordotomy: clinical features, mechanisms, and clinical importance', *Journal of Neurosurgery,* vol. 95, no. 3, pp. 425-431.

Nagy, Z, Hutton, C, David, G, Hinterholzer, N, Deichmann, R, Weiskopf, N & Vannesjo, SJ 2023, 'HiHi fMRI: a data-reordering method for measuring the hemodynamic response of the brain with high temporal resolution and high SNR', *Cerebral Cortex,* vol. 33, no. 8, pp. 4606-4611.

Napadow, V, Sclocco, R & Henderson, LA 2019, 'Brainstem neuroimaging of nociception and pain circuitries', *PAIN Reports,* vol. 4, no. 4.

Niven, JE & Laughlin, SB 2008, 'Energy limitation as a selective pressure on the evolution of sensory systems', *Journal of Experimental Biology,* vol. 211, no. 11, pp. 1792-1804.

Nolte, J 2013, *The Human Brain in Photographs and Diagrams*, Fourth edition. edn, Elsevier - Health Sciences Division, Saint Louis.

Olson, I, Suryanarayana, SM, Robertson, B & Grillner, S 2017, 'Griseum centrale, a homologue of the periaqueductal gray in the lamprey', *IBRO Rep,* vol. 2, pp. 24-30.

Olszewski, J & Baxter, D 1954, *Cytoarchitecture of the Human Brain Stem*, Lippincott, Philadelphia.

Ostrowsky, K, Magnin, M, Ryvlin, P, Isnard, J, Guenot, M & Mauguière, F 2002, 'Representation of Pain and Somatic Sensation in the Human Insula: a Study of Responses to Direct Electrical Cortical Stimulation', *Cerebral Cortex,* vol. 12, no. 4, pp. 376-385.

Penfield, W & Rasmussen, T 1950, *The cerebral cortex of man; a clinical study of localization of function*, Macmillan, Oxford, England.

Petrovic, P, Kalso, E, Petersson, KM & Ingvar, M 2002, 'Placebo and Opioid Analgesia-- Imaging a Shared Neuronal Network', *Science,* vol. 295, no. 5560, pp. 1737-1740.

Piovesan, EJ, Kowacs, PA, Tatsui, CE, Lange, MC, Ribas, LC & Werneck, LC 2001, 'Referred Pain After Painful Stimulation of the Greater Occipital Nerve in Humans: Evidence of Convergence of Cervical Afferences on Trigeminal Nuclei', *Cephalalgia,* vol. 21, no. 2, pp. 107-109.

Price, JL & Amaral, DG 1981, 'An autoradiographic study of the projections of the central nucleus of the monkey amygdala', *J Neurosci,* vol. 1, no. 11, pp. 1242-59.

Purves, D, Augustine, GJ & Fitzpatrick, D 2001, *Neuroscience, 2nd Edition*, 2nd edn, Sinauer Associates, Sunderland, MA.

Raj, D, Anderson, AW & Gore, JC 2001, 'Respiratory effects in human functional magnetic resonance imaging due to bulk susceptibility changes', *Phys Med Biol,* vol. 46, no. 12, pp. 3331-40.

Reynolds, DV 1969, 'Surgery in the Rat during Electrical Analgesia Induced by Focal Brain Stimulation', *Science,* vol. 164, no. 3878, pp. 444.

Roeder, Z, Chen, Q, Davis, S, Carlson, JD, Tupone, D & Heinricher, MM 2016, 'Parabrachial complex links pain transmission to descending pain modulation', *Pain,* vol. 157, no. 12, pp. 2697-2708.

Sachs, E 1911, 'ON THE RELATION OF THE OPTIC THALAMUS TO RESPIRATION, CIRCULATION, TEMPERATURE, AND THE SPLEEN', *J Exp Med,* vol. 14, no. 4, pp. 408-32.

Sanchez-Panchuelo, RM, Besle, J, Beckett, A, Bowtell, R, Schluppeck, D & Francis, S 2012, 'Within-Digit Functional Parcellation of Brodmann Areas of the Human Primary Somatosensory Cortex Using Functional Magnetic Resonance Imaging at 7 Tesla', *The Journal of Neuroscience,* vol. 32, no. 45, pp. 15815.

Satpute, AB, Wager, TD, Cohen-Adad, J, Bianciardi, M, Choi, J-K, Buhle, JT, Wald, LL & Barrett, LF 2013, 'Identification of discrete functional subregions of the human periaqueductal gray', *Proceedings of the National Academy of Sciences,* vol. 110, no. 42, pp. 17101-17106.

Sauro, MD & Greenberg, RP 2005, 'Endogenous opiates and the placebo effect: a meta-analytic review', *J Psychosom Res,* vol. 58, no. 2, pp. 115-20.

Schafer, SM, Geuter, S & Wager, TD 2018, 'Mechanisms of placebo analgesia: A dual-process model informed by insights from cross-species comparisons', *Prog Neurobiol,* vol. 160, pp. 101-122.

Schellekens, W, Petridou, N & Ramsey, NF 2018, 'Detailed somatotopy in primary motor and somatosensory cortex revealed by Gaussian population receptive fields', *Neuroimage,* vol. 179, pp. 337-347.

Sclocco, R, Beissner, F, Bianciardi, M, Polimeni, JR & Napadow, V 2018, 'Challenges and opportunities for brainstem neuroimaging with ultrahigh field MRI', *Neuroimage,* vol. 168, pp. 412-426.

Scott, DJ, Stohler, CS, Egnatuk, CM, Wang, H, Koeppe, RA & Zubieta, JK 2008, 'Placebo and nocebo effects are defined by opposite opioid and dopaminergic responses', *Arch Gen Psychiatry,* vol. 65, no. 2, pp. 220-31.

Sessle, B 2000, 'Acute and chronic craniofacial pain: Brainstem mechanisms of nociceptive transmission and neuroplasticity, and their clinical correlates', *Critical Reviews In Oral Biology & Medicine,* vol. 11, no. 1, pp. 57-91.

Sherrington, CS 1893, 'Experiments in Examination of the Peripheral Distribution of the Fibres of the Posterior Roots of Some Spinal Nerves. Part I', *Philosophical Transactions of the Royal Society of London. Series B: Biological Sciences,* vol. 184, pp. 641-763.

Sherrington, CS 1898, 'Experiments in Examination of the Peripheral Distribution of the Fibres of the Posterior Roots of Some Spinal Nerves. Part II', *Philosophical Transactions of the Royal Society of London, Series B: Biological Sciences,* vol. 190, pp. 45-186.

Shipley, MT, Ennis, M, Rizvi, TA & Behbehani, MM 1991, 'Topographical Specificity of Forebrain Inputs to the Midbrain Periaqueductal Gray: Evidence for Discrete Longitudinally Organized Input Columns', in Depaulis, A & Bandler, R (eds.), *The Midbrain Periaqueductal Gray Matter: Functional, Anatomical, and Neurochemical Organization*, Springer US, Boston, MA.

Singewald, N & Sharp, T 2000, 'Neuroanatomical targets of anxiogenic drugs in the hindbrain as revealed by Fos immunocytochemistry', *Neuroscience,* vol. 98, no. 4, pp. 759-70.

Smith, JJ, Timoshevskaya, N, Ye, C, Holt, C, Keinath, MC, Parker, HJ, Cook, ME, Hess, JE, Narum, SR, Lamanna, F, Kaessmann, H, Timoshevskiy, VA, Waterbury, CKM, Saraceno, C, Wiedemann, LM, Robb, SMC, Baker, C, Eichler, EE, Hockman, D, Sauka-Spengler, T, Yandell, M, Krumlauf, R, Elgar, G & Amemiya, CT 2018, 'The sea lamprey germline genome provides insights into programmed genome rearrangement and vertebrate evolution', *Nature Genetics,* vol. 50, no. 2, pp. 270-277.

Song, H, Kim, M, Kim, E, Lee, J, Jeong, I, Lim, K, Ryu, SY, Oh, M, Kim, Y & Park, J-U 2024, 'Neuromodulation of the peripheral nervous system: Bioelectronic technology and prospective developments', *BMEMat,* vol. 2, no. 1, pp. e12048.

Soper, WY & Melzack, R 1982, 'Stimulation-produced analgesia: Evidence for somatotopic organization in the midbrain', *Brain Research,* vol. 251, no. 2, pp. 301-311.

Standring, S 2008, 'Gray's Anatomy: The Anatomical Basis of Clinical Practice', Elsevier, United Kingdom.

Stephenson-Jones, M, Samuelsson, E, Ericsson, J, Robertson, B & Grillner, S 2011, 'Evolutionary conservation of the basal ganglia as a common vertebrate mechanism for action selection', *Curr Biol,* vol. 21, no. 13, pp. 1081-91.

Szikszay, TM, Adamczyk, WM, Carvalho, GF, May, A & Luedtke, K 2020, 'Offset analgesia: somatotopic endogenous pain modulation in migraine', *Pain,* vol. 161, no. 3, pp. 557-564.

Taber, E, Brodal, A & Walberg, F 1960, 'The raphe nuclei of the brain stem in the cat. I. Normal topography and cytoarchitecture and general discussion', *The Journal of Comparative Neurology,* vol. 114, pp. 161-87.

Toi, PT, Jang, HJ, Min, K, Kim, SP, Lee, SK, Lee, J, Kwag, J & Park, JY 2022, 'In vivo direct imaging of neuronal activity at high temporospatial resolution', *Science,* vol. 378, no. 6616, pp. 160-168.

Torebjörk, H & Hallin, R 1973, 'Perceptual changes accompanying controlled preferential blocking of A and C fibre responses in intact human skin nerves', *Experimental Brain Research,* vol. 16, no. 3, pp. 321-332.

Tracey, I 2005, 'Nociceptive processing in the human brain', *Current Opinion in Neurobiology,* vol. 15, no. 4, pp. 478-487.

Tracey, I, Ploghaus, A, Gati, JS, Clare, S, Smith, S, Menon, RS & Matthews, PM 2002, 'Imaging attentional modulation of pain in the periaqueductal gray in humans', *J Neurosci,* vol. 22, no. 7, pp. 2748-52.

Treede, R-D, Kenshalo, DR, Gracely, RH & Jones, AKP 1999, 'The cortical representation of pain', Elsevier B.V.

Tu, Y, Wilson, G, Camprodon, J, Dougherty, DD, Vangel, M, Benedetti, F, Kaptchuk, TJ, Gollub, RL & Kong, J 2021, 'Manipulating placebo analgesia and nocebo hyperalgesia by changing brain excitability', *Proc Natl Acad Sci U S A,* vol. 118, no. 19.

Vanderah, T & Gould, DJ 2020, *Nolte's The Human Brain: An Introduction to its Functional Anatomy*, 8th edition. edn, Elsevier.

Vase, L, Skyt, I & Hall, KT 2016, 'Placebo, nocebo, and neuropathic pain', *PAIN,* vol. 157.

Vedantam, A, Bruera, E, Hess, KR, Dougherty, PM & Viswanathan, A 2019, 'Somatotopy and Organization of Spinothalamic Tracts in the Human Cervical Spinal Cord', *Neurosurgery,* vol. 84, no. 6, pp. E311-E317.

Wager, TD, Rilling, JK, Smith, EE, Sokolik, A, Casey, KL, Davidson, RJ, Kosslyn, SM, Rose, RM & Cohen, JD 2004, 'Placebo-Induced Changes in fMRI in the Anticipation and Experience of Pain', *Science,* vol. 303, no. 5661, pp. 1162-1167.

Waite, P & Ashwell, K 2004, 'Chapter 29. Trigeminal Sensory System'.

Wall, PD 1979, 'On the relation of injury to pain the John J. Bonica Lecture', *Pain,* vol. 6, no. 3, pp. 253-264.

Wall, PD & Taub, A 1962, 'Four aspects of trigeminal nucleus and a paradox', *Journal of neurophysiology,* vol. 25, pp. 110-126.

Watkins, LR, Griffin, G, Leichnetz, GR & Mayer, DJ 1980, 'The somatotopic organization of the nucleus raphe magnus and surrounding brain stem structures as revealed by HRP slow-release gels', *Brain Res,* vol. 181, no. 1, pp. 1-15.

Wiberg, M & Blomqvist, A 1984, 'The spinomesencephalic tract in the cat: its cells of origin and termination pattern as demonstrated by the intraaxonal transport method', *Brain Res,* vol. 291, no. 1, pp. 1-18.

Wiberg, M, Westman, J & Blomqvist, A 1987, 'Somatosensory projection to the mesencephalon: An anatomical study in the monkey', *Journal of comparative neurology (1911),* vol. 264, no. 1, pp. 92-117.

Wilder-Smith, CH, Schindler, D, Lovblad, K, Redmond, SM & Nirkko, A 2004, 'Brain functional magnetic resonance imaging of rectal pain and activation of endogenous inhibitory mechanisms in irritable bowel syndrome patient subgroups and healthy controls', *Gut,* vol. 53, no. 11, pp. 1595.

Xu, Y, Zhu, SW & Li, QW 2016, 'Lamprey: a model for vertebrate evolutionary research', *Zool Res,* vol. 37, no. 5, pp. 263-9.

Yaksh, TL, Yeung, JC & Rudy, TA 1976, 'Systematic examination in the rat of brain sites sensitive to the direct application of morphine: observation of differential effects within the periaqueductal gray', *Brain Research,* vol. 114, no. 1, pp. 83-103.

Yezierski, RP 1988, 'Spinomesencephalic tract: Projections from the lumbosacral spinal cord of the rat, cat, and monkey', *Journal of Comparative Neurology,* vol. 267, no. 1, pp. 131-146.

Youssef, AM, Macefield, VG & Henderson, LA 2016, 'Pain inhibits pain; human brainstem mechanisms', *NeuroImage,* vol. 124, pp. 54-62.

Zemlan, FP, Leonard, CM, Kow, LM & Pfaff, DW 1978, 'Ascending tracts of the lateral columns of the rat spinal cord: a study using the silver impregnation and horseradish peroxidase techniques', *Exp Neurol,* vol. 62, no. 2, pp. 298-334.

Zhang, SP, Bandler, R & Carrive, P 1990, 'Flight and immobility evoked by excitatory amino acid microinjection within distinct parts of the subtentorial midbrain periaqueductal gray of the cat', *Brain research,* vol. 520, no. 1, pp. 73-82.

Appendix A:

Differential activation of lateral parabrachial nuclei and their limbic projections during head compared with body pain: A 7-Tesla functional magnetic resonance imaging study

NeuroImage 299 (2024) 120832

Contents lists available at ScienceDirect

NeuroImage

journal homepage: www.elsevier.com/locate/ynimg

Differential activation of lateral parabrachial nuclei and their limbic projections during head compared with body pain: A 7-Tesla functional magnetic resonance imaging study

Rebecca V Robertson [a], Noemi Meylakh [a], Lewis S Crawford [a], Fernando A Tinoco Mendoza [a], Paul M Macey [b], Vaughan G Macefield [c], Kevin A Keay [a], Luke A Henderson [a,*]

[a] School of Medical Sciences (Neuroscience), Brain and Mind Centre, University of Sydney, 2006, Australia
[b] UCLA School of Nursing and Brain Research Institute, University of California, Los Angeles, California, 90095, USA
[c] Department of Neuroscience, Monash University, Melbourne, VIC, Australia

ARTICLE INFO

Keywords:
Brainstem
Parabrachial nucleus
Hypothalamus
Thalamus
Ultra-high field MRI

ABSTRACT

Pain is a complex experience that involves sensory, emotional, and motivational components. It has been suggested that pain arising from the head and orofacial regions evokes stronger emotional responses than pain from the body. Indeed, recent work in rodents reports different patterns of activation in ascending pain pathways during noxious stimulation of the skin of the face when compared to noxious stimulation of the body. Such differences may dictate different activation patterns in higher brain regions, specifically in those areas processing the affective component of pain. We aimed to use ultra-high field functional magnetic resonance imaging (fMRI at 7-Tesla) to determine whether noxious thermal stimuli applied to the surface of the face and body evoke differential activation patterns within the ascending pain pathway in awake humans (n=16). Compared to the body, noxious heat stimulation to the face evoked more widespread signal changes in prefrontal cortical regions and numerous brainstem and subcortical limbic areas. Moreover, facial pain evoked significantly different signal changes in the lateral parabrachial nucleus, substantia nigra, paraventricular hypothalamus, and paraventricular thalamus, to those evoked by body pain. These results are consistent with recent preclinical findings of differential activation in the brainstem and subcortical limbic nuclei and associated cortices during cutaneous pain of the face when compared with the body. The findings suggest one potential mechanism by which facial pain could evoke a greater emotional impact than that evoked by body pain.

1. Introduction

Pain acts as a warning signal that drives behavioural changes that remove an individual from danger. Signals arising from noxious stimuli applied to the body ascend from the dorsal horn of the spinal cord, while those arising from the head and orofacial regions arise from the spinal trigeminal nucleus. These signals ascend in multiple pathways terminating in a number of subcortical and cortical structures in which the pain experience is processed. Ascending projections to the somatosensory cortices via the ventrocaudal thalamus code sensory perceptual aspects of pain, including stimulus intensity, quality, and location (Willis and Westlund, 1997). Ascending projections to the midbrain, specifically to the dorsal periaqueductal gray matter (PAG), are responsible for triggering active coping responses, that includes fight or flight behaviours. These PAG-evoked behavioural reactions remove an individual from danger and are the usual responses to superficial/cutaneous pain (Bandler et al., 2000). Further, ascending projections to the lateral parabrachial nucleus in the brainstem relay their noxious inputs to the cingulate and insular cortices, the amygdala, and the hypothalamus, and this network of projections is critical for emotional aspects of pain including fear of pain, and suffering (Bernard et al., 1996).

Emerging evidence from human studies suggests that pain originating from the head and orofacial region is more emotionally intense and distressing than pain originating from the body. Studies in people suggest that despite reporting similar perceived intensities at each site, pain-related fear is rated higher for the head when compared with the body (Schmidt et al., 2016). A recent preclinical study in mice, using

* Corresponding author.
E-mail address: luke.henderson@sydney.edu.au (L.A. Henderson).

https://doi.org/10.1016/j.neuroimage.2024.120832
Received 28 June 2024; Received in revised form 16 August 2024; Accepted 2 September 2024
Available online 3 September 2024

activity-dependent anatomical tracing technology showed that the lateral parabrachial nucleus (lPB) is activated more strongly by noxious stimuli applied to the head, when compared with the hind-paw, and furthermore lPB activation following stimulation of the head is strongly bilateral (Rodriguez et al., 2017). These pain responsive lPB neurons were shown to project to multiple targets including the paraventricular nucleus of the hypothalamus, the central nucleus of the amygdala, the bed nucleus stria terminalis (BNST), the paraventricular thalamic nucleus (PVT) and the substantial nigra (SN). This study also revealed that there is a direct projection from neurons in the trigeminal ganglion to the lPB in mice. The authors speculated that this pathway provides an additional route by which noxious stimuli in the head and orofacial region could activate the lPB and its output targets to evoke stronger emotional reactions than those which arise from noxious stimulation of the body.

Although this preclinical study provides compelling evidence for differential activation of specific subcortical structures such as the lPB, hypothalamus and amygdala during head versus body pain, similar comparisons in humans are yet to be made. In a recent study, we used ultra-high field (7-Tesla) functional magnetic resonance imaging (fMRI) to define signal changes in the PAG, hypothalamus, and amygdala in awake humans during noxious stimuli applied to the face (Robertson et al., 2022). We found that acute facial pain evoked robust signal intensity increases in the lateral PAG and decreases of a similar size, in multiple hypothalamic and amygdala subnuclei. Our study characterised only the signal changes in response to noxious heat applied to the face, comparison of differences in activity in the PAG, hypothalamus, and amygdala during noxious stimuli applied to the face *versus* the body has not yet been conducted. Similarly, there have been no attempts to compare activation patterns in the lPB during noxious stimuli applied to different body regions either, therefore it remains unknown whether the recently reported differences in pattern and intensity of lPB activation during face versus hind-paw stimulation in preclinical studies, is also present in humans. It is also unknown whether in humans the lPB is also embedded in a common functional network that includes the SN, hypothalamus, amygdala, BNST, and PVT as described in preclinical studies. Defining the functional networks in which different emotional encoding of face *versus* body pain is represented could provide an important platform, for determining the role of such circuitry in chronic pain conditions, especially those originating in the orofacial region, which are distressing and drive severe disability in this cohort of patients.

The aim of this study was to use ultra-high field fMRI to explore subcortical activation patterns during noxious stimulation of the face and body in awake humans. We hypothesized that noxious heat stimuli applied to the face would evoke larger signal intensity changes in the lPB, hypothalamus, amygdala, BNST, PVT, and SN, than noxious stimuli applied to the body. In addition, we also hypothesized that noxious stimulation of the face would evoke greater signal intensity changes in the prefrontal and cingulate cortices which are known to be involved in emotional processing.

2. Materials and methods

2.1. Participants

Sixteen healthy people (7 females; mean[±SEM] age 25.8 ± 1.4 years, range 20-35 years) were recruited for the study. Informed written consent was obtained for all procedures, which were conducted with the approval of the local Institutional Human Research Ethics Committees, and which were consistent with the Declaration of Helsinki, apart from registration in a public database. All experiments were conducted at the Melbourne Brain Centre Imaging Unit, University of Melbourne.

Before entering the MRI scanner, an MRI compatible Thermal Sensory Analyser unit connected to a 30 × 30mm thermode (TSA-II, Medoc) was placed onto the volar surface of each participant's right forearm. The thermode temperature was increased from a baseline temperature of 32°C to one of a series of ten randomly ordered temperatures within the range 44°C-48.5°C, in 0.5°C increments. Participants verbally reported the perceived pain intensity of these stimuli using an 11-point scale, where 0 indicated no pain, and 10 indicated the worst pain imaginable. The temperature that elicited a moderate pain intensity (approximately 5 out of 10) was used for the remainder of the experiment.

2.2. MRI scanning and data acquisition

Participants lay supine in a Siemens MAGNETOM 7-Tesla MRI system (Siemens Healthcare, Erlangen, Germany) with a combined tight-fitting single-channel transmit and 32-channel receive head coil (Nova Medical, Wilmington MA, USA). A T1-weighted anatomical image set covering the whole brain was collected (repetition time 5000 ms, echo time 3.1 ms, raw voxel size=0.73 × 0.73 × 0.73 mm, 224 sagittal slices, scan time 7 mins). Next, four scans of 134 gradient echo echo-planar fMRI volumes using blood oxygen-dependent (BOLD) contrast and covering the entire brain were collected over 335 seconds each. Images were acquired in an interleaved collection pattern with a multi-band factor of four and an acceleration factor of three (124 axial slices, repetition time 2500 ms; echo time 26 ms; voxel size: 1.0 × 1.0 × 1.2 mm thick).

During each of the fMRI scans, a repeated series of brief noxious stimuli were delivered via the thermode to four different parts of the body. Two series were delivered to the face—one on the right corner of the mouth (lips) and another on the right cheek—two series were delivered to the body—one series on the thenar eminence (thumb) and another on the plantar surface of the big toe (Fig. 1A). For each fMRI scan, following a 90-second baseline period, a series of 8 noxious thermal stimuli reaching the target (moderate) temperature were applied. The thermode temperature was raised over 2.5-seconds and held at the target temperature for 10-seconds before being lowered over 2.5-seconds to the baseline temperature (32°C), at which it was held for 15-seconds. This was repeated 7 times for a total of 8 noxious stimulation periods. This procedure, with a series of 8 noxious stimuli was repeated a further three times for a total of four sets of fMRI scans in each participant. Between scans, the thermode was moved between the four body sites. Following each of the four fMRI scans, participants were asked to rate the intensity of pain on an 11-point visual analogue scale (VAS).

2.3. Pain intensity and temperature analysis

Pain intensity ratings were calculated for each individual, for each of the four fMRI scan series, by taking the mean, of the mean pain intensity ratings on the 11-point visual analogue scale following each scan. The mean pain intensity ratings were compared between stimulus sites using a repeated measures one-way ANOVA ($p<0.05$, Bonferroni corrected for multiple comparisons). Given the same individualised stimulus temperature was used for all four sites, these were simply averaged across individuals.

2.4. MRI Image processing

Statistical Parametric Mapping v12 (SPM12; Wellcome Trust Centre for Neuroimaging, UK) and custom software were used for image analysis. The first 5 brain volumes of each fMRI image series were removed to allow for scanner equilibration leaving 129 fMRI volumes for each fMRI scan. The fMRI image sets were slice-time corrected, motion corrected, and the 6 directional movement parameters inspected to ensure there was no greater than 1 mm of linear movement or 0.5 degrees of rotation movement in any direction. Images were linearly detrended to remove global signal changes, physiological noise relating to cardiac frequency band 60-120 beats/minute +1 harmonic), and filtered to remove respiratory (frequency band 8-25 beats/minute +1 harmonic)

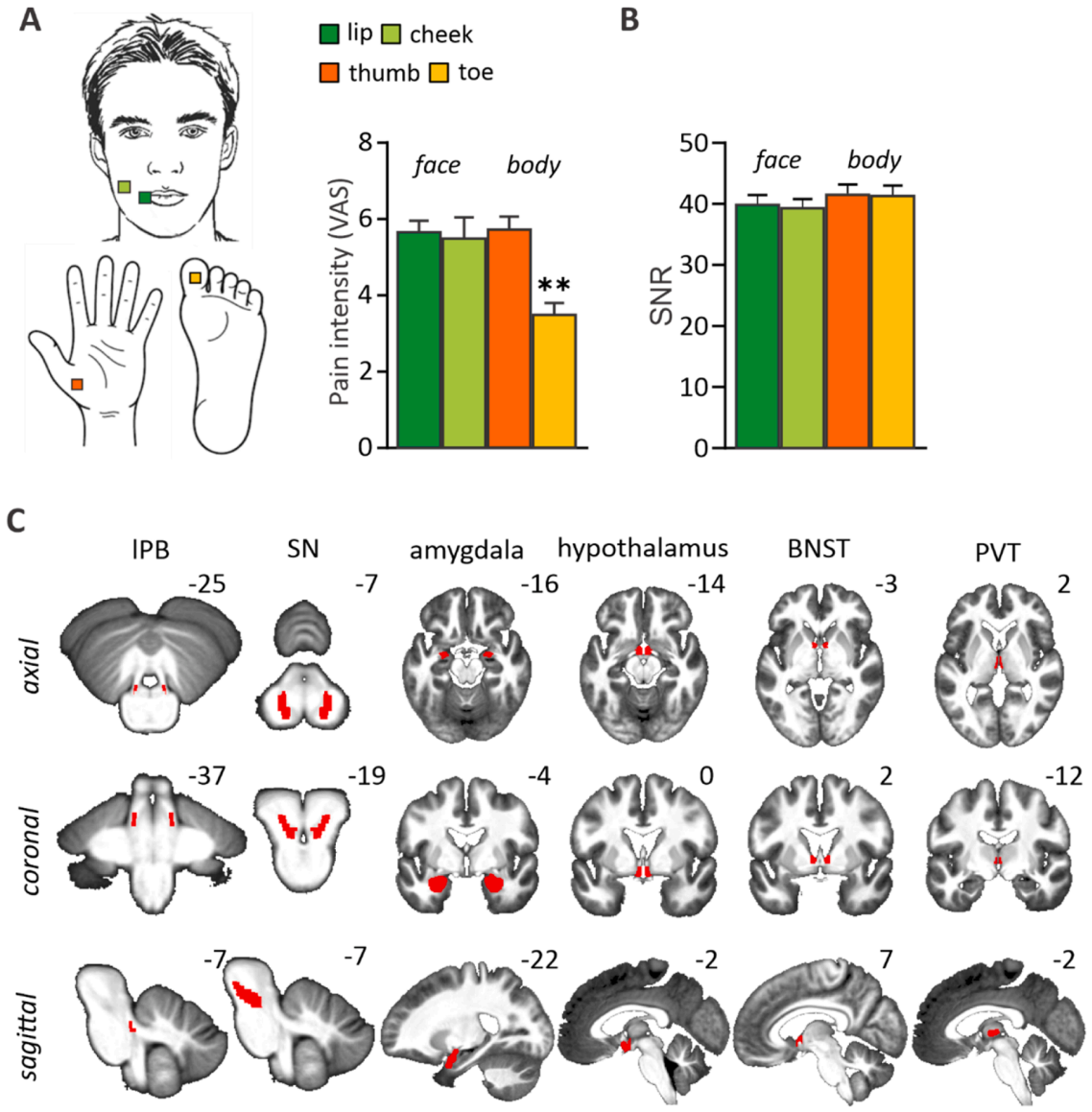

Fig. 1. A: Schematic representation of the locations of noxious stimulation and the mean (±SEM) pain intensity ratings for each of the four stimulation sites; two on the face (lip and cheek) and two on the body (thumb and big toe). **B**: Mean (±SEM) signal to noise ratio (SNR) for each whole-brain scan; **C** Schematic summary for output targets of the lateral parabrachial nucleus (lPB) nucleus. The locations of each of the regions of interest analysed are shown to the right with each region shaded in red overlaid onto axial, coronal and sagittal T1-weighted anatomical slices. Slice locations are indicated to the top right of each image in Montreal Neurological Institute space. BNST, bed nucleus of the stria terminalis; PVT, paraventricular thalamus; SN, substantia nigra; VAS, visual analogue scale.

noise using the Dynamic Retrospective Filtering toolbox (Särkkä et al., 2012), and the 6-parameter movement related signal changes were modelled and removed using a linear modelling of realignment parameters (LMRP) procedure (Macey et al., 2004). The fMRI images were then co-registered to their own T1-weighted anatomical image set, and underwent distortion correction using the SynBOLD DisCO toolbox (Yu et al., 2023).

Following anatomical co-registration, two spatial normalization procedures were then performed: i) *whole brain:* the entire T1-weighted image was spatially normalized into Montreal Neurological Institute (MNI) space and the normalization parameters applied to the fMRI image sets; ii) *brainstem:* to improve the spatial normalization of the brainstem, the spatially unbiased infra-tentorial template (SUIT) toolbox was used (Diedrichsen, 2006). For both the fMRI and T1 image sets, the brainstem and cerebellum were isolated and then normalised to the brainstem- and cerebellum-only SUIT template in Montreal Neurological Institute (MNI) space. During both the whole brain and brainstem spatial normalization procedures, the fMRI images were resliced into 1mm isotropic voxels, and the images spatially smoothed using a 2mm full-width-at-half maximum (FWHM) Gaussian filter. A small smoothing kernel was used to allow for the accurate investigation of signal intensity changes within small brainstem and subcortical nuclei (Sclocco et al., 2018). To explore changes in cortical regions, the whole brain images were also separately smoothed using a 5mm FWHM Gaussian filter.

2.5. fMRI image quality assessment

To assess the signal quality of the fMRI image sets, for each participant we calculated signal:noise ratios as the mean divided by the standard deviation over the scan for each stimulus location and for the whole brain image sets. Significant signal:noise differences between stimulation sites were determined using a repeated measures one-way ANOVA ($p<0.05$, Bonferroni corrected for multiple comparisons).

2.6. fMRI statistical analysis

A repeated box-car model convolved with a hemodynamic delay function was used to determine signal intensity changes that matched the 8 noxious stimulus periods. The resultant brain maps for each participant (lip, cheek, thumb, toe: whole brain and brainstem only) were entered into second-level full-factorial analyses with participant and body location entered as factors (individual pain ratings entered as a nuisance covariate). Two second level analyses were then performed: *i) whole brain (5mm smoothed images):* significant signal intensity increases and decreases as well as significant signal intensity change differences between face stimuli (lip and cheek) and body stimuli (thumb and toe) were determined ($p<0.05$, family wise error corrected for multiple comparisons, minimum cluster size 50 contiguous voxels); *ii) whole brain and brainstem regions of interest analysis (2mm smoothed images):* significant signal intensity increases and decreases as well as significant signal intensity change differences between face stimuli (lip and cheek) and body stimuli (thumb and toe) were determined ($p<0.05$, false discovery rate corrected for multiple comparisons, minimum cluster size 5 contiguous voxels). Since we aimed to explore fine detail within the lPB, SN, hypothalamus, amygdala, BNST and PVT, we created bilateral masks of these regions on the mean T1-weighted and fMRI image sets using two brain atlases (Duvernoy, 2012; Mai and Majtanik, 2017), and the analysis was restricted to these regions of interest (Fig. 1C). The lPB and SN regions were assessed using the 2mm smoothed brainstem isolated images whereas the hypothalamus, amygdala, BNST and PVT were assessed using the 2mm smoothed whole brain images. In addition, given that noxious stimulation of the toe resulted in lower pain intensity ratings than that of the other three stimulation sites (Fig. 1), we also assessed if signal changes during toe stimulation were driving any differences between the face versus body. We performed a second level conjunction analysis to determine whether face versus arm and face versus toe stimulations evoked similar signal intensity change differences in these subcortical and brainstem structures ($p<0.05$ false discovery rate corrected).

Clusters displaying significant signal intensity increases or decreases during face or body stimulation and those displaying significant differences between face and body stimuli were overlaid onto a mean T1-weighted anatomical image for visualization purposes. The location of individual nuclei were determined based on macro-anatomical features and with the help of brain atlases (Duvernoy, 2012; Mai and Majtanik, 2017). For each significant cluster, the β values (estimate of relative neural activation) were extracted for each of the four stimulation sites, with mean (±SEM) values plotted. Finally, to assess signal intensity changes differences between each of the four stimulation sites independently in more detail, two-sample paired *t*-tests were performed to compare β values from all four stimulation sites ($p<0.05$, Bonferroni corrected).

3. Results

3.1. Participant pain ratings, stimulus temperatures and image quality

The mean (±SEM) pain intensity ratings for the four stimuli were: lip 5.7±0.3, cheek 5.6±0.5, thumb 5.8±0.3, toe 3.6±0.3 (Fig. 1A). The mean pain intensity elicited when noxious stimuli were delivered to the toe was significantly lower compared to those when noxious stimuli were applied to either the lip, cheek, or thumb ($F[1.7, 25.4]$, $p = 0.002$; Fig. 1A). Despite these significant differences in pain rating, the same temperature was applied to all four body sites in each individual (mean ±SEM temperature: 48.2±0.1°C). There were no significant differences between stimulation sites with respect to whole brain and brainstem signal to noise ratios (mean±SEM signal:noise lip 40.10±1.38, cheek 39.52±1.28; thumb 41.74±1.45; toe 41.57±1.46, $p>0.05$, Fig. 1B).

3.2. Whole brain signal intensity changes during face and body noxious thermal stimuli

Analysis of whole brain images revealed that each of the noxious stimuli evoked signal intensity increases and decreases in pain processing regions that have been previously described (Fig. 2A). These included signal increases in the insula, putamen and mid-cingulate, orbitofrontal, and dorsolateral prefrontal cortices and signal decreases in the medial prefrontal cortex and precuneus. Comparison of head versus body noxious stimuli revealed significantly different signal intensity changes during head stimulation in multiple brain regions critical for emotional processing including in the medial, orbital, ventrolateral and dorsolateral prefrontal cortices as well as in the secondary somatosensory cortex and putamen (Fig. 2B, Table 1). Within the medial and orbital prefrontal cortices and the putamen, signal intensity increased during lip and cheek stimulation and changed very little during thumb and toe stimulation. In contrast, in the dorsolateral and ventrolateral prefrontal cortices, secondary somatosensory and primary motor cortices, signal intensity decreased during lip and cheek stimulation and increased during thumb and toe stimulation. Between all four stimulation sites, t-test revealed consistently significant changes ($p<0.05$) between face and body regions and no significant changes ($p>0.05$) within face and body with the exception of i) ipsilateral mPFC: no significant difference between lip and both body regions while a significant difference between cheek and lip ($p=0.036$); ii) ipsilateral vlPFC: no significant change between toe and both face regions; and iii) ipsilateral putamen, with no significant difference between toe and lip (Fig. 2B).

3.3. Brainstem and subcortical signal intensity changes during face and body noxious thermal stimuli

Significant bilateral signal intensity decreases occurred in the lPB during noxious stimulation of the face (Fig. 3A, Table 2). No significant signal changes were observed during noxious stimulation of the body. Similarly, bilateral signal decreases were also found in the hypothalamus, specifically in the paraventricular and medial preoptic nuclei, and the lateral hypothalamic area (Fig. 3B, Table 2). No significant signal changes were observed in the hypothalamus during noxious stimulation of the body. There were no significant signal increases or decreases during face or body stimulation in the amygdala. Noxious stimulation of the face evoked significant signal intensity increases in the BNST contralateral to the stimulus, but not ipsilaterally. Noxious stimulation of the body did not evoke signal changes in BNST. (Fig. 3C, Table 2). Noxious stimulation of the face produced a bilateral decrease in signal in the posterior part of the PVT, and an increase in the anterior part of the PVT but only on the side contralateral to the stimulus. Noxious stimulation of the body produced an increase in signal in the posterior part of the PVT again on the side contralateral to the stimulus. (Fig. 3D, Table 2). Since pain intensities were significantly lower during toe stimulation, we assessed whether the face versus body signal differences were being driven by altered signal changes during toe stimulation. A conjunction analysis revealed that both the arm and toe stimulations were equally driving the signal changes and thus the reported face versus body differences were not due to differences in pain intensities (see Supplementary Fig. 1, Supplementary Table 1).

3.4. Signal differences during face versus body noxious thermal stimuli

Analysis of signal intensity change differences between face and body stimulation revealed significant differences in numerous regions of interest. Both the ipsilateral and contralateral lPB displayed significant decreases during noxious face stimulation and small signal increases during body stimulation (Fig. 4A, Table 3). Similarly, in the ipsilateral SN signal decreased during face and increased during body noxious stimulation in two separate sites: one caudal and a second more rostral

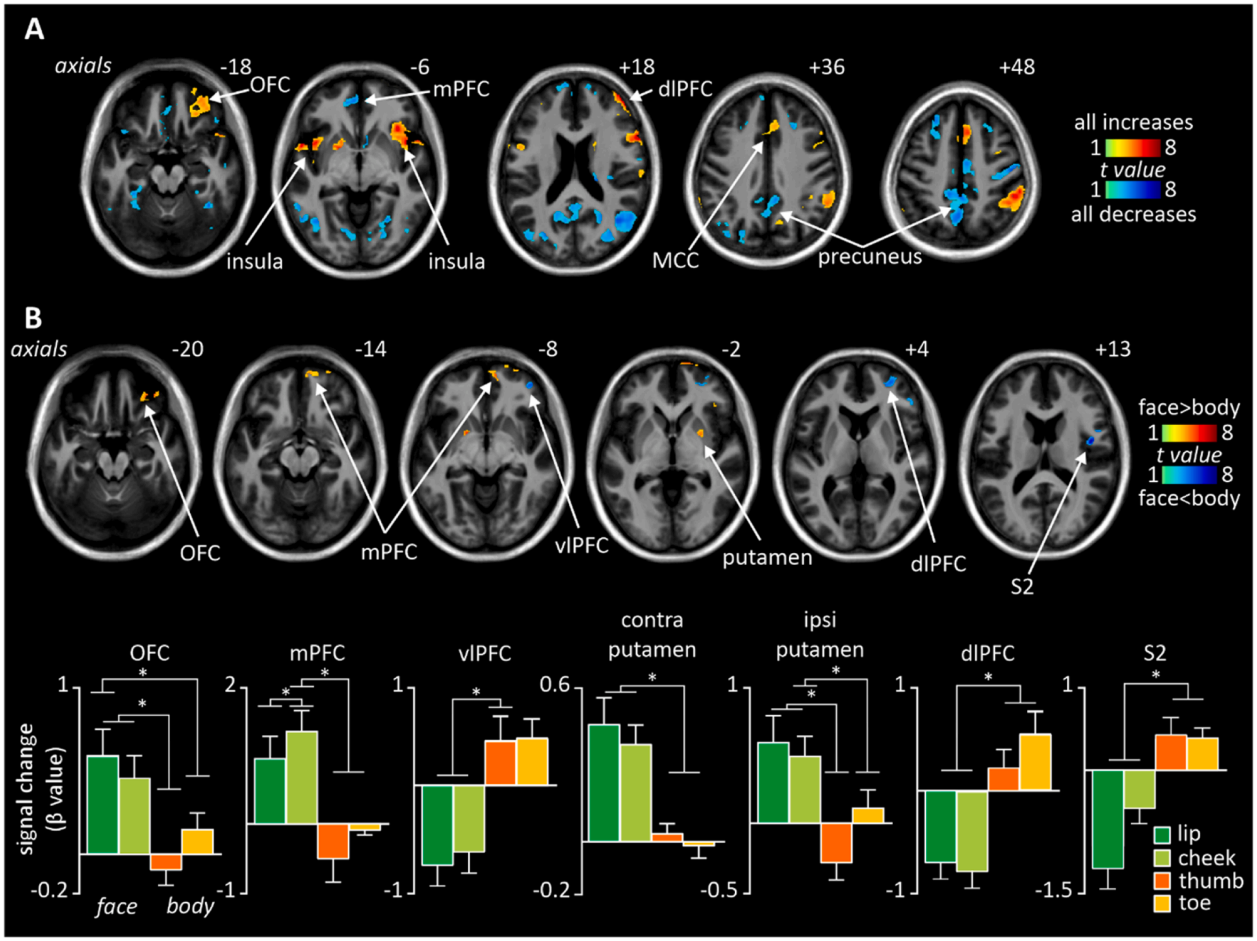

Fig. 2. *Whole brain signal intensity changes during noxious heat stimuli applied to the face and body. n=16.* **A:** Significant signal intensity increases (*hot* colour scale) and decreases (*cool* colour scale) during noxious stimuli applied to all four sites (lip, cheek, thumb, toe) overlaid onto a series of axial mean T1-weighted anatomical images. Slice locations in Montreal Neurological Institute Space are indicated at the top right of each slice. **B:** Significant signal intensity differences during face versus body stimulation (face>body: *hot* colour scale; face<body: *cool* colour scale). Significantly different signal intensity changes occurred in multiple emotional processing regions including the dorsolateral prefrontal cortex (dlPFC), medial prefrontal cortex (mPFC), orbitofrontal cortex (OFC) and ventrolateral prefrontal cortex (vlPFC). Below and to the right are plots of mean±SEM signal intensity changes (β values) for seven significantly different clusters. * $p<0.05$ two-sided paired *t*-test. ACC, anterior cingulate cortex; MCC, mid-cingulate cortex; S2, secondary somatosensory cortex.

Table 1
Locations, cluster sizes (number of voxels), and *t*-values for regions that displayed signal changes during either face or body noxious stimulation. Cluster locations are shown in Montreal Neurological Institute (MNI) space. dlPFC: dorsolateral prefrontal cortex; M1: primary motor cortex; mPFC: medial prefrontal cortex; S2: secondary somatosensory cortex; vlPFC: ventrolateral prefrontal cortex

brainstem region	MNI coordinates			t value	cluster size	mean±SEM signal intensity change			
	x	y	Z			*lip*	*cheek*	*thumb*	*toe*
face>body									
ipsi mPFC	9	58	-9	5.63	470	0.29±0.17	0.61±0.18	-0.45±0.10	-0.26±0.12
	16	69	-2	5.37	182	0.95±0.33	1.37±0.28	-0.51±0.26	-0.07±0.10
	28	62	-11	5.32	125	0.74±0.28	1.54±0.25	-0.04±0.18	0.21±0.16
ipsi vlPFC	39	31	1	5.19	67	0.81±0.25	0.69±0.13	0.01±0.13	0.36±0.19
ipsi putamen	27	3	-2	5.04	156	0.59±0.21	0.50±0.15	-0.29±0.10	0.11±0.15
contra putamen	-18	4	-7	6.40	69	0.46±0.11	0.38±0.08	0.03±0.04	-0.01±0.06
ipsi OFC	37	39	-19	5.61	261	0.52±0.14	0.40±0.10	-0.08±0.09	0.13±0.09
contra cerebellar cortex	-17	-66	-24	4.71	80	0.23±0.10	0.45±0.10	-0.20±0.10	-0.19±0.12
face>body									
ipsi dlPFC	32	51	2	5.79	459	-0.71±0.15	-0.79±0.16	0.14±0.19	0.44±0.22
ipsi vlPFC	40	48	-5	5.77	164	-0.75±0.20	-0.64±0.18	0.42±0.22	0.44±0.19
	49	34	5	4.52	97	-0.94±0.29	-1.01±0.28	0.23±0.25	0.51±0.23
ipsi S2	45	-4	13	6.90	280	-1.19±0.27	-0.48±0.18	0.42±0.20	0.37±0.13
ipsi M1	50	5	15	5.11	65	-1.47±0.36	-0.10±0.33	0.75±0.27	0.91±0.25

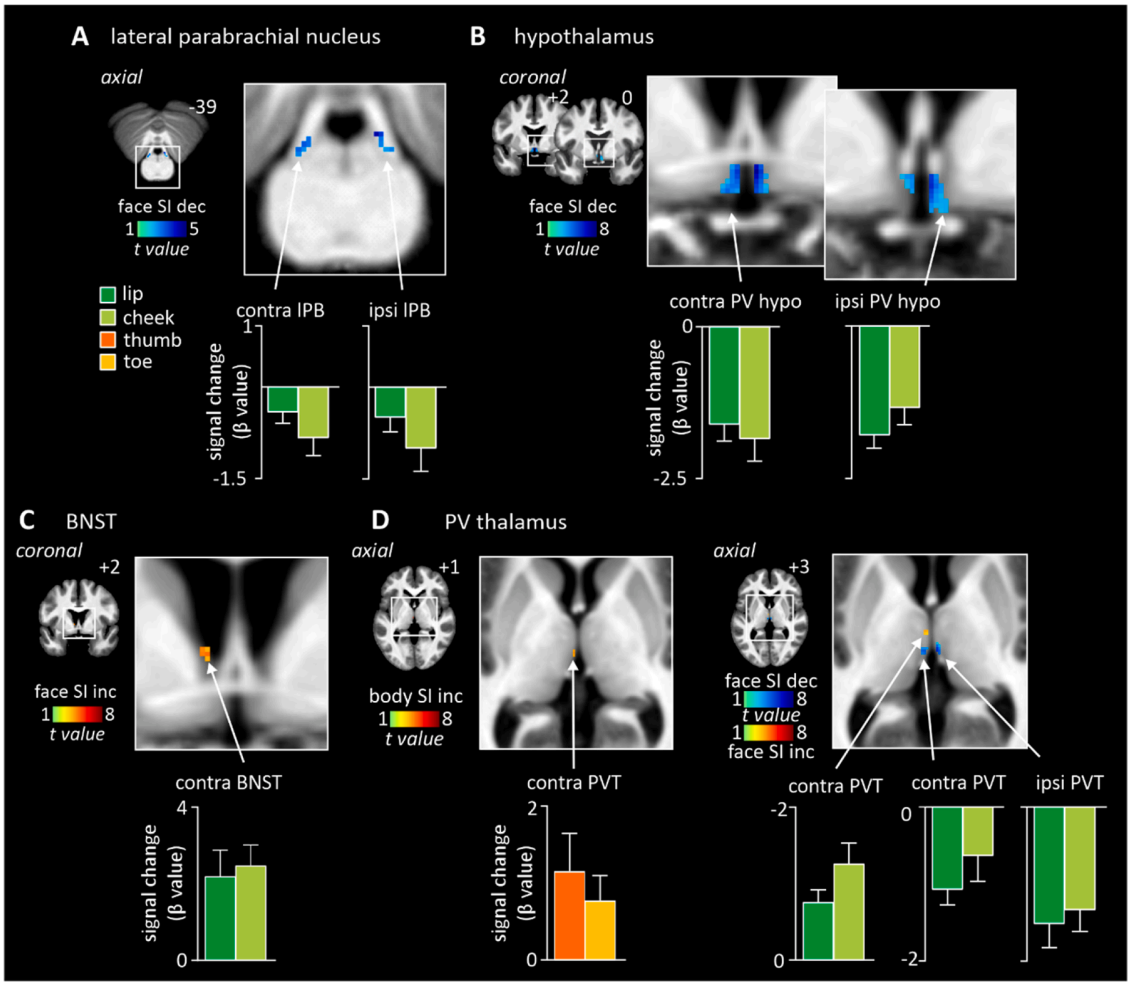

Fig. 3. *Significant changes in signal during noxious heat stimuli applied to the face and body. N=16.* **A:** Significant signal intensity (SI) decreases (*cool* colour scale) bilaterally in the lateral parabrachial nucleus (lPB) during noxious face stimuli overlaid onto a T1-weighted axial anatomical slice. Plots of mean±SEM β values are shown below; **B:** Significant signal decreases bilaterally within the hypothalamus during noxious face stimuli; **C:** Significant signal increases (*hot* colour scale) within the bed nucleus stria terminalis (BNST) contralateral to the noxious face stimuli; **D:** Significant signal increases and decreases within the paraventricular (PVT) thalamus during noxious face and body stimuli. contra: contralateral, ipsi: ipsilateral. Significant clusters are overlaid onto a mean T-weighted anatomical image and slice locations are indicated to the top right in Montreal Neurological Institute space.

Table 2
Locations, cluster sizes (number of voxels), and *t*-values for regions that displayed signal changes during either face or body noxious stimulation. Cluster locations are shown in Montreal Neurological Institute (MNI) space. BNST: bed nucleus stria terminalis, lPB: lateral parabrachial nucleus, PV thalamus: paraventricular thalamus.

brainstem region	MNI coordinates			t value	cluster size	mean±SEM signal intensity change			
	x	y	z			*lip*	*cheek*	*thumb*	*toe*
lPB									
face decrease	7	-39	-23	4.30		-0.49±0.24	-1.00±0.38		
	-7	-37	-23	2.79		-0.41±0.18	-0.83±0.29		
hypothalamus									
face decrease	3	2	-9	7.25	97	-1.34±0.28	-1.79±0.21		
	-1	3	-9	5.34	59	-1.85±0.37	-1.61±0.27		
BNST									
face increase	-5	2	1	4.15	9	2.19±0.68	2.47±0.54		
PV thalamus									
face increase	-1	-9	-1	5.99	34	0.76±0.16	1.26±0.27		
body increase	-1	-17	1	3.50	5			1.16±0.49	0.77±0.32
face decrease	4	-20	-1	6.13	67	-1.52±0.31	-1.34±0.28		
	-2	-20	3	4.42	21	-1.07±0.20	-0.64±0.33		

region (Fig. 4B, Table 3).

In the hypothalamus, while noxious stimulation of both face and body evoked signal intensity decreases in the region encompassing the paraventricular/medial preoptic nuclei and lateral hypothalamic area, the signal decreased more during face compared with body stimulation (Fig. 4C, Table 3). In the PVT, the posterior region displayed bilateral

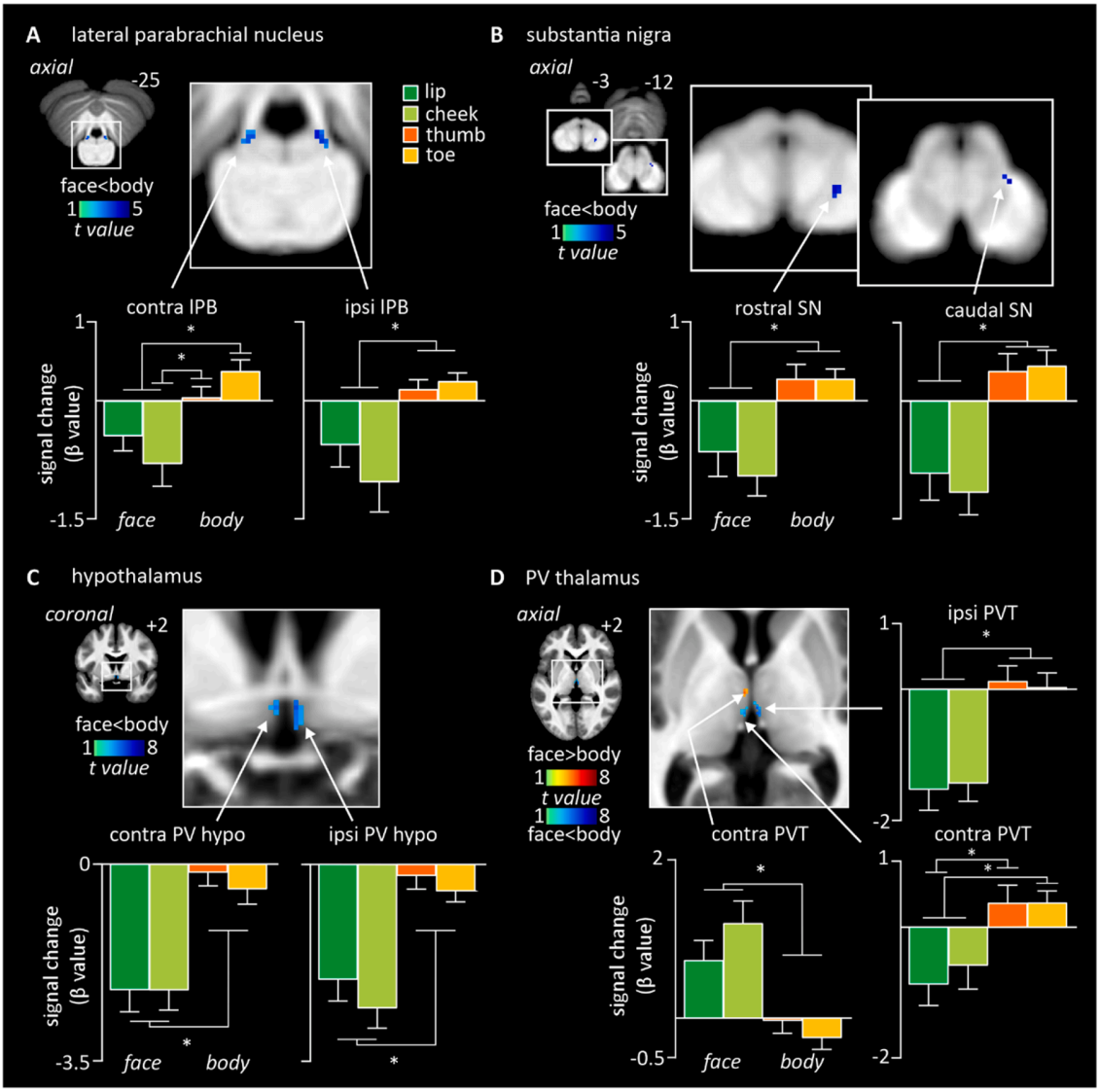

Fig. 4. *Significant differences in signal intensity changes during noxious heat stimuli applied to the face compared with the body. n=16.* * $p<0.05$ paired two-sided *t*-test. **A:** Significantly greater signal decreases during face versus body noxious stimuli in the lateral parabrachial nucleus (lPB; *cool* colour scale) overlaid onto a T1-weighted axial anatomical slice. Plots of mean±SEM β values are shown below; **B:** Significant signal intensity differences within the substantia nigra (SN); **C:** paraventricular hypothalamus (PV hypo); and **D**: paraventricular thalamus. PB, parabrachial; PV, paraventricular; PVT, paraventricular thalamus; SI signal intensity; SN, substantia nigra. contra: contralateral, ipsi: ipsilateral.

Table 3
Locations, cluster sizes (number of voxels), and t-values for regions that displayed significantly different signal changes during face compared with body noxious stimulation. Cluster locations are shown in Montreal Neurological Institute (MNI) space.

brainstem region	MNI coordinates			t value	cluster size	mean±SEM signal intensity change			
	x	y	z			*lip*	*cheek*	*thumb*	*toe*
lPB									
face < body	7	-39	-23	5.00	22	0.56±0.28	-1.03±0.38	0.14±0.12	0.25±0.12
	-7	-38	-25	3.57	25	-0.44±0.19	-0.80±0.29	0.04±0.14	0.38±0.14
SN									
face < body	11	-27	-12	4.22	5	-0.92±0.34	-1.17±0.28	0.38±0.22	0.45±0.20
	12	-17	-3	3.99	10	-0.67±0.26	0.97±0.25	0.26±0.18	0.25±0.12
hypothalamus									
face < body	3	2	-9	4.72	33	-2.05±0.38	-2.56±0.35	-0.20±0.24	-0.48±0.19
	-1	3	-9	4.21	14	-2.24±0.38	2.24±0.35	-0.14±0.24	-0.44±0.26
PV thalamus									
face < body	3	-18	1	4.91	60	-1.52±0.31	-1.42±0.27	0.13±0.23	0.03±0.22
	-2	-20	3	4.14	32	-0.87±0.32	-0.58±0.36	0.37±0.27	0.37±0.17
face > body	-2	-12	2	4.14	8	0.73±0.25	1.20±0.28	-0.03±0.16	-0.25±0.15

signal intensity decreases during face noxious stimuli and either no change (ipsilateral) or an increase (contralateral) in signal during body stimulation (Fig. 4D, Table 3). In addition, the anterior region of the contralateral PVT displayed significant increases in signal intensity during face noxious stimulation whereas there was no change during body stimulation (Fig. 4D; Table 3). We found no significant differences in signal intensity between face and body in either the amygdala or BNST. Between all four stimulation sites, t-test revealed consistently significant changes ($p<0.05$) between face and body regions and no significant changes ($p>0.05$) within face and body except for: i) contralateral lPB: no significant change between lip and thumb; and ii) contralateral PV: body greater than face, with no significant change between toe and cheek (Fig. 4).

4. Discussion

In this study we found that noxious heat stimuli applied to the face evoked larger signal intensity changes in a distinct set of brain regions known to be critical for emotional processing, when compared those evoked by noxious heat stimuli applied to the body. These signal differences were found in subcortical and brainstem regions, specifically the lateral parabrachial nucleus, the paraventricular nucleus of hypothalamus, the paraventricular nucleus of thalamus, the substantia nigra, the BNST, as well as cortical regions including the dorsolateral, ventrolateral, medial, orbital prefrontal cortices. It has been suggested that head and orofacial pain evokes a greater emotional reaction to that evoked by pain in other body regions, and the altered signal changes reported in this study are consistent with this idea (Rodriguez et al., 2017).

The data we present shows that cutaneous facial pain evokes a profound decrease in signal intensity bilaterally in the lPB, the paraventricular nucleus of the hypothalamus and the medial preoptic area as well as in the ipsilateral substantia nigra and increased signal intensity in the BNST. Signal intensity increases were also seen in the PVT following both facial pain and body pain, the signal changes evoked by facial pain were also bilateral in this region. The characteristics of these changes are consistent with the signal differences that we found between face and body pain, with facial pain evoking signal decreases in the ipsilateral and contralateral lPB, the ipsilateral SN, and bilaterally in the paraventricular hypothalamus and PVT. These differences were striking as body pain did not evoke significant signal intensity changes in the majority of structures evaluated, whereas pain applied to the face had a strong impact on these regions.

The data we report are consistent with recent preclinical work that showed significantly greater expression of the immediate early gene c-Fos, a robust indicator of neuronal activation, in neurons of lPB during facial compared with body noxious stimulation (Rodriguez et al., 2017). It is important to note that the c-Fos increases were observed bilaterally in the preclinical study, which is identical to the lPB signal increases seen in this study. It is now well-established that the lPB is an important region for pain processing and that it is also a critical relay for ascending nociceptive information whose targets include; the midbrain periaqueductal gray matter, the hypothalamus, the amygdala, the BNST and the PVT (Bernard et al., 1996, Raver et al., 2020, Chiang et al., 2020, Gauriau and Bernard, 2002, Roeder et al., 2016, Fulwiler and Saper, 1984). The importance of these lPB networks in integrating the complex behavioural components of the pain experience is highlighted from work in preclinical models. Recent studies have shown that there are at least two distinct lPB neuronal populations: the first which projects to the midbrain periaqueductal gray matter and ventromedial hypothalamus and is critical for mediating active coping responses to painful stimuli, including fight-flight reactions, and a second population that projects to the central amygdala and BNST which plays an important role in aversive memory processes, and which are likely a critical component of circuits that mediate fear avoidance behaviours that are characteristic of both acute and chronic pain states (Chiang et al., 2020).

Consistent with these projection patterns we found significant differences in face versus body pain signal changes in the hypothalamus and, in particular, the region encompassing the paraventricular (PV) and medial preoptic nuclei (MPO) of the hypothalamus. Direct stimulation of neurons in the PV and MPO hypothalamus can produce analgesia via descending projections (Condes-Lara et al., 2007, Condes-Lara et al., 2006, Zhang and Ennis, 2007). In addition, corticotropin releasing factor (CRF) containing PV hypothalamic neurons also coordinate the hypothalamo-pituitary-adrenal response to acute pain (Daviu et al., 2020), that is characterised by increased circulating adrenocorticotropic hormone levels and increased systemic glucocorticoid levels (Halasz et al., 1962). Since these CRF neurons are under tonic inhibitory control, their activation likely results from dis- inhibition (Herman et al., 2016) which is consistent with signal decreases identified here. Whether there are differences in the endocrine responses to face versus body pain remains unknown, but our data would suggest that head and orofacial pain results in greater glucocorticoid release than body pain. Furthermore, the PV hypothalamus projects directly onto brainstem sympathetic premotor vasoconstrictor neurons, and also directly onto sympathetic preganglionic vasoconstrictor neurons in the intermediolateral cell column of the spinal cord to bring about changes in blood pressure (Saper et al., 1976). While no study has compared sympathetic activity changes during face versus body stimuli, it has been shown that skin conductance responses, a measure of sympathetic drive to the skin and often linked to changes in emotion are greater during fear conditioning associated with face versus body noxious stimuli (Meier et al., 2014).

Interestingly, we did not find significant signal differences between face and body signal changes in either the amygdala or the BNST, although we have previously reported signal decreases in the amygdala during facial pain (Robertson et al., 2022) and in this study we report signal increases during face pain in the BNST. Given the higher threat value of tissue damaging or potentially damaging stimuli in the head and oro-facial region when compared to the same stimuli in other body regions (Schmidt et al., 2016, Meier et al., 2014), we predicted differential signal intensity change patterns in the amygdala because of its well-documented role in threat evaluation as part of both the acute and chronic pain experience (Veinante et al., 2013). A comprehensive review of fear conditioning studies has shown that in almost half of the studies examined there was no amygdala activation (Sehlmeyer et al., 2009), this lack of consistency in fear conditioning studies may result from rapid habituation effects (Bach et al., 2011, Marschner et al., 2008). We know of no other studies that have compared amygdala activation patterns during face versus body pain, although a previous study has reported a significant correlation between face pain and fear ratings, indicating increased amygdala signal changes in those who perceived face stimulation as more threatening than hand stimulation (Schmidt et al., 2016).

In addition to differential signal changes between body and face noxious pain in the PV hypothalamus, we found similar signals changes both in terms of direction and bilaterality, in the PVT. The PVT is now recognised as an important node in the forebrain networks responsible for generating emotional states and translating them into behavioural responses (Barson et al., 2020). It is involved in both conditioned and unconditioned emotional responses via its projections to various forebrain regions including to the PV hypothalamus (Csaki et al., 2000) and prefrontal cortex (Huang et al., 2006). It has been proposed that the PVT can be divided into two major divisions based on both anatomical relations and functional organisation. The anterior PVT connects with the ventral hippocampus and infralimbic cortex, and the posterior PVT connects with the BNST, amygdala, and nucleus accumbens (Barson et al., 2020). While there is evidence that these divisions are likely more complex than first appreciated (Gao et al., 2020), it is thought that the anterior PVT plays a more prominent role in arousal, whereas the posterior PVT is involved in assigning valence in stimulus-response relationships. Consistent with the idea of a greater emotional value head and orofacial pain when compared with body pain, we found robust

bilateral signal decreases in the posterior PVT during face pain and very little signal change during body pain. Furthermore, it has been suggested that when compared to the anterior PVT, the posterior PVT is more responsive during exposure to stressful contexts in preclinical studies (i.e., elevated plus maze, foot-shock, and forced swim test) (Pliota et al., 2020, Zhu et al., 2011). Furthermore, in rats neuronal activity evoked by noxious mechanical stimulation, as measured by c-fos expression, increases more in the posterior PVT, compared with anterior PVT (Bullitt, 1990). It has also been revealed that the PAG projects strongly into the PVT, with the ventrolateral PAG column projecting to primarily the posterior PVT and the dorsolateral PAG to the anterior PVT (Boorman et al., 2021). The outputs of the lPB and the PAG to the PV thalamus provides afferent drive onto prefrontal cortical regions, which also project back to the hypothalamus, including the medial hypothalamus (Floyd et al., 2001). This loop, in addition to direct ascending PV hypothalamic inputs from the lPB and PAG (Floyd et al., 1996) is likely critical for mediating the endocrine responses to pain.

Consistent with differential changes in the PVT, we also found differential changes in its output territories, including multiple subdivisions of the prefrontal cortex. While noxious stimuli applied to the face and body evoked significant increases in signal intensity in well-described cortical pain circuits, including in the prefrontal cortex, we also found discrete differences between face and body pain in the medial, orbital, ventrolateral and dorsolateral prefrontal cortices. In the medial and orbital prefrontal cortices, signal intensity increased during face and changed very little during body pain, whereas in the dorsolateral and ventrolateral prefrontal cortices, signal decreased during face and increased to a lesser extent during body pain. It has been reported that areas such as the orbital and medial prefrontal cortices are critical for emotional processing and are strongly implicated in the process of fear conditioning (Giustino and Maren, 2015). While our study shows signal intensity differences in the orbitofrontal cortex during face versus body pain, a previous study explored brain activation patterns during face compared with body pain-related fear and found enhanced brain activation in the orbitofrontal cortex and medial thalamus during face versus body fear conditioning (Meier et al., 2014). In addition to the dorsolateral prefrontal cortex, the orbitofrontal and medial prefrontal cortices have been linked to mood and negative affective responses to multimodal stimuli as well as to variability in acute pain perception (Kohoutova et al., 2022, Rao et al., 2018, Ceko et al., 2022, Meylakh et al., 2024, Crawford et al., 2023). Given these functions, the differential signal changes observed in these limbic cortical regions, potentially reflecting direct inputs from the PVT, likely contribute significantly to the differences in emotional responses to acute face versus body pain.

Some limitations of the present study should be noted. Firstly, we attempted to match perceived pain intensities during face and body pain by assessing pain intensity during noxious stimuli placed on the forearm prior to entering the MRI scanner. Using the same noxious stimulus temperature on all four body sites resulted in significantly lower perceived pain intensity during toe stimulation compared with the three other sites, perhaps owing to the thicker skin of the toe pad. However, to overcome this variability, we entered each individual's mean perceived pain intensity for each of the four stimulus sites as nuisance variables so that the effects of pain intensity were factored out of the analysis. Additionally, an examination of face compared to toe pain and face compared to thumb pain revealed that the signal differences were not mediated by the reduced pain rating in the toe and thus we are confident that the signal change represent differential brain processing of face compared with body noxious stimuli. Secondly, although we measured pain intensity, we did not measure the emotional component of the stimulus. It would have been advantageous to explore the relationship between the affective quality of each stimulus and regions of brain signal changes and this is an issue that could be addressed in future investigations. Finally, we have previously shown a crude somatotopic map (head versus body) in the midbrain periaqueductal gray matter, which is likely linked to the expression of different pain-related defensive behaviours (Tinoco Mendoza et al., 2023), given this somatotopic organization we did not explore differences in this brainstem region despite it being connected to the lPB. There is currently no evidence of a somatotopic organization in the other brainstem or subcortical regions that we have explored; if a somatotopic organization does exist it could potentially change some aspects of our interpretation of the current results.

In conclusion, we found differential noxious-evoked signal changes in brainstem and forebrain regions between the face and body that likely underpin the reported differences in emotional component of face compared with body pain. These differences may also reflect the reported differences in the emotional aspect of chronic head pain compared with chronic body pain. Furthermore, they highlight the need to account for body location when exploring pain-related signal changes in brainstem and subcortical regions given that we have uncovered significant difference in activation pattern.

Declaration of generative AI in scientific writing

No generative AI was used in scientific writing.

Data requirements

Due to the ethics requirements of this study, participant raw data will remain confidential and will not be shared.

CRediT authorship contribution statement

Rebecca V Robertson: Writing – original draft, Visualization, Validation, Formal analysis, Data curation, Conceptualization. **Noemi Meylakh:** Writing – review & editing, Validation, Data curation. **Lewis S Crawford:** Writing – review & editing, Validation, Data curation. **Fernando A Tinoco Mendoza:** Writing – review & editing, Validation, Data curation. **Paul M Macey:** Writing – review & editing, Software. **Vaughan G Macefield:** Writing – review & editing, Data curation. **Kevin A Keay:** Writing – review & editing, Supervision, Project administration, Funding acquisition, Conceptualization. **Luke A Henderson:** Writing – original draft, Visualization, Validation, Supervision, Project administration, Funding acquisition, Formal analysis, Data curation, Conceptualization.

Declaration of competing interest

The authors declare there are no conflicts of interest.

Data availability

The data that has been used is confidential.

Acknowledgements

We wish to thank the many volunteers in this study. The authors acknowledge the facilities, scientific and technical assistance from the National Imaging Facility, a National Collaborative Research Infrastructure Strategy capability, at the Melbourne Brain Centre Imaging Unit, The University of Melbourne. This work was funded by the National Health and Medical Research Council of Australia Grant 1130280.

Supplementary materials

Supplementary material associated with this article can be found, in the online version, at doi:10.1016/j.neuroimage.2024.120832.

References

Bach, D.R., Weiskopf, N., Dolan, R.J., 2011. A stable sparse fear memory trace in human amygdala. J. Neurosci. 31, 9383–9389.

Bandler, R., Keay, K.A., Floyd, N., Price, J., 2000. Central circuits mediating patterned autonomic activity during active vs. passive emotional coping. Brain Res. Bull. 53, 95–104.

Barson, J.R., Mack, N.R., Gao, W.J., 2020. The Paraventricular Nucleus of the Thalamus Is an Important Node in the Emotional Processing Network. Front. Behav. Neurosci. 14, 598469.

Bernard, J.F., Bester, H., Besson, J.M., 1996. Involvement of the spino-parabrachio -amygdaloid and -hypothalamic pathways in the autonomic and affective emotional aspects of pain. Prog. Brain Res. 107, 243–255.

Boorman, D.C., Brown, R., Keay, K.A., 2021. Periaqueductal gray inputs to the paraventricular nucleus of the thalamus: Columnar topography and glucocorticoid (in)sensitivity. Brain Res. 1750, 147171.

Bullitt, E., 1990. Expression of c-fos-like protein as a marker for neuronal activity following noxious stimulation in the rat. J. Comp. Neurol. 296, 517–530.

Ceko, M., Kragel, P.A., Woo, C.W., Lopez-Sola, M., Wager, T.D., 2022. Common and stimulus-type-specific brain representations of negative affect. Nat. Neurosci. 25, 760–770.

Chiang, M.C., Nguyen, E.K., Canto-Bustos, M., Papale, A.E., Oswald, A.M., Ross, S.E., 2020. Divergent neural pathways emanating from the lateral parabrachial nucleus mediate distinct components of the pain response. Neuron 106, 927–939 e5.

Condes-Lara, M., Martinez-Lorenzana, G., Rojas-Piloni, G., Rodriguez-Jimenez, J., 2007. Branched oxytocinergic innervations from the paraventricular hypothalamic nuclei to superficial layers in the spinal cord. Brain Res. 1160, 20–29.

Condes-Lara, M., Rojas-Piloni, G., Martinez-Lorenzana, G., Rodriguez-Jimenez, J., Lopez Hidalgo, M, Freund-Mercier, M.J, 2006. Paraventricular hypothalamic influences on spinal nociceptive processing. Brain Res. 1081, 126–137.

Crawford, L., Mills, E., Meylakh, N., Macey, P.M., Macefield, V.G., Henderson, L.A., 2023. Brain activity changes associated with pain perception variability. Cereb. Cortex. 33, 4145–4155.

Csaki, A., Kocsis, K., Halasz, B., Kiss, J., 2000. Localization of glutamatergic/ aspartatergic neurons projecting to the hypothalamic paraventricular nucleus studied by retrograde transport of [3H]D-aspartate autoradiography. Neuroscience 101, 637–655.

Daviu, N., Fuzesi, T., Rosenegger, D.G., Rasiah, N.P., Sterley, T.L., Peringod, G., Bains, J. S., 2020. Paraventricular nucleus CRH neurons encode stress controllability and regulate defensive behavior selection. Nat. Neurosci. 23, 398–410.

Diedrichsen, J., 2006. A spatially unbiased atlas template of the human cerebellum. Neuroimage 33, 127–138.

Duvernoy, H.M., 2012. The human brain stem and cerebellum: surface, structure, vascularization, and three-dimensional sectional anatomy, with MRI. Springer Science & Business Media.

Floyd, N.S., Keay, K.A., Arias, C.M., Sawchenko, P.E., Bandler, R., 1996. Projections from the ventrolateral periaqueductal gray to endocrine regulatory subdivisions of the paraventricular nucleus of the hypothalamus in the rat. Neurosci. Lett. 220, 105–108.

Floyd, N.S., Price, J.L., Ferry, A.T., Keay, K.A., Bandler, R., 2001. Orbitomedial prefrontal cortical projections to hypothalamus in the rat. J. Comp. Neurol. 432, 307–328.

Fulwiler, C.E., Saper, C.B., 1984. Subnuclear organization of the efferent connections of the parabrachial nucleus in the rat. Brain Res. 319, 229–259.

Gao, C., Leng, Y., Ma, J., Rooke, V., Rodriguez-Gonzalez, S., Ramakrishnan, C., Deisseroth, K., Penzo, M.A., 2020. Two genetically, anatomically and functionally distinct cell types segregate across anteroposterior axis of paraventricular thalamus. Nat. Neurosci. 23, 217–228.

Gauriau, C., Bernard, J.F., 2002. Pain pathways and parabrachial circuits in the rat. Exp. Physiol. 87, 251–258.

Giustino, T.F., Maren, S., 2015. The role of the medial prefrontal cortex in the conditioning and extinction of fear. Front. Behav. Neurosci. 9, 298.

Halasz, B., Pupp, L., Uhlarik, S., 1962. Hypophysiotrophic area in the hypothalamus. J. Endocrinol. 25, 147–154.

Herman, J.P., McKlveen, J.M., Ghosal, S., Kopp, B., Wulsin, A., Makinson, R., Scheimann, J., Myers, B., 2016. Regulation of the hypothalamic-pituitary-adrenocortical stress response. Compr. Physiol. 6, 603.

Huang, H., Ghosh, P., Van Den Pol, A.N., 2006. Prefrontal cortex-projecting glutamatergic thalamic paraventricular nucleus-excited by hypocretin: a feedforward circuit that may enhance cognitive arousal. J. Neurophysiol. 95, 1656–1668.

Kohoutova, L., Atlas, L.Y., Buchel, C., Buhle, J.T., Geuter, S., Jepma, M., Koban, L., Krishnan, A., Lee, D.H., Lee, S., Roy, M., Schafer, S.M., Schmidt, L., Wager, T.D., Woo, C.W., 2022. Individual variability in brain representations of pain. Nat. Neurosci. 25, 749–759.

Macey, P.M., Macey, K.E., Kumar, R., Harper, R.M., 2004. A method for removal of global effects from fMRI time series. Neuroimage 22, 360–366.

Mai, J.K., Majtanik, M., 2017. Human brain in standard MNI space: a comprehensive pocket atlas. Elsevier.

Marschner, A., Kalisch, R., Vervliet, B., Vansteenwegen, D., Buchel, C., 2008. Dissociable roles for the hippocampus and the amygdala in human cued versus context fear conditioning. J. Neurosci. 28, 9030–9036.

Meier, M.L., De Matos, N.M., Brugger, M., Ettlin, D.A., Lukic, N., Cheetham, M., Jancke, L., Lutz, K., 2014. Equal pain-unequal fear response: enhanced susceptibility of tooth pain to fear conditioning. Front. Hum. Neurosci. 8, 526.

Meylakh, N., Crawford, L.S., Mills, E.P., Macefield, V.G., Vickers, E.R., Macey, P.M., Keay, K.A., Henderson, L.A., 2024. Altered cortico-brainstem connectivity during spontaneous fluctuations in pain intensity in painful trigeminal neuropathy. eNeuro.

Pliota, P., Bohm, V., Grossl, F., Griessner, J., Valenti, O., Kraitsy, K., Kaczanowska, J., Pasieka, M., Lendl, T., Deussing, J.M., Haubensak, W., 2020. Stress peptides sensitize fear circuitry to promote passive coping. Mol. Psychiatry 25, 428–441.

Rao, V.R., Sellers, K.K., Wallace, D.L., Lee, M.B., Bijanzadeh, M., Sani, O.G., Yang, Y., Shanechi, M.M., Dawes, H.E., Chang, E.F., 2018. Direct electrical stimulation of lateral orbitofrontal cortex acutely improves mood in individuals with symptoms of depression. Curr. Biol. 28, 3893–3902 e4.

Raver, C., Uddin, O., Ji, Y., Li, Y., Cramer, N., Jenne, C., Morales, M., Masri, R., Keller, A., 2020. An amygdalo-parabrachial pathway regulates pain perception and chronic pain. J. Neurosci. 40, 3424–3442.

Robertson, R.V., Crawford, L.S., Meylakh, N., Macey, P.M., Macefield, V.G., Keay, K.A., Henderson, L.A., 2022. Regional hypothalamic, amygdala, and midbrain periaqueductal gray matter recruitment during acute pain in awake humans: A 7-Tesla functional magnetic resonance imaging study. Neuroimage 259, 119408.

Rodriguez, E., Sakurai, K., Xu, J., Chen, Y., Toda, K., Zhao, S., Han, B.X., Ryu, D., Yin, H., Liedtke, W., Wang, F., 2017. A craniofacial-specific monosynaptic circuit enables heightened affective pain. Nat. Neurosci. 20, 1734–1743.

Roeder, Z., Chen, Q., Davis, S., Carlson, J.D., Tupone, D., Heinricher, M.M., 2016. Parabrachial complex links pain transmission to descending pain modulation. Pain. 157, 2697–2708.

Saper, C.B., Loewy, A.D., Swanson, L.W., Cowan, W.M., 1976. Direct hypothalamo-autonomic connections. Brain Res. 117, 305–312.

Särkkä, S., Solin, A., Nummenmaa, A., Vehtari, A., Auranen, T., Vanni, S., Lin, F.-H, 2012. Dynamic retrospective filtering of physiological noise in BOLD fMRI: DRIFTER. Neuroimage 60, 1517–1527.

Schmidt, K., Forkmann, K., Sinke, C., Gratz, M., Bitz, A., Bingel, U., 2016. The differential effect of trigeminal vs. peripheral pain stimulation on visual processing and memory encoding is influenced by pain-related fear. Neuroimage 134, 386–395.

Sclocco, R., Beissner, F., Bianciardi, M., Polimeni, J.R., Napadow, V., 2018. Challenges and opportunities for brainstem neuroimaging with ultrahigh field MRI. Neuroimage 168, 412–426.

Sehlmeyer, C., Schoning, S., Zwitserlood, P., Pfleiderer, B., Kircher, T., Arolt, V., Konrad, C., 2009. Human fear conditioning and extinction in neuroimaging: a systematic review. PLoS. One 4, e5865.

Tinoco Mendoza, F.A., Hughes, T.E.S., Robertson, R.V., Crawford, L.S., Meylakh, N., Macey, P.M., Macefield, V.G., Keay, K.A., Henderson, L.A., 2023. Detailed organisation of the human midbrain periaqueductal grey revealed using ultra-high field magnetic resonance imaging. Neuroimage 266, 119828.

Veinante, P., Yalcin, I., Barrot, M., 2013. The amygdala between sensation and affect: a role in pain. J. Mol. Psychiatry 1, 9.

Willis, W.D., Westlund, K.N., 1997. Neuroanatomy of the pain system and of the pathways that modulate pain. J. Clin. Neurophysiol. 14, 2–31.

Yu, T., Cai, L.Y., Torrisi, S., Vu, A.T., Morgan, V.L., Goodale, S.E., Ramadass, K., Meisler, S.L., Lv, J., Warren, A.E.L., Englot, D.J., Cutting, L., Chang, C., Gore, J.C., Landman, B.A., Schilling, K.G., 2023. Distortion correction of functional MRI without reverse phase encoding scans or field maps. Magn. Reson. ImAging 103, 18–27.

Zhang, Y.H., Ennis, M., 2007. Inactivation of the periaqueductal gray attenuates antinociception elicited by stimulation of the rat medial preoptic area. Neurosci. Lett. 429, 105–110.

Zhu, L., Wu, L., Yu, B., Liu, X., 2011. The participation of a neurocircuit from the paraventricular thalamus to amygdala in the depressive like behavior. Neurosci. Lett. 488, 81–86.

Appendix B:

The acute effects of non-concussive head impacts in sport: A randomized control trial

The acute effects of non-concussive head impacts in sport: A randomised control trial.

Nathan Delang
n.delang@griffith.edu.au

School of Health Sciences and Social Work, Griffith University, Gold Coast, Queensland, Australia https://orcid.org/0000-0002-9925-278X
Rebecca V. Robertson
The University of Sydney School of Medical Sciences
Fernando A. Tinoco Mendoza
The University of Sydney School of Medical Sciences
Luke A. Henderson
The University of Sydney School of Medical Sciences
Caroline Rae
Neuroscience Research Australia
Stuart J. McDonald
Monash University Central Clinical School
Ben Desbrow
Griffith University School of Allied Health Sciences
Christopher Irwin
Griffith University School of Allied Health Sciences
Aimie L. Peek
The University of Sydney School of Medical Sciences
Elizabeth A. Cairns
The University of Sydney Brain and Mind Centre
Paul J. Austin
The University of Sydney School of Medical Sciences
Michael A. Green
Neuroscience Research Australia
Nicholas W. Jenneke
The University of Sydney School of Medical Sciences
Jun Cao
University of New South Wales School of Biomedical Sciences
William T. O'Brien
Monash University Central Clinical School
Shane Ball
The University of Sydney School of Health Sciences
Michael E. Buckland
Royal Prince Alfred Hospital
Katherine Rae
The Sports Clinic, The University of Sydney, Sydney, New South Wales, Australia
Iain S. McGregor
The University of Sydney Brain and Mind Centre
Danielle McCartney
The University of Sydney Brain and Mind Centre

Research Article

Keywords: Subconcussion, contact sport, neural, astroglial, metabolites

Posted Date: September 3rd, 2024

DOI: https://doi.org/10.21203/rs.3.rs-4765251/v1

Abstract

Background

Head impacts, particularly, *non-concussive* impacts, are common in sport. Yet, their effects on the brain are poorly understood. Here, we investigated the acute effects of non-concussive impacts on brain microstructure, chemistry, and function using magnetic resonance imaging (MRI) and other techniques.

Results

Fifteen healthy male soccer players completed this randomised, controlled, crossover trial. Participants completed a soccer heading task ('Heading'; the Intervention) and an equivalent 'Kicking' task (the Control); followed by a series of MRI sequences between ~ 60–120 minutes post-tasks. Blood was also sampled, and cognitive function assessed, pre-, post-, 2.5 hours post-, and 24 hours post-tasks. Brain chemistry: Heading increased total *N*-acetylaspartate ($p = 0.012$) and total creatine ($p = 0.010$) levels in the primary motor cortex (but not the dorsolateral prefrontal cortex) as assessed via proton magnetic resonance spectroscopy. Glutamate-glutamine, myoinositol, and total choline levels were not altered in either region. Brain structure: Heading had no effect on diffusion weighted imaging metrics. However, two blood biomarkers expressed in brain microstructures, glial fibrillary acidic protein and neurofilament light, were elevated 24 hours ($p = 0.014$) and ~ 7-days ($p = 0.046$) post-Heading (*vs.* Kicking), respectively. Brain function: Heading decreased tissue conductivity in five brain regions (p's < 0.001) as assessed via electrical properties tomography. However, no differences were identified in: (1) connectivity within major brain networks as assessed via resting-state functional MRI; (2) cerebral blood flow as assessed via pseudo continuous arterial spin labelling; (3) electroencephalography frequencies; or (4) cognitive (memory) function.

Conclusions

This study identified chemical, microstructural and functional brain alterations in response to an acute non-concussive soccer heading task. These alterations appear to be subtle, with some only detected in specific regions, and no corresponding functional deficits (e.g., cognitive, adverse symptoms) observed. Nevertheless, our findings emphasise the importance of exercising caution when performing repeated non-concussive head impacts in sport.

Trial registration

ACTRN12621001355864. Date of registration 7/10/2021. URL https//www.anzctr.org.au/Trial/Registration/TrialReview.aspx?id=382590&isReview=true

Key Points

1. The effects of non-concussive head impacts on the brain are poorly understood. Employing a variety of magnetic resonance imaging sequences after controlled head impacts can interrogate parameters that have not been investigated in previous research.
2. This study observed acute alterations to select chemical, functional and microstructural parameters in the absence of overt cognitive deficits or reported symptoms, after participants completed a controlled soccer heading task.
3. These findings highlight the 'silent' physiological changes that can occur after non-concussive head impacts and emphasise the importance of exercising caution when performing repeated head impacts in sport.

1.0 Background

Athletes participating in contact/collision sports such as American football, rugby and association football (soccer) can sustain hundreds of head impacts each sporting season [1]. High strength, unanticipated and/or poorly located head impacts can cause *concussion*, a type of mild traumatic brain injury (mTBI) that is accompanied by a host of unpleasant symptoms (e.g., headache, blurred vision, nausea) [2]. Head impacts that do not elicit clinical signs or symptoms are termed '*subconcussive*', or increasingly '*non-concussive*', impacts [1, 3]. These impacts are exceedingly common, accounting for > 99% of all head impacts incurred in sport [4, 5]. They also have the potential to cause long-term harm, with some evidence suggesting that chronic traumatic encephalopathy (an incurable neurodegenerative disease related to head trauma [6]) can develop in the presence of non-concussive impacts exclusively [7]. Despite this, the effects of non-concussive impacts on the brain remain poorly understood [8].

Several observational studies have investigated the microstructural and physiological sequelae of non-concussive impacts in sport; specifically, those incurred over the course of a sporting season [9–12]. These studies have employed various assessment techniques, including *central methods* (e.g., magnetic resonance imaging [MRI] sequences such as diffusion weighted imaging [DWI], magnetic resonance spectroscopy [MRS] and functional MRI [fMRI]), *peripheral methods* (e.g., blood biomarkers), and *functional tests* (e.g., cognitive tasks) [8, 13–15]. Recent systematic reviews summarising their findings indicate that non-concussive impacts have the potential to alter brain microstructure, chemistry and function [8, 13–15]. However, results are inconsistent [8, 13–15]. It is also noted that observational studies have inherent limitations (e.g., confounders, biases) and cannot establish causation.

Interventional studies (particularly, randomised controlled trials [RCTs]) are increasingly being used to investigate the effects of non-concussive impacts on the brain [16]. When using these designs, impacts are administered in the form of a controlled non-concussive soccer heading task (SHT) [16]. Studies employing a SHT have shown that non-concussive impacts can elicit significant alterations in neuroelectric (via electroencephalography [EEG]) [17], cognitive [18, 19], neurovascular [20], neuroophthalmologic [21, 22], and vestibular [23, 24], function in healthy soccer athletes. SHTs have also been reported to increase blood concentrations of neurofilament light (Nf-L; a biomarker of axonal pathology) [25, 26], glial fibrillary acidic protein (GFAP; a biomarker of astrocyte pathology) [27], and certain inflammatory markers [28]. However, no interventional studies have investigated the microstructural and physiological effects of non-concussive impacts in sport using MRI techniques. This is important, as MRI has the capacity to interrogate regional chemical, functional and microstructural parameters that have not previously been investigated and allow researchers to predict the functional consequences of any changes observed.

The primary aim of this study was to investigate the acute effects of non-concussive impacts, administered in the form of a controlled SHT, on brain microstructure, function and chemistry using MRI techniques. It was hypothesised that non-concussive impacts would result in unfavourable changes to these parameters, as per previous observational studies.[8, 13, 15] The secondary aim was to investigate the effects of non-concussive impacts on neuroelectric activity (via EEG), cognitive function and blood biomarkers of neuronal and astroglial damage (i.e., Nf-L, GFAP) and inflammation (e.g., interleukin [IL]-6, etc).

2.0 Methods

2.1 Study Design

A randomised, controlled, crossover trial was conducted at Neuroscience Research Australia (NeuRA; Randwick, NSW). The trial was approved by the University of Sydney's Human Research Ethics Committee (2021/515) and registered prospectively with the Australian New Zealand Clinical Trials Registry (ACTRN12621001355864). All research was completed in accordance with the Declaration of Helsinki.

2.2 Participants

Healthy individuals aged between 18–35 years and with ≥ 5 years of soccer heading experience were recruited. The full eligibility criteria are presented in Figure S1. Briefly, the key exclusion criteria were: (1) a head, neck, face or eye injury (including a confirmed or suspected concussion) within the last 12 months; (2) an uncontrolled physical or mental health condition; (3) a neurological disorder; (4) a contraindication to MRI; or (5) pregnant or lactating.

2.3 Enrolment

Each volunteer completed a face-to-face screen with the trial coordinator (N.D.) and physician (K.R.). Here, they were informed about the nature and risks of experimental procedures, before providing written informed consent and being assessed for eligibility. Eligible participants were familiarised with the cognitive function tasks (Section 2.7.4 Cognitive Function Acquisition) and asked to provide demographic information (including an indication of 'usual' [non-specific] concussion symptoms as per the Concussion Recognition Tool [CRT]-5) [29].

2.4 Randomisation and Allocation Concealment

Participants were randomised to one of two possible treatment orders in a 1:1 ratio at the beginning of their first test session. Specifically, they were assigned a unique identification code (by N.D.) that was linked to a treatment order via a pre-populated randomisation schedule. The schedule was generated in a series of balanced blocks (and one 'block' of one) by an investigator (E.C.) using an online random number generator (https://www.sealedenvelope.com/simple-randomiser/v1/lists). The schedule could only be accessed by the investigator and one other researcher (P.A.), neither of whom had contact with participants. The balanced blocks also varied in size so that the final treatment order within each block could not be predicted. Treatment allocation was then concealed using sealed, opaque envelopes.

2.5 Treatments

Treatments were administered by the trial coordinator (N.D.) and a second investigator (D.M.) on the outdoor fields of Paine Reserve (Randwick, NSW; ~500 m from NeuRA).

2.5.1 Intervention ('Heading' Task)

The intervention was a SHT ('Heading'). A JUGS Soccer Machine™ (JUGS® Australia, Cheltenham, Victoria, Australia) was used to launch FIFA regulation size 5 soccer balls at a speed of 35 $km \cdot h^{-1}$. Participants performed 20 headers in 20 minutes from ~ 12 meters to the JUGS. They were instructed to hit the ball with their forehead and to direct it back towards the JUGS. Unsuccessful headers (i.e., where there was no contact between the head and the ball) were re-administered.

2.5.2 Control ('Kicking' Task)

The control was a soccer kicking task ('Kicking'). It was administered exactly as the intervention, except that participants kicked (rather than headed) the ball (which was launched along the ground).

2.6 Treatment Sessions

Participants completed two treatment sessions, Heading or Kicking, separated by ≥ 7 days.

2.6.1 Standardisation Procedures

Prior to each treatment session, participants were instructed to: (1) avoid soccer heading and playing other contact sports (> 7 days); (2) avoid using alcohol (> 24 hours), caffeine (> 12 hours), anti-inflammatory medication (> 4 days) and central nervous system (CNS) active drugs (> 7 days); (3) avoid moderate to strenuous exercise (> 12 hours); (4) spend > 8 hours in bed overnight; (5) consume a standardised breakfast (at home) and (6) consume 500 mL of water before arriving at the clinic.

2.6.2 Experimental Procedures

Experimental procedures are summarised in Fig. 1. Briefly, participants arrived at NeuRA between ~ 7:30–8:30 AM and verbally acknowledged compliance to the standardisation procedures. A urine sample was collected to confirm avoidance of CNS active drugs (DrugCheck® NxStep Onsite Urine Drug Test) and to assess hydration status (urine specific gravity [U_{SG}]; Palette Digital Refractometer, ATAGO, USA). If U_{SG} was > 1.024, likely indicating hypohydration [30], participants consumed 500 mL of water [31]. Participants then completed a series of baseline assessments ('Pre'; Section 2.7 Data Collection), before they were walked to the outdoor field to receive their assigned treatment (i.e., Heading or Kicking). Following treatment, participants returned to NeuRA to complete a series of post-treatment assessments ('Post' and '2.5 hrs Post'). They left between 12:30 – 1:30 PM but returned the following day to complete their 24-hour post-treatment assessments ('24 hrs Post'). Participants were instructed to adhere to the same standardisation procedures ahead of this visit.

Insert Fig. 1 *approximately here*

2.7 Data Collection

2.7.1. MRI Acquisition (Primary Outcome)

MRI commenced ~ 60 minutes post-treatment and took ~ 60 minutes to complete. The timing of this assessment was selected with consideration for pragmatic factors (e.g., participant transportation) and prior research suggesting that SHTs can elicit immediate alterations in neurovascular and corticomotor function [18, 20]. All images were collected by a registered radiographer using a 3T MRI scanner (Ingenia CX, Philips) with a 32-channel head coil. Participants were placed supine into the MRI scanner with their head secured in a tight-fitting head coil with headphones to prevent movement. Images were collected in the following order (time of acquisition post-treatment provided in mean ± SD): (1) T_1-weighted anatomical (+ 68 ± 6 mins); (2) proton MRS (^{1}H-MRS; +78 ± 7 mins); (3) electrical properties tomography (EPT; +94 ± 7 mins); (4) blood-oxygen-level-dependent (BOLD) resting-state fMRI (rs-fMRI; +102 ± 12 mins); (5) pseudo continuous arterial spin labelling (pCASL; +111 ± 8 mins); and (5) DWI (+ 117 ± 8 mins). Scans were conducted to measure brain chemistry (^{1}H-MRS), function (EPT, rs-fMRI and pCASL) and microstructure (DWI). Participants were instructed to remain awake and focused on a crosshair (displayed on a screen) throughout functional scans.

T1-weighted anatomical: A high-resolution 3-dimensional anatomical image set covering the entire brain was acquired for accurate image registration and segmentation (211 sagittal slices; repetition time [TR]/echo time [TE] = 7.3/3.4 ms; flip angle = 8°; slice thickness = 0.9 mm; voxel size = 0.75x0.75x0.9 mm).

^{1} H-MRS: Single voxel ^{1}H-MRS was collected from two brain regions: the left dorsolateral prefrontal cortex (dlPFC) and primary motor cortex (M1) in the somatotopic region representing the dominant foot, as these regions have demonstrated neurometabolic alterations in previous observational studies of non-concussive impacts [32–34]. Data from ^{1}H-MRS were collected using a semiadiabatic Localization by Adiabatic SElective Refocusing (sLASER) sequence (VAriable Power and Optimized Relaxations [VAPOR] water suppression; 64 averages; 2048 data

points; TE = 31 ms for dlPFC and 33 ms for M1, TR = 5000 ms; voxel size = 15 mm^3). Second order shimming was conducted using the auto-shimming function with the vendor-supplied (Phillips) sLASER sequence; only spectra with full width at half maximum (FWHM) values less than 15 Hz were accepted (otherwise scans were repeated).

EPT: Scans were acquired using a balanced fast field echo (bFFE) sequence (TR/TE = 2.54/1.27 ms; flip angle = 25°; nonselective radiofrequency [RF] pulses; compressed SENSE factor 1; RF shimming calibrated with full coverage 2D dual refocusing echo acquisition mode [DREAM]; voxel size = 1 mm^3).

rs-fMRI: A rs-fMRI series consisting of 250 whole brain BOLD fMRI image volumes was collected (TR/TE = 1500/30 ms; 75 axial slices; voxel size = 2 mm^3).

pCASL: A resting pCASL series covering the entire brain was acquired (TR/TE = 4188/10.7 ms; 24 axial slices; voxel size = 3x3x6 mm; 384 images). Four background suppression pulses were applied to maximise the sensitivity to blood perfusion [35].

DWI: A DWI set covering the entire brain was acquired using a single-shot multi-section spin-echo echo-planar pulse sequence (TR/TE = 3000/75 ms; flip angle = 90°; 57 axial slices; voxel size = 2.5 mm^3). For each slice, diffusion gradients were applied along 32 phase-encoding directions at b-value = 1000 s/mm^2, 64 phase-encoding directions at b-value = 3000 s/mm^2, and one volume acquired at b-value = 0 s/mm^2. Anatomical and diffusion image sets were visually inspected for artifacts; no participants were excluded from the analysis.

2.7.2 EEG Acquisition

A 15-minute resting EEG recording was acquired ~ 2 hours post-treatment using a 64-channel EEG system (ANT Neuro, Netherlands). Electrodes were placed according to the standard 10–20 system [36], with reference electrodes placed on opposing mastoid processes, and an electrode placed on the orbicularis oculi muscle to monitor eye movements. Participants were tested while seated in a quiet room and instructed to relax, close their eyes and let their mind wander. Continuous EEG data were acquired at a sampling rate of 1000 Hz with online band-pass filtered between 0.01 and 100 Hz.

2.7.3 Blood Acquisition

Blood was collected into a 6.0 mL pre-treated EDTA vacutainer and 3.5 mL serum vacutainer at Pre, Post, 2.5 hrs Post and 24 hrs Post. Each vacutainer was centrifuged for 15 minutes at 1500 g and 4˚C within 30 minutes of collection (following coagulation of the serum sample), with plasma and serum stored at − 80˚C until analysis.

2.7.4 Cognitive Function Acquisition

Cognitive function was assessed at Pre, Post, 2.5 hrs Post and 24 hrs Post using two computerised tasks from the Cambridge Neuropsychological Test Automated Battery (CANTAB): the Paired Associate Learning (PAL; ~8 minutes duration) and Spatial Working Memory (SWM; ~4 minutes duration) tasks [37, 38]. These tasks have demonstrated sensitivity to the effects of SHTs [18]. Participants completed the tasks in a quiet room and were instructed to take their time and minimise errors.

2.8 Data Processing and Analysis

2.8.1 MRI Processing and Analysis

[1] H-MRS: All analysis specifics, including visualisation of voxel placement and sample spectra, are presented in Table S1 (MRSinMRS Acquisition and Analysis Checklist) [39]. The spectrum and unsuppressed water spectrum for each participant were analysed by N.D. (unblinded) using Totally Automatic Robust Quantitation in NMR (TARQUIN; v4.3.10) [40]. Pre-processing consisted of eddy current correction, lipid filtering, automatic referencing water residual removal using Hankel singular value decomposition, zero-order phase correction, and automatic referencing using zero filling. The neurometabolites of interest were: total *N*-acetylaspatate (tNAA; NAA + *N* acetyl glutamate), myo-inositol (mI), total choline (tCho; choline-containing compounds), total creatine (tCr; creatine + phosphocreatine), and glutamate/glutamine (Glx). Neurometabolites were analysed and reported as water-referenced levels (using the default TARQUIN processing) rather than using internal neurometabolite references (e.g., tCr), as several neurometabolites including tCr may be influenced by non-concussive impacts [15].

The quality of all spectra were examined using the line width/FWHM of fitted spectra and signal-to-noise ratio (SNR) using TARQUIN's default processing. Data were excluded if FWHM > 15 Hz or SNR was < 5 (no data were discarded on this basis; Table S1). In addition, the accuracy of voxel placement was visually inspected through heat maps. Data from poorly placed voxels were discarded. Tissue parcellation (grey and white matter) within each voxel was reported (Table S1).

EPT: Data were processed by J.C. (blinded to treatment) to produce conductivity maps according to methods described by Cao and colleagues [41]. In brief, T1-weighted turbo field echo images were co-registered and segmented into white matter, grey matter and

cerebrospinal fluid using FSL [42], to alleviate boundary artifacts. Within each tissue type, an average parabolic phase fitting method was used to reduce artifacts amplified in the Laplacian [43], and the second derivatives of the fitted phase were taken to calculate conductivity. The conductivity maps of each participant from both sessions were normalised into Montreal Neurological Institute (MNI) space (voxel size 2 mm isotropic) using statistical parametric mapping (SPM) 12 [44].

rs-fMRI: Using SPM 12 [44], and custom software, fMRI images were processed by N.D. (unblinded). Images were slice-time and motion corrected, and global signal drifts removed using the detrending method described by Macey and colleagues [45]. Physiological noise was corrected (cardiac frequency band 60–120 beats per minute + 1 harmonic; respiratory frequency band 8–25 breaths per minute + 1 harmonic) using the DRIFTER toolbox [46], and the six-parameter movement-related signal changes modelled and removed using a linear modelling of realignment parameters procedure [45]. The fMRI images were then co-registered to participant's T1 anatomical image, the T1 image then spatially normalised to the MNI template and normalisation parameters applied to the fMRI images. The fMRI images were then spatially smoothed using a 6 mm FWHM Gaussian filter. Independent components analysis (ICA) was performed using the Group ICA toolbox [47] to define major brain networks [48–50]. Thirty independent components were extracted using the Infomax ICA algorithm [51], and major networks identified by visual inspection. We selected nine components from six major brain networks: the salience, sensorimotor, visual, default mode, cerebellar and executive control networks (Figure S2).

pCASL: Using SPM 12 [44], pCASL data were analysed by N.D. (unblinded). All pCASL sets were realigned, co-registered to each participant's source image, and a mean cerebral blood flow (CBF) map created using the subtraction method from the ASL toolbox [52]. Each participant's source images were spatially normalised to MNI space and the parameters applied to the CBF maps. The CBF maps were smoothed using a 6 mm FWHM Gaussian filter.

DWI: During acquisition, a coding error occurred that corrupted the acquisitions with diffusion gradients at b-value = 1000 s/mm^2. Consequently, b-1000 DWI were removed from the image set. Using SPM12 [44], the remaining images were processed by N.J. (blinded to treatment). Images were corrected for motion, eddy current and b0 distortion. Elements of the diffusion tensor were computed from the images using a linear model, then fractional anisotropy (FA) and mean diffusivity (MD) whole-brain maps were derived. The FA and MD maps were resliced into 1.5 mm isotropic voxel sizes and co-registered to each individual's T1-weighted anatomical image to ensure all images were in the same three-dimensional space. Subsequently, they were spatially normalised to MNI space using the previously calculated parameters from T1 images and spatially smoothed using a 5 mm FWHM Gaussian filter.

In addition, a fixel-based analysis (FBA) was conducted using MRtrix3 [53], to determine tract-specific quantities of fibre density (FD), fibre cross section (FC) and a combination of both (FDC). Data were processed by M.G. (blinded to treatment) according to previous published methods [54].

2.8.2 EEG Processing and Analysis

Processing of EEG data were performed in Matlab (Version R2020b; MathWorks, Inc., Natick, MA, USA) and the FieldTrip toolbox by N.D. (unblinded) [55]. Prior to processing, data were bandpass filtered between 0.01 and 35 Hz. Initially, large artefacts and poor-quality channels were identified via visual inspection and removed from the data. Following this, an ICA was conducted to remove typical eye artefacts (e.g., blinks and saccades). Poor quality channels were reconstructed via interpolation from neighbouring channels. Finally, the EEG signals were re-referenced to the average of the mastoid electrodes and down sampled to 200 Hz to enhance processing speed. Estimates of cortical power were produced using the fast Fourier transform, at the following frequencies: 0.02–0.09 (at steps of 0.01 Hz), 0.1–0.9 (at steps of 0.1 Hz), and 1–30 (at steps of 1 Hz). The cortical power at each frequency was computed by averaging the power across all EEG channels. Four frequency bands were included for analysis: infra-slow (0.03–0.06 Hz), theta (4–8 Hz), alpha (9–12 Hz), and beta (13–25 Hz).

2.8.3 Blood Biomarkers Analysis

Nf-L and GFAP: Plasma samples were analysed using a Simoa HD-X Analyzer (Quanterix, Lexington, MA) using commercially available Simoa kits as per manufacturer's instructions [56]. Samples were tested in duplicate by a scientist (W.O.) blinded to treatment. GFAP Discovery assays (Item 102336) were used to quantify GFAP, with participant samples analysed on the same plate, and all samples measuring above the lower limit of quantification (LLOQ; 0.686 pg/mL). For Nf-L, NF-Light V2 Advantage assays (Item 104073) were used, with all Pre and 24 hrs Post samples from the same participant were analysed on the same plate, and the remaining samples analysed separately later (once additional funding was sourced). All samples measured above the LLOQ for Nf-L (1.38 pg/mL).

Inflammatory Markers: Serum samples were analysed by a Contract Research Organisation (Eve Technologies, Calgary, AB, Canada). The Human Cytokine 15-Plex Assay Array was performed to determine concentrations of: granulocyte-macrophage colony-stimulating factor, interferon gamma, IL-1β, IL-1RA, IL-2, IL-4, IL-5, IL-6, IL-8, IL-10, IL-12p40, IL-12p70, IL-13, monocyte chemoattractant protein-1 (MCP-1), and tumour necrosis factor-α. The analyses were performed in duplicate by a laboratory technician blinded to treatment. Only Pre and 24 hrs Post samples were analysed due to funding constraints.

2.8.4 Cognitive Function Outcomes

The PAL task measures visual memory and learning [37]. The outcome measures were: number of attempts required to complete the task ('attempts') and number of errors made (adjusted for attempts if the participant did not complete the task; 'adjusted errors'). The SWM task measures working memory, executive functions, and strategy [38]. The outcome measures were: number of errors ('errors') and a strategy score (calculated based on the randomness of participants' opening boxes, where lower scores indicated better strategy; 'strategy').

2.8.5 Treatment Characteristics

An impact monitoring mouthguard (Prevent Biometrics™, Edina, MN, USA) was used to measure linear and rotational acceleration of head impacts (peak linear acceleration [PLA]; peak rotational acceleration [PRA]). This device has demonstrated a high degree of accuracy in controlled and field environments (concordance correlation coefficient > 0.8) [57]. Participants were also asked to rate how 'well' they performed each header on an 11-point scale (-5='very poorly'; to + 5='very well') and the 'strength' of each header on a 5-point scale (1='very low'; to 5='very high'). Mean heart rate (HR) throughout the 20-minute activity was determined using a chest strap monitor (Polar H10 HR Sensor).

2.8.6 Adverse Event Monitoring

Participants were monitored for signs of concussion (adverse event [AE]) using Parts 1–3 of the CRT-5 [29], at Post, 2.5 hrs Post, 4–8 hrs Post and 24 hrs Post Task (Fig. 1). Parts 1 and 2 were used to identify 'red flag' and 'observable sign(s)' of concussion. Part 3 was used to identify possible (non-specific) 'symptoms' of concussion. Participants answered 'yes', 'no' or 'maybe' to the 'red flag(s)', 'observable sign(s)' and potential 'symptoms'. Responses were documented, reviewed and escalated to the trial physician, as necessary.

2.9 Sample Size

A target sample size of 15 was selected with consideration of practical factors such as time, cost, and resource allocation, rather than formal power analysis. This pragmatic approach reflects the current lack of interventional studies investigating the acute effects of non-concussive impacts on brain structure, function and chemistry using MRI.

2.10 Statistical Analyses

The EPT, fMRI, ASL and DWI data were analysed using Matlab (Version R2023b; MathWorks, Inc., Natick, MA, USA) and EEG data using Matlab (Version R2020b). The remaining data were analysed using R (Version 4.2.2) [58].

2.10.1 Electrical Properties Tomography (EPT), Resting-State Functional Magnetic Resonance Imaging (rs-fMRI), Arterial Spin Labelling (ASL) and Diffusion Weighted Imaging (DWI)

Second level, random effects, paired analyses were conducted to determine significant differences at a voxel-by-voxel level ($p < 0.05$, false discovery rate [FDR] corrected, minimum cluster = 10 contiguous voxels). For the rs-fMRI network analyses, each analysis was restricted by creating a mask of the relevant network using both treatments' scan images ($p < 0.05$, FDR corrected). Significant differences for all MRI scans were then overlaid onto a mean T1-weighted anatomical image set.

2.10.2 Diffusion Weighted Imaging (DWI) Fixel-Based Analysis

A general liner model was fitted to every fixel to compare between treatments for all metrics (FD, FC, FDC). A whole brain tractogram consisting of two million streamlines was used for statistical inference using connectivity-based fixel enhancement [54]. Data were analysed between treatment using non-parametric permutation testing (5000 permutations; $p < 0.05$, family wise-error [FWE] corrected).

2.10.3 Electroencephalography (EEG)

Global cortical power of each frequency band (i.e., infraslow, theta, alpha and beta) between treatments were compared using paired t-tests with significance set a $p < 0.05$. In addition, to identify a group of channels where significant differences existed, the spatial distribution of power differences between treatments and within infraslow, theta, alpha and beta bands, were examined using cluster-based permutation tests (4000 permutations; $p < 0.05$, corrected using the 'cluster' function) [59].

2.10.4 Other Data

Continuous variables (neurometabolites [^{1}H-MRS], blood biomarkers, treatment characteristics) were analysed using linear mixed-effects models and the 'lme4' and 'emmeans' packages [60, 61]. The models included Treatment, Time, and Treatment $\times$ Time interaction as fixed effects and had a random intercept (Participant) and slope (Treatment), as appropriate. The models were generated using the restricted maximum likelihood criterion and no covariance structure was specified (unstructured). If the residuals were non-normally distributed

(Shapiro–Wilk test, $p < 0.05$) or heteroskedastic (Levene test, $p < 0.05$), the data were square-root transformed (and if unimproved, log-transformed) and reanalysed. If an appropriate model could not be generated, the 'best' of those described above (i.e., simplest model violating the fewest assumptions) was utilised. Note: As plasma Nf-L concentrations can remain elevated for 22 days following SHTs [25], a separate analysis was conducted, using Session (1 or 2), Treatment Order (Heading–Kicking or Kicking–Heading) and Session × Treatment Order interaction as a fixed effects and a random intercept (Participant) and slope (Treatment Order).

Count variables (cognitive function) were analysed using generalised linear mixed-effects models and the 'glmmTMB' and 'emmeans' packages [61, 62]. These models included the same fixed and random effects structure as above, and were fitted to a Poisson distribution, unless over-dispersed, and/or zero-inflated. In these instances, a negative binomial, zero-inflated Poisson, or zero-inflated negative binomial distribution was substituted, respectively (with both parts of the zero-inflated models containing the same fixed effects).

Two-sided pairwise comparisons were used to compare estimated marginal means across Treatment and/or Time if a significant main effect of Treatment, Time, or a Treatment × Time interaction (or equivalent for Nf-L) was observed. Data were presented as mean ± SD unless non-normally distributed (in which case, data were presented as Median [IQR]). Statistical significance was accepted as $p < 0.05$ (Dunn–Šidák-corrected) and effect sizes were calculated as Hedges' g [63].

3.0 Results

3.1 Participant and Treatment Characteristics

Recruitment commenced in November 2021 and concluded 12 months later. Eighteen volunteers signed informed consent and 15 were randomised (Fig. 2). Of those randomised, 14 received both treatments (i.e., as intended) and one received one treatment (i.e., Heading only) after being unable to complete the second session for personal reasons. All 15 participants were included in the final sample (except where the analytical technique employed could not handle missing data) (Table 1). Participants completed their sessions between seven and 25 days apart (9 ± 4 days). Note that due to difficulties with recruitment, only male participants completed this trial.

Table 1
Participant Characteristics

ID	Age (years)	BMI (kg/m^2)	Dominant Foot	Predominant playing position	Number of headers in last 12 months[a]	Number of years heading experience	Number of previous concussions	Length of time since last concussion (years)	Time of season[b]	Days between trials
1	24	28.1	Right	Centre Midfield	528	18	0	NA	Pre-Season	25[c]
2	22	23.6	Right	Centre Attacking Midfield	928	14	0	NA	Pre-Season	7
3	25	24.2	Right	Centre Back	160	13	0	NA	In-Season	7
4	29	24.0	Right	Centre Defending Midfield	192	20	0	NA	In-Season	7
5	18	19.0	Right	Wide Back	336	9	0	NA	Off-Season	8
6	34	28.4	Right	Centre Defensive Midfield	1520	28	2	17	In-Season	7
7	20	23.3	Right	Wing	144	8	1	8	In-Season	8
8	20	29.7	Right	Centre Back	96	8	2	4	In-Season	7
9	27	25.6	Right	Centre Back	1760	14	0	NA	Post-Season	8
10	22	24.0	Right	Centre Back	0	5	0	NA	Off-Season	8
11	32	28.2	Right	Centre Back	540	25	0	NA	Post-Season	7
12	20	25.1	Right	Striker	1248	8	0	NA	Post-Season	NA[d]
13	29	25.8	Left	Centre Back	832	23	2	5	Post-Season	8
14	27	24.3	Right	Centre Midfield	12	19	0	NA	Off-Season	8
15	27	24.3	Right	Centre Back	204	20	5	4	Off-Season	9
Mean ± SD	25 ± 5	25.2 ± 2.7			567 ± 549	16 ± 7				9 ± 4

[a]The number of head impacts in the last 12 months was subjectively assessed via a standardised questionnaire.[27]

[b]Pre-Season: (Scheduled training prior to In-Season but after Off-Season - possible infrequent games); In-Season (Scheduled training and frequent competitive games [at least weekly]); Post-Season (No/minimal scheduled training and between In-Season and Off-Season - possible infrequent games); Off-Season (No scheduled training/games)

[c]Participant had longer than anticipated time between trials due to being diagnosed with SARS-CoV-2 between Trial 1 and 2.

[d]Participant did not complete Trial 2 due to family reasons.

Insert Fig. 2 *approximately here*

Insert Table 1 *approximately here*

Treatment characteristics are summarised in Table S2. The average PLA and PRA of headers was 15.8 ± 5.6 g and 1271 ± 602 rad/s^2, respectively. No head impacts were recorded on Kicking. Participants rated the strength of headers as 3 (IQR: 2–4) on a 5-point scale and how well they performed each header as 1 (IQR: -1–3) on a -5 to 5 scale. Mean HR tended to be higher during Heading than Kicking (81 ± 12; 79 ± 12 bpm, $p = 0.081$, g = 0.159).

3.2 Magnetic Resonance Imaging (MRI)

Only the 14 participants who received both treatments could be included in the MRI analyses, except for the ^{1}H-MRS analysis (details below).

3.2.1 Proton Magnetic Resonance Spectroscopy (^{1}H-MRS)

Fifteen participants were included in the dlPFC analyses. Only 14 were included in the M1 analyses due to inaccurate voxel placement (on both sessions; ID: 1). Heading increased tNAA ($p = 0.012$, g = 0.593) and tCr ($p = 0.010$, g = 0.702) levels in the M1 compared to Kicking. No other significant differences were observed in either region (Table 2; all p's > 0.05).

Table 2
Neurometabolite levels between trials assessed using Magnetic Resonance Spectroscopy

ROI	Metabolite	Kicking		Heading		*p* value	Hedges' g
		n	Concentration (mM)	*n*	Concentration (mM)		
dlPFC							
	Glx	14	7.04 ± 1.57	15	7.95 ± 1.76	0.156	0.514
	tNAA	14	9.04 ± 0.89	15	8.74 ± 0.76	0.333	-0.343
	tCr	14	5.99 ± 0.89	15	5.95 ± 0.36	0.993	-0.063
	tCho	14	1.74 ± 0.26	15	1.71 ± 0.17	0.659	-0.137
	mI	14	3.12 ± 0.67	15	3.02 ± 0.65	0.619	-0.142
M1							
	Glx	13	6.99 ± 1.01	14	7.55 ± 1.57	0.287	0.404
	tNAA	13	9.02 ± 0.50	14	9.43 ± 0.71	0.012	0.593
	tCr	13	5.53 ± 0.31	14	5.82 ± 0.44	0.010	0.702
	tCho	13	1.56 ± 0.15	14	1.56 ± 0.12	0.894	-0.034
	mI	13	2.88 ± 0.54	14	2.76 ± 0.36	0.511	-0.241

Abbreviations: dlPFC – dorsolateral prefrontal cortex, Glx – glutamate and glutamine, M1 – primary motor cortex, mI – myo-inositol, mM (millimolar), tNAA – total *N*-acetyl aspartate (*N*-acetyl aspartate and *N*-acetyl glutamate), ROI – region of interest, tCho – total choline (choline-containing compounds), tCr – total creatine (creatine and phosphocreatine). Data presented as mean ± SD. **Bold** values represent statistically significant changes ($p < 0.05$).

Insert Table 2 *approximately here*

3.2.2 Electrical Properties Tomography (EPT)

Heading significantly reduced tissue conductivity in 11 clusters located in the white matter of the frontal, occipital, temporal and parietal lobes, and cerebellum. The location, size and *T* values of these clusters are presented in Fig. 3. No increases in conductivity were observed.

Insert Fig. 3 *approximately here*

3.2.3 Resting-State Functional Magnetic Resonance Imaging (rs-fMRI)

Heading had no significant effects on network connectivity strengths in any of the six brain networks identified (i.e., the salience, sensorimotor, visual, default mode, cerebellar and executive control).

3.2.4 Pseudo Continuous Arterial Spin Labelling (pCASL)

Heading had no significant effects on resting CBF in any brain region.

3.2.5 Diffusion Weighted Imaging (DWI)

Heading had no significant effects on FA or MD in any brain region. In the fixel-based analysis, Heading had no significant effects on FB, FC or FBC in any brain region (example images from the analysis provided in Figure S3).

3.3 Electroencephalography (EEG)

Of the 14 participants who received both treatments, 12 were included in these analyses. Indeed, EEG data could not be collected for one participant (on Kicking) due to technical difficulties and was unreadable for another (on both treatments).

Heading had no significant effects on infraslow, theta, alpha or beta frequency bands (Table S3). For cluster analyses, no significant differences for any individual band was identified (all $p > 0.05$, Fig. 4A). However, Heading tended to decrease alpha frequency power in five left posterior channels (Fig. 4B; $p = 0.066$).

Insert Fig. 4 *approximately here*

3.4 Blood Biomarkers

3.4.1 Plasma Neurofilament-Light (Nf-L) and Glial Fibrillary Acidic Protein (GFAP)

Fifteen participants were included. Nine of the 120 samples (7.5%) could not be collected due to difficulties with vascular access.

For Nf-L, the mean ± SD intra-assay coefficient of variation (CV) for the duplicate samples was 6.0 ± 5.1%. There was no significant interaction between Treatment and Time ($p = 0.510$; Fig. 5A). However, a significant interaction between Session and Treatment Order ($p < 0.001$) was observed (Fig. 5B). Post hoc comparisons showed that participants had higher plasma Nf-L concentrations on Session 2 with Treatment Order Heading–Kicking ($n = 8$) than Kicking–Heading ($n = 7$) (6.60 [IQR: 4.64–7.63] vs. 3.70 [IQR: 3.47–4.82] pg/mL; $p = 0.046$; g = 1.201). No significant difference between Treatment Orders were observed at Session 1 (5.18 [IQR: 3.85–5.51] vs. 3.76 [IQR: 3.34–4.92] pg/mL; $p = 0.765$, g = 0.370).

Insert Fig. 5 *approximately here*

For GFAP, the mean ± SD intra-assay CV for the duplicate samples was 5.5 ± 5.1%. A significant interaction between Treatment and Time was observed ($p = 0.043$; Fig. 5C). Post hoc comparisons showed that Heading increased GFAP concentrations at 24 hrs Post compared to Kicking (81.0 [IQR: 65.2–88.2] vs. 66.5 [IQR: 59.3–77.1] pg/mL; $p = 0.014$; Hedges' g = 0.637). No other significant differences were observed.

3.4.2 Serum Inflammatory Markers

Fifteen participants were included. Three of 60 samples (5%) could not be collected due to difficulties with vascular access. The mean intra-assay CV for the samples ranged from 11.8 ± 11.7% (MCP-1) to 36.0 ± 27.6% (IL-6). Due to extremely high CVs, the utility of data is limited. We have provided the results of these analyses in Table S6 for completeness, but recommend they be interpreted with a high degree of caution.

3.5 Cognitive Function

Fifteen participants were included. No significant Treatment, Time or Treatment × Time interactions were observed (all p's > 0.05; Table S4). Note: SWM errors were not formally analysed as participants demonstrated a high degree of accuracy on all treatments and time points (i.e., achieved zero errors on 81% of occasions) (Table S4).

3.6 Adverse Event (AE) Monitoring

The frequency of possible (but non-specific) symptoms of concussion are presented in Table S5. The most commonly reported symptom was 'Pressure in the head' (9/15; 60%) Post-Heading, followed by Headache (6/15; 40%) 2.5 hrs Post-Heading. Both abated within 24 hours. The remaining symptoms were relatively infrequent. No participants experienced a concussion.

4.0 Discussion

This RCT investigated the acute effects of non-concussive impacts on brain function, chemistry and microstructure utilising MRI and other methods. Contrary to our hypothesis, significant changes were only observed in select outcomes. With respect to brain function, several regions displayed significant reductions in tissue conductivity, as assessed via EPT, while no changes in brain network connectivity (assessed via rs-fMRI) or CBF (assessed via pCASL) were found. Accompanying this, a non-significant trend toward reduced alpha frequency power (assessed via EEG) was noted in the left parietal/occipital cortex. Non-concussive impacts regionally altered brain chemistry (assessed via ^{1}H-MRS) as assessed via, with increases in tNAA and tCr observed within the M1 (but not the dlPFC). We found no significant effects of non-concussive impacts on brain microstructure, as assessed via DWI. However, two blood biomarkers (GFAP and Nf-L) expressed in brain

microstructures, were significantly elevated 24 hours and ~ 7-days post Heading, respectively. These changes were observed in the absence of significant adverse symptoms and detectable alterations in cognitive function.

No previous studies have used EPT to investigate the effects of non-concussive (or concussive) impacts on the electrical properties of the brain. Our finding of reduced tissue conductivity in several brain regions is, therefore, novel and indicates that white matter conductivity is affected by non-concussive impacts. White matter is typically more susceptible to injury from biomechanical forces than grey matter due to its anisotropic and rheological properties [64–66]. However, it is unclear why almost no alterations were observed within frontal regions (i.e., where the soccer balls were received). The more posterior alterations could represent a contrecoup mechanism, whereby the movement of the brain within the skull produces a secondary impact elsewhere [67].

The largest cluster demonstrating reduced conductivity (> 200 voxels) was located posteriorly across the left optic radiation, which transmits visual information to the visual cortex [68]. Our participants did not experience symptoms related to vision (e.g., double vision, blank or vacant look). However, previous interventional studies have shown that non-concussive impacts can affect oculomotor and neuro-ophthalmologic function [21, 22]. Interestingly, this general region of the brain also tended to demonstrate reduced alpha activity (as assessed via EEG), which may be reflective of increased excitability to visual regions or visual processing [69, 70]. That said, a previous interventional study utilising EEG found that whole brain and channel-wise alpha power was unaltered following a SHT when compared to the control trial [17]. Thus, the effect of non-concussive impacts on EEG metrics and in relation to visual function requires further investigation.

Other functional metrics including brain network connectivity via rs-fMRI, CBF via pCASL and cognitive (memory) function, showed no significant changes from non-concussive impacts. Previous observational studies have detected increases in brain network connectivity (in sensorimotor, visual and cerebellum networks) [50] and CBF following non-concussive impacts [71, 72]. In these studies, longer exposure periods (e.g., a full season) and different contact sports (e.g., American Football) could potentially produce stronger effects. However, observational studies also often have significant limitations (e.g., confounders, biases) that are difficult to control [73]. That said, one interventional study did find that non-concussive impacts altered performance on the same neurocognitive tasks used in this investigation [18]. Specifically, errors on both the SWM and PAL tasks were increased following heading, compared to baseline [18]. However, this study utilised a more demanding SHT (i.e., 20 headers in 10 minutes, at a speed of ~ 39km/hr and distance of 6 meters) [18]. Ultimately, with neither brain network connectivity nor CBF demonstrating significant effects (including brain regions involved in memory [74]), it is not surprising that cognitive function was unaltered in the current study.

Two recent meta-analyses have investigated the effects of non-concussive impacts on brain chemistry via ^{1}H-MRS [15, 75]. Both included observational studies only, as interventional studies were lacking. Neither meta-analysis reported significant differences in tNAA, tCr, tCho, and Glx levels between ‘cases’ (i.e., individuals exposed to non-concussive impacts) and controls [15, 75]. However, one found that tNAA (considered a biomarker of energy utilisation and neuronal health in mTBI [32, 76]) and tCr (considered a biomarker of energy homeostasis [76]) levels decreased from the pre-season to the mid-/post-season period [15]. In contrast, our study found that non-concussive impacts *increased* tNAA and tCr levels within the M1. This could be indicative of mitochondrial hypermetabolism in this region [76]. Again, the inconsistent findings could be due to methodological differences between studies. Alternatively, these studies may be detecting the same response along a temporal continuum (e.g., initial hypermetabolism as seen in concussive impacts [77], followed by delayed hypometabolism). Finally, the absence of frontal alterations (i.e., in the dlPFC) could be representative of a contrecoup mechanism as suggested earlier.

The current study used two analytical approaches to interrogate DWI data. No significant effects were observed on FA or MD, nor on the FBA metrics of FC, FD or FDC; suggesting that microstructural tissue alterations were not readily apparent [78]. Two recent systematic reviews have summarised the effects of non-concussive impacts on brain microstructure via DWI [13, 79]. Both reviews (which again included observational studies, only) concluded that non-concussive impacts typically, albeit somewhat inconsistently, decrease FA and increase MD in predominantly white matter regions [13, 79]. As previously noted, the inconsistent findings could be due to methodological differences between studies. No studies have previously investigated the effects of non-concussive impacts on DWI using FBA.

While no significant microstructural alterations were observed using DWI, two blood biomarkers expressed in brain microstructures, Nf-L and GFAP, were significantly elevated post Heading. First, a large effect size was observed in an axonal injury marker, Nf-L, ~ 7-days post Heading. Three previous interventional studies have likewise shown that non-concussive impacts increase blood Nf-L concentrations and that concentrations can remain elevated for a prolonged period (e.g., > 22 days) [25, 26, 80]. Though, in these cases, changes emerged within 24 hours. This could be because a more intensive SHT was employed (e.g., one study administered 40 headers in 20 minutes at a speed of 77.4 km/hr) [25]. Alternatively, we might have been unable to detect an effect at 24 hrs because of treatment order effects. Nonetheless, the observed change in plasma Nf-L concentration suggests some degree of microstructural disruption to axons or other neural components [81]. The disparity between this finding and those from DWI metrics, may reflect a greater sensitivity of the blood biomarker to subtle microstructural damage.

Second, a moderate effect size increase in plasma concentrations of an astroglial pathology marker, GFAP, was observed 24 hrs post Heading. Two previous interventional studies have investigated the effects of non-concussive impacts on plasma GFAP concentrations [27, 80]. One found no difference 2 hrs or 24 hrs post Heading (compared to a Kicking control) [80], while the other found that concentrations were increased 2 hrs, but not 24 hrs, post-Heading (compared to baseline) [27]. The significant and delayed response observed in our trial could be due to the fact that our SHT was more intensive than that utilised in previous investigations [27, 80]. Nevertheless, the observed change in plasma GFAP concentration is indicative of an astrocytic response, which may reflect astrogliosis, or disruption to astrocyte integrity [27, 82]. The extent of this alteration appears subtle, given that no alterations to astrocyte activation were observed in DWI metrics, infraslow oscillations (via EEG) or CBF (via pCASL) [83, 84].

Our study was not without limitations. First, it had a relatively small sample size; thus, may be under-powered to detect additional effects. Second, we could not blind participants or researchers involved in trial activities to treatments. Third, we are unable to comment on the effect of the SHT on serum inflammatory markers due to extremely high CVs between duplicate samples. Finally, our study only included young, healthy males. Thus, results may not be generalisable to other populations.

5.0 Conclusions

this RCT demonstrates that non-concussive impacts; specifically, those administered in the form of a controlled SHT, can alter select markers of brain function, chemistry and microstructure. These include changes to tissue conductivity, brain concentrations of tNAA and tCr, and plasma Nf-L and GFAP concentrations. These alterations appear to be subtle, with some only detected in specific regions and no corresponding functional deficits (e.g., cognitive, adverse symptoms) observed. Nevertheless, our findings suggest that non-concussive impacts have the potential to elevate metabolism and impair neuronal/glial cell functioning, particularly in mid- to posterior- brain regions. These observations substantiate suggestions that prolonged exposure to non-concussive impacts has long term consequences for the brain health and suggest that individuals should exercise caution when performing repeated non-concussive impacts in sport.

Abbreviations

^{1}H-MRS	proton magnetic resonance spectroscopy
bFFE	balanced fast field echo
BOLD	blood-oxygen-level-dependent
CBF	cerebral blood flow
CNS	central nervous system
CRT	concussion recognition tool
CV	coefficient of variation
dlPFC	dorsolateral prefrontal cortex
DREAM	dual refocusing echo acquisition mode
DWI	diffusion weighted imaging
EEG	electroencephalography
EPT	electrical properties tomography
FA	fractional anisotropy
FBA	fixel-based analysis
FC	fibre cross section
FD	fibre density
FDC	fibre density + cross section
FDR	false discovery rate
fMRI	functional magnetic resonance imaging
FWE	family wise-error
FWHM	full width at half maximum
GFAP	glial fibrillary acidic protein
Glx	glutamate/glutamine
HR	heart rate
ICA	independent components analysis
IL	interleukin
LLOQ	lower limit of quantification
M1	primary motor cortex
MCP-1	monocyte chemoattractant protein-1
MD	mean diffusivity
mI	myo-inositol
MNI	Montreal Neurological Institute
MRI	magnetic resonance imaging
MRS	magnetic resonance spectroscopy
mTBI	mild traumatic brain injury
NeuRA	Neuroscience Research Australia
Nf-L	neurofilament light
PAL	paired associate learning
pCASL	pseudo continuous arterial spin labelling

^{1}H-MRS	proton magnetic resonance spectroscopy
PLA	peak linear acceleration
PRA	peak rotational acceleration
RCT	randomised controlled trial
RF	radiofrequency
rs-fMRI	resting-state functional magnetic resonance imaging
SHT	soccer heading task
sLASER	semiadiabatic Localization by Adiabatic SElective Refocusing
SNR	signal-to-noise ratio
SPM	statistical parametric mapping
SWM	spatial working memory
TARQUIN	Totally Automatic Robust Quantitation in NMR
tCho	total choline
tCr	total creatine
TE	echo time
tNAA	total N-acetylaspatate
TR	repetition time
U_{SG}	urine specific gravity
VAPOR	VAriable Power and Optimized Relaxations

Declarations

Ethics Approval and Consent to Participate:

The trial was approved by the University of Sydney's Human Research Ethics Committee (2021/515) and registered prospectively with the Australian New Zealand Clinical Trials Registry (ACTRN12621001355864). All research was completed in accordance with the Declaration of Helsinki. Informed consent was obtained from all individual participants included in the study.

Consent for publication:

Not applicable.

Competing Interests:

The authors have no competing interests to declare that are relevant to the content of this article.

Funding:

This study was primarily supported by funding from the Lambert Initiative for Cannabinoid Therapeutics (a philanthropically funded centre for medicinal cannabis research at the University of Sydney). Additional funding support was provided internally from Griffith University and Monash University.

Author Contributions:

N.D., L.A.H., C.R., S.J.M., B.D., C.I., E.A.C., P.J.A., S.B., M.E.B., K.R., I.S.M., & D.M. conceptualised the research project. N.D., R.V.R., F.A.T., K.R., & D.M. contributed to data collection. N.D., R.V.R., F.A.T., L.A.H., C.R., S.J.M., B.D., C.I., A.L.P, M.A.G., N.W.J., J.C., W.T.O., & D.M. contributed to

data analysis and interpretation of results. N.D. and D.M. drafted the manuscript. All authors critically reviewed and edited the manuscript prior to submission.

Acknowledgements:

The authors acknowledge the facilities and scientific and technical assistance of the National Imaging Facility, a National Collaborative Research Infrastructure Strategy (NCRIS) capability, at NeuRA Imaging, NeuRA, UNSW Node. We also acknowledge and greatly appreciate the technical expertise of Paul M. Macey and Judy Zhu in the development of software codes. the Randwick City Council for their approval to use the sporting fields for treatment sessions. The ongoing financial support of Barry and Joy Lambert is gratefully acknowledged by the research team.

Availability of Data and Materials:

The data that support the findings of this study are available from the corresponding author, upon reasonable request.

References

1. Bailes JE, et al. Role of subconcussion in repetitive mild traumatic brain injury: A review. J Neurosurg JNS. 2013;119(5):1235–45.
2. Patricios JS et al. *Consensus statement on concussion in sport: the 6th International Conference on Concussion in Sport–Amsterdam, October* 2022. British Journal of Sports Medicine, 2023. 57(11): pp. 695–711.
3. Nowinski CJ et al. 'Subconcussive' is a dangerous misnomer: hits of greater magnitude than concussive impacts may not cause symptoms. Br J Sports Med, 2024: p. bjsports-2023-107413.
4. Stemper BD, et al. Comparison of Head Impact Exposure Between Concussed Football Athletes and Matched Controls: Evidence for a Possible Second Mechanism of Sport-Related Concussion. Ann Biomed Eng. 2019;47(10):2057–72.
5. King DA, et al. Head impact exposure from match participation in women's rugby league over one season of domestic competition. J Sci Med Sport. 2018;21(2):139–46.
6. Nowinski CJ et al. Applying the Bradford Hill criteria for causation to repetitive head impacts and chronic traumatic encephalopathy. Front Neurol, 2022. 13.
7. McKee AC, Alosco ML, Huber BR. Repetitive head impacts and chronic traumatic encephalopathy. Neurosurg Clin North Am. 2016;27(4):529–35.
8. Mainwaring L, et al. Subconcussive head impacts in sport: a systematic review of the evidence. Int J Psychophysiol. 2018;132:39–54.
9. Churchill NW, et al. Structural, functional, and metabolic brain markers differentiate collision versus contact and non-contact athletes. Front Neurol. 2017;8:390.
10. Miller JR, et al. Comparison of preseason, midseason, and postseason neurocognitive scores in uninjured collegiate football players. Am J Sports Med. 2007;35(8):1284–8.
11. Rogatzki MJ, et al. Biomarkers of brain injury following an American football game: A pilot study. Int J ImmunoPathol Pharmacol. 2016;29(3):450–7.
12. Bazarian JJ, et al. Persistent, long-term cerebral white matter changes after sports-related repetitive head impacts. PLoS ONE. 2014;9(4):e94734.
13. Tayebi M, et al. The role of diffusion tensor imaging in characterizing injury patterns on athletes with concussion and subconcussive injury: a systematic review. Brain Injury. 2021;35(6):621–44.
14. Karantali E, et al. Neurofilament light chain in patients with a concussion or head impacts: a systematic review and meta-analysis. European Journal of Trauma and Emergency Surgery; 2021.
15. Delang N, et al. The effect of contact/collision sport participation without concussion on neurometabolites: A systematic review and meta-analysis of magnetic resonance spectroscopy studies. J Neurochem. 2023;167(5):615–32.
16. Bevilacqua ZW, Huibregtse ME, Kawata K. *In* vivo protocol of controlled subconcussive head impacts for the validation of field study data. JoVE (Journal Visualized Experiments), 2019(146): p. e59381.
17. Parr JVV et al. Soccer heading immediately alters brain function and brain-muscle communication. Front Hum Neurosci, 2023. 17.
18. Di Virgilio TG, et al. Evidence for acute electrophysiological and cognitive changes following routine soccer heading. EBioMedicine. 2016;13:66–71.

19. Ashton J, et al. Immediate effects of an acute bout of repeated soccer heading on cognitive performance. Sci Med Footb. 2021;5(3):181–7.
20. Smirl JD et al. An acute bout of soccer heading subtly alters neurovascular coupling metrics. Front Neurol, 2020. 11.
21. Kawata K, et al. Effect of repetitive sub-concussive head impacts on ocular near point of convergence. Int J Sports Med. 2016;37(05):405–10.
22. Nowak MK, et al. Neuro-Ophthalmologic Response to Repetitive Subconcussive Head Impacts: A Randomized Clinical Trial. JAMA Ophthalmol. 2020;138(4):350–7.
23. Hwang S, et al. Vestibular dysfunction after subconcussive head impact. J Neurotrauma. 2017;34(1):8–15.
24. Kaminski TW, et al. Self-reported head injury symptoms exacerbated in those with previous concussions following an acute bout of purposeful soccer heading. Res sports Med. 2020;28(2):217–30.
25. Wallace C, et al. Heading in soccer increases serum neurofilament light protein and SCAT3 symptom metrics. BMJ open sport Exerc Med. 2018;4(1):e000433.
26. Wirsching A, et al. Association of acute increase in plasma neurofilament light with repetitive subconcussive head impacts: a pilot randomized control trial. J Neurotrauma. 2019;36(4):548–53.
27. Nowak MK, et al. Neuro-ophthalmologic and blood biomarker responses in ADHD following subconcussive head impacts: a case-control trial. Front Psychiatry. 2023;14:1230463.
28. Huibregtse ME, et al. Acute time-course changes in CCL11, CCL2, and IL-10 levels after controlled subconcussive head impacts: a pilot randomized clinical trial. J Head Trauma Rehabil. 2020;35(5):308–16.
29. Echemendia RJ, et al. The concussion recognition tool 5th edition (CRT5): background and rationale. Br J Sports Med. 2017;51(11):870–1.
30. Armstrong LE, et al. Human hydration indices: acute and longitudinal reference values. Int J Sport Nutr Exerc Metab. 2010;20(2):145–53.
31. McCartney D, Desbrow B, Irwin C. The effect of fluid intake following dehydration on subsequent athletic and cognitive performance: a systematic review and meta-analysis. Sports medicine-open. 2017;3(1):1–23.
32. Vike NL et al. American football position-specific neurometabolic changes in high school athletes–a magnetic resonance spectroscopic study. J Neurotrauma, 2022(ja).
33. Bari S, et al. Dependence on subconcussive impacts of brain metabolism in collision sport athletes: an MR spectroscopic study. Brain Imaging Behav. 2019;13(3):735–49.
34. Poole VN, et al. Sub-concussive hit characteristics predict deviant brain metabolism in football athletes. Dev Neuropsychol. 2015;40(1):12–7.
35. Alsop DC, et al. Recommended implementation of arterial spin-labeled perfusion MRI for clinical applications: A consensus of the ISMRM perfusion study group and the European consortium for ASL in dementia. Magn Reson Med. 2015;73(1):102–16.
36. Oostenveld R, Praamstra P. The five percent electrode system for high-resolution EEG and ERP measurements. Clin Neurophysiol. 2001;112(4):713–9.
37. Cambridge Cognition. Paired Associates Learning (PAL). 2023 23rd May 2023]; https://www.cambridgecognition.com/cantab/cognitive-tests/memory/paired-associates-learning-pal/.
38. Cambridge Cognition. Spatial Working Memory (SWM). 2023 23rd May 2023]; https://www.cambridgecognition.com/cantab/cognitive-tests/executive-function/spatial-executive-function-swm/.
39. Lin A, et al. Minimum reporting standards for in vivo magnetic resonance spectroscopy (MRSinMRS): experts' consensus recommendations. NMR Biomed. 2021;34(5):e4484.
40. Wilson M, et al. A constrained least-squares approach to the automated quantitation of in vivo 1H magnetic resonance spectroscopy data. Magn Reson Med. 2011;65(1):1–12.
41. Cao J, et al. Repeatability of brain phase-based magnetic resonance electric properties tomography methods and effect of compressed SENSE and RF shimming. Phys Eng Sci Med. 2023;46(2):753–66.
42. Zhang Y, Brady M, Smith S. Segmentation of brain MR images through a hidden Markov random field model and the expectation-maximization algorithm. IEEE Trans Med Imaging. 2001;20(1):45–57.
43. Katscher U et al. *Estimation of breast tumor conductivity using parabolic phase fitting*. in *Proceedings of the 20th Annual Meeting of ISMRM, Melbourne, Australia*. 2012.
44. Friston KJ, et al. Statistical parametric maps in functional imaging: A general linear approach. Hum Brain Mapp. 1994;2(4):189–210.
45. Macey PM, et al. A method for removal of global effects from fMRI time series. NeuroImage. 2004;22(1):360–6.
46. Särkkä S, et al. Dynamic retrospective filtering of physiological noise in BOLD fMRI: DRIFTER. NeuroImage. 2012;60(2):1517–27.

47. Calhoun VD, et al. A method for making group inferences from functional MRI data using independent component analysis. Hum Brain Mapp. 2001;14(3):140–51.
48. Manning KY, et al. Longitudinal changes of brain microstructure and function in nonconcussed female rugby players. Neurology. 2020;95(4):e402–12.
49. Li W, Kong X, Ma J. Effects of combat sports on cerebellar function in adolescents: a resting-state fMRI study. Br J Radiol. 2022;95(1130):20210826.
50. Li W, et al. Effects of combat sports on functional network connectivity in adolescents. Neuroradiology. 2021;63(11):1863–71.
51. Amari S, Cichocki, Yang H. A new learning algorithm for blind signal separation. Adv Neural Inf Process Syst, 1995. 8.
52. Wang Z, et al. Empirical optimization of ASL data analysis using an ASL data processing toolbox: ASLtbx. Magn Reson Imaging. 2008;26(2):261–9.
53. Tournier JD, et al. MRtrix3: A fast, flexible and open software framework for medical image processing and visualisation. NeuroImage. 2019;202:116137.
54. Raffelt DA, et al. Connectivity-based fixel enhancement: Whole-brain statistical analysis of diffusion MRI measures in the presence of crossing fibres. NeuroImage. 2015;117:40–55.
55. Oostenveld R et al. *FieldTrip: open source software for advanced analysis of MEG, EEG, and invasive electrophysiological data.* Computational intelligence and neuroscience, 2011. 2011.
56. Jonathan R et al. *Utility of Acute and Subacute Blood Biomarkers to Assist Diagnosis in CT Negative Isolated Mild Traumatic Brain Injury.* Neurology, 2023: p. 10.1212/WNL.0000000000207881.
57. Kieffer EE, et al. A Two-Phased Approach to Quantifying Head Impact Sensor Accuracy: In-Laboratory and On-Field Assessments. Ann Biomed Eng. 2020;48(11):2613–25.
58. Core Team R. R: A Language and Environment for Statistical Computing. R Foundation for Statistical Computing: Vienna, Austria; 2023.
59. Maris E, Oostenveld R. Nonparametric statistical testing of EEG-and MEG-data. J Neurosci Methods. 2007;164(1):177–90.
60. Bates D et al. *Package 'lme4'.* URL http://lme4. r-forge. r-project. org, 2009.
61. Lenth R et al. *Package 'emmeans'*. 2019.
62. Magnusson A, et al. Package 'glmmtmb'. R Package Version. 2017;0(2):0.
63. Cohen J. Statistical Power Analysis for the Behavioral Sciences. Routledge; 1988.
64. Park E, Baker AJ. *The Pathophysiology of Concussion*, in *Tackling the Concussion Epidemic: A Bench to Bedside Approach*, T.A. Schweizer and A.J. Baker, Editors. 2022, Springer International Publishing: Cham. pp. 25–41.
65. Giordano C, et al. The influence of anisotropy on brain injury prediction. J Biomech. 2014;47(5):1052–9.
66. Grevesse T, et al. Opposite rheological properties of neuronal microcompartments predict axonal vulnerability in brain injury. Sci Rep. 2015;5:9475.
67. Payne WN, De Jesus O, Payne AN. Contrecoup Brain Injury. StatPearls Publishing; 2022. Treasure Island (FL).
68. Ramos-Fresnedo A et al. Chap. 2 - *Supratentorial White Matter Tracts*, in *Comprehensive Overview of Modern Surgical Approaches to Intrinsic Brain Tumors*, K. Chaichana and A. Quiñones-Hinojosa, Editors. 2019, Academic Press. pp. 23–35.
69. Romei V et al. Resting electroencephalogram alpha-power over posterior sites indexes baseline visual cortex excitability. NeuroReport, 2008. 19(2).
70. Hanslmayr S, et al. Visual discrimination performance is related to decreased alpha amplitude but increased phase locking. Neurosci Lett. 2005;375(1):64–8.
71. Brett BL, et al. Longitudinal alterations in cerebral perfusion following a season of adolescent contact sport participation compared to non-contact athletes. Volume 40. NeuroImage: Clinical; 2023. p. 103538.
72. Slobounov SM, et al. The effect of repetitive subconcussive collisions on brain integrity in collegiate football players over a single football season: a multi-modal neuroimaging study. Volume 14. Neuroimage: clinical; 2017. pp. 708–18.
73. Boyko EJ. Observational research — opportunities and limitations. J Diabetes Complicat. 2013;27(6):642–8.
74. Balsters JH, Robertson IH, Calhoun VD. BOLD Frequency Power Indexes Working Memory Performance. Front Hum Neurosci. 2013;7:207.
75. Joyce JM, et al. Magnetic resonance spectroscopy of traumatic brain injury and subconcussive hits: A systematic review and meta-analysis. J Neurotrauma. 2022;39(21–22):1455–76.
76. Rae CD. A guide to the metabolic pathways and function of metabolites observed in human brain 1H magnetic resonance spectra. Neurochem Res. 2014;39(1):1–36.
77. Giza CC, Hovda DA. The new neurometabolic cascade of concussion. Neurosurgery. 2014;75(0 4):S24–33.

78. Baliyan V, et al. Diffusion weighted imaging: Technique and applications. World J Radiol. 2016;8(9):785–98.
79. Koerte IK, et al. Diffusion Imaging of Sport-related Repetitive Head Impacts—A Systematic Review. Neuropsychol Rev. 2023;33(1):122–43.
80. Nowak MK, et al. ADHD May Associate With Reduced Tolerance to Acute Subconcussive Head Impacts: A Pilot Case-Control Intervention Study. J Atten Disord. 2022;26(1):125–39.
81. Arslan B, Zetterberg H. *Neurofilament light chain as neuronal injury marker – what is needed to facilitate implementation in clinical laboratory practice?* Clinical Chemistry and Laboratory Medicine (CCLM), 2023. 61(7): p. 1140–9.
82. Abdelhak A, et al. Blood GFAP as an emerging biomarker in brain and spinal cord disorders. Nat Reviews Neurol. 2022;18(3):158–72.
83. Howarth C. The contribution of astrocytes to the regulation of cerebral blood flow. Front NeuroSci. 2014;8:87930.
84. Hughes SW, et al. 1*0 - Infraslow (< 0.1Hz) oscillations in thalamic relay nuclei: basic mechanisms and significance to health and disease states.* In: Van Someren EJW, et al. editors. Progress in Brain Research. Elsevier; 2011. pp. 145–62.

Figures

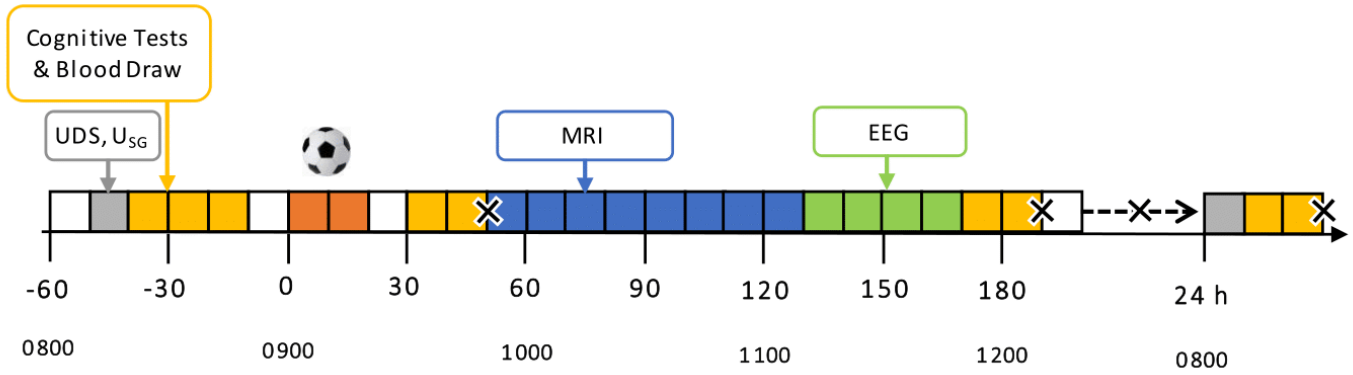

Figure 1

Experimental procedures.

Grey represents UDS and U_{SG} checks; Yellow represents the cognitive tests and blood draw; Orange represents the trial intervention (soccer task); Blue represents MRI; Green represents EEG. Crosses (X) are used to signify adverse event (concussion symptom) checks. Abbreviations: EEG – electroencephalography; MRI – magnetic resonance imaging; UDS – urine drug screen; U_{SG} – urine specific gravity.

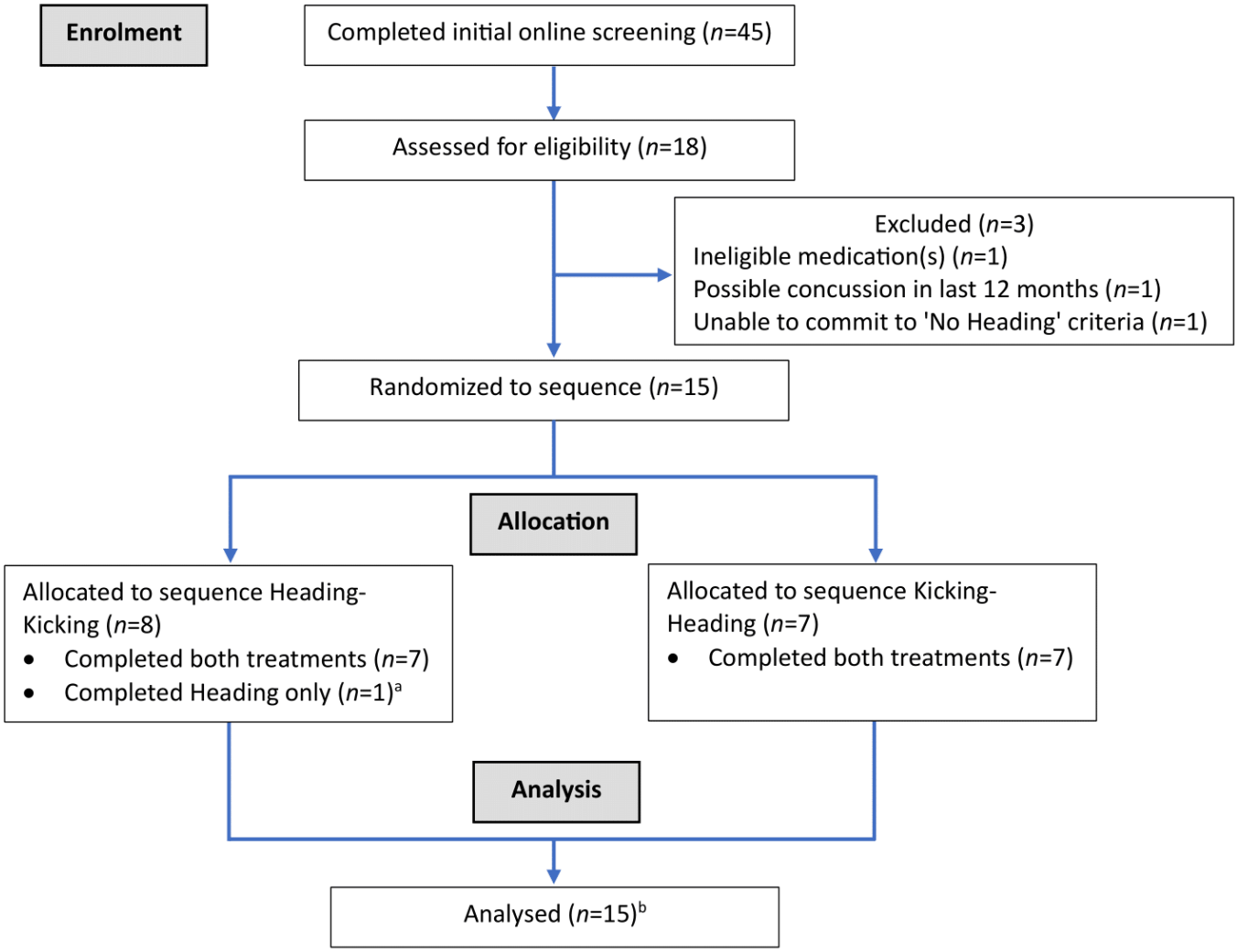

Figure 2

CONSORT Participant Flow Diagram.

[a]Did not complete second trial (Kicking) due to family reasons. [b]All participants who were randomised were included in the final (analytical) sample (except where the specific analytical technique could not handle missing data).

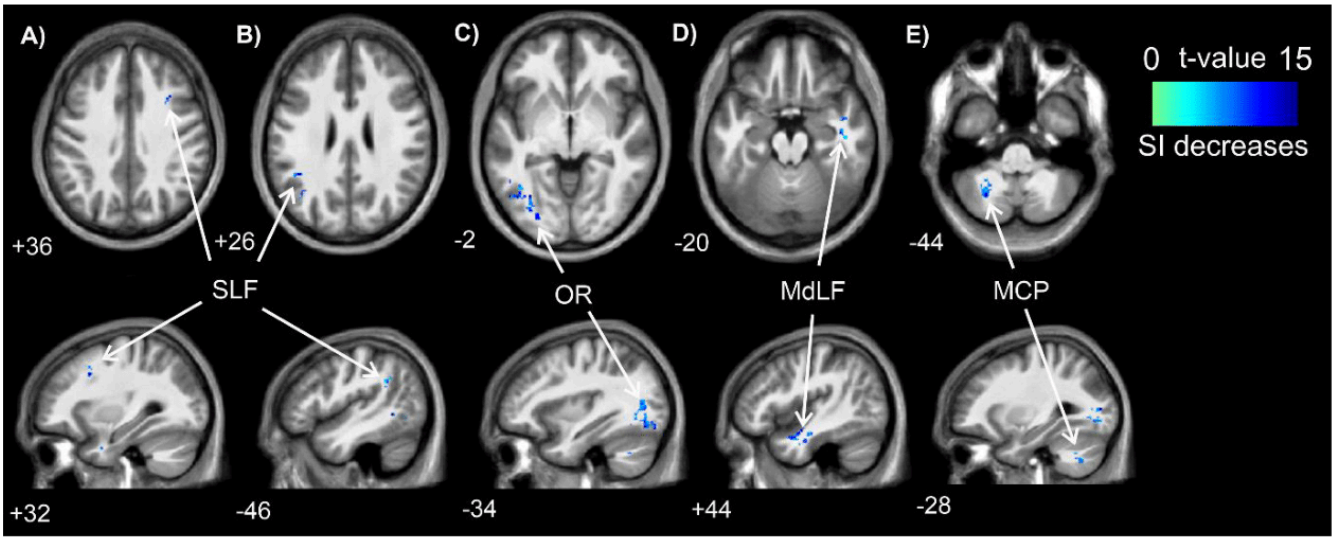

Region	Peak MNI coordinate			Cluster Size	Peak *T* value	Peak *P* value (FDR $p<0.05$)	Direction of change
	X	Y	Z				
A) Right SLF (anterior)							
	32	14	36	13	12.83	**<0.001**	Reduced for Heading
B) Left SLF (posterior)							
	-44	-48	10	12	15.72	**<0.001**	Reduced for Heading
	-48	-48	30	37	14.03	**<0.001**	Reduced for Heading
	-38	-64	26	14	12.04	**<0.001**	Reduced for Heading
C) Left OR							
	-34	-74	-14	207	22.80	**<0.001**	Reduced for Heading
D) Right MdLF							
	38	4	-36	16	14.63	**<0.001**	Reduced for Heading
	44	-4	-20	25	14.08	**<0.001**	Reduced for Heading
	42	-12	-16	18	13.44	**<0.001**	Reduced for Heading
	46	-8	-30	15	12.59	**<0.001**	Reduced for Heading
E) Left MCP							
	-24	-64	-42	25	13.04	**<0.001**	Reduced for Heading
	-32	-60	-38	13	11.75	**<0.001**	Reduced for Heading

Figure 3

Locations of significant clusters from electrical properties tomography data (*above*) and statistical details (*below*) between treatment sessions.

Cooler (blue) colours represent higher t values and a decrease in signal intensity. Location of each sagittal and axial slice in Montreal Neurological Institute space are indicated at the bottom left of each slice. Abbreviations: MCP – middle cerebellar peduncle; MdLF – middle longitudinal fasciculus; MNI – Montreal Neurological Institute; OR – optic radiation; SI – signal intensity; SLF – superior longitudinal fasciculus.

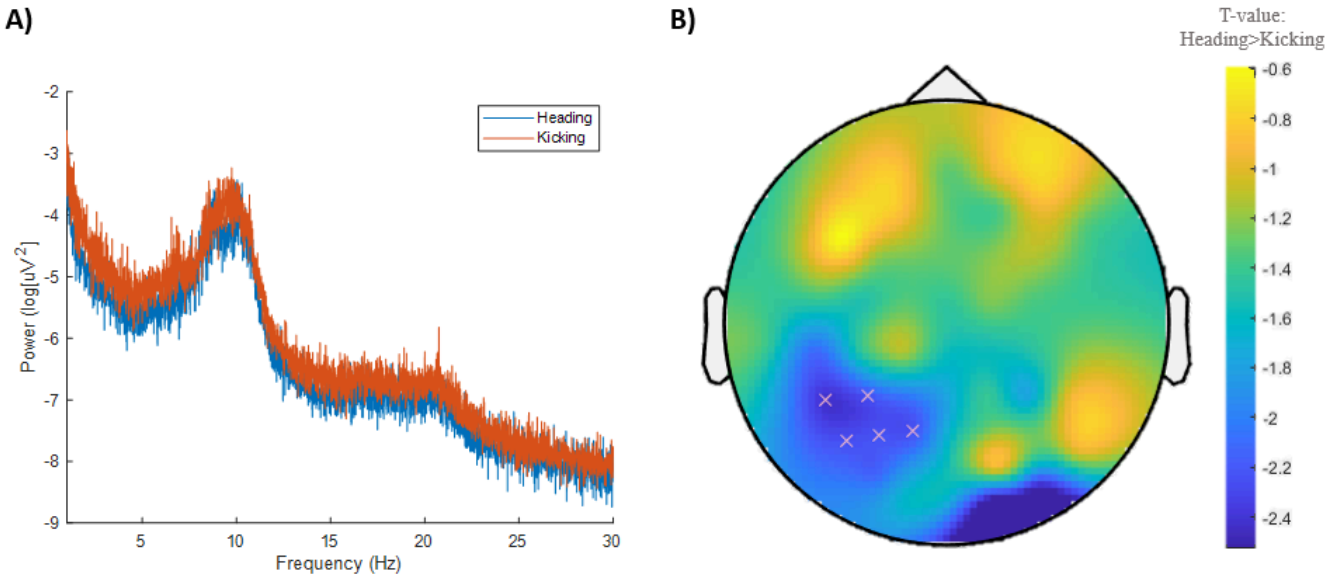

Figure 4

Electroencephalography data between treatment sessions.

(A) Power spectra across all frequencies between treatment sessions. (B) A trend (p=0.066) for reduced alpha frequency power in five left posterior channels on Heading. Cooler (blue) colours represent higher t values and a decrease in power (scale provided on right).

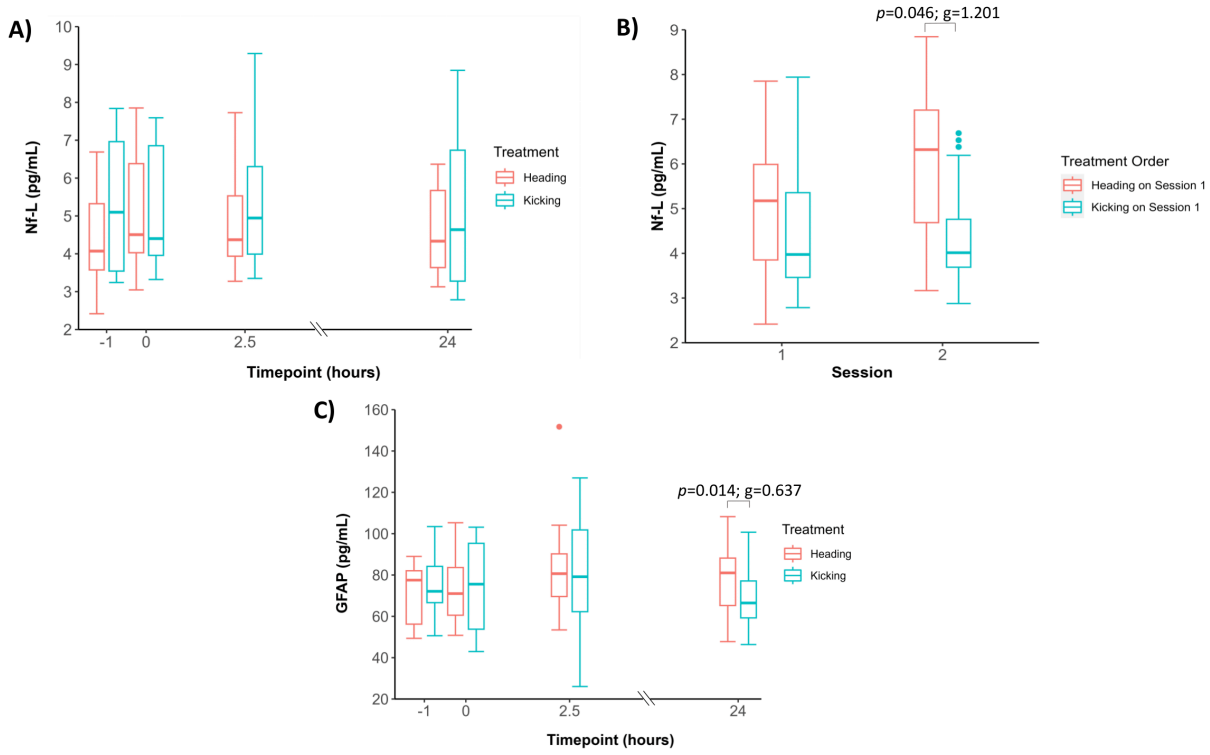

Figure 5

Plasma biomarker concentrations.

(A) Nf-L concentration between treatment and timepoint. (B) Nf-L concentration between sessions and treatment order. Session 2 was ≥7 days (mean=9 days) after session 1. (C) GFAP concentration between treatment and timepoint. Note that the simplest model violating the

fewest assumptions (i.e., untransformed) was used for analysis of GFAP, although still failed Shapiro-Wilk test of residuals (p<0.05).
Abbreviations: GFAP – glial fibrillary acidic protein; mL – millilitre; Nf-L – neurofilament light; pg – picogram.

Supplementary Files

This is a list of supplementary files associated with this preprint. Click to download.

- SupplementaryFiles7.docx